The Development of a Robotic System for Zygomatic Implant Placement

Mohammed Yahya Mansoor Al-Jarsha
(BDS (IRQ), MSc (UK-UofG))

Submitted in fulfilment of the requirements
for the Degree of Doctor of Philosophy (PhD)

Department of Oral and Maxillofacial Surgery
Glasgow Dental Hospital and School

School of Medicine, Dentistry, and Nursing
College of Medical, Veterinary, and Life Sciences

University of Glasgow

April 2025

Thesis Abstract

Oral rehabilitation with zygomatic implant placement is a predictable treatment option to restore the function of lost maxillary dentition. It is particularly indicated in cases of severe resorption of the maxilla and also after maxillectomies.

Today, the placement of almost all dental implants including zygomatic implants is achieved with the aid of a physical or a digital guide. Static guides are widely used to physically guide the placement of dental and zygomatic implants. Dynamic navigation technology provides digital guidance through monitoring of a computer screen during the implant osteotomy preparation and implant placement. Robotic-assisted implant dentistry can be regarded as a combination guide in the sense that it provides haptic physical guidance in addition to the digital real-time monitoring of the drilling stages on screen.

On the other hand, robotic placement of dental and zygomatic implants also relies on digital guidance principles, but the drilling and implant placement is not performed by a human operator. This technique has shown to produce a highly predictable accuracy in conventional dental implants and also demonstrated promising results with zygomatic implants. A deeper analysis of the possible sources of error involved in the digitally guided zygomatic implant placement techniques would inform the surgeons and may lead to better treatment outcomes in relation to placement accuracy. Such level of analysis would also benefit operators performing digitally guided conventional dental implant placement as it has not been done with this type of implants either.

Chapter 1: reviews the literature in relation to the importance of accurate implant positioning, the revolution of digital planning and guiding protocols, including robotic-assisted and robotic-guided approaches.

Chapter 2: is presented as a published journal article. This chapter analysed the registration error; one of the major human-related sources of error for the digital guidance protocol. This analysis served to optimise and standardise the registration process for the next stages of the project, by selecting the configuration of registration markers expected to produce the best registration accuracy.

Chapter 3: is presented as a published journal article. This chapter investigated the precision of drill calibration; another major human-related sources of error for the digital guidance protocol. The results served to optimise and standardise the drill calibration process for the next stages of the project, by selecting the best single drill that is expected to produce the best drill calibration accuracy.

Chapter 4: describes the processes involved in the initial development and testing phases of the integrated robotic system.

Chapter 5: is presented in the traditional chapter format. This chapter includes the final phases of *in vitro* testing of the newly developed integrated robotic system in this project. This blindly-analysed comparative study investigated the application error (i.e., execution error); the last major human-related source of error for the digital guidance protocol. The control groups involved operator placement under digital guidance (i.e., dynamic navigation) while the test group involved task-autonomous robotic placement using the new system.

In conclusion, this project investigated (*in vitro*) the accuracy of a newly developed dynamically guided robotic system to achieve zygomatic implant placement. The results demonstrated that the robotic system is highly accurate with clinically acceptable margin of errors. The translation into clinical application would require further developments mainly pertaining to the automation of the preparatory and within-procedure checks as the process was time-consuming when compared to manual placement. The project also contributes to our knowledge of the magnitude of the possible human-related sources of error in placing zygomatic implants under dynamic navigation guidance and suggests solutions to minimising them whether *in vitro* or in clinical scenarios.

Table of Contents

List of Tables

List of Figures

Presentations

Poster: Dynamic Navigation in Dental Implantology, SoMDN PGR day on the 17th of May 2021.

Oral Presentation: Dynamic Navigation Surgery in the Placement of Pterygoid Implants, Oral Surgery/Oral Medicine journal club on the 5th of October 2021.

Oral Presentation: Dynamic Navigation for Dental Implant Placement, The Digital Dentistry Week (BDS 1 Part B) on the 14th of March 2022.

Oral Presentation: Development of a Robotic System for Zygomatic Implant Placement, SOHRC Craniofacial Symposium on the 24th May 2022.

Oral Presentation: Using Dynamic Surgical Navigation in Augmented Areas, Oral Surgery/Oral Medicine journal club on the 1st of November 2022.

Oral Presentation: Reducing Human Error in Dynamic Navigation for Dental Implantology, BSODR Annual Meeting 2023 on the 7th of September 2023.

Poster: The Robotic Placement of Zygomatic Implants Guided by Dynamic Navigation, IADR General Session on the 16th of March 2024.

Publications

AL-JARSHA, M. Y., ALMEZYAD, O., ALOTAIBI, N., NAUDI, K. B., ROBERTSON, D. P. & AYOUB, A. F. 2024. The Accuracy of Intraoral Registration for Dynamic Surgical Navigation in the Edentulous Maxilla. Int J Oral Maxillofac Implants, 21-46.

AL-JARSHA, M. Y., AYOUB, A. F., ALMGRAN, M. M., LIU, C. H., ROBERTSON, D. P. & NAUDI, K. B. 2024. The precision of drill calibration for dynamic navigation. J Dent, 146, 105032.

AL-JARSHA, M. Y., DIAO, Y., ZHAO, G., IMRAN, M. A., AYOUB, A. F., ROBERTSON, D. P. & NAUDI, K. B. 2025. Dynamic Navigation-Guided Robotic Placement of Zygomatic Implants. J Dent, 153, 105463 (Manuscript was accepted pre-Viva, but published post-Viva).

Submitted Manuscripts

AL-JARSHA, M. Y., DIAO, Y., ZHAO, G., IMRAN, M. A., AYOUB, A. F., ROBERTSON, D. P. & NAUDI, K. B. Accuracy of an Integrated Robotic Arm with Dynamic Navigation System for Zygomatic Implant Placement – a comparative in vitro study

Acknowledgement

All praise and thanks be to Allah Almighty for giving me strength and patience to be able to start and finish this journey.

Firstly, I want to express my deepest gratitude to my supervisors Dr Kurt Naudi, Professor Ashraf Ayoub and Dr Douglas Robertson for their continuous guidance, insight, and support throughout my PhD study. I am so grateful for all the knowledge and skills you have helped me develop.

My appreciation extends to my reviewing committee Prof Andrea Sherriff and Dr Marta Czesnikiewicz-Guzik for their advice and support that contributed to achieve a more relaxing study environment.

Special thanks to my family; my mother, father, brother, sister, and my fiancée for being patient and understanding for my prolonged absence. Thank you for your endless love, encouragement, advice and support during my PhD study. I am proud to have each one of you in my family.

I would also like to thank my colleagues who gave me some of their time to help with my study endeavours; Dr Yufeng Diao, Dr Zhen Meng, Jiaming Yang, Kan Chen, Noura AlOtaibi, Hamideh Saghafi, and Omar Almezyad.

Author's Declaration

I confirm that the work presented in this thesis is my own and, at the time of submission, is not being considered for any other academic qualification. Where information has been delivered from other sources, I confirm that this has been indicated in this thesis and in the Statement of contribution below.

November 2024

Statement of contribution

The vast majority of the following work has been directly performed by the principal investigator (Mohammed Y. Al-Jarsha).

Exceptions include the intellectual work described in section 4.3 (suggesting the different possible methods for the coordinates transfer), the sophisticated coding and the stereophotogrammetry described in section 4.5 in addition to the hardware solutions provided in section 4.7.

The abovementioned parts were contributed to by members of the engineering team at the School of Engineering/University of Glasgow: Yufeng Diao, Zhen Meng, Jiaming Yang, and Kan Chen. However, the principal investigator was involved in all the practical work of testing and validating the hardware and software modifications, even in these parts.

Abbreviations

2D	2-dimensional
3D	3-dimensional
AC	Alternating current
AI	Artificial intelligence
ANOVA	Analysis of variance
CAD/CAM	Computer-aided design/Computer-aided manufacturing
CBCT	Cone beam computed tomography
Conf.	Configuration
CSV	Comma separated values
DICOM	Digital imaging and communications in medicine
DN	Dynamic navigation
DOF	Degrees of freedom
EM	Electromagnetic
FDA	The United States' food and drug administration
ICC	Intra-class correlation coefficient
IQR	Interquartile range
NASA	The national aeronautics and space administration
ND	NaviDent®
QZP	The quad zygoma protocol
RD	Registration deviation
ROS	Robot operating system
RViz	ROS 3D visualisation environment and interactive interface
sa-RASS	Semi-autonomous robotic assisted surgery system
SQ	Spread quality
STL	Standard triangle/tessellation language
TCP	Transmission control protocol
TM	Transformation matrix
TTL	Transistor-transistor logic
USB	Universal serial bus
V	Volts
XG	X-Guide®
ZI	Zygomatic implant

Chapter 1

Review of Literature

1.1. Introduction

Dental implants are designed and manufactured to restore the function of missing teeth (Bagheri et al., 2020). Being anchored to the bone, they are a favourable replacement option with high success rates (Scherer et al., 2015). Surgical and restorative treatments based on dental implants have improved significantly over the years. New treatment protocols as well as improved training and education methods have led to better outcomes (Sanz et al., 2019).

1.2. The importance of the accurate position of dental implants

The position of dental implants should be based on the required prosthetic rehabilitation without compromising the basic biological principles of hard and soft tissue remodelling during the healing process and after implant abutment connection. The aesthetic contour of the final restoration and the health of the surrounding soft and hard tissues are dependent on the position of the implant neck (i.e., shoulder). Gingival recession is likely to be severe if the implant shoulder is placed more buccally (i.e., towards the cheeks and lips). This was also true if the implant was proclined or was placed deeper than ideal, due to the lack of keratinised mucosa (Bagheri et al., 2020).

The vertical discrepancy between the implant shoulder and the peaks of the alveolar bone on the adjacent teeth should be minimal. This would allow the best aesthetic “emergence profile” of the restoration as the diameter of the gingiva widens from the occlusal surface of the implant towards the gingival margin (Bagheri et al., 2020). Placing the implant more coronally will result in a short-looking restoration with a questionable longevity if its crown height is less than 8 mm (Misch, 2014). More apically positioned implants would encourage bone loss around the implant with subsequent gingival recession (Bagheri et al., 2020). The vertical position of the smile line is critical in the aesthetic area as the implant-supported restoration may require augmentation with a pink part compensating for lost alveolar bone height. The transition line separating the pink part of the restoration from the patient’s gingiva should not be visible during smiling (Misch, 2014).

To minimise the risk of nerve injuries and perforations, a minimum 2 mm safety distance should be kept between the apex of the implant and the inferior alveolar nerve. The implant should also be 1 mm away from the floor of the maxillary sinus or any external bone surface (Bagheri et al., 2020). The minimum distance between an implant and an adjacent natural tooth should be 1.5 mm. Inter-implant distance should be at least 3 mm (Misch, 2014), or the resultant narrow crestal alveolar bone can result in resorption of this bone (Bagheri et al., 2020, Behnia et al., 2020).

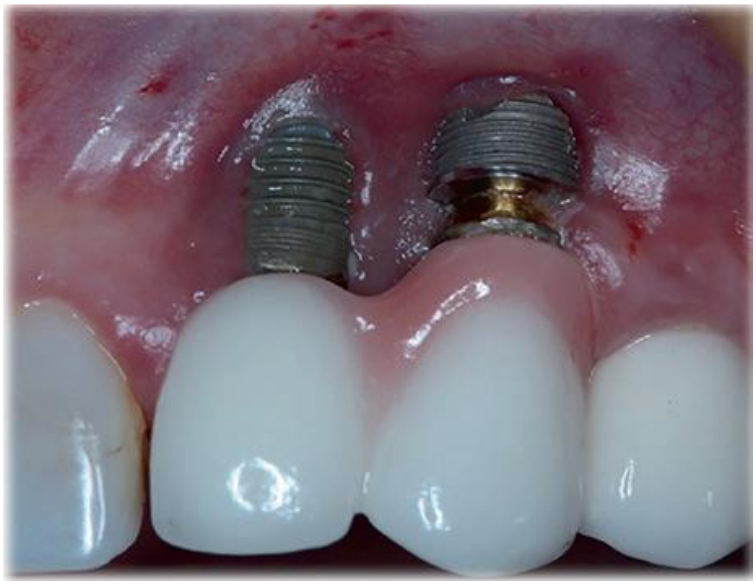

Figure 1-1: Gingival recession and implant exposure due to wrong position of the dental implant (more buccally and apically)(Behnia et al., 2020). © 2020, Springer Nature Switzerland AG, with permission.

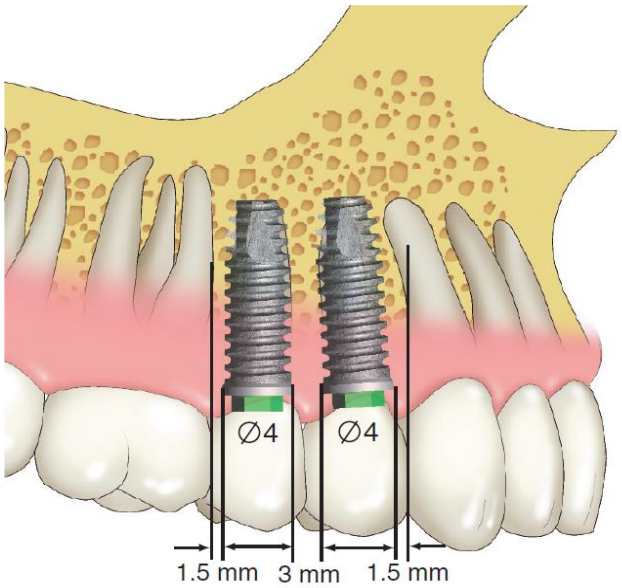

Figure 1-2: Key implant position in relation to adjacent natural teeth and other implants (Misch, 2014). © 2014 Elsevier Science & Technology Journals, with permission.

Accurate 3-dimensional (3D) dental implant positions are critical when multiple restorations and the immediate provision of a prosthesis are required. The predictability of an immediate temporary success would be limited if a trial-and-error approach was used to find the appropriate multiunit abutments as a consequence of ill-fitting prosthesis due to a mismatch between the planned and the achieved implant positions (Chen and Nikoyan, 2020). This would also have the potential of causing fatigue and failure of the components even if the implant positional error was as little as 0.15 mm (Bolding and Reebye, 2021, Pan et al., 2021). Angular deviations of around 3 degrees can negatively impact the health of the peri-implant tissue (Poli et al., 2023).

In summary, the accurate 3D position of the dental implant will contribute to its long-term success as a result of favorable prosthetic and aesthetic outcomes. Implant-supported prosthetic designs would also avoid the need to use cemented restorations (i.e., more designs would be screw-retained) (Parra-Tresserra et al., 2021).

The accuracy of the implant placement according to the pre-planned position is crucial. Deviations from the planned ideal position are measured at the entry point (implant platform or collar) and at the implant apex as well as the central axis angular deviation (in degrees)(Jorba-García et al., 2021, Zhan et al., 2020, Pyo et al., 2019).

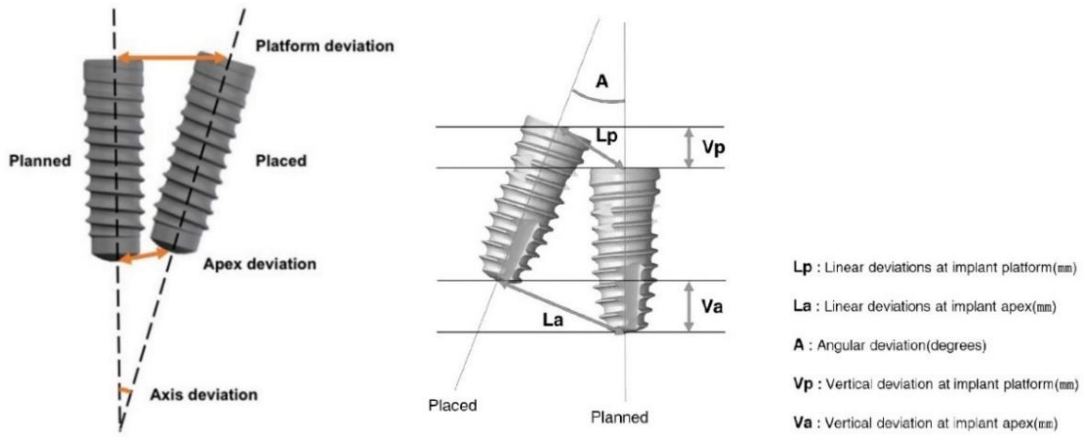

Figure 1-3. Parameters to measure implant placement accuracy compared to the planned positions. The left section is from (Zhan et al., 2020) © 2020 American Dental Education Association, with permission. The right section is from (Pyo et al., 2019), with permission (Open Access Article).

The sources of inaccuracies of implant placement include human error, imaging-related errors, guide manufacturing errors and registration errors ("deviation between the corresponding points on CT image and surgical site other than the fiducial points after registration"). Achieving a zero-level deviation is considered unrealistic (Kaewsiri et al., 2019), but aiming to reduce these errors to as low as reasonably achievable should be the aim of any technique used for implant placement.

1.3. The revolution of 3D imaging and planning software

Despite concerns of increased radiation dose (Kunzendorf et al., 2021), 3D imaging in the form of cone beam computed tomography (CBCT) have almost entirely replaced the need for 2-dimenstional (2D) panoramic radiography for dental implant planning. This is attributed to its advantage in providing 3D details of the adjacent anatomic structures, bone volume as well as the available restorative space (Anadioti and Kohltfarber, 2021). It has also been reported that there is a tendency towards selecting larger implant dimensions when relying on 2D imaging for planning, possibly due to variations in the shape and inclination of alveolar bone as well as the inherent degree of magnification and distortion in panoramic 2D images (Fortes et al., 2019).

The placement of dental implants without a physical or digital guide "mental navigation" has been the routine practice for many years. But the fact that this method produces the highest implant positional deviations has been confirmed in previous published literature (Vercruyssen et al., 2014).

The development of 3D dental planning software was the next natural evolution. This advancement had enabled excellent dentist-patient communication (Parra-Tresserra et al., 2021). Radiographic guides were then implemented in the pre-treatment CBCT to aid in planning the exact location of the implants guided by the prosthetic design (Anadioti and Kohltfarber, 2021).

The combination of 3D imaging and 3D planning software contributed to the development of a “digital workflow” that has gradually replaced the traditional methods of implant planning (Sanz et al., 2019). Today, it is possible to produce a physical template via prototyping technology with the aim of guiding the surgeon to the planned implant positions during surgery (Zhou et al., 2018). Figure 1-4 shows a screenshot from a 3D planning software.

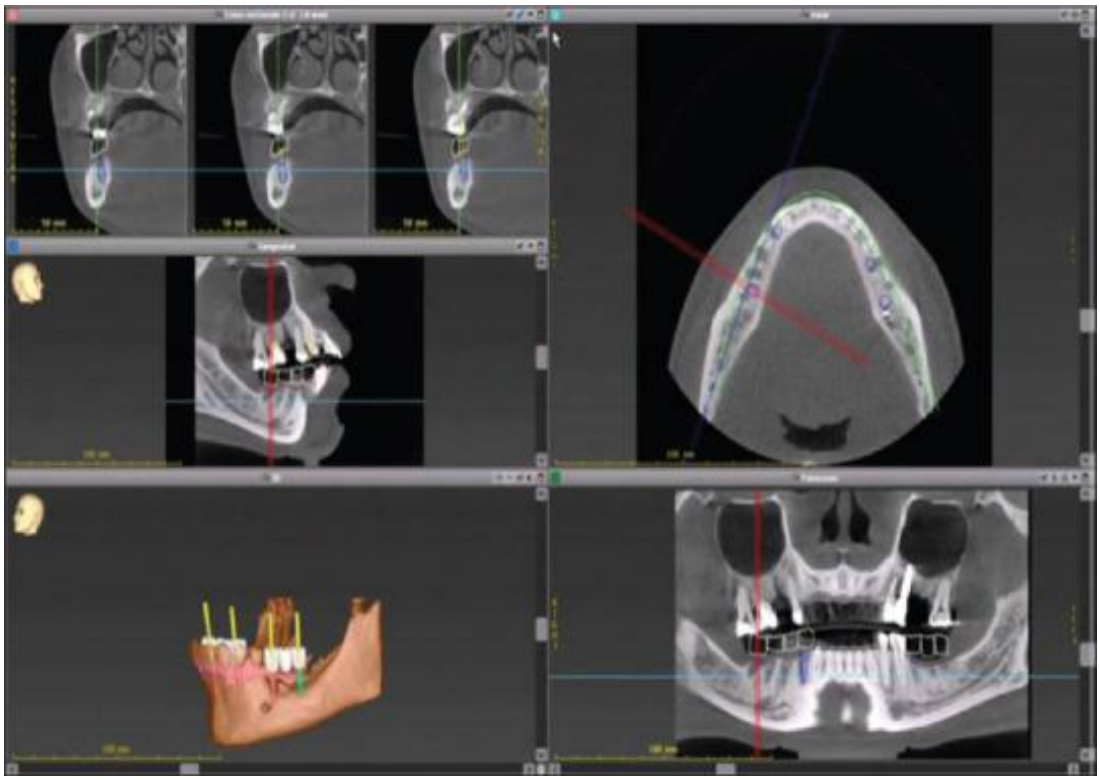

Figure 1-4. An example 3D planning software screenshot showing the advantage of planning in multiple cross-sectional views based on the patient specific CBCT (Kalaivani et al., 2020), with permission (Open Access Article).

Artificial intelligence (AI) is being incorporated into the planning software to assist in the process. Identification of anatomical structures including the alveolar bone, the segmentation of maxillary sinus plus the detection of the mandibular canal have been developed and validated (Altalhi et al., 2023).

1.4. Guided dental implant surgery

Guided by 3D imaging and planning technology, different surgical protocols used for implant site preparation have emerged. These can either be performed free-hand or assisted by static, dynamic and most recently robotic guidance (Chen and Nikoyan, 2020, Bolding and Reebye, 2021). The aim of guided surgical protocols is to reduce the human error associated with free-hand 'mental' navigation. The magnitude of such error relies on the surgeon's individual work style in preparing the site for implant placement. The effect of such factor is considerably less with guided surgery, especially for inexperienced surgeons (Vercruyssen et al., 2014, Scherer et al., 2015, Bolding and Reebye, 2021).

A recent large expert survey across Europe showed a moderate consensus (84%) that implant placement should be "guide oriented". However, only 8% thought that the implant should be "fully guided" (i.e., all drilling steps together with implant placement are guided rather than only guiding the initial drilling step(s)) (Sanz et al., 2019).

1.4.1. Static guidance

Surgical static guides are plastic devices which enable the surgeon to place the implant according to the preoperative surgical plan (Kalaivani et al., 2020). In the late 1980s and early 1990s, the guides were fabricated primarily for radiographical evaluation (Pesun and Gardner, 1995). This was followed by extensive research to improve the design, fabrication method and mode of fixation to tissues (Tallarico et al., 2019, Ashry et al., 2021). The term "static" appropriately describes this type of physical guide in which the implant position is predetermined and cannot be adjusted during the surgery (Block and Emery, 2016).

The earliest form of vacuum-formed stents (i.e., stents that were produced using a thermal-forming material sheet plus a vacuum device such as Biostar® and MiniSTAR® machines) were mainly used for professional communication reasons and their surgical benefit was limited to marking the osteotomy site with limited vertical control. On the other hand, most of current surgical static guides incorporate openings to accept manufacturer-specific metal cylinders (sleeves) related to that particular implant system.

The sleeve controls the width and direction of each drill up until implant placement, while it is also possible to use other cylinders from the manufacturer-specific guided surgical kit for vertical depth control (i.e., as physical stoppers) (Gargallo-Albiol et al., 2019).

The fabrication methods of the guides utilize patient-specific 3D imaging as well as scanned dentition data (Chen and Nikoyan, 2020). The guides can be manually made, produced through stereolithographic CAD/CAM technology (i.e., milling), or 3D printing technology. The latter two are computerised and more precise as the manual fabrication steps are eliminated (Kalaivani et al., 2020, Lo Russo et al., 2023, Htay et al., 2023, Salazar Rios et al., 2023). See figure 1-5.

Static guides can be also classified according to the mode of support or fixation to oral tissues (Chen and Nikoyan, 2020, Kalaivani et al., 2020). Tooth-supported surgical guides rely on support from the remaining teeth. Mucosa-supported guides are used in completely edentulous patients. Bone-supported guides are fixed to the bone using mini-pins (Gargallo-Albiol et al., 2019, Kalaivani et al., 2020, Vinci et al., 2020). See figure 1-5.

Variations in sleeve design include the closed metallic, closed non-metallic and open types. The closed metallic sleeves may result in bone overheating during drilling due to poor access of the external irrigation to the underlying bone. On the other hand, the open sleeve design allows better access for both the drill and the irrigation solution to the implant osteotomy site and is easy to apply in limited inter-arch space situations (Kalaivani et al., 2020, Ashry et al., 2021).

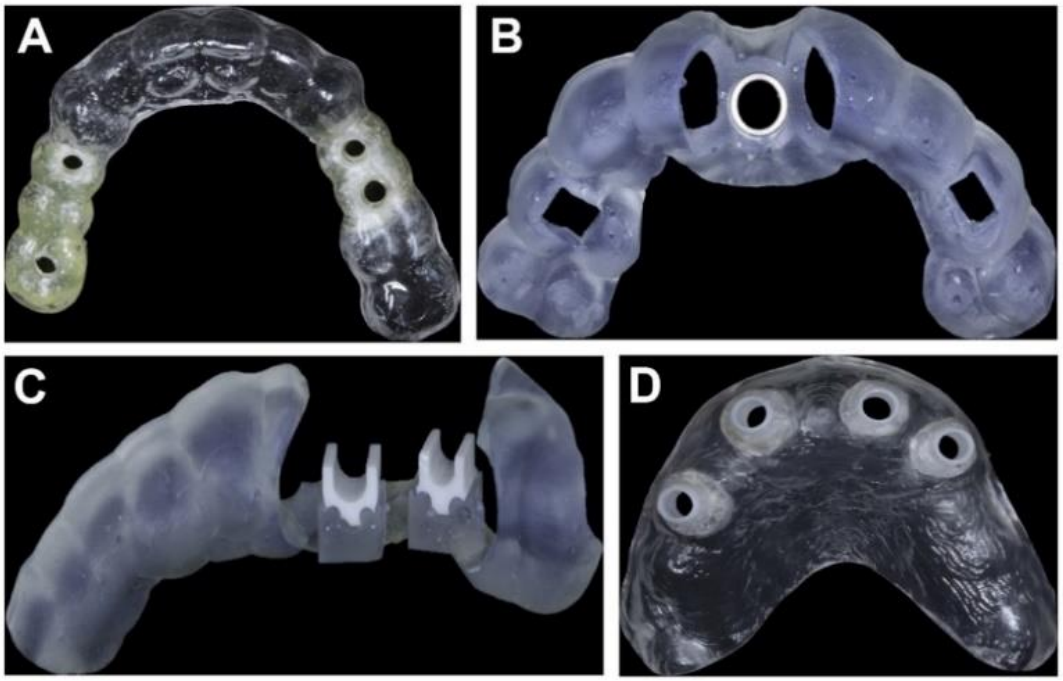

Figure 1-5. Examples of static guides. (A) Closed tooth-supported, vacuum stent. (B) Closed tooth-supported, 3D printed. (C) Open tooth-supported, 3D printed. (D) Closed mucosa-supported. Adapted from (Gargallo-Albiol et al., 2019). © 2019 Elsevier GmbH, with permission.

Today, the accuracy benefits of static guides are well established in comparison to free-hand mental navigation (Vercruyssen et al., 2014). Nevertheless, inaccuracies can still arise from the instability of the guide at the time of surgery, in addition to the inherent manufacturing errors. The metal sleeve has to be 0.2 - 0.5 mm larger than the diameter of the drill (Chen and Nikoyan, 2020).

According to a recent meta-analysis, other clinical factors such as the involved jaw (maxilla versus mandible), could influence the accuracy of the static-guided dental implant placement (Zhou et al., 2018). Implants placed under static guidance show a tendency for a more superficial final position than planned, probably due to the difficulty in monitoring the implant's crestal depth location in the presence of the static guide, as the implants were placed prior to the removal of the static guide (Block et al., 2017a, Parra-Tresserra et al., 2021).

Even with the introduction of open sleeve designs, static guides are difficult to use where there is limited vertical or horizontal space due to the minimum bulk required for the guiding components, which can result in limited visualisation and access (Golob Deeb et al., 2019, Jorba-García et al., 2019).

This effect might be mitigated by decreasing the drilling distance below the guided sleeve via using shorter implants or reducing sleeve heights, which have shown to increase the accuracy of this method (El Kholy et al., 2019). Comparing the effect of the inter-occlusal gap size in dentate patients using static guides versus freehand showed that gap size had an influence on the error in angulation only in both groups (Schneider et al., 2021).

1.4.2. Dynamic guidance

Dynamic guidance or dynamic navigation (DN) can be defined as "*a real-time coordination of the surgeon's hands and eyes by 3-dimensional visualization of the implant preparation with high magnification*" (Parra-Tresserra et al., 2021). The dynamic guidance does not physically restrict the surgeon's hand, but continuously tracks the tip of the drill and illustrates its position on a computer screen in relation to a planned implant position on a patient's CBCT scan. This leads to real-time guidance throughout the course of drilling and implant placement (Parra-Tresserra et al., 2021, Block et al., 2017b). Visual feedback cues built in the software alert the surgeon to their current drill (or implant) position and orientation in relation to the preoperative plan (Parra-Tresserra et al., 2021). See figures 1-6 and 1-7.

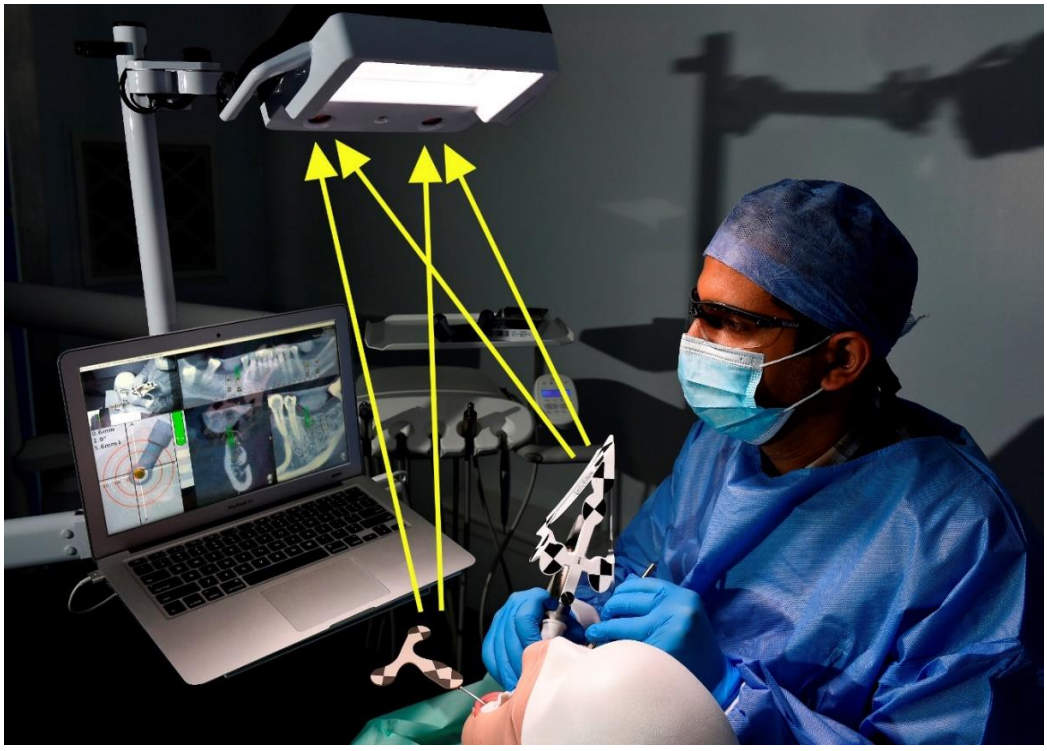

Figure 1-6. Dynamic navigation device with optical tracking during implant surgery training. The yellow arrows represent the directions of reflected light paths from the markers to the stereoscopic camera.

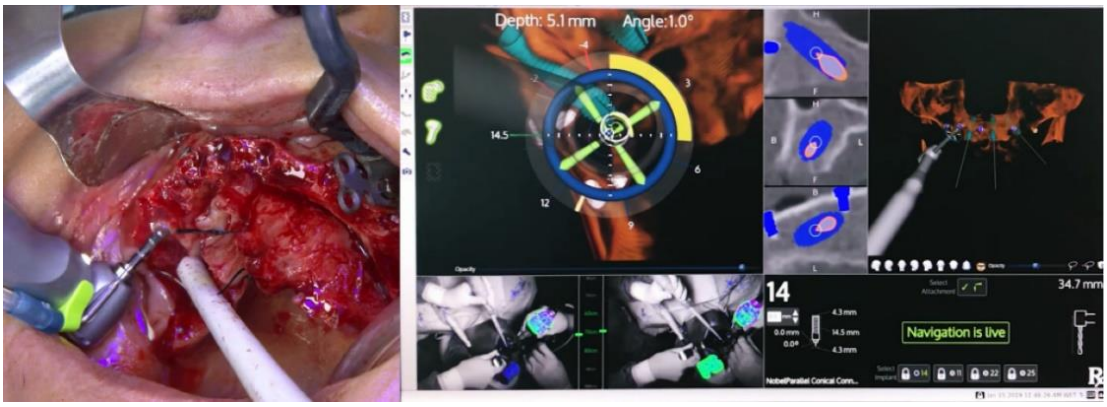

Figure 1-7. Side-by-side clinical and virtual real-time display showing visual cues of the current deviations from the planned implant position (Lopes et al., 2020), with permission (Open Access Article).

The development in medical imaging and stereotaxy plus the challenging high accuracy requirement in neurosurgery inspired the development of navigation surgery (Brown, 1979). Research of the oral and maxillofacial applications of the technology started as early as 1992 (Ewers et al., 2005). Micron tracking technology and the increasing power of the microprocessors and video trackers allowed the precise matching of the virtual plan of the CBCT to tracking markers. These markers are attached to the surgical handpiece and to the patient's anatomic surgical site (Aydemir and Arısan, 2020).

"Registration" is the process of determining the relation between the CBCT and the patient's relevant anatomic structure at the time of surgery. Fiducial markers, usually in the form of bone-anchored screws, are inserted before the preoperative scanning around the surgical region. These are digitised immediately before surgery to synchronise the preoperative planning and the surgical site (Fitzpatrick et al., 1998, Wu et al., 2019b). Two types of dynamic navigation systems based on the method of tracking are available for clinical use:

A. Optical navigation systems: these can be classified as active or passive depending on whether the tracking tags were emitting or reflecting light, respectively. An example of an active optical tracking systems is DCarer® (Yizhimei, Suzhou, China) (Figure 1-8, A) (Wu et al., 2019b). Passive reflective marker system examples include X-Guide® (X-Nav Technologies, LLC, USA) (Figure 1-7) and Navident® (ClaroNav Technology Inc., Canada) (Figures 1-6 and 1-8, B).

The light reflected from the patterns on the markers is picked up by a stereoscopic camera (Block et al., 2017a, Golob Deeb et al., 2019, Lopes et al., 2020).

B. Electromagnetic (EM) navigation systems: e.g. Aurora® and 3D Guidance®, NDI - Northern Digital Inc, Waterloo, ON, Canada (Lin et al., 2020) (Figure 1-9). Although EM systems may implement automatic registration functions (Lin et al., 2020), metal instruments and/or a metal operating table could cause interference problems with such systems (Wu et al., 2019b, Gao et al., 2021, Bolding and Reebye, 2021).

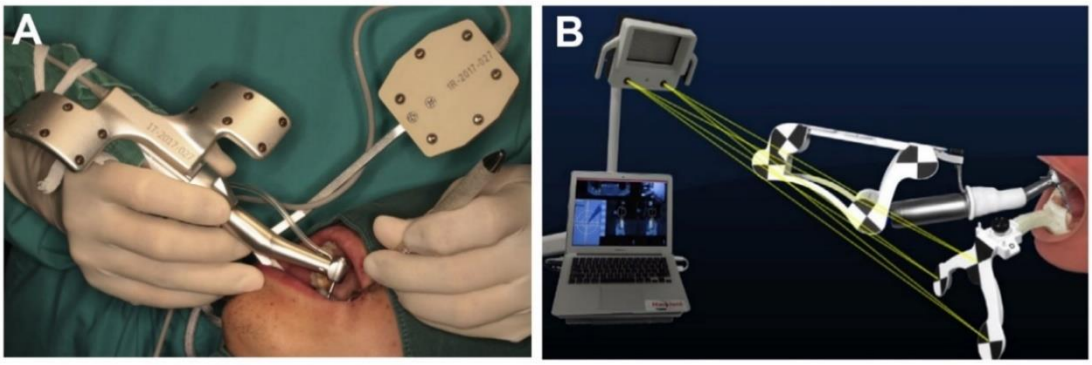

Figure 1-8. (A) Active optical tracking through battery-powered lights fixed on the surgical handpiece and the stent. (Wu et al., 2019b). © 2019 Elsevier, with permission. (B) Passive optical tracking through reflective patterns fixed on the surgical hand piece and the stent (Golob Deeb et al., 2019). © 2019 John Wiley and Sons, with permission.

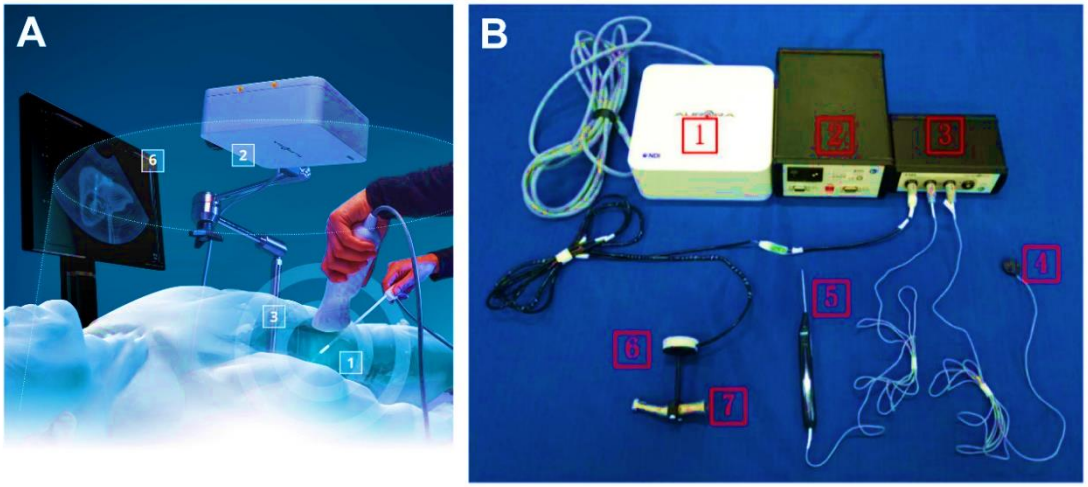

Figure 1-9. (A) Electromagnetic sensors embedded in the surgical instrument emit small currents once they enter the EM field. The signals are then interpreted by sensor tracking data for real-time navigation in relation to patient's image sets. The picture is provided courtesy of NDI, with permission (B) Components of the NDI Aurora EM tracking system 1: planar EM field generator, 2: system control unit, 3: sensor interface unit, 4: standard reference sensor for patients, 5: positioning probe for registration and calibration, 6: sensor of handpieces, 7: dental handpiece (Gao et al., 2021). © 2021 John Wiley and Sons, with permission.

After the registration process described above for mapping the CBCT space and the patient's real-world space, the DN software also needs to recognise the spatial relationship between the drill and the tracker that is attached to the handpiece. Drill calibration is the process that can achieve this input via two stages; drill axis calibration followed by drill length calibration. Registration and drill calibration steps provide input information to the DN system, which allows the tracking to be produced as an output on the screen showing the real-time spatial relationship between the tip of the drill and the implant trajectory planned on the patient's CBCT (ClaroNavInc., 2021, X-NavTechnologiesLLC, 2020).

A major advantage of DN is ensuring accuracy during the actual execution of the surgical plan (Parra-Tresserra et al., 2021). Therefore, DN-based implant surgery is considered the most accurate available implant placement technique according to multiple published studies (Golob Deeb et al., 2019, Chen and Nikoyan, 2020). It has been used in complex cases with limited access and it is possible to adjust the planned positions during surgery (Pellegrino et al., 2019).

However, accuracy data for DN systems are still scarce, with most of the published studies based on case reports and *in vitro* studies (Jorba-García et al., 2021, Wei et al., 2021, Parra-Tresserra et al., 2021). This might partially explain the reluctance of experts in Europe to use DN more routinely (Sanz et al., 2019). Previous authors reported the fact that surgeons might trust surgical experience more than advanced technology as a potential reason for the reduced adoption of the systems (Sanz et al., 2019).

Some studies reported on the advantages of DN over the static guidance approach due to the increased predictability. This is readily available as a result of real-time tracking. DN offers surgical safety due to the real time monitoring of vital structures during surgery. This encouraged the development of flapless surgeries, simpler planning steps (no physical guide fabrication is required), improved surgeon ergonomics, and better perception of bone quality. The facility of a direct view of the surgical filed is the main advantage of DN. The inaccuracies of ill-fitting or fractured static guides are also eliminated with the use of DN (Pellegrino et al., 2019, Parra-Tresserra et al., 2021, Wachol et al., 2023).

Nevertheless, DN guidance is also associated with some inaccuracies due to CBCT related errors, bite registration errors, the stability of the navigation tracker attached to the jaw, optical tracking noise, and fiducial registration errors (Chen and Nikoyan, 2020). However, the tracing of the patient's teeth was reported to reduce registration error if at least 3 stable teeth were traced (Stefanelli et al., 2020b). Local contributing factors, including variable bone quality, still contribute to the accuracy of the DN guided placement of dental implants. Dense bone will cause deflection of the drills during bone cutting as well as with the placement of the implants (Parra-Tresserra et al., 2021).

The main drawbacks of the current DN systems are their cost and the required training to be able to use them (DeLong et al., 2019, Chen and Nikoyan, 2020, Cristache et al., 2021). However, some studies reported decreased cost per patient (Pellegrino et al., 2019, Parra-Tresserra et al., 2021). Deeb and colleages explored dental implant training in predoctoral students using DN and reported that a plateau was achived after 3-5 attemtps (Golob Deeb et al., 2019) while senior dental students requried 10 attemtps according to another study (Zhan et al., 2020).

Operator's skill is an important factor influencing the accuracy of DN. There is a consensus in the published literature that guided approaches, especially dynamic navigation, are associated with a steep operator learning curve (DeLong et al., 2019, Demian et al., 2019, Pellegrino et al., 2019). Augmented reality (augmenting the virtual surgical plan into the real environment through semi-transparent glasses) might help mitigate the effect of this factor. Augmented reality will eliminate the uncomfortable tilting of the neck to monitor the 3D movement of the surgical instruments on the screen. The planning can be seen directly reflected on the surgical site throughout the course of the surgical procedure (Ayoub and Pulijala, 2019). In fact, the paradigm shift of looking at a screen instead of the patient was claimed to result in reduced tactile feedback and other cues from the surgical site and was thought to result in more errors due to the lack of physical guidance during DN (Bolding and Reebye, 2021).

Another recognised limitation of optical DN is that all the markers on the surgical tools and those attached to the patient's surgical field have to be within the line-of-sight of the camera (Lopes et al., 2020, Bolding and Reebye, 2021). EM DN systems such as TianShu-ESNS incorporate a virtual calibration method and avoids this issue. Nevertheless, metal object interference with the magnetic field is a unique limitation of the EM systems (Gao et al., 2021, Bolding and Reebye, 2021).

Some studies reported increased total time of the operation due to time spent for manual registration and setting up the device before the surgical work commences (Lin et al., 2020).

In some recent studies, a double-factor or "hybrid" guidance is being advocated to improve accuracy and overcome some shortcomings of either single method. In this protocol, the DN workflow is used, but in the presence of a static guide (Pomares-Puig et al., 2023, Yotpibulwong et al., 2023, Chhabra et al., 2023). The validity of this technique could be defended in edentulous cases or partially dentate cases with insufficient number of teeth to stabilise the guide, and where the accuracy of DN alone is slightly diminished due to difficulties with the registration process.

1.4.3. Robotic guidance

The fundamental rationale behind the development of robotic surgical devices has always been the reduction of human error which may arise from poor ergonomics due to surgical space requirements and/or fatigue of the surgeon (Wu et al., 2019a).

In the mid- 1980s, the National Aeronautics and Space Administration (NASA) developed a robotic system to surgically operate on astronauts in space and soldiers on the battlefield (Ahmad et al., 2021). Subsequently, the United States' Food and Drug Administration (FDA) approved the first robotic system for laparoscopic surgery in 2000. Ever since then, robots have been increasingly used across various surgical specialties in multiple surgical procedures (Wu et al., 2019a). In implant dentistry, the first study of robot-assisted surgery involved helping the surgeon by holding a drilling guide (Boesecke et al., 2001, Ahmad et al., 2021).

The past 2 decades have witnessed intensive research involving robotic real-time guidance and assistance in the field of dental implantology, mainly with 3 degrees of freedom (DOF) active joints leaving the final effector joints to be manipulated by the surgeon (Figure 1-10) (Yu et al., 2015, Wu et al., 2019a, Ahmad et al., 2021). See section 1.6 for the definition of DOF.

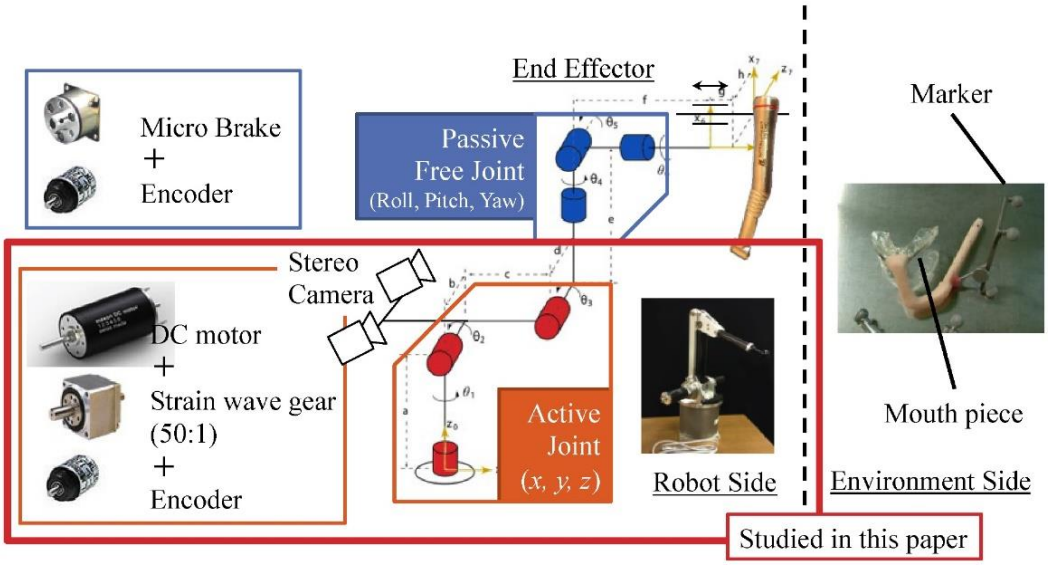

Figure 1-10. A diagram showing the design of a stereovision-based robot navigation system including active and passive robotic arm joints, an end effector, a stereo camera and an environment of markers for tracking (Yu et al., 2015) © 2015 IEEE, with permission.

In 2017, two major breakthroughs related to robotic dental surgical systems were announced; the FDA approval of the first commercially available robotic haptic feedback guidance system “Yomi” (Neocis Inc., USA) and the world’s first autonomous dental implant placement robotic system (ADIR system) (Beihang University in Beijing and the Fourth Military Medical University Hospital, China)(Wu et al., 2019a, Bolding and Reebye, 2021, Wang et al., 2024a, Jia et al., 2023).

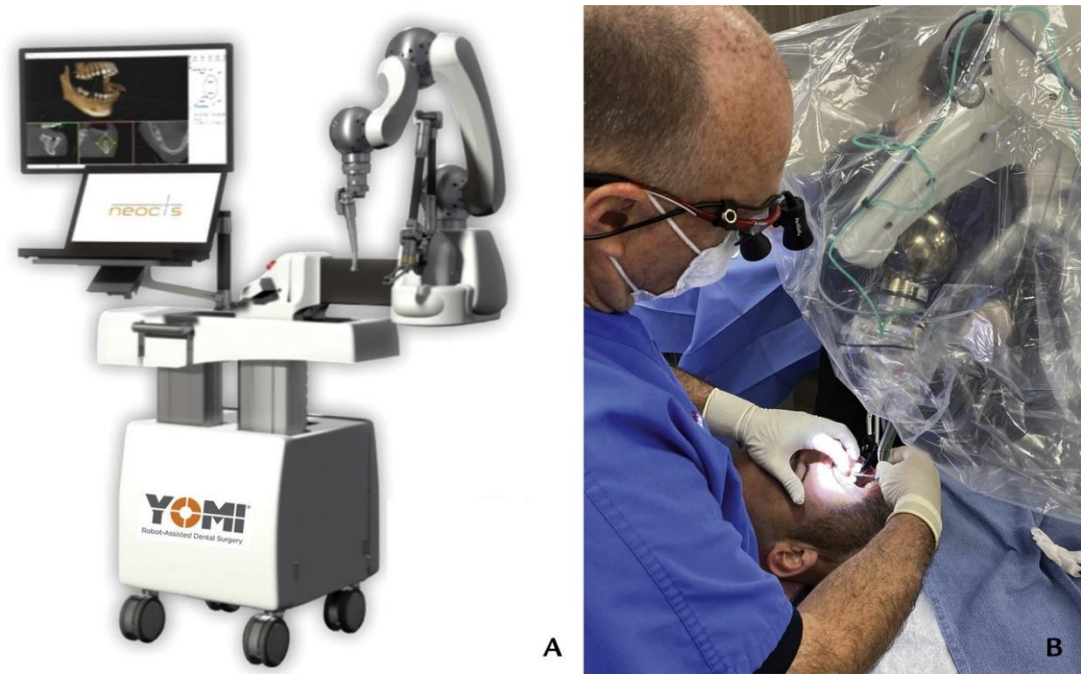

Figure 1-11. (A) Yomi robotic system (B) The Yomi robotic system draped during its clinical use (Bolding and Reebye, 2021). © 2021 by the Editorial Council for the Journal of Prosthetic Dentistry, with permission.

One limitation of the Yomi system is that it requires a rigid connection to the patient alveolar bone via a splint to register and track the position of the jaw. This high sensitivity to surgical site movement may explain why the validation studies of its clinical accuracy were performed under general rather than local anesthesia (Bolding and Reebye, 2021). Other obstacles currently facing the wide use of the Yomi system is its high cost and the lack of robust validation studies (Wu et al., 2019a, Bolding and Reebye, 2021, Ahmad et al., 2021). The high price of any robotic guidance system is related to the precise manufacturing and assembling requirements of its mechanical structure (Li et al., 2020).

The semi-autonomous robotic assisted surgery system (sa-RASS) is similar to Yomi, it requires the surgeon to handle the handpiece during the procedure. It was recently tested for single tooth implants (Ding et al., 2023). This type of robotic assistance is also termed “passive”. DentRobot® is another example of available passive robots (Xu et al., 2023a).

Autonomous robotic systems can be “semi-active” or “active” depending on whether the human operator needs to move the robotic arm close to the area of surgery before the drilling commences. In active robots, there is no human intervention required during the preparation of the implant bed. Remebot® is an example of a semi-active system whereas Yakebot® is one of the few commercially available active systems (Xu et al., 2023a).

The ADIR system includes a mechanical robot, DentalNavi software (for planning and navigation), an implantation foundation (connecting the robot to the implantation tools), and an image-guided foundation (connecting the navigation software to the robotic software). The outcome of its *in vitro* validation reported a mean entry deviation of 0.705 ± 0.145 mm, a mean apical deviation of 0.998 ± 0.232 mm, and a mean axial deviation of 2.077 ± 0.455 degrees. This system is claimed to be intelligent and capable of executing surgical tasks without interferences from the surgeon. Nevertheless, these claims are premature as they are not yet backed up by robust studies, especially in relation to the validation of robot intelligence-generated procedures (Wu et al., 2019a, Ahmad et al., 2021).

Remebot®, an autonomous brain surgery robot, was modified and validated for dental implant placement in recent years (Li et al., 2023b). This validation was through a retrospective case series in which 59 implants were placed in 10 patients with the Remebot® system. Their results demonstrated promising implant placement accuracy, with sub-millimetre coronal and apical deviations and an angular deviation of 1.27° ± 0.59° (Li et al., 2023b).

Another example of a 6 degrees of freedom (DOF) autonomous robotic system was investigated *in vitro* for zygomatic implant placement (Shengchi et al., 2018, Cao et al., 2020). The prototype robotic system showed lower deviations than that observed with the manual zygomatic implant placement under dynamic navigation. Angular zygomatic implant deviations were 1.52° ± 0.58° and 2.07° ± 0.30° for the robotic and manual DN groups, respectively in the second investigation (Cao et al., 2020). The angular deviations in the robotic system were 2.76° ± 1.39° in the first investigation (Shengchi et al., 2018).

Robotic surgery provides sustained accuracy and greater flexibility in assisting dental implant surgery (Wu et al., 2019a, Ahmad et al., 2021). However, current robotic systems are still lacking insertion torque and force feedback sensing which limits their use for immediate function implantology (Wu et al., 2019a). Current research in the area of dental robotics also includes the introduction of markerless navigation robotics in partially dentate cases, where the remaining teeth serve as “natural markers” (Ma et al., 2020).

The methodology of these previously published studies could be questioned on the basis of the lack of proper control groups and/or the lack of blind analysis which might have introduced analysis bias. A very recent meta-analysis also highlighted the possibility of funding bias when reporting the results of the robotic systems (Sankar et al., 2025). A more detailed critical appraisal of the previously investigated guiding protocols for zygomatic implants is provided in section 1.7.

A study by Milner and colleagues investigated the patients’ perceptions on robotics in restorative dentistry. The results demonstrated that dental patients expect robotic dental treatment to be much cheaper and there is also a lack of trust in the robotic systems to carry out invasive procedures safely (Milner et al., 2020). Nevertheless, the future of robotics seems promising as the systems become even more easily available and reliable (Wu et al., 2019a).

1.5. The anatomy of the zygomatic area in relation to zygomatic implants

Zygomatic bones are a pair of irregularly-shaped facial bones. They form the prominences of the cheeks and parts of the orbital floor and its lateral wall. They also form a portion of the boundaries of the temporal and infratemporal fossae. The zygomatic bone articulates medially with the maxilla, laterally with the temporal bone, posteriorly with the greater wing of sphenoid, and superiorly with the frontal bone (Marwan et al., 2020).

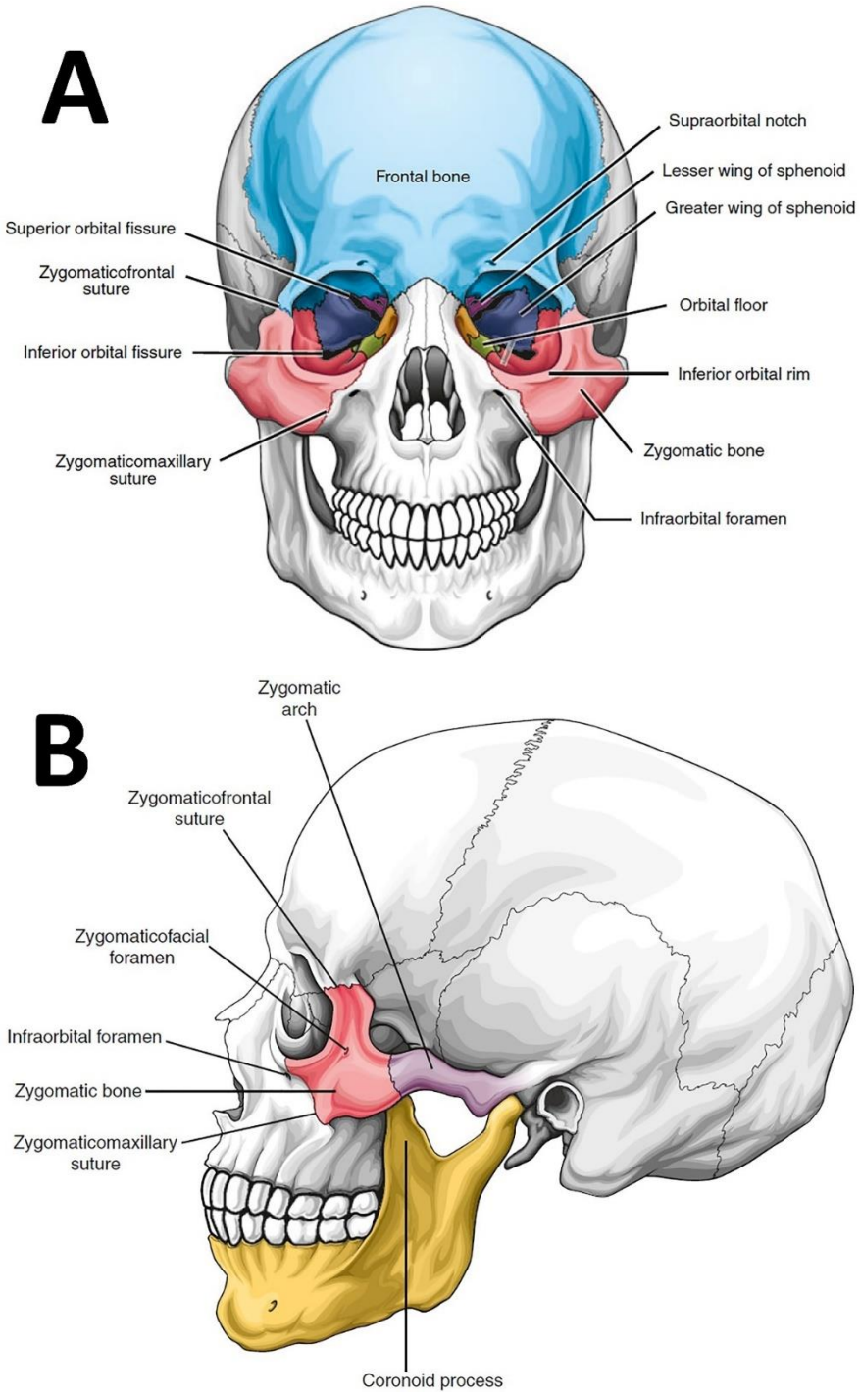

Figure 1-12. Anatomic relationships of the zygomatic bone. (A) frontal view. (B) lateral view (Marwan et al., 2020). © 2020, Springer Nature Switzerland AG, with permission.

Besides its role in maintaining facial aesthetics, the zygomatic bone protects the eye, transmits reactionary and masticatory forces from the maxilla, and constitutes an important part of the masticatory system via the attachment of the masseter muscle to the zygomatic arch (Wang and Dechow, 2016). The trabecular bone of the zygoma was investigated in relation to its volume and mineral dentistry as it is important for implant osseointegration (Nkenke et al., 2003, Chow, 2020). The strong cortical bone of the zygoma provides a good primary stability for zygomatic implants (Chow, 2020).

Planning ZIs involves the identification of the appropriate implant pathways based on the surrounding anatomical restrictions (Aparicio et al., 2021b). This is then followed by implementing a surgical guiding technique to ensure accurate execution of the plan (Aparicio et al., 2022).

The ZAGA classes are widely used to explain the ZI planned trajectory (Aparicio et al., 2021a). According to this classification, the trajectory could have an intra-sinus path (ZAGA-0), such as in cases with flat anterior maxillary wall. It could also be mostly intra-sinus but can be seen through the slightly concave maxillary wall (ZAGA-1). When the ZI trajectory is mostly extra-sinus and the implant body is in contact with most of the concave maxillary wall, it is classified as ZAGA-2.

In the ZAGA-3 and ZAGA-4 classes, the middle of the implant body does not touch the maxillary wall due to the degree of its concavity. The difference between the ZAGA-3 and ZAGA-4 is the location of the implant head in relation to the alveolar bone. If the implant head is located buccally outside the alveolar bone due to the severe degree of alveolar atrophy, then it is considered to be ZAGA-4. Otherwise, it is ZAGA-3 (Aparicio, 2011). See figure 1-13 (Aparicio et al., 2021a).

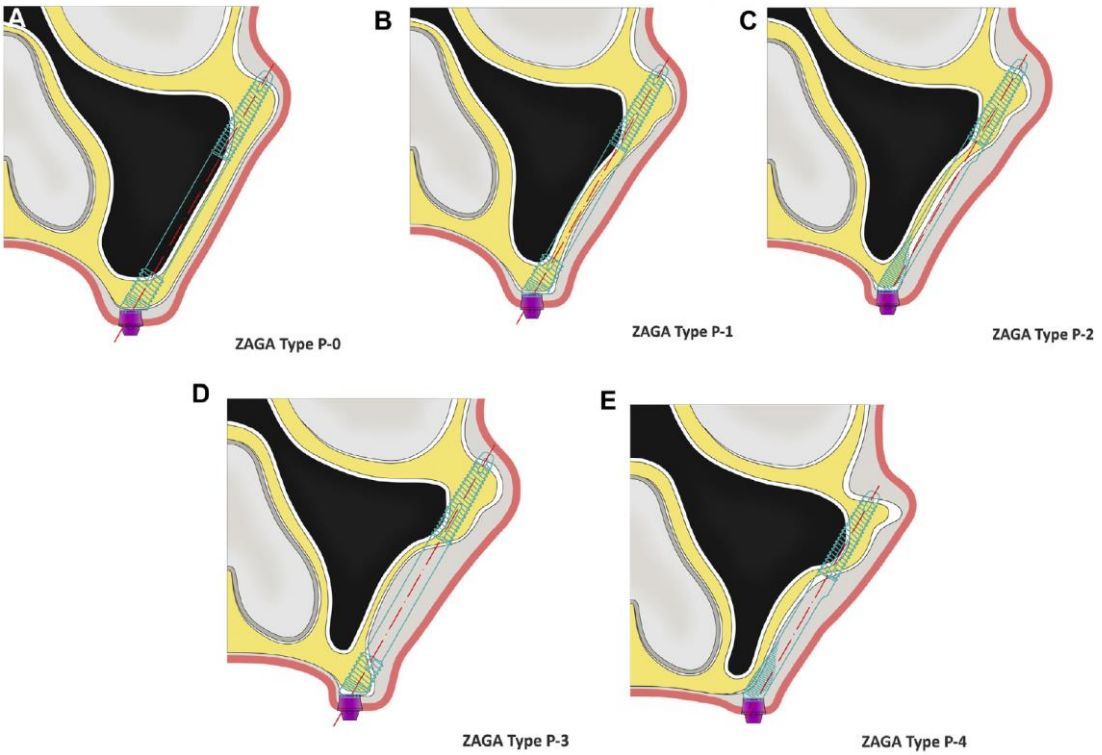

Figure 1-13. A diagrammatic representation of the ZAGA classification for ZI planning. (A) A total intrasinus path for the zygomatic implant (ZAGA-0). (B and C) the implant path is the more or less partially intrasinus (ZAGA-1 and ZAGA-2). (D) An intra-alveolar extramaxillary path (ZAGA-3). (E) An extra-alveolar and extramaxillary path (ZAGA-4) (Aparicio et al., 2021a) © 2021 Elsevier Inc., with permission.

1.6. Robotic arms: basic principles

Robotic arms, also known as mechanical manipulators, are devices that are designed to perform specific tasks effectively and swiftly. Their components include a collection of joints connecting multiple links and move them in relation to each other. The spatial relationship between the tool and the base of the arm is determined by the angles of the joints in the robotic arm (Craig, 2005, UniversalRobotsA/S, 2022).

The geometry and specifications of the robotic arms are usually described with terms like degrees of freedom (DOF), pose repeatability, reach, and maximum payload (UniversalRobotsA/S, 2018, Craig, 2005).

DOF is the number of independent movements the far end of the robot can achieve. All robotic arms that require the tool to be at a specific orientation in addition to reaching a certain position would require six degrees of freedom. This specification is determined by the type of joints included in the robotic arm design (Pennestri` et al., 2005).

The types of joints commonly used in robotic arms include revolute and prismatic joints. Revolute joints add a single rotational DOF in one plane, while prismatic joints add a single translational DOF due to their linear sliding action. Incorporating more complex joint types would add more DOFs and therefore reduces the total number of joints and links required to achieve the six degrees of freedom (e.g., a spherical joint would add three degrees of rotational freedom) (Pennestri` et al., 2005, Craig, 2005).

Pose repeatability refers to the ability of a robot to return repeatedly to a given position and orientation. It is the ability of a robotic mechanism to repeat the same motion and can be described as robotic precision. The resolution of a robotic arm is another term for denoting the smallest increment of motion that the arm can control or detect. It depends on the mechanical specifications of the motors in the joints and the distance between the tool and joint axes. On the other hand, the accuracy of the robotic arm refers to the magnitude of error in reaching a specific position compared to a more accurate gold standard (Craig, 2005).

The accuracy of the robotic arm therefore also relies on the calibration procedures performed at the manufacturing stage while programming the robotic arm, not only on the quality of the hardware components (Craig, 2005).

The reach of a robotic arm is the maximum horizontal distance between the centre of the robotic arm base and the end of its last joint. It is related to the overall work volume (i.e., workspace) in which the robotic arm can operate. As mentioned earlier, more resolution are expected for robotic arms that have smaller work volumes because of the shorter distances between the joints (Craig, 2005).

Maximum payload is the maximum magnitude of weight carried by the robotic arm at reduced speed while maintaining its rated pose repeatability. The payload parameter should be correctly input into the robotic arm control system. Incorrect payload input (e.g., more than the actual weight of the tool) would cause the robotic arm to go higher than the required position during motion (Craig, 2005).

1.7. Guided zygomatic dental implants

Zygomatic implant (ZI) treatment has been an effective option in the management of the atrophic edentulous maxilla as well as for defects resulting from maxillectomies. The reported success/survival rates for ZIs are around 97%, with the most common complications being related to local inflammations (35.7%) and sinusitis (12.5%) (Vrielinck et al., 2003, Bedrossian, 2021, Zhou et al., 2021, Davó et al., 2023, Brennand Roper et al., 2023). Bedrossian and Bedrossian explained the management of nine ZI complications, five of which were related in improper positioning. These included orbital involvement, intracranial involvement, overextended implant, vestibular dehiscence, and implant failure (Bedrossian and Bedrossian, 2018). Brånemark introduced the zygomatic implant not only as a solution to obtain posterior maxillary anchorage but also to expedite the rehabilitation process (Parel et al., 2001, Brånemark et al., 2004, Davó et al., 2023). These implants are anchored in the remote bone site of the zygoma where they are expected to be osseointegrated. The resulting long

prosthetic cantilever passing through the maxillary sinus zone would provide a level of functional rehabilitation (Parel et al., 2001). The classic Brånemark approach for rehabilitation involved placing 2 ZIs in the premolar/molar region and other 2 to 4 conventional dental implants in the anterior region (Brånemark et al., 2004).

The quad zygoma protocol (QZP), was initially described by Duarte and colleagues and then refined by Davó and colleagues (Duarte et al., 2007, Davó and David, 2021). This involves the palcement of 4 ZIs; two on either side of the zygoma, thus excluding the need for conventional anterior dental implants (Davó and David, 2021, Kämmerer et al., 2023). One of the major challenges is surgically achieving the anatomically accurate pre-planned position of the zygomatic implants due to limited available space and the increased length of these implants when compared to conventional dental implants (Vrielinck et al., 2003, Chrcanovic et al., 2010, Van Steenberghe et al., 2003). See figure 1-14.

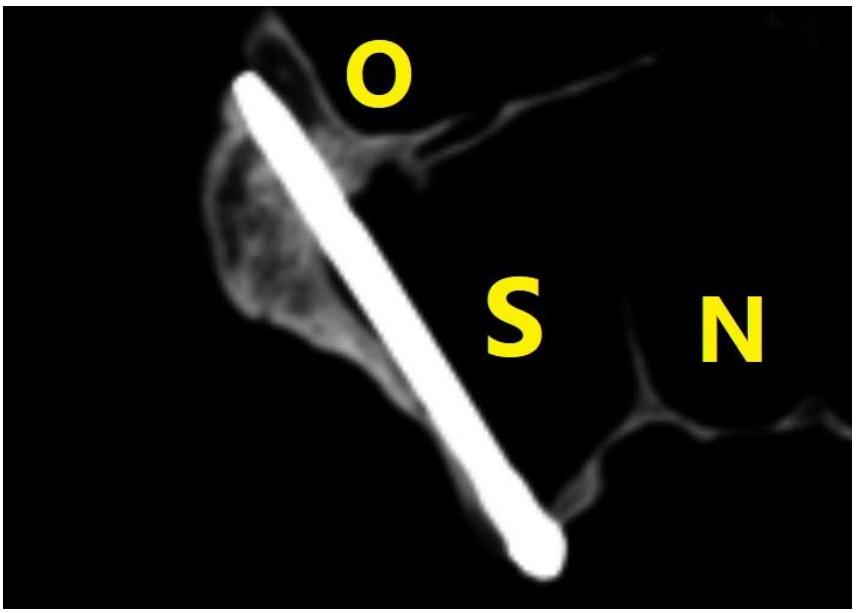

Figure 1-14. The ideal placement of a right zygomatic implant. The implant is anchored and subsequently osseointegrated into the zygoma. Alveolar anchorage depends on the level of crestal bone resorption and the curvature of the lateral wall of the maxillary sinus. O = orbital cavity; S = maxillary sinus; N = nasal cavity.

Misalignment of zygomatic implants could cause orbital injury, damage to the maxillary sinus as well as loss of osseointegration if the top of the implant is not fully engaged within the maximum width of the zygomatic bone (Van Steenberghe et al., 2003, Molinero-Mourelle et al., 2016).

Many implant guiding systems have been developed to improve the accuracy of the zygomatic implant placement. These include static guides (Grecchi et al., 2021) and real-time dynamic navigation systems (Hung et al., 2017). Robotic-assisted surgery is currently being investigated *in vitro* (Shengchi et al., 2018, Cao et al., 2020). Table 1-1 summarises some examples of previous studies within this field with their accuracy results.

N.	Study	Design	Test Groups	Sample size (per arm)	Reported accuracy (deviations)		
					Entry point (mm)	Exit point (mm)	Angular (°)
1	(Xing Gao et al., 2021)	Case Series (4)	Free-hand (+ pre-planning)	14	4.986 ± 2.66	6.114 ± 4.28	8.357 ± 5.3
2	(Tao et al., 2020)	Clinical	DN vs. free-hand	48 DN 48 FH	1.45 ± 0.60 1.50 ± 0.64	1.96 ± 0.44 2.04 ± 0.79	2.66 ± 1.13 2.50 ± 1.13
3	(Fan et al., 2023)	Clinical + Cadaver (Meta analysis)	Free-hand Static Guide DN	10 45 102	2.04 1.19 1.81	3.23 1.80 2.95	4.92 2.15 3.49
4	(Hernández-Alfaro et al., 2023)	Clinical	Static Guide	20	0.62 ± 0.19 BP 0.76 ± 0.19 MD	0.42 ± 0.13 BP 1.06 ± 0.37 MD	0.79 ± 0.41 axial
5	(Vosselman et al., 2021)	Cadaver	Static Guide	10	1.20 ± 0.61	2.12 ± 1.24	2.97 ± 1.43
6	(Grecchi et al., 2021)	Cadaver	Static Guide (Ti, long flange)	40 Zyg. 20 Pter.	0.93 ± 1.23 1.35 ± 1.45	1.35 ± 0.78 1.81 ± 1.47	1.69 ± 1.12 4.15 ± 3.53
7	(Schiroli et al., 2016)	Cadaver	Static Guide	6 (5)	< 1	3.86	4.5
8	(Chrcanovic et al., 2010)	Cadaver	Static Guide	16	-	-	8.06 ± 6.40 AP 11.20 ± 9.75 CC
9	(Vrielinck et al., 2003)	Prospective Clinical	Static Drill Guide	18 Zyg. 6 Pter.	2.77 ± 1.61 3.57 ± 2.99	4.46 ± 3.61 7.77 ± 6.09	5.14 ± 2.59 10.18 ± 6.07
10	(Zhou et al., 2021)	Case Series (4)	DN	9	1.56 ± 0.54	1.87 ± 0.63	2.52 ± 0.84
11	(Qin et al., 2019b)	*In vitro*	DN	4	1.22	1.70	0.4 to 2.9
12	(Qin et al., 2019a)	*In vitro*	DN	32	1.328	2.326	1.094 to 2.395
13	(Hung et al., 2017)	Clinical pilot	DN	40	1.35 ± 0.75	2.15 ± 0.95	2.05 ± 1.02
14	(Hung et al., 2016)	Case Report - hemimaxillectomy	DN	3	1.07 ± 0.15	1.20 ± 0.46	1.37 ± 0.21
15	(Chen et al., 2011)	Case Report	DN	3	1.127 ± 0.295	1.64 ± 0.19	1.12 ± 0.39
16	(Watzinger et al., 2001)	Cadaver - hemimaxillectomy	DN	10	-	1.3 ± 0.8	-
17	(Shengchi et al., 2018)	*In vitro*	Robotics (+DN)	12	2.34 ± 0.79	2.57 ± 1.73	2.76 ± 1.39
18	(Cao et al., 2020)	*In vitro*	DN + Robotics vs. DN only	12 DN+R 4 DN only	0.79 ± 0.19 0.96 ± 0.28	1.49 ± 0.48 2.26 ± 0.32	1.52 ± 0.58 2.07 ± 0.30
19	(Li et al., 2023a)	*In vitro*	Remebot®	10	0.78 ± 0.34	0.80 ± 0.25	1.33 ± 0.14
20	(Deng et al., 2023b)	*In vitro*	Remebot® 1S Remebot® 2S	13 13	1.22 ± 0.76 0.57 ± 0.19	2.13 ± 0.83 1.07 ± 0.48	1.58 ± 0.88 0.91 ± 0.51
21	(Deng et al., 2023c)	Clinical	Remebot® 2S	8	0.97 ± 0.50	1.27 ± 0.67	1.48 ± 0.61

Table 1-1: Examples of published studies reporting the accuracy of placing zygomatic implants free-hand (un-assisted) and guided with different modalities. DN = dynamic navigation, FH = free-hand, Zyg. = zygomatic, Pter. = pterygoid, AP = anterior-posterior, CC = caudal-cranial, BP = buccopalatally, MD = mesiodistally, R = robotics, 1S = one-stage protocol, 2S = two-stage protocol.

According to table 1-1, all three accuracy parameters were generally improved when moving from free-hand to static guidance, and then from static to dynamic navigation guidance. However, ZIs placed under dynamic navigation and robotic guidance demonstrated similar accuracy results.

Free-hand ZIs showed 1.5 to 5 mm mean entry point deviation, 2 to 6 mm mean exit point deviation, and 2.5 to 8.5° mean angular deviation. Static guided ZIs showed 0.9 to 2.8 mm mean entry point deviation, 1.4 to 4.5 mean exit point deviation, and 1.7 to 11.2° mean angular deviation. DN guided ZIs showed 1.1 to 1.8 mm mean entry point deviation, 1.2 to 2.3 mm mean exit point deviation, and 1.1 to 2.5° mean angular deviation. Robotically placed ZIs showed 0.6 to 2.3 mm mean entry point deviation, 0.8 to 2.6 mm mean exit point deviation, and 0.9 to 2.7° mean angular deviation.

Gao and colleagues highlighted the inadequate accuracy of free-hand ZI placement despite the use of virtual surgical planning (Xing Gao et al., 2021). This is supported by the reported five surgical complications due to inaccurate positioning of ZIs by Bedrossian and Bedrossian, mentioned earlier in this section (Bedrossian and Bedrossian, 2018). However, another clinical study by Tao et. al. reported much higher accuracy for the free-hand protocol, indicating the sensitivity of the free-hand placement accuracy to the level of surgical training in this protocol (Tao et al., 2020).

Three of the other four ZI placement complications in Bedrossians' publication (Bedrossian and Bedrossian, 2018) were mostly related to handling the surgical flap, which is a requirement for most static guided ZI protocols (Vosselman et al., 2021, Grecchi et al., 2021), as the flapless approach with static guided ZI placement found to be problematic (Schiroli et al., 2016). These complications include paraesthesia of the maxillary nerve branch (V2) due to flap reflection, subperiosteal infections, and sinus infections due to debris entrapped underneath the flap (Bedrossian and Bedrossian, 2018).

Reducing errors and complications is essential for zygomatic implant placement (Molinero-Mourelle et al., 2016, Bhalerao et al., 2023). Static guides have the disadvantage of the required production time in addition to the necessity for mucoperiosteal flap reflection to fix the guide in place (Grecchi et al., 2021, Hernández-Alfaro et al., 2023). These drawbacks are eliminated if a DN protocol is applied in these cases (Bhalerao et al., 2024).

There is a well-reported need for considerable operator training for DN protocols with simple conventional dental implant procedures (Golob Deeb et al., 2019, Zhan et al., 2020, Wang et al., 2022b, Yan et al., 2024). The same requirement for a steep learning curve has shown to be applicable for ZI placement procedures, particularly in relation to operation time (Wang et al., 2024c).

Using robotics for implant placement to circumvent the requirement for operator training is an attractive approach. The literature is still scarce on the application of robotic assistance for zygomatic implant placement. Shengchi, Cao and other members of that research team in China investigated one of the first systems *in vitro* (Shengchi et al., 2018, Cao et al., 2020). The deviation evaluation method used in their studies was vague and seem to involve a process of segmentation for the post-operative ZIs before analysis (Cao et al., 2020). In addition, despite getting accurate results, this research team have not published any follow-up studies on their prototype robotic system, yet. This could be related to the complex architecture of their robotic system and/or having difficulties in making the procedure time practical for clinical scenarios.

Therefore, up until 2023, there was a lack of well-conducted studies in robotic guided ZI placement that justified conducting the research project presented in this thesis.

Later on, the ROSA One® robot was tried in a clinical case using a flapless protocol in France and considered to be a safe technique (Olivetto et al., 2023). At the same time, Li and colleagues in China have been testing the Remebot® system (Li et al., 2023a).

Both of these commercially available robotic systems are semi-active and were originally designed for neurosurgical applications (Olivetto et al., 2023). In September 2023, Deng and colleagues proposed a two-stage protocol to implement the Remebot® system in a clinical trial on 6 cases (Deng et al., 2023c). The overall accuracy was comparable to using the dynamic navigation manually without a robot in a previously published cases series (Hung et al., 2016)(table 1-1).

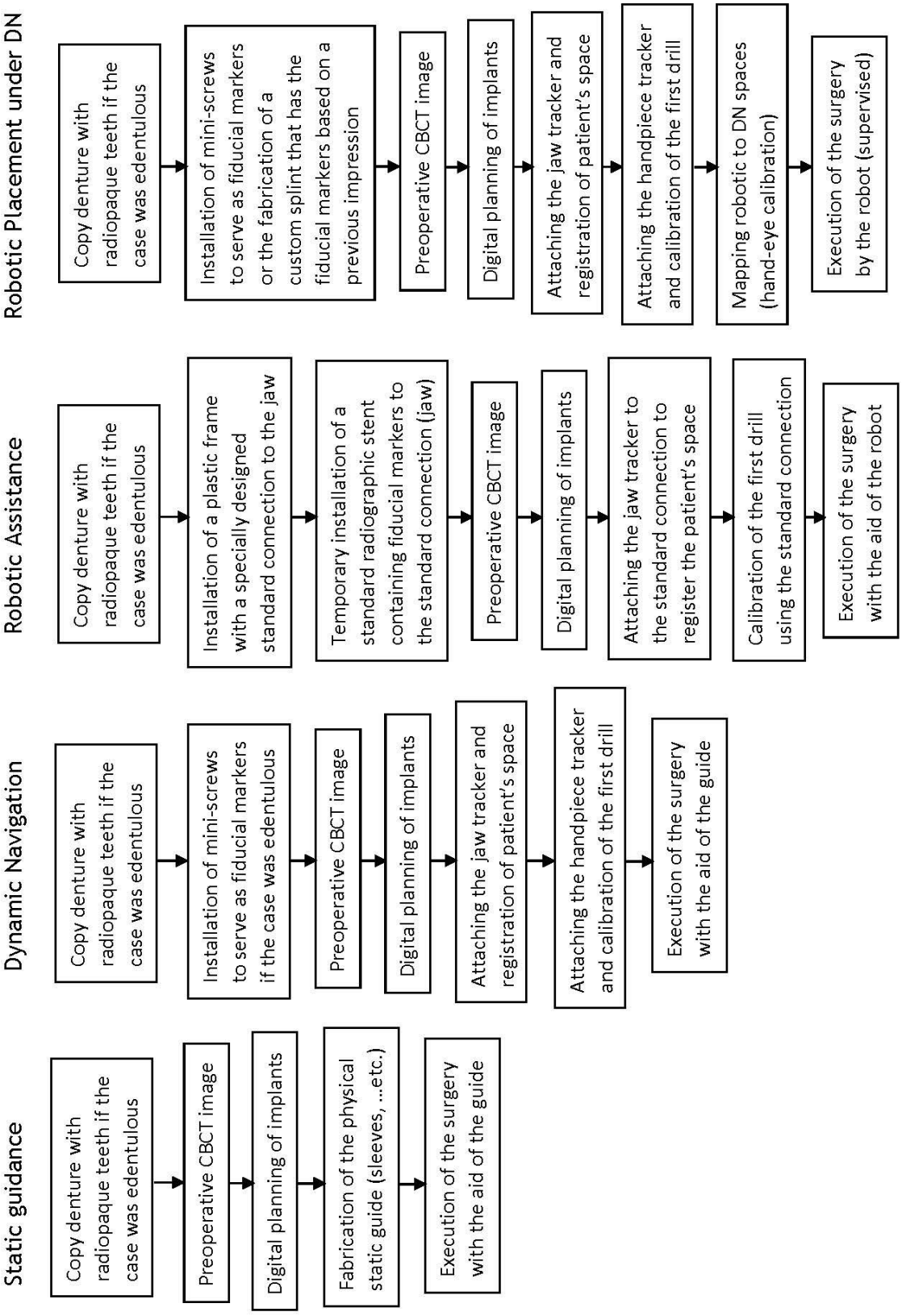

Figure 1-15: A flow diagram showing the main procedural steps for implant guiding techniques. DN = dynamic navigation.

Chapter 2

The Accuracy of Intraoral Registration for Dynamic Surgical Navigation in the Edentulous Maxilla

2.1. Preface

In the previous chapter, we showed the importance of accurate dental and zygomatic implant position and the currently available clinical protocols to ensure that accurate positioning.

The most commonly used of these guiding protocols is dynamic navigation via optical tracking. This method of guidance still involves multiple sources of error. Some of them are related to the technical side while others are related to the operator side. One of the operator-related error sources arise during the manual mapping of the 3D space of the CBCT to the real-world space of the patient, a procedure known as registration. The mapping process relies on common landmarks between the two spaces. These can be healthy teeth in partially dentate cases, but have to be pre-placed small landmarks (e.g., fixation screws) in edentulous cases. These later landmarks are termed fiducial markers, and the protocol related to using them is termed fiducial registration. When using teeth as landmarks in partially dentate cases, the operator is required to go over several parts of the tooth surface rather than mere single points. This process is known as tracing registration.

Therefore, this chapter aimed at comparing the accuracy of the registration process using different registration protocols and different configuration of landmarks within each protocol. This optimisation of the registration process standardises the best protocol and landmark configurations that resulted in the minimum magnitude of error in cases of edentulous maxillae.

This chapter is presented as a published journal article (with minor variations form the published version in order to improve clarity):

Al-Jarsha, M. Y., Almezyad, O., Alotaibi, N., Naudi, K. B., Robertson, D. P. & Ayoub, A. F. 2024. The Accuracy of Intraoral Registration for Dynamic Surgical Navigation in the Edentulous Maxilla. International Journal of Oral and Maxillofacial Implants, 39(3), 21-46.

2.2. Author declaration and contribution

Conceptualisation: The formulation of research aims and goals in this publication is totally of my own conceptualisation.

Data Curation: I completed all data processing to extract measurements from all the pictures from all three operators using ImageJ software in this publication.

Formal Analysis: I was responsible for application of all statistical analyses to synthesise all study processed data, including descriptive tests, normality tests, inter-operator agreement tests, and multiple comparisons in this publication.

Investigation: I participated in the practical experiment and data collection (in picture format) as one of the three operators in this publication.

Methodology: I designed the experiment in this publication through selection of the configurations to be tested, standardising the procedural steps that was conducted by all operators, and creation of data collection sheets.

Project Administration: I participated in the management and coordination for the experiment execution in this publication.

Visualisation: I was responsible for the creation and preparation of all figures and tables for data visualisation and presentation in this publication.

Writing – original draft: I wrote the complete original draft for this publication.

Writing – review and editing: I completed the pre-publication revisions (up to version 4) based on feedback from the other co-authors. I also completed all the editing requested by the journal as well as post-acceptance proof reading.

2.3. The Accuracy of Intraoral Registration for Dynamic Surgical Navigation in the Edentulous Maxilla

Mohammed Y. Al-Jarsha[1,2], Omar Almezyad[1], Noura AlOtaibi[1,3], Kurt B Naudi[1,*], Douglas P. Robertson[4], Ashraf F Ayoub[1].

The international journal of oral & maxillofacial implants. 2024 Jun 21:(3):21-46. https://doi.org/10.11607/jomi.10531.

[1] Department of Oral Surgery, School of Medicine, Dentistry and Nursing, College of Medical, Veterinary and Life Sciences, University of Glasgow, Glasgow, United Kingdom.

[2] Department of Oral and Maxillofacial Surgery, College of Dentistry, University of Baghdad, Baghdad, Iraq.

[3] Department of Maxillofacial Surgery, King Saud University, Riyadh, 12372, Saudi Arabia.

[4] Department of Restorative Dentistry, School of Medicine, Dentistry and Nursing, College of Medical, Veterinary and Life Sciences, University of Glasgow, Glasgow, United Kingdom.

* Corresponding author (Kurt.BusuttilNaudi@glasgow.ac.uk)

2.4. Abstract

Purpose: Despite the high clinical accuracy of dynamic navigation, inherent sources of error exist. The purpose of this study was to improve the accuracy of dynamic navigated surgical procedures in the edentulous maxilla by identifying the optimal configuration of intraoral points that results in the lowest possible registration error for direct clinical implementation.

Materials and Methods: Six different four-area configurations (left and right sides; n = 12) were tested by three operators against two negative controls (left and right sides) and one positive control (three-area and eight-area configurations, respectively) using a skull model. The two dynamic navigation systems (X-Guide and NaviDent) and the two registration methods (bone surface tracing and fiducial markers) produced four registration groups: XG tracing, ND tracing, XG fiducial, and ND fiducial. The accuracy of the registration was checked at the frontal process of the zygoma. Intra- and interoperator reliabilities were reported for each registration group. Multiple comparisons were conducted to find the best configuration with the minimum registration error.

Results: Ranking revealed one configuration in the tracing groups (Conf.3) and two configurations in the fiducial groups (Conf.3 and Conf.5) that had the best accuracy. When the inferior surfaces of the zygomatic buttress were excluded, fiducial registration produced better accuracy with both systems (P = .006 and < .0001). However, bilaterally tracing 1-cm areas at these surfaces resulted in similar registration accuracy as placing fiducial markers there (P = .430 and .237). NaviDent performed generally better (P = .049, .001 and .002), but the values had a wider margin of uncertainty. Changing the distribution of the four tracing areas or fiducial markers had a less pronounced effect with X-Guide than with the NaviDent system.

Conclusion: For surgery in the edentulous maxilla, four fiducial markers placed according to Conf.3 or Conf.5 resulted in the lowest registration error. Where implants are being placed bilaterally, an additional 2 sites may further reduce the error. For bilateral zygomatic implant placement, it is optimal to place two fiducial markers on the inferior surfaces of the maxillary tuberosities, two on their buccal surfaces, and another two on the anterior labial surface of the alveolar bone. Utilising the inferior zygomatic buttress is recommended over the inferior maxillary tuberosities in other types of maxillary surgeries.

Keywords: dynamic navigation, fiducial, implants, maxilla, registration, tracing.

2.5. Introduction

Although dynamic navigation facilitates the execution of pre-surgical plans, the process involves multiple steps that may lead to errors in the final outcome (Widmann et al., 2009). These sources of error can be operator- or non—operator-related (Widmann et al., 2009). Examples of non-operator sources of error are machine calibration, imaging method/settings and the software utilised for surface matching (Hamilton et al., 2022, Park et al., 2020, Chackartchi et al., 2020, Widmann et al., 2010). Operator-related errors mainly include inaccuracies in the registration process, instrument calibration, and execution (application) errors (Widmann et al., 2009). There are no published acceptable thresholds for each of these errors and the effect of variation in each step is often reported in terms of final outcome accuracy (i.e., implant deviations) (Ma et al., 2022, Wu et al., 2023b).

Registration is the process of matching two defined structures between the image space and the patient space guided by common landmarks (either surface areas or fiducial markers) (Maurer et al., 1997, Qin et al., 2019a). The registration process provides input information to the software from the patient and is essential to commence the dynamic navigation procedures (X-NavTechnologiesLLC, 2020, ClaroNavInc., 2021).

The existing guidelines for the registration process for implant-guided surgeries using dynamic navigation recommend tracing five or six teeth in partially dentate cases (Stefanelli et al., 2020a), and the localisation of more than four fiducial markers in edentulous cases (Widmann et al., 2009, Ledderose et al., 2012). However, a recent study reported satisfactory accuracy of flapless zygomatic implant placement relying on only four fiducial markers (Bhalerao et al., 2022, Bhalerao et al., 2023). The subjective accuracy check performed by the clinician is still a crucial requirement after the standard registration process (X-NavTechnologiesLLC, 2020, ClaroNavInc., 2021). There is a lack of standardisation in selecting ideal locations for fiducial markers or tracing areas to achieve the best registration and maximise the accuracy of the dynamic navigation-guided surgery (Wu et al., 2023b, X-NavTechnologiesLLC, 2020, ClaroNavInc., 2021, Wei et al., 2023, Zhou et al., 2021). West et al. provided clinically beneficial guidelines where the surgical site is close to the centroid of the fiducials (West et al., 2001).

In maxillary surgeries, the oral cavity is the best area for the registration process of patient-to-image spaces (Qin et al., 2019a). The solid, smooth surface of teeth is ideal for tracing, and the alveolar arches are optimal sites to place stable fiducial markers that do not interfere with the surgical procedure or patient comfort (Bhalerao et al., 2022, Mohagheghi et al., 2014). This requires further investigation to achieve the best possible configuration of marker locations to maximise the registration accuracy, particularly in the clinical situations where the surgical site extends beyond the oral cavity (Ledderose et al., 2012, Fan et al., 2019). Previous studies investigated several configurations of fiducial markers that include the palatal area (Qin et al., 2019a, Fan et al., 2019). Qin et al. tested the accuracy of a software-localisation algorithm for a prototype dynamic navigation system, including one standard configuration of fiducial markers without comparison groups (Qin et al., 2019a). Fan et al. investigated the target registration error for different configurations of fiducial markers. However, their study did not consider a configuration of four properly spaced fiducial markers (both of the four-marker fiducial distributions were triangular in shape) (Fan et al., 2019).

In the present study, to reduce patient discomfort in future clinical application, palatal fiducial markers were not used.

2.6. Aim of the study

The main study aim was the objective assessment of various configurations of tracing areas and fiducial markers to maximise the registration accuracy for dynamic navigation involving an edentulous maxilla. The null hypotheses were as follows: *(1)* There would be no difference in the registration accuracy between these configurations; *(2)* the tracing registration method would produce the same accuracy as the fiducial registration method; and *(3)* increasing the number of registration areas has no effect on further increasing the registration accuracy.

2.7. Materials and Methods

This *in vitro* investigation was carried out on a life-size skull model with a radiopaque surface (foam cortical shell skull, Sawbones). The teeth component was removed. Prior to imaging, eight circular areas (diameter: 1 cm) were marked on the skull to represent the tracing areas. These were distributed as four areas on each side: the inferior surface of the zygomatic buttress, the buccal (lateral) surface of the tuberosity area, the inferior surface of the tuberosity, and the anterior surface of the alveolus at the central incisor region (figure 2-1). A CBCT scan was then taken (OP 3D Vision, KaVo; 13 x 16—cm field of view, 120 KVp and 0.4 mm voxel size). Two dynamic navigations systems were used in the study; NaviDent (version 3.0.3, ClaroNav) and X-Guide (version 3.1.1.11, X-Nav Technologies). After collecting data for the tracing groups, a fiducial marker was placed in the centre of each tracing area, and another CBCT scan was captured. The fiducial markers were plate-fixation screws (1.2x6 mm, Stryker Leibinger). Data were then recorded for the fiducial groups using both systems. This resulted in four registration study groups; XG tracing, ND tracing, XG fiducial and ND fiducial.

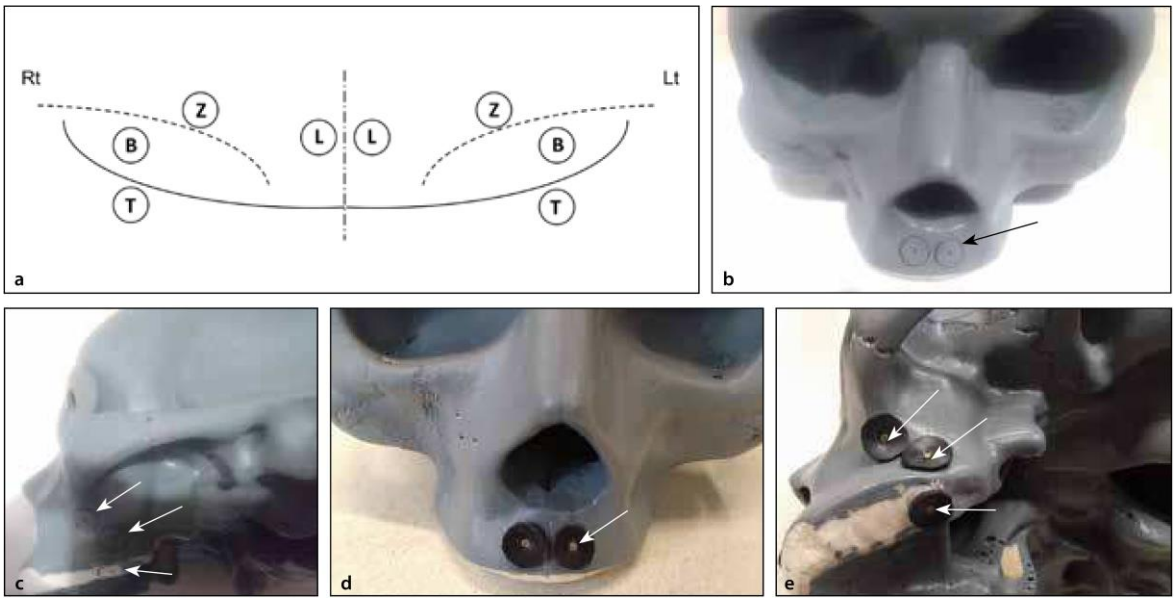

Figure 2-1. The eight areas that were tested as potential registration areas. (a) Diagrammatic representation of these areas. Z = zygomatic buttress; B = buccal area of the tuberosity behind the zygomatic buttress; T = inferior area of the tuberosity; L = labial area of the alveolus; Rt = right; Lt = left. (b to e) The locations of the tracing areas and the fiducial markers (arrows) on the skull.

2.7.1. Sample size calculation

Based on the previously reported mean ± SD target registration errors of 1.10 ± 0.16 mm and 1.53 ± 0.20 mm by Fan et. al. (Fan et al., 2019), a minimum sample size of five registration cycles per configuration was required to achieve statistical significance (assuming normal distribution, alpha was set at < .05 and sample power set at 0.8; G*Power software version 3.1.9.6). However, fiducial markers in both configurations by Fan et al. were distributed as triangles. Due to the differences between the present study and Fan et al.'s study, it was decided to set the sample size at six repetitions per operator instead of five. Three operators carried out the registration and accuracy-check processes. Thus, each of the eight configurations (left and right sides) was registered 18 times in every registration group. Before the experiment, each operator received comprehensive training sessions to ensure standardisation of the experimental protocol.

2.7.2. Selection of configurations

A total of eight configurations were tested per registration group (figure 2-2). Of these, six different configurations had their mirror images tested (left and right versions of the configurations; n = 12), with four different fiducial markers utilised per configuration, then switched for the contralateral configurations (figure 2-2a to 2-2f). Additionally, one positive-control configuration (all eight fiducial areas marked on the model; n =1) was considered (figure 2-2g). Then, one negative-control configuration (left and right versions; n = 2) were considered, each utilising only three fiducial markers on just one side (figure 2-2h). These controls were included to compare against the registration accuracy of the four-area configurations. The assumptions were that the negative controls are the least accurate, while the positive controls are the most accurate.

2.7.3. Selecting the accuracy-check areas

This was measured at the frontal process of the zygoma which is of high relevance in maxillary surgeries, particularly for zygomatic implant placement, orbital floor reconstruction, and zygomatic complex fractures (Bedrossian, 2021, He et al., 2020). Figure 2-3 demonstrates the six points used for accuracy measurements for every configuration (three planes per side).

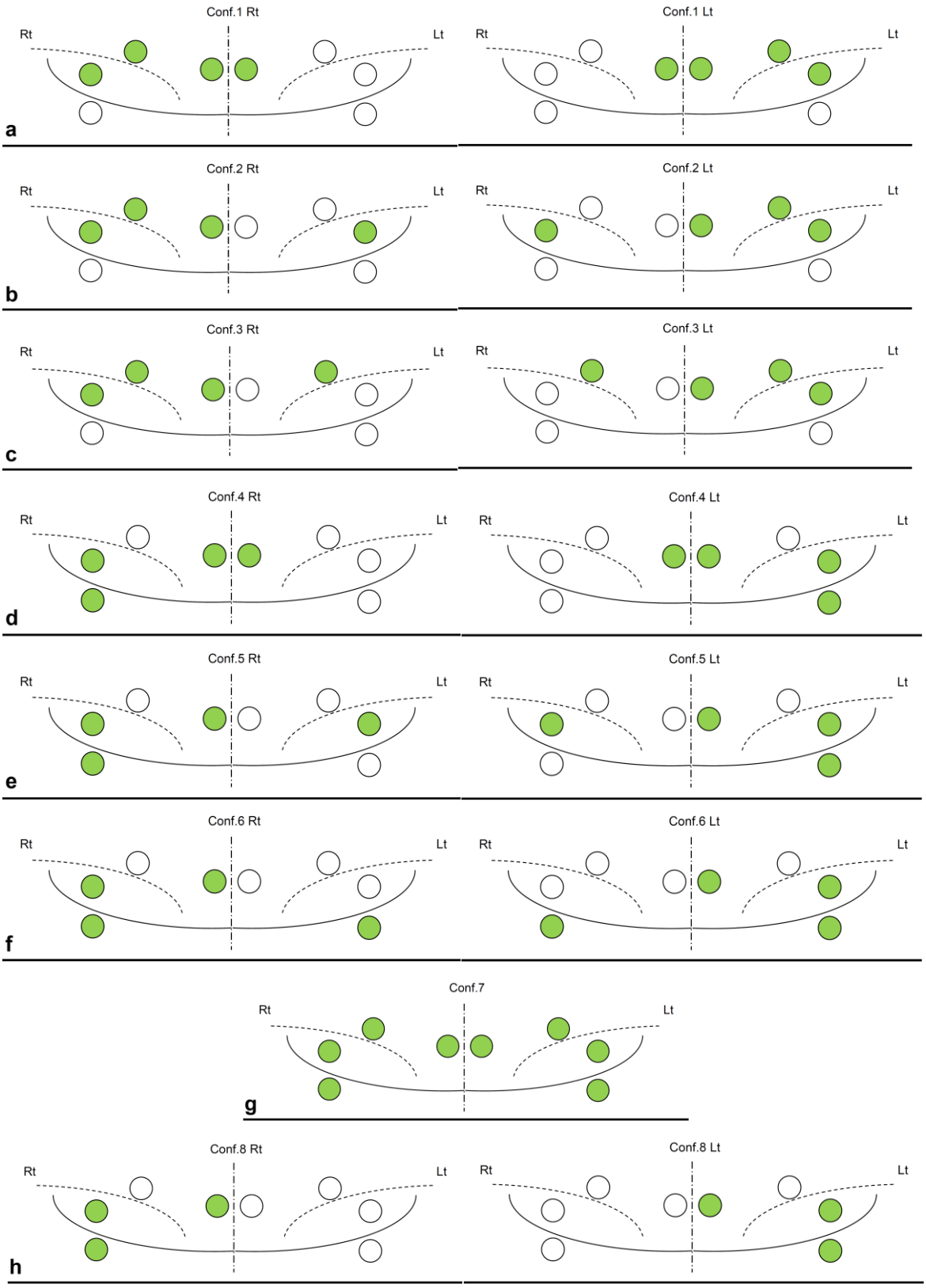

Figure 2-2. Diagramatic representations of the 15 configurations that were tested for registration error (green-filled circles represent the fiducial markers or tracing areas used): (a to f) Right and left sides of Conf.1 to Conf.6, respectivley; (g) Conf.7; and (h) right and left sides of Conf.8. Conf.7 represents the positive control (eight filled circles), and Conf.8 represent the negative controls (three filled circles). The first six configurations and the negative control had mirror images, as the distribution of the tracing areas/fiducials was asymmetric. In these configurations, the side on which three tracing areas/fiducials were included is used to reference the configuration side (i.e., if the left side had three markers, it was considered to be the left configuration).

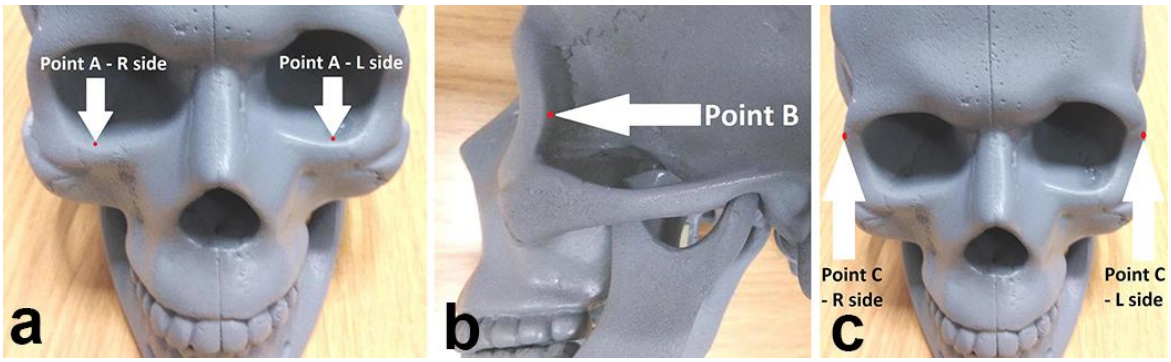

Figure 2-3. Target accuracy checking points on the skull model (arrows). All six points were marked with an indelible marker pen for precise identification. Vector deviation values can be calculated for each side, and grouping by points allows for specific deviation assessments by plane. (a) Point A is located on the most inferior surface of the orbital floor medial to the zygomatico-maxillary suture (to check for vertical deviation). (b) Point B is located on the most posterior surface of the frontal zygomatic process (to check for coronal deviation). (c) Point C is located on the most lateral surface of the frontal zygomatic process (to check for medio-lateral deviation).

2.7.4. Registration process

The registration process followed the manufacturer's instructions (e.g., point disparity < 1 mm in the XG tracing group). All settings were optimised prior to commencing data acquisition (W/L setting at 1100/200, surface threshold setting at -40 HU, identical panoramic curves for both dynamic navigation systems). All operators received training sessions before the experiment. The tracer tool is the instrument used to perform the registration process via tracing a surface or localising a fiducial marker in the patient space (X-NavTechnologiesLLC, 2020, ClaroNavInc., 2021). It is also the registration accuracy-check instrument used by the clinician before proceeding with other dynamic navigation steps (X-NavTechnologiesLLC, 2020, ClaroNavInc., 2021). All present accuracy-check processes in our study were carried out using the system-specific tracer tool, which was recalibrated before each round of registration processes. Each round comprises a set of 15 registration cycles performed by a single operator (see figure 2-2), and the values of each accuracy check were recorded using the same tracer tool calibration. Each operator completed six rounds of registration per group.

2.7.5. Assessment of the registration accuracy

After each round of registration, the accuracy data were assessed in the form of screen captures: six screen captures per registration, and each screen capture corresponded to one of the six accuracy check points shown in figure 2-3. One of the operators (M.A.) extracted distance measurements from all collected screenshots via ImageJ software (version 1.53o, National Institutes of Health). These were recorded in Excel spreadsheets (Microsoft). Distance scaling was standardised against the diameter of the on-screen tracer tip (2 mm for X-Guide, 1 mm for NaviDent). These values were obtained from the system manufacturers (X-NavTechnologiesLLC, 2020, ClaroNavInc., 2021).

In every screenshot, the distance between the centre of the tracer circle and the surface on which the target accuracy checking point is located was recorded (figure 2-4). The absolute distance values were recorded and the directions of each of these deviations were also kept for later graphical presentation (i.e., whether the tracer was detected as being inside or outside the surface).

For example, in figure 2-4a, the position of the tracer circle appears to be outside the surface being contacted in the real world of point B (bottom left against top left sections of the screen capture). The middle bottom section is reserved for point C deviation while the bottom right section is for point A deviations. In figure 2-4b, the position of the tracer circle appears to be inside the surface being contacted in the real world of point C (second row in the middle section of the screen capture). The first row is reserved for point A while the third row is for point B deviations.

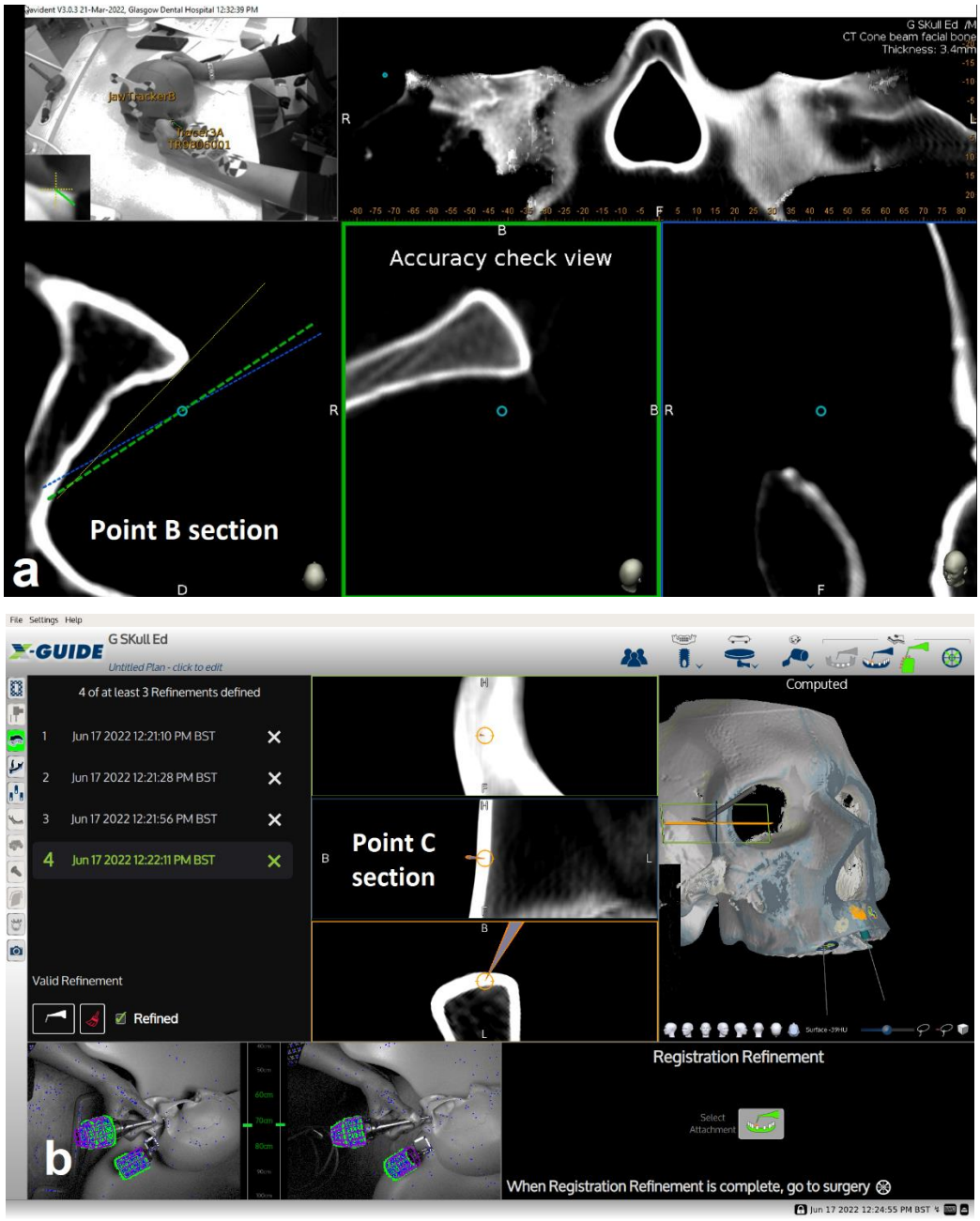

Figure 2-4. Data extraction process from the screen captures. (a) Example measurement of point B deviation in NaviDent. (b) Example of point C deviation measurement in X-Guide. The other sections of the screenshots were used for measuring the remaining point deviations. Each configuration accuracy is ultimately represented by six distance deviation values.

2.7.6. Processing the collected data

The measurement method's reproducibility (or level of uncertainty) was validated for each registration group. The screenshots for the six accuracy checking points were captured repeatedly (six times for each accuracy checking point; n = 36). This was done after a single registration process by the same operator to account for variation in target point localisation and any other contributing factors that could affect the measurement reproducibility for the same configuration (Min et al., 2017).

One negative (left side) and one positive control configuration were tested for reproducibility (two sets of 36 screenshots, totaling 72 screenshots to determine deviation measurement reproducibility) in each of the four registration groups. The reproducibility results were expressed in terms of maximum range in each group, which was selected from the 12 range values obtained in each group. This was recorded as the final outcome of measurement method reproducibility, and this was done for each of the four registration groups.

The original deviation data, which were derived directly from the screenshots (see figure 2-4) without any mathematical changes, were first illustrated to show their relative frequencies, direction, and magnitude in each plane.

The absolute deviation values were then grouped by plane (vertical, coronal, or medio-lateral). For each instance of a registration, the plane deviation was calculated as the average of the 2 points representing that plane:

- Vertical conf. deviation = $\frac{\text{Point A Rt deviation} + \text{Point A Lt deviation}}{2}$
- Coronal conf. deviation = $\frac{\text{Point B Rt deviation} + \text{Point B Lt deviation}}{2}$
- Medio-lateral conf. deviation = $\frac{\text{Point C Rt deviation} + \text{Point C Lt deviation}}{2}$

The accuracy data were then converted into vectors (root mean squares) to simplify its reporting (West et al., 2001):

- Right side 3D vector deviation = $\sqrt{(\text{Point A Rt deviation})^2 + (\text{Point B Rt deviation})^2 + (\text{Point C Rt deviation})^2}$
- Left side 3D vector deviation = $\sqrt{(\text{Point A Lt deviation})^2 + (\text{Point B Lt deviation})^2 + (\text{Point C Lt deviation})^2}$
- Configuration average vector deviation = $\frac{\text{Right side vector deviation} + \text{Left side vector deviation}}{2}$

The specific right- and left-side vector deviations were used to group the data by side (ipsilateral or contralateral), whereas the average vector deviations were utilised for further statistical analysis.

2.7.7. Statistical Analysis

SPSS statistics (version 26, IBM) was used for statistical analysis. For each data subset (e.g., plane, vector, or registration group), Shapiro-Wilk normality test was used to determine the normality of distribution. Intra- and interoperator reliability in each registration group were reported in terms of intra-class correlation coefficient (ICC). Intraoperator reliability statistics were based on six values (average vector deviations) per operator, grouped by configuration. Interoperator reliability statistics were based on the median values of each configuration. Kruskal-Wallis multiple comparisons test was performed between configurations in each study group (GraphPad, version 9, Prism) with statistical significance set at < .05. GraphPad was also used to create the graphical representations.

2.7.8. Supplementary accuracy data

Because all of the four-area configurations were asymmetric and the results displayed high interoperator agreement in the fiducial groups, an additional configuration was tested by one operator (Conf.9). It included six fiducial markers distributed in a symmetric manner (figure 2-5). The operator repeated the registration for this additional configuration 18 times.

The accuracy data obtained from this process was compared against Conf.7 (which had eight fiducial markers) and against the best four-area configurations resulting from the earlier phase of analysis.

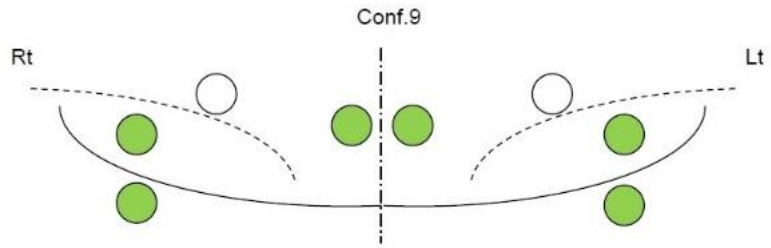

Figure 2-5. Diagramatic representation of the additional symmetric configuration (Conf.9) of six fiducial markers (green circles) that was tested for registration error.

2.8. Results

2.8.1. Results from the original raw data

The level of uncertainty (reproducibility) in the measurement method was 0.7 mm for the X-Guide system and 1.8 mm for the NaviDent system. Figure 2-6 shows the frequency distributions of the original deviations from all operators and tested configurations. Negative values denote that the tip of the tracer tool was inside the surface being contacted.

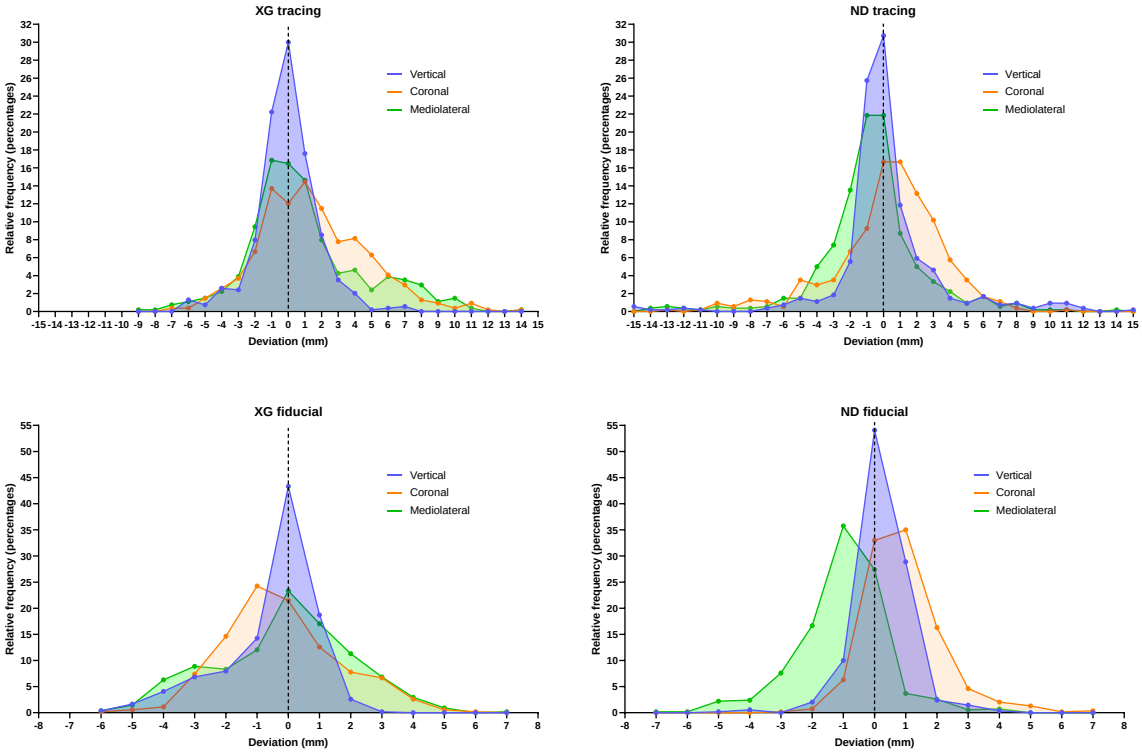

Figure 2-6. Area charts depicting the percentage of deviations categorised by plane, direction and magnitude. Positive values on the x-axes represent outside deviations while negative values represent inside deviations. The total number of measured values under each curve = 540. XG = X-Guide, ND = NaviDent.

2.8.2. Results after segregation of the original data into planes

The results of grouping by plane are shown in figure 2-7. In general, the smallest deviations were at the vertical plane, while most of the inaccuracies were at the coronal and the mediolateral planes. The maximum limits for deviations were considerably different between the tracing and the fiducial groups (10.85 mm and 5.40 mm, respectively). The detailed results for this subset of data are provided as appendix tables 2-1 through 2-6.

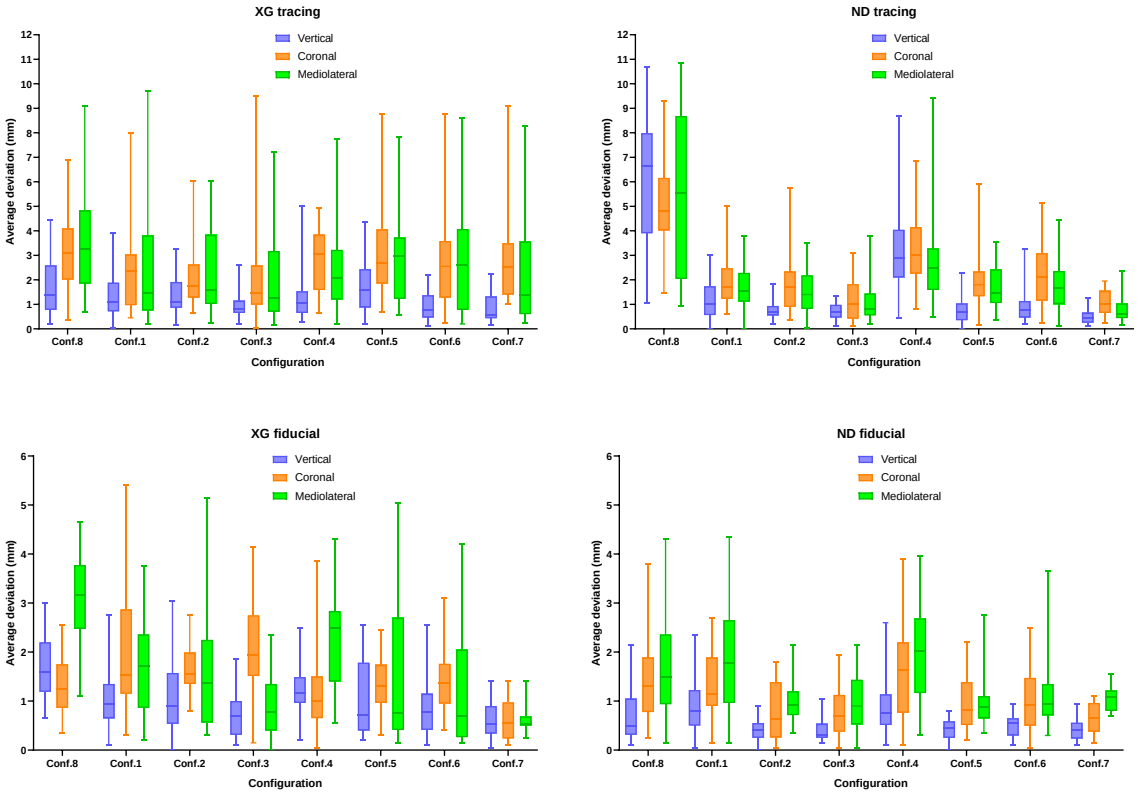

Figure 2-7. Box plots showing the target registration accuracy values by deviation plane. The error bars represent the total ranges. Number of values in each box = 36 (except Conf.7 boxes [n = 18]). XG = X-Guide; ND = NaviDent.

Configuration	Registration Group	n	Shapiro-Wilk p value	Mean ± SD (mm)	Median (IQR) (mm)	Min. (mm)	Max. (mm)
Conf.1	XG tracing	36	**.017**	1.33 ± 0.85	1.10 (1.18)	0.05	3.90
	ND tracing	36	.166	1.18 ± 0.75	1.03 (1.18)	0.00	3.00
	XG fiducial	36	**.009**	1.03 ± 0.54	0.95 (0.70)	0.10	2.75
	ND fiducial	36	.125	0.84 ± 0.50	0.80 (0.73)	0.05	2.35
Conf.2	XG tracing	36	**.022**	1.36 ± 0.80	1.10 (1.05)	0.15	3.25
	ND tracing	36	**.003**	0.76 ± 0.39	0.68 (0.39)	0.20	1.85
	XG fiducial	36	**.041**	1.08 ± 0.70	0.90 (1.04)	0.00	3.05
	ND fiducial	36	.724	0.42 ± 0.20	0.40 (0.30)	0.00	0.90
Conf.3	XG tracing	36	**.001**	0.93 ± 0.47	0.80 (0.50)	0.20	2.60
	ND tracing	36	.481	0.71 ± 0.35	0.70 (0.53)	0.10	1.35
	XG fiducial	36	**.045**	0.73 ± 0.42	0.70 (0.69)	0.10	1.85
	ND fiducial	36	**.002**	0.42 ± 0.24	0.30 (0.29)	0.15	1.05
Conf.4	XG tracing	36	**.000**	1.39 ± 1.16	1.05 (0.89)	0.30	5.00
	ND tracing	36	**.026**	3.21 ± 1.81	2.88 (1.95)	0.45	8.70
	XG fiducial	36	.281	1.21 ± 0.51	1.18 (0.53)	0.20	2.50
	ND fiducial	36	**.003**	0.90 ± 0.55	0.75 (0.63)	0.10	2.60
Conf.5	XG tracing	36	.145	1.17 ± 1.05	1.60 (1.56)	0.20	4.35
	ND tracing	36	**.003**	0.77 ± 0.54	0.70 (0.69)	0.00	2.30
	XG fiducial	36	**.000**	1.07 ± 0.78	0.73 (1.39)	0.20	2.55
	ND fiducial	36	.452	0.43 ± 0.22	0.45 (0.34)	0.00	0.80
Conf.6	XG tracing	36	.137	0.90 ± 0.50	0.78 (0.91)	0.10	2.20
	ND tracing	36	**.000**	0.91 ± 0.61	0.75 (0.68)	0.20	3.25
	XG fiducial	36	**.004**	0.90 ± 0.62	0.78 (0.74)	0.10	2.55
	ND fiducial	36	.181	0.51 ± 0.23	0.55 (0.35)	0.10	0.95
Conf.7 (positive control)	XG tracing	18	**.010**	0.81 ± 0.58	0.58 (0.90)	0.15	2.25
	ND tracing	18	**.035**	0.51 ± 0.35	0.45 (0.41)	0.15	1.25
	XG fiducial	18	.540	0.62 ± 0.37	0.53 (0.56)	0.05	1.40
	ND fiducial	18	.600	0.42 ± 0.22	0.40 (0.33)	0.10	0.95
Conf.8 (negative control)	XG tracing	36	**.007**	1.76 ± 1.24	1.38 (1.81)	0.20	4.45
	ND tracing	36	**.032**	5.94 ± 2.67	6.65 (4.09)	1.05	10.70
	XG fiducial	36	.388	1.66 ± 0.59	1.60 (1.01)	0.65	3.00
	ND fiducial	36	**.000**	0.78 ± 0.62	0.50 (0.74)	0.10	2.15

Appendix table 2-1. Descriptive statistics for average vertical deviations. Shapiro-Wilk values < .05 indicate the lack of distribution normanlity.

Configuration	Comparison Group	XG tracing	ND tracing	XG fiducial	ND fiducial
Conf.1	Against Conf.8	> 0.999	**< 0.0001**	**0.002**	0.733
	Against Conf.7	**0.094**	0.011	**0.077**	0.005
Conf.2	Against Conf.8	> 0.999	**< 0.0001**	**0.001**	0.083
	Against Conf.7	0.043	**0.751**	**0.097**	**> 0.999**
Conf.3	Against Conf.8	**0.017**	**< 0.0001**	**< 0.0001**	**0.039**
	Against Conf.7	**> 0.999**	**> 0.999**	**> 0.999**	**> 0.999**
Conf.4	Against Conf.8	0.873	0.740	0.121	0.399
	Against Conf.7	**0.211**	< 0.0001	0.002	0.002
Conf.5	Against Conf.8	> 0.999	**< 0.0001**	**0.0002**	0.191
	Against Conf.7	0.002	**> 0.999**	**0.216**	**> 0.999**
Conf.6	Against Conf.8	**0.008**	**< 0.0001**	**< 0.0001**	> 0.999
	Against Conf.7	**> 0.999**	**0.197**	**0.915**	**> 0.999**

Appendix table 2-2. Results of multiple comparisons for average vertical deviations using independent-samples Kruskal-Wallis tests with Dunn's correction in terms of p values.

Configuration	Registration Group	n	Shapiro-Wilk p value	Mean ± SD (mm)	Median (IQR) (mm)	Min. (mm)	Max. (mm)
Conf.1	XG tracing	36	**.000**	2.30 ± 1.62	2.35 (2.08)	0.45	8.00
	ND tracing	36	**.004**	1.96 ± 1.03	1.73 (1.25)	0.60	5.00
	XG fiducial	36	**.002**	1.92 ± 1.15	1.53 (1.73)	0.30	5.40
	ND fiducial	36	.300	1.30 ± 0.68	1.15 (0.99)	0.15	2.70
Conf.2	XG tracing	36	**.000**	2.16 ± 1.33	1.75 (1.35)	0.65	6.05
	ND tracing	36	**.003**	1.81 ± 1.15	1.73 (1.44)	0.35	5.75
	XG fiducial	36	.710	1.63 ± 0.49	1.55 (0.64)	0.80	2.75
	ND fiducial	36	**.003**	0.80 ± 0.55	0.63 (1.13)	0.05	1.80
Conf.3	XG tracing	36	**.000**	2.17 ± 1.94	1.48 (1.60)	0.05	9.50
	ND tracing	36	**.023**	1.19 ± 0.84	1.00 (1.41)	0.10	3.10
	XG fiducial	36	.962	2.06 ± 0.85	1.95 (1.24)	0.15	4.15
	ND fiducial	36	.343	0.78 ± 0.47	0.70 (0.75)	0.05	1.95
Conf.4	XG tracing	36	.176	2.77 ± 1.19	3.05 (2.25)	0.65	4.95
	ND tracing	36	.497	3.18 ± 1.49	3.03 (1.90)	0.80	6.85
	XG fiducial	36	**.006**	1.20 ± 0.76	1.00 (0.85)	0.05	3.85
	ND fiducial	36	.369	1.65 ± 0.98	1.63 (1.44)	0.10	3.90
Conf.5	XG tracing	36	**.002**	3.18 ± 1.82	2.70 (2.21)	0.70	8.75
	ND tracing	36	**.000**	1.99 ± 1.09	1.80 (1.01)	0.15	5.90
	XG fiducial	36	.580	1.34 ± 0.55	1.30 (0.78)	0.30	2.45
	ND fiducial	36	.065	0.91 ± 0.51	0.83 (0.88)	0.20	2.20
Conf.6	XG tracing	36	**.027**	2.82 ± 1.93	2.55 (2.31)	0.25	8.75
	ND tracing	36	.372	2.22 ± 1.21	2.10 (1.94)	0.25	5.15
	XG fiducial	36	.259	1.40 ± 0.60	1.38 (0.81)	0.40	3.10
	ND fiducial	36	.104	1.03 ± 0.67	0.93 (0.98)	0.05	2.50
Conf.7 (positive control)	XG tracing	18	**.001**	2.81 ± 1.91	2.53 (2.10)	1.00	9.10
	ND tracing	18	.373	1.04 ± 0.54	1.00 (0.90)	0.25	1.95
	XG fiducial	18	.082	0.64 ± 0.44	0.55 (0.74)	0.10	1.40
	ND fiducial	18	.132	0.63 ± 0.33	0.65 (0.59)	0.15	1.10
Conf.8 (negative control)	XG tracing	36	.729	3.14 ± 1.60	3.10 (2.09)	0.35	6.90
	ND tracing	36	.316	5.08 ± 2.00	4.80 (2.14)	1.45	9.30
	XG fiducial	36	.539	1.28 ± 0.58	1.25 (0.89)	0.35	2.55
	ND fiducial	36	**.029**	1.36 ± 0.75	1.30 (1.11)	0.25	3.80

Appendix table 2-3. Descriptive statistics for average coronal deviations. Shapiro-Wilk values < .05 indicate the lack of distribution normanlity.

Configuration	Comparison Group	XG tracing	ND tracing	XG fiducial	ND fiducial
Conf.1	Against Conf.8	0.072	**< 0.0001**	0.122	> 0.999
	Against Conf.7	**> 0.999**	0.036	< 0.0001	0.004
Conf.2	Against Conf.8	**0.037**	**< 0.0001**	0.141	**0.006**
	Against Conf.7	**> 0.999**	**0.168**	< 0.0001	**> 0.999**
Conf.3	Against Conf.8	**0.009**	**< 0.0001**	**0.0005**	**0.005**
	Against Conf.7	**0.716**	**> 0.999**	< 0.0001	**> 0.999**
Conf.4	Against Conf.8	> 0.999	0.061	> 0.999	> 0.999
	Against Conf.7	**> 0.999**	< 0.0001	**0.065**	0.0001
Conf.5	Against Conf.8	> 0.999	**< 0.0001**	> 0.999	0.083
	Against Conf.7	**> 0.999**	0.026	0.003	**0.862**
Conf.6	Against Conf.8	> 0.999	**< 0.0001**	> 0.999	0.364
	Against Conf.7	**> 0.999**	0.005	0.001	**0.310**

Appendix table 2-4. Results of multiple comparisons for average coronal deviations using independent-samples Kruskal-Wallis tests with Dunn's correction in terms of p values.

Configuration	Registration Group	n	Shapiro-Wilk p value	Mean ± SD (mm)	Median (IQR) (mm)	Min. (mm)	Max. (mm)
Conf.1	XG tracing	36	**.000**	2.59 ± 2.51	1.45 (3.06)	0.20	9.70
	ND tracing	36	.303	1.73 ± 0.89	1.53 (1.17)	0.00	3.80
	XG fiducial	36	.213	1.72 ± 0.99	1.73 (1.50)	0.20	3.75
	ND fiducial	36	.203	1.86 ± 1.05	1.78 (1.69)	0.15	4.35
Conf.2	XG tracing	36	**.001**	2.28 ± 1.65	1.58 (2.83)	0.25	6.05
	ND tracing	36	.512	1.53 ± 0.89	1.40 (1.38)	0.05	3.50
	XG fiducial	36	**.002**	1.54 ± 1.06	1.38 (1.69)	0.30	5.15
	ND fiducial	36	.063	0.98 ± 0.41	0.93 (0.49)	0.35	2.15
Conf.3	XG tracing	36	**.000**	1.90 ± 1.76	1.25 (2.47)	0.15	7.20
	ND tracing	36	**.000**	1.06 ± 0.75	0.83 (0.90)	0.20	3.80
	XG fiducial	36	**.008**	0.92 ± 0.70	0.78 (0.95)	0.00	2.35
	ND fiducial	36	.289	0.96 ± 0.50	0.90 (0.91)	0.05	2.15
Conf.4	XG tracing	36	**.003**	2.52 ± 1.73	2.08 (2.03)	0.20	7.75
	ND tracing	36	**.000**	2.72 ± 1.68	2.50 (1.69)	0.50	9.40
	XG fiducial	36	.144	2.27 ± 1.02	2.50 (1.44)	0.55	4.30
	ND fiducial	36	.142	2.00 ± 0.99	0.99 (1.53)	0.30	3.95
Conf.5	XG tracing	36	**.025**	2.84 ± 1.72	2.98 (2.50)	0.55	7.85
	ND tracing	36	.162	1.71 ± 0.88	1.48 (1.38)	0.35	3.55
	XG fiducial	36	**.000**	1.56 ± 1.48	0.75 (2.29)	0.15	5.05
	ND fiducial	36	**.000**	0.96 ± 0.45	0.88 (0.45)	0.35	2.75
Conf.6	XG tracing	36	**.005**	2.66 ± 1.96	2.63 (3.30)	0.20	8.60
	ND tracing	36	**.027**	1.73 ± 1.07	1.65 (1.35)	0.10	4.45
	XG fiducial	36	**.000**	1.23 ± 1.22	0.70 (1.79)	0.15	4.20
	ND fiducial	36	**.000**	1.11 ± 0.66	0.95 (0.64)	0.30	3.65
Conf.7 (positive control)	XG tracing	18	**.002**	2.08 ± 2.07	1.38 (2.96)	0.25	8.30
	ND tracing	18	**.001**	0.87 ± 0.66	0.63 (0.60)	0.15	2.35
	XG fiducial	18	**.002**	0.63 ± 0.28	0.53 (0.19)	0.25	1.40
	ND fiducial	18	.321	1.06 ± 0.26	1.08 (0.41)	0.70	1.55
Conf.8 (negative control)	XG tracing	36	.056	3.35 ± 1.89	3.28 (2.99)	0.70	9.10
	ND tracing	36	**.002**	5.53 ± 3.52	5.53 (6.65)	0.95	10.85
	XG fiducial	36	.658	3.11 ± 0.83	3.18 (1.30)	1.10	4.65
	ND fiducial	36	**.038**	1.73 ± 1.04	1.50 (1.42)	0.15	4.30

Appendix table 2-5. Descriptive statistics for average mediolateral deviations. Shapiro-Wilk values < .05 indicate the lack of distribution normanlity.

Configuration	Comparison Group	XG tracing	ND tracing	XG fiducial	ND fiducial
Conf.1	Against Conf.8	0.064	**< 0.0001**	**0.0002**	> 0.999
	Against Conf.7	**> 0.999**	0.009	0.009	**0.122**
Conf.2	Against Conf.8	0.132	**< 0.0001**	**< 0.0001**	**0.004**
	Against Conf.7	**> 0.999**	**0.073**	**0.067**	**> 0.999**
Conf.3	Against Conf.8	**0.002**	**< 0.0001**	**< 0.0001**	**0.002**
	Against Conf.7	**> 0.999**	**> 0.999**	**> 0.999**	**> 0.999**
Conf.4	Against Conf.8	0.509	0.259	0.134	> 0.999
	Against Conf.7	**> 0.999**	< 0.0001	< 0.0001	0.016
Conf.5	Against Conf.8	> 0.999	**< 0.0001**	**< 0.0001**	**0.001**
	Against Conf.7	**0.405**	0.014	**0.209**	**> 0.999**
Conf.6	Against Conf.8	0.447	**< 0.0001**	**< 0.0001**	**0.033**
	Against Conf.7	**> 0.999**	0.023	**> 0.999**	**> 0.999**

Appendix table 2-6. Results of multiple comparisons for average mediolateral deviations using independent-samples Kruskal-Wallis tests with Dunn's correction in terms of p values.

2.8.3. Results after 3D vector calculations

Descriptive statistics and normality testing

The average vector data from the right and left sides were merged for each configuration (n = 36). Shapiro-Wilk normality testing revealed that the data departed significantly from normality. Table 2-1 and figure 2-8 summarise these results.

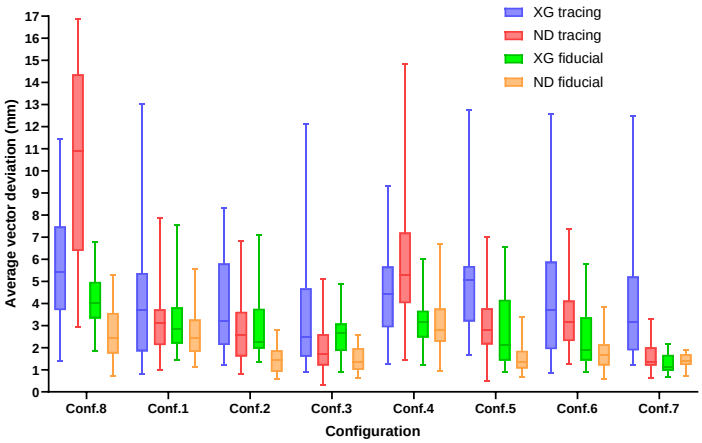

Figure 2-8. A box plot of overall target registration error (average vector) categorised by the registration method and navigation system. The error bars represent the total ranges. Number of values in each box = 36 (except Conf.7 boxes [n = 18]). XG = X-Guide; ND = NaviDent.

Configuration	Registration Group	n	Shapiro-Wilk p value	Mean ± SD (mm)	Median (IQR) (mm)	Min. (mm)	Max. (mm)
Conf.1	XG tracing	36	**.002**	4.12 ± 2.79	3.71 (3.54)	0.81	13.01
	ND tracing	36	**.004**	3.21 ± 1.50	3.10 (1.62)	0.99	7.89
	XG fiducial	36	**.004**	3.15 ± 1.37	2.83 (1.64)	1.46	7.57
	ND fiducial	36	**.023**	2.68 ± 1.06	2.42 (1.47)	1.14	5.54
Conf.2	XG tracing	36	**.001**	3.87 ± 2.12	3.21 (3.69)	1.23	8.33
	ND tracing	36	**.017**	2.76 ± 1.39	2.59 (2.02)	0.82	6.81
	XG fiducial	36	**.000**	2.85 ± 1.23	2.25 (1.80)	1.35	7.11
	ND fiducial	36	.238	1.44 ± 0.57	1.46 (0.97)	0.58	2.81
Conf.3	XG tracing	36	**.000**	3.32 ± 2.49	2.48 (3.09)	0.90	12.10
	ND tracing	36	.052	1.94 ± 1.03	1.72 (1.42)	0.33	5.11
	XG fiducial	36	.473	2.57 ± 0.92	2.67 (1.24)	0.91	4.87
	ND fiducial	36	**.028**	1.46 ± 0.54	1.35 (0.99)	0.61	2.57
Conf.4	XG tracing	36	.165	4.44 ± 1.95	4.41 (2.76)	1.27	9.33
	ND tracing	36	**.034**	5.69 ± 2.67	5.28 (3.19)	1.45	14.82
	XG fiducial	36	.158	3.21 ± 1.12	3.17 (1.22)	1.20	6.00
	ND fiducial	36	**.012**	3.07 ± 1.36	2.82 (1.50)	0.94	6.70
Conf.5	XG tracing	36	**.002**	4.98 ± 2.28	5.06 (2.50)	1.68	12.74
	ND tracing	36	.078	3.08 ± 1.30	2.82 (1.64)	0.50	6.99
	XG fiducial	36	**.001**	2.77 ± 1.62	2.10 (2.75)	0.88	6.54
	ND fiducial	36	**.006**	1.51 ± 0.62	1.37 (0.79)	0.68	3.38
Conf.6	XG tracing	36	**.007**	4.19 ± 2.63	3.69 (3.95)	0.87	12.59
	ND tracing	36	**.026**	3.28 ± 1.46	3.17 (1.83)	1.28	7.36
	XG fiducial	36	**.000**	2.41 ± 1.32	1.91 (1.95)	0.88	5.80
	ND fiducial	36	**.060**	1.79 ± 0.79	1.69 (0.96)	0.60	3.82
Conf.7 (positive control)	XG tracing	18	**.002**	3.85 ± 2.70	3.16 (3.35)	1.20	12.47
	ND tracing	18	**.019**	1.64 ± 0.74	1.36 (0.83)	0.61	3.29
	XG fiducial	18	**.000**	1.42 ± 0.87	1.12 (0.79)	0.65	4.43
	ND fiducial	18	.496	1.45 ± 0.31	1.42 (0.50)	0.73	1.90
Conf.8 (negative control)	XG tracing	36	.543	5.48 ± 2.30	5.42 (3.79)	1.39	11.45
	ND tracing	36	.061	10.50 ± 4.27	10.90 (7.99)	2.91	16.88
	XG fiducial	36	.969	4.14 ± 1.14	4.03 (1.65)	1.85	6.77
	ND fiducial	36	.321	2.64 ± 1.22	2.44 (1.83)	0.73	5.27

Table 2-1. Descriptive statistics for the accuracy results of the tested configurations. Shapiro-Wilk p values < .05 indicate the lack of distribution normality. IQR = interquartile range; XG = X-Guide; ND = NaviDent.

Reliability of the registration methods

The results of intra- and interoperator reliability are presented as ICCs (table 2-2). Two operators showed poor intraoperator reliability in the X-Guide tracing group (ICC score < 0.5). All other intra- and interoperator reliability ranged from moderate (0.5 – 0.75) to good (0.75 – 0.9) and even excellent correlations (> 0.9).

Registration Group	ICC within each operator (6 readings/operator)			ICC between all operators
	Operator.1 (M.A.)	Operator.2 (O.A.)	Operator.3 (N.A.)	
XG tracing	0.539	0.043	0.023	0.557
ND tracing	0.900	0.906	0.946	0.964
XG fiducial	0.808	0.763	0.781	0.958
ND fiducial	0.883	0.924	0.862	0.860

Table 2-2. Average ICCs in each registration group. ICC = intra-class correlation coefficient; XG = X-Guide; ND = NaviDent.

Determining the best configuration

There was a common trend when ranking these configurations. Aside from the positive control (Conf.7), Conf.5 and Conf.6 were generally the best, followed by Conf.2 and Conf.3, then Conf.1, then Conf.4 (see figure 2-8, table 2-1, and appendix table 2-16 on page 77). The exception was the XG tracing group, in which the positive control configuration (Conf.7) was associated with higher deviation values than expected (median: 3.16 mm; range: 1.20 to 12.47 mm). The results of multiple comparisons were tabulated (table 2-3), and these data were combined with the ranking of means/medians shown in table 2-1. Regarding the median (range), Conf.3 had the best accuracy in the tracing groups: XG tracing = 2.48 mm (0.90 to 12.10 mm); ND tracing = 1.72 mm (0.33 to 5.11 mm). Meanwhile, Conf.3, Conf.5 and Conf.6 had the best accuracy in the fiducial groups: ND fiducial Conf.3 = 1.35 mm (0.61 to 2.57 mm); ND fiducial Conf.5 = 1.37 mm (0.68 to 3.38 mm); XG fiducial Conf.6 = 1.91 mm (0.88 to 5.80 mm). Further multiple comparisons were carried out among these best configurations to comment on the effect of the registration method (tracing vs fiducial) and the navigation device (X-Guide vs NaviDent). The results are reported in tables 2-4 and 2-5, respectively.

The fiducial registration method yielded significantly better accuracy values than the tracing method, but only in the configurations where the zygomatic buttress areas were excluded (Conf.6 in X-Guide and Conf.5 in NaviDent).

When comparing Conf.3, which includes the bilateral zygomatic buttress areas, the accuracy of tracing method was not significantly different from fiducial method. Table 2-5 shows that, in their tested versions, the NaviDent system generally produced better accuracy than X-Guide except when tracing non-zygomatic buttress configurations.

Configuration	Comparison Group	XG tracing	ND tracing	XG fiducial	ND fiducial
Conf.1	Against Conf.8	**.028**	**< .0001**	**.020**	> .999
	Against Conf.7	**> .999**	.003	< .0001	.0002
Conf.2	Against Conf.8	**.028**	**< .0001**	**.001**	**< .0001**
	Against Conf.7	**> .999**	**.068**	< .0001	**> .999**
Conf.3	Against Conf.8	**< .0001**	**< .0001**	**< .0001**	**< .0001**
	Against Conf.7	**> .999**	**> .999**	.0003	**> .999**
Conf.4	Against Conf.8	.561	**.110**	**.075**	> .999
	Against Conf.7	**> .999**	< .0001	< .0001	< .0001
Conf.5	Against Conf.8	> .999	**< .0001**	**< .0001**	**< .0001**
	Against Conf.7	**.320**	.005	.0003	**> .999**
Conf.6	Against Conf.8	.064	**< .0001**	**< 0.0001**	**.022**
	Against Conf.7	**> .999**	.002	.009	**> .999**

Table 2-3. Multiple comparison results using independent-samples Kruskal-Wallis tests with Dunn's correction in terms of p values. P < .05 indicates statistical significance. Analysis conducted in GraphPad. XG = X-Guide; ND = NaviDent.

Zygomatic buttress available	P value	Zygomatic buttress in the way of surgery	P value
XG tracing Conf.3 against XG fiducial Conf.6	.430 Non-significant	XG tracing Conf.6 against XG fiducial Conf.6	**.006** XG fiducial is better
ND tracing Conf.3 against ND fiducial Conf.3	.237 Non-significant	ND tracing Conf.5 against ND fiducial Conf.5	**< .0001** ND fiducial is better

Table 2-4. Multiple comparison results for the effect of registration method using independent-samples Kruskal-Wallis tests with Dunn's correction in terms of p values. The significance level was set at < .05. Analysis conducted in GraphPad. XG = X-Guide; ND = NaviDent.

Zygomatic buttress available	P value	Zygomatic buttress in the way of surgery	P value
XG tracing Conf.3 against ND tracing Conf.3	**.049** ND tracing is better	XG tracing Conf.6 against ND tracing Conf.5	> .9999 Non-significant
XG fiducial Conf.6 against ND fiducial Conf.3	**.001** ND fiducial is better	XG fiducial Conf.6 against ND fiducial Conf.5	**.002** ND fiducial is better

Table 2-5. Multiple comparison results for the effect of dynamic navigation device using independent-samples Kruskal-Wallis tests with Dunn's correction in terms of p values. The significance level was set at < .05. Analysis conducted in GraphPad. XG = X-Guide; ND = NaviDent.

Determining whether the best configuration is significantly better

Among the four-area configurations in each registration group, the question of whether the distribution of these four areas changes the accuracy with a statistical significance was answered through Kruskal-Wallis multiple comparison tests of the best against the worst configuration in each registration group. The results are shown in tables 2-6 and 2-7. The p values in these tables suggest that the specific distribution (configuration) of four areas had no statistically significant effect on the registration accuracy in X-Guide. However, the contrary was observed with NaviDent.

Zygomatic buttress available	P value	Zygomatic buttress in the way of surgery	P value
XG tracing best (Conf.3) against XG tracing worst (Conf.5)	.001 Conf.3 is better	XG tracing best (Conf.6) against XG tracing worst (Conf.5)	**.526** Non-significant
XG fiducial best (Conf.6) against XG fiducial worst (Conf.4)	**.092** Non-significant	XG fiducial best (Conf.6) against XG fiducial worst (Conf.4)	**.092** Non-significant

Table 2-6. Multiple comparison results for the effect of configuration in the X-Guide system using independent-samples Kruskal-Wallis tests with Dunn's correction in terms of p values. The significance level was set at < .05. Analysis conducted in GraphPad. XG = X-Guide.

Zygomatic buttress available	P value	Zygomatic buttress in the way of surgery	P value
ND tracing best (Conf.3) against ND tracing worst (Conf.4)	< .0001 Conf.3 is better	ND tracing best (Conf.5) against ND tracing worst (Conf.4)	.030 Conf.5 is better
ND fiducial best (Conf.3) against ND fiducial worst (Conf.4)	< .0001 Conf.3 is better	ND fiducial best (Conf.5) against ND fiducial worst (Conf.4)	< .0001 Conf.5 is better

Table 2-7. Multiple comparison results for the effect of configuration in the NaviDent system using independent-samples Kruskal-Wallis tests with Dunn's correction in terms of p values. The significance level was set at < .05. Analysis conducted in GraphPad. ND = NaviDent.

Determining the effect of the asymmetric distribution of the registration areas/fiducials

Figure 2-9 shows the results when separating the vector data by side (into ipsilateral vectors and contralateral vectors). Ipsilateral deviations denote the right vectors for right-side configurations and left vectors for left-side configurations (see figure 2-2 on page 39).

The general pattern shows less deviation for ipsilateral vectors. However, in both NaviDent groups (tracing and fiducials), the deviations on the left side were lower than the right side in the symmetric configurations (Conf.7 and Conf.9).

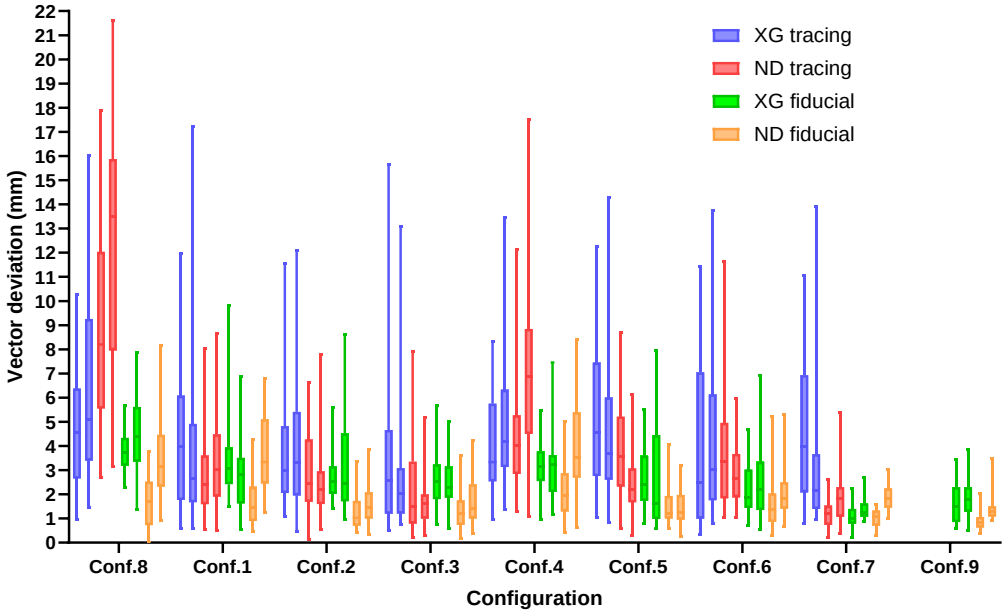

Figure 2-9. A box plot demonstrating the effect of tracing area/fiducial distribution among sides in the same configuration on the target registration accuracy. In every configuration, each registration group was presented as two adjacent boxes with the same colour: the left one shows ipsilateral vectors and the right one shows contralateral vectors. Conf. 7 (the positive control) and Conf.9 (six fiducial markers) are both symmetric, and thus the left and right boxes represent the left and right vectors, respectively. Number of values in each box = 36 (except Conf.7 and Conf.9 boxes [n = 18]). XG = X-Guide; ND = NaviDent.

Determining the effect of the number of fiducials in the symmetric configurations

There was no statistically significant difference in the average vector deviations when changing the number of fiducials from six to eight in both systems (figure 2-10). However, with six fiducial markers (Conf.9), significantly smaller deviations were produced in the NaviDent system when compared to the best four-area configuration (not including the zygomatic buttress area) tested in that system (Conf.5) (table 2-8). See appendix table 2-8 on page 75 for descriptive statistics of Conf.9.

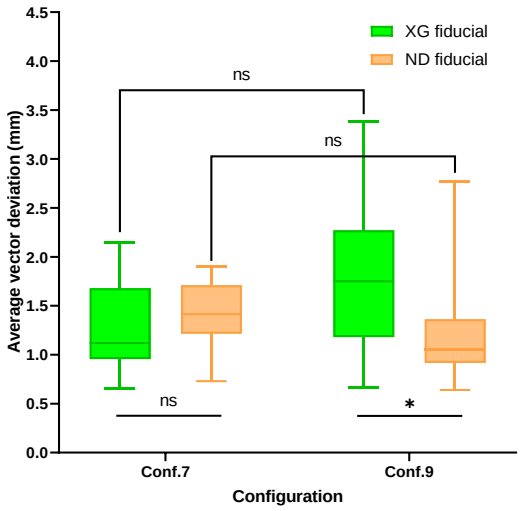

Figure 2-10. A box plot of overall target registration error (average vector) categorised by the registration modality and navigation system for symmetric configurations: Conf. 7 (the positive control with eight fiducial markers) and Conf.9 (six fiducial markers). The error bars represent the total ranges. The number of values in each box = 18. Independent-samples Kruskal-Wallis tests with Dunn's correction p values: * < .05, ns > .05. The analysis was conducted in GraphPad. XG = X-Guide; ND = NaviDent; ns = not significant.

Zygomatic buttress available	P value	Zygomatic buttress in the way of surgery	P value
ND fiducial Conf.3 against ND fiducial Conf.9	.067 Non-significant	ND fiducial Conf.5 against ND fiducial Conf.9	**.025** Conf.9 is better
XG fiducial Conf.6 against XG fiducial Conf.9	.091 Non-significant	XG fiducial Conf.6 against XG fiducial Conf.9	.091 Non-significant

Table 2-8. Results of Mann-Whitney tests for the effect of number of fiducial markers in terms of p values. The significance level was set at < .05. Conf. 9 has six fiducial markers while other configurations only have four. Analysis conducted in GraphPad. XG = X-Guide; ND = NaviDent.

2.9. Discussion

The crucial importance of minimising registration errors has been well documented (Widmann et al., 2009, Rußig and Schulze, 2013). Factors affecting registration accuracy in dynamically guided dental implant surgery include the distance between the surgical site and the fiducial marker in addition to voxel size (Rußig and Schulze, 2013).

Widmann et al. advised using more than four registration markers for fiducial point-based registration (Widmann et al., 2009, Widmann et al., 2010).

However, the present findings showed that four fiducial markers would be sufficient, at least for ipsilateral side surgeries (table 2-3 and figure 2-9). Regarding the measurement of registration errors, the surface of the CBCT scan itself was used to reduce confounding sources of errors arising from matching a second surface to the CBCT surface in the form of shell-to-shell deviations (Park et al., 2020).

Measuring registration errors based on screenshot images has already been reported (Ledderose et al., 2012). When selecting the four-area configurations to be tested, one of these areas was always crossing the midline, as this has been shown to greatly influence the resulting accuracy (X-NavTechnologiesLLC, 2020, ClaroNavInc., 2021). The same effect was observed in the present results when comparing the negative control with any other configurations that have one tracing area or fiducial marker crossing the midline. This can also be seen when comparing Conf.1 and Conf.4, in which the fourth fiducial marker is located close to the midline, to any other four-area configuration in which the fourth fiducial is further away (see table 2-1 and figures 2-2 and 2-8). This supports the rejection of the first null hypothesis (i.e., registration accuracy was affected by the specific configuration).

Although the reproducibility of the accuracy measurement method revealed an additional margin/source of error, no further effort was put to modify it. This method of judging the outcome of a particular registration process was similar to the clinical scenario wherein the clinicians must decide whether to repeat the registration process based on the subjective observation of what is on-screen (Scheyer et al., 2020). The present study merely supplemented this with the objective measurements from the same screen captures.

The significantly higher measurement error in NaviDent (1.8 mm) could be caused by the adaptive contrast algorithm implemented (in which the surface definition is continuously changing according to the bone density in that area), leading to inconsistent demarcation of the surface on repeated approaches. Other dynamic navigation systems (especially in their prototype versions) may have provided more details about the target registration error (e.g., InVivo Dental (Kim et al., 2015), IGOIS (Xiaojun et al., 2009) and BrainLAB (Lan et al., 2022)).

The NaviDent and X-Guide systems, in their current versions, completely rely on subjective assessment via the typical circle representation on an “accuracy check” screen (X-NavTechnologiesLLC, 2020, ClaroNavInc., 2021).

The distribution of deviations by direction (figures 2-6 and 2-7 on pages 46 and 47) supports the improved margin of safety in the fiducial-based registration over tracing-based registration. The percentages of deviation values > 2 mm in the XG fiducial group were relatively higher compared to ND fiducial group, probably due to the shape of the tracer tip. The sharp end of the X-Guide tracer may contribute to the higher human localisation errors than the ball end of the NaviDent tracer (which locks itself over the centre of the screw head).

Fiducial registration procedures produced less deviations than tracing flat surface areas (table 2-1 and figure 2-8). This supports the rejection of the second null hypothesis (i.e., tracing and fiducial registration methods do not produce similar registration accuracies). These results are consistent with the previous studies (Ledderose et al., 2012). In dentate cases, tracing five or six teeth proved more reliable than tracing three or four teeth (Stefanelli et al., 2020a).

Lan et al. investigated the use of non-invasive adhesive markers attached to the palatal area for an edentulous maxillary model and reported that at least six markers were required for acceptable accuracy. Their target positions for accuracy check were still close to the centroid of the fiducial markers (Lan et al., 2022). That is not the case with the target position located away from the fiducial markers (figures 2-6, 2-7, and 2-8). This is mainly due to operator- and system-related errors in localising the matching points/areas, which can be minimised by increasing the number of points/areas, but these errors can never be eliminated (Maurer et al., 1997, Rußig and Schulze, 2013). Software-related fiducial localisation error may be minimised via alternative fiducial marker materials (e.g., silicon nitride), as it produces a less distorted image of the fiducial screw head by avoiding metal artifacts (Du et al., 2019).

The mixed patterns of distribution and the wide ranges of error seen in table 2-1 (on page 53) emphasise the importance of completing the accuracy checking process prior to commencing the surgical procedure.

Intraoperator agreement values reflect the consistency of results when the same configuration is repeatedly tested. The interoperator agreement had a high value, promoting the generalisation of the present conclusions and also supporting the rejection of the first null hypothesis (Fan et al., 2019). According to the present intra-class correlation coefficients, only the XG tracing group showed poor intra- and interoperator reliabilities. This could suggest that the tracing algorithm for X-Guide produces a wider variation in accuracy when the target area is far. However, this may not be the case if teeth were traced instead of small flat surfaces. The X-Guide tracing algorithm can still be of value in the "refinement" of a fiducial registration process to improve its accuracy (via supplementing the original registration with tracing information from exposed bone surfaces).

The results in table 2-3 indicate that four-area configuration registration can be as good as eight-area registration, particularly when one registration area is located far from the other three (Conf.2, Conf.3, Conf.5 and Conf.6; see figure 2-8). This partially supports the acceptance of the third null hypothesis (i.e., increasing the number of registration areas does not necessarily improve the registration accuracy). With tracing methods, it is important for the registration areas to be close to the target surgical site (Conf.3) rather than being widely separated. In contrast, with fiducial-based registration, their wide separation (Conf.5) looks to be equally important as the close proximity to the target surgical site. Multiple comparisons showed that these three potential four-area configurations (Conf.3, Conf.5, and Conf.6) had no statistically significant differences from their corresponding positive controls (eight-areas), except in the XG fiducial group, wherein the positive control was significantly better. This again supports the dependency of accepting or rejecting the third null hypothesis on the specific method and configuration being tested.

There was a systematic discrepancy when comparing the right with the left vector values of Conf.7 (the positive control) in the ND tracing and fiducial groups (see figure 2-9). Despite the symmetric distribution of the registration areas, the registration error was consistently less on the left than on the right side. This might be explained by the method in which the software operates during the registration process (it forces the direction of registration from right to left). Therefore, the order of registration may have had an impact on the values of the right and left vector deviations.

The smaller vertical deviations (see figures 2-6 and 2-7 on pages 46 and 47) might be related to the shape of the skull surface. The present authors suggest that, compared to vertical deviations, coronal and lateral deviations may become more pronounced because the skull is rotated along a vertical axis between the image and patient spaces. Software matching algorithms seem to better avoid rotations along horizontal axes, probably due to more step-surface irregularities in the vertical plane.

In summary, out of the three null hypotheses stated earlier, only the second null hypothesis can be rejected with confidence. The acceptance of the first and third null hypotheses is dependent on the specific configurations being compared and also on whether the registration was done by tracing or by fiducial marker method.

Pre-determining fiducial marker positions has a substantial clinical impact, particularly in edentulous scenarios. Inadequate fiducial placement may require the exposure of bone to allow trace registration of the exposed surface areas to improve (refine) the registration accuracy (X-NavTechnologiesLLC, 2020, ClaroNavInc., 2021). Therefore, studying the ideal number and the best configuration of fiducial markers can have a valuable clinical impact.

It is, however, very difficult to comment on what is "sufficient" or "acceptable" registration accuracy due to the fact that this source of error is complicated by many other types of errors during dynamic navigation procedures that, based on their direction, may increase or reduce the clinical effect of the registration error (Widmann et al., 2009). The present authors therefore believe that it is neither correct nor clinically sound to state registration error in terms of the final accuracy of the surgical procedure, especially given that the other sources of error could be greater (e.g., application or execution human error) (Widmann et al., 2009, Fan et al., 2019). The present results serve to improve the standardisation of the registration step rather than comment on its clinical significance. That is, to optimise the registration protocol for subsequent steps given the available tools and algorithms for registration. The clinical impact would rely on the direction and magnitude of the other sources of errors in dynamic navigation.

When the inferior surfaces of the zygomatic buttress were excluded, fiducial registration produced significantly better accuracy with both dynamic navigation systems. However, tracing 1-cm areas at these surfaces bilaterally (Conf.3) resulted in similar registration accuracy as placing fiducial markers there. This finding highlights the possibility of using trace registration on the bone surfaces as an alternative to fiducial registration in some clinical situations, on the conditions that bone exposure of these surfaces is not problematic and that they are located close to the surgical site without being affected by the surgery.

The main limitation of this study is not including more configurations and variations in the registration method (e.g., more than four areas, combining tracing and fiducial methods in the same registration process). Another limitation is not accounting for more anatomical variations to confirm the generalisation of the conclusions. Each configuration and its mirror image were implemented to have two different anatomies, but more models with different anatomies could have been more effective. Both of the above-mentioned limitations were directly related to time constrains of this study.

2.10. Conclusions

The minimum number of fiducial markers to achieve good (i.e., plateau) bilateral accuracy for maxillary surgeries is six. The best configuration would be to have 3 fiducial markers on either side distributed as wide as possible but still close to the surgical site (e.g., Conf.9 for zygomatic implant placement and Conf.3 [mirrored] for maxillary surgeries not involving the zygomatic buttress areas). Increasing the number of fiducial markers beyond six has a negligible effect in further increasing the registration accuracy, as described earlier.

Four fiducial markers could be enough for unilateral surgeries on the condition that three fiducial markers are placed on three different planes on the surgical side and the fourth as far as possible on the other side, close to the level of the surgical site (e.g., Conf.3, Conf.5 and Conf.6). There were statistically significant differences between the suggested best configurations and the other four-area configurations included herein when the NaviDent system was involved. However, the same effect was not observed with the X-Guide system as the differences were not significant.

Even with the best accuracy configurations using the tracing method, the fiducial method still produced significantly better accuracy, supporting the use of fiducial registration as a primary registration method in edentulous cases.

The authors also recommend keeping records for the target registration accuracy checks (even if they were in the form of subjective screen captures) for each surgical procedure. These records will allow retrospective analysis of their effect on the overall accuracy of the surgeries. Consequently, the correlation with the details of the utilised registration methods/configurations would serve as feedback to improve clinical results and establish thresholds for what a “sufficient” registration accuracy is in each procedure.

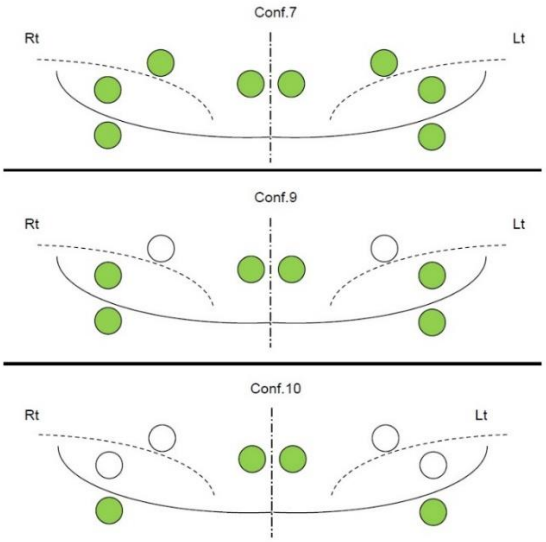

Appendix figure 2-1. Diagramatic representations of the three symmetric configurations that were tested for registration error. The filled circles represent the fiducial markers that were registered per configuration. Conf.7 represents the positive control (eight filled circles), Conf. 9 and 10 were tested by a single operator to supplement the previous data.

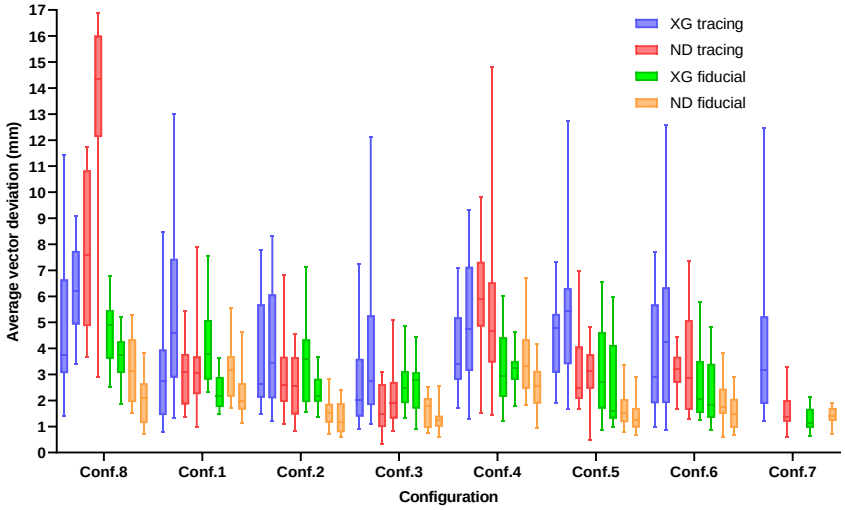

Appendix figure 2-2. A box plot of overall target registration error (average vector) categorised by the registration modality and navigation system. The error bars represent the total ranges. Each modality was presented as two adjacent boxes with the same colour: the left and right boxes represent the left and right configurations, respectively. Conf. 7 (positive control) is symmetric and therefore has no sides. Number of values in each box = 18. . XG = X-Guide; ND = NaviDent.

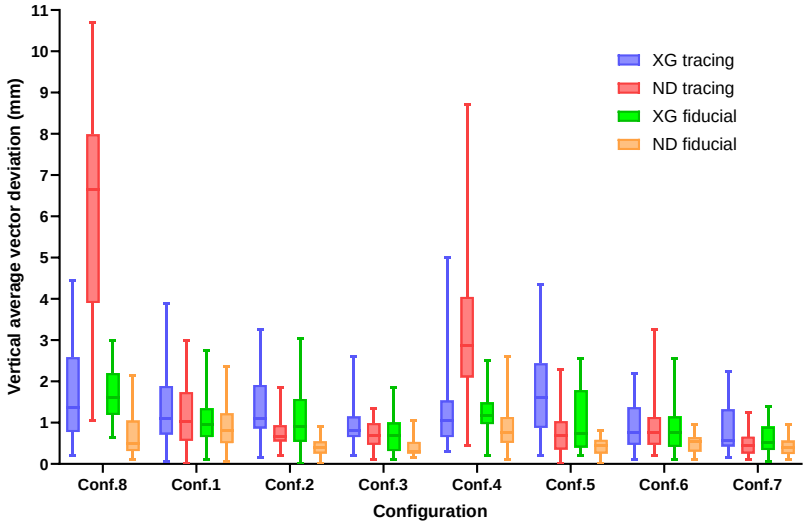

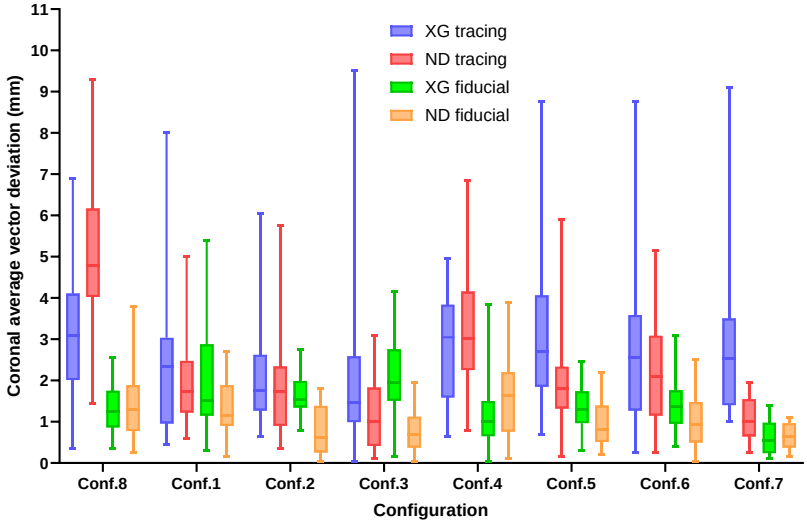

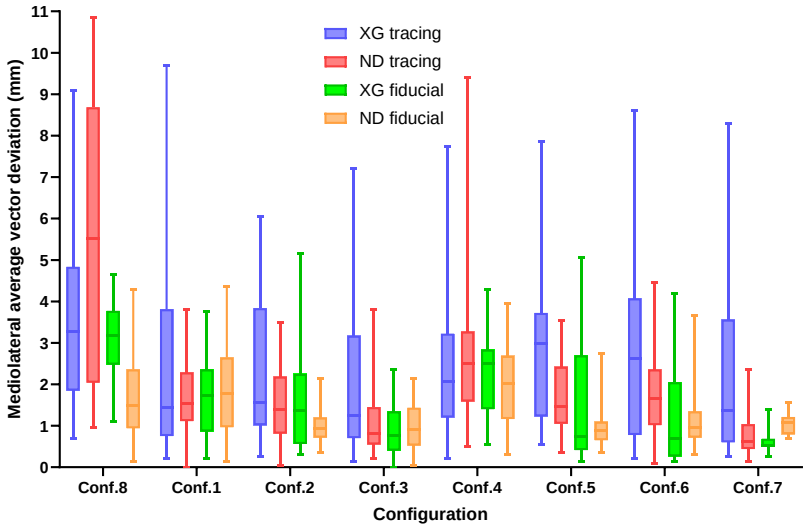

Appendix figure 2-3. Box plots showing the target registration accuracy values by deviation plane. The error bars represent the total ranges. Number of values in each box = 36 (except Conf.7 boxes [n = 18]). XG = X-Guide; ND = NaviDent.

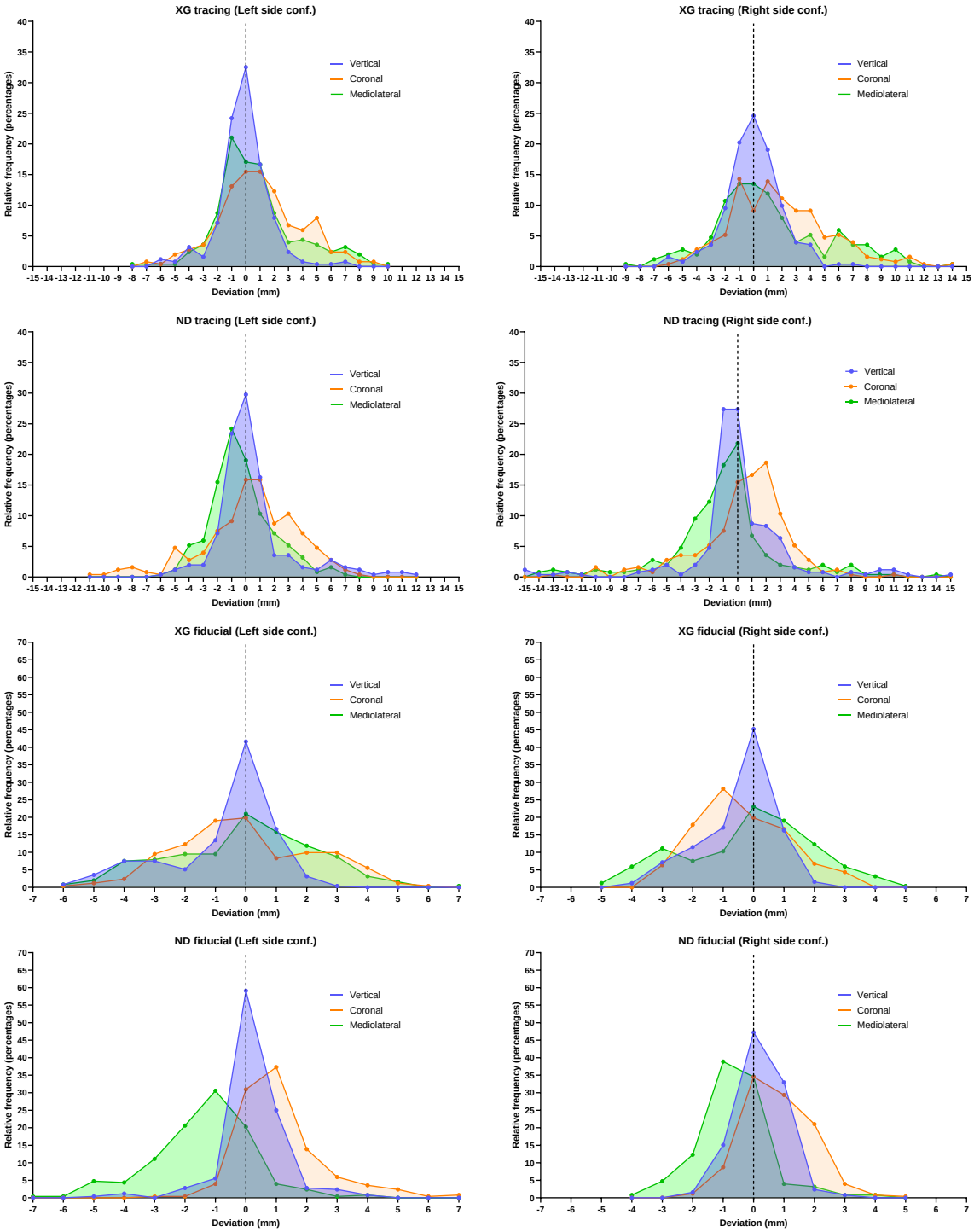

Appendix figure 2-4. Area charts depicting the percentage of deviations for the left and right side configurations. The total number of measured values under each curve = 252. XG = X-Guide; ND = NaviDent. Larger area located close to the doted line in the centre indicates more accurate registration procedure for that direction.

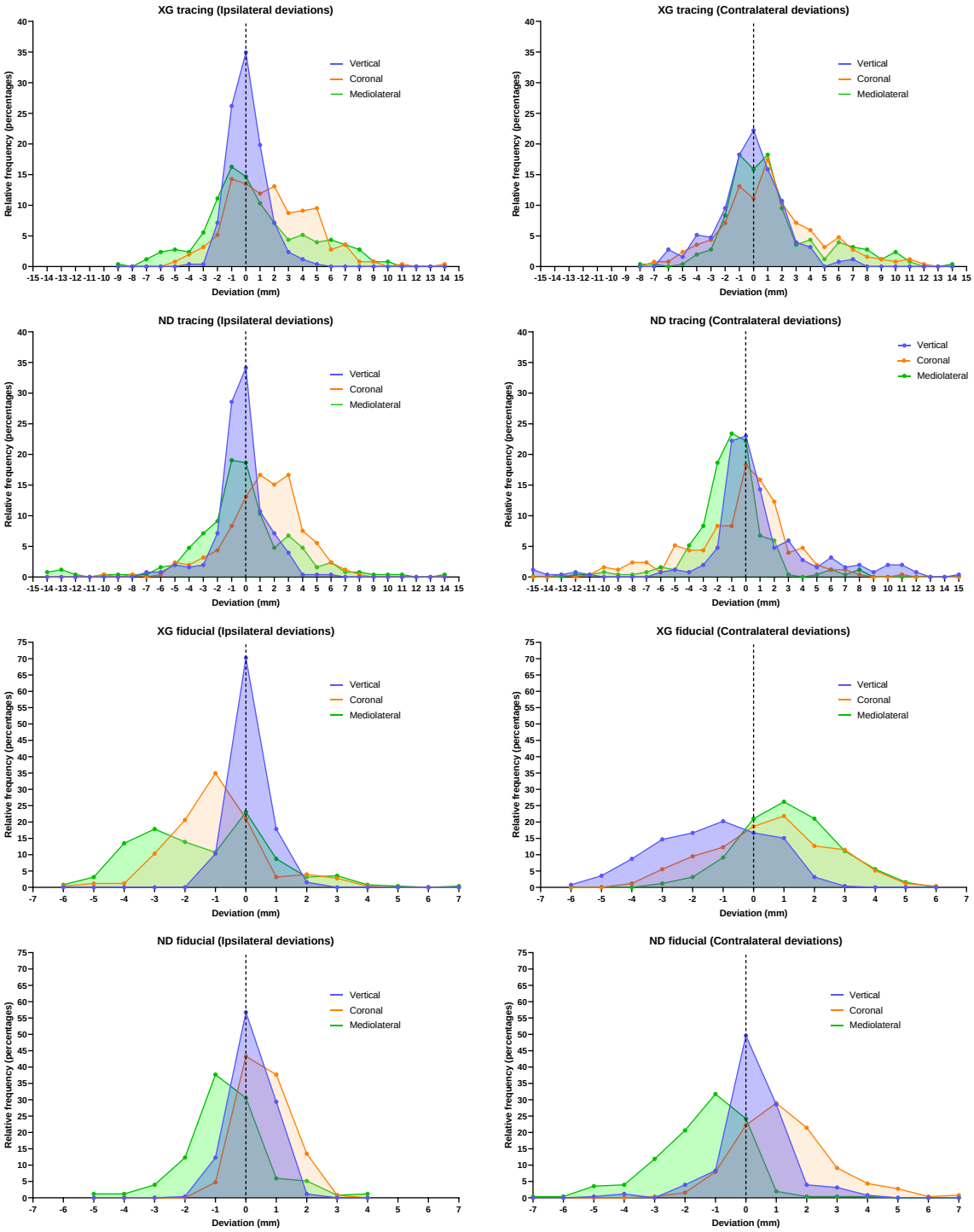

Appendix figure 2-5. Area charts depicting the percentage of ipsilateral and contralateral deviations. The total number of measured values under each curve = 252. XG = X-Guide; ND = NaviDent.

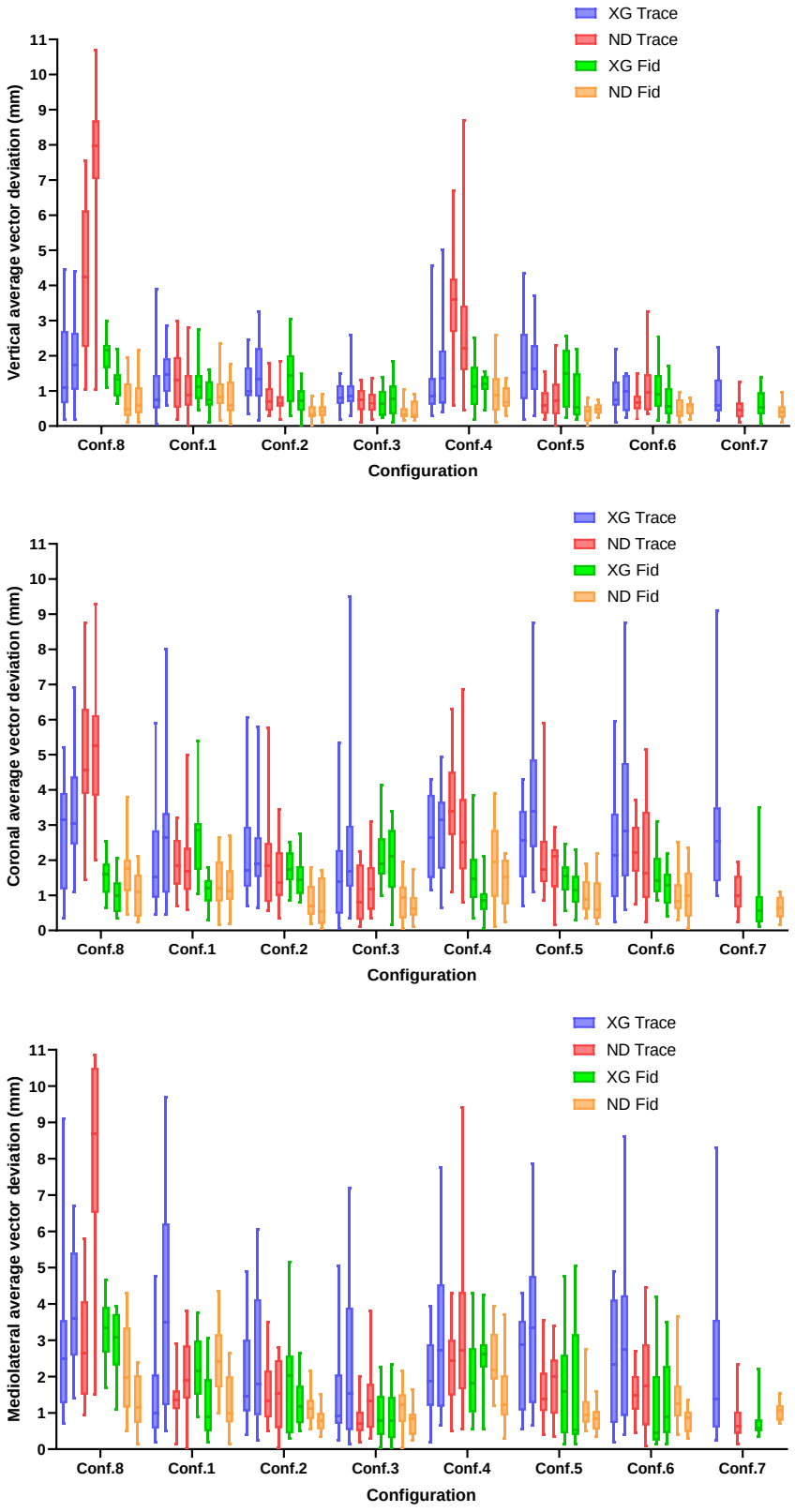

Appendix figure 2-6. Box plots showing the target registration accuracy values by deviation plane. The error bars represent the total ranges. Each modality was presented as two adjacent boxes with the same colour: the left and right boxes represent the left and right configurations, respectively. Conf. 7 is symmetric and therefore has no sides. Number of values in each box = 18. XG = X-Guide; ND = NaviDent.

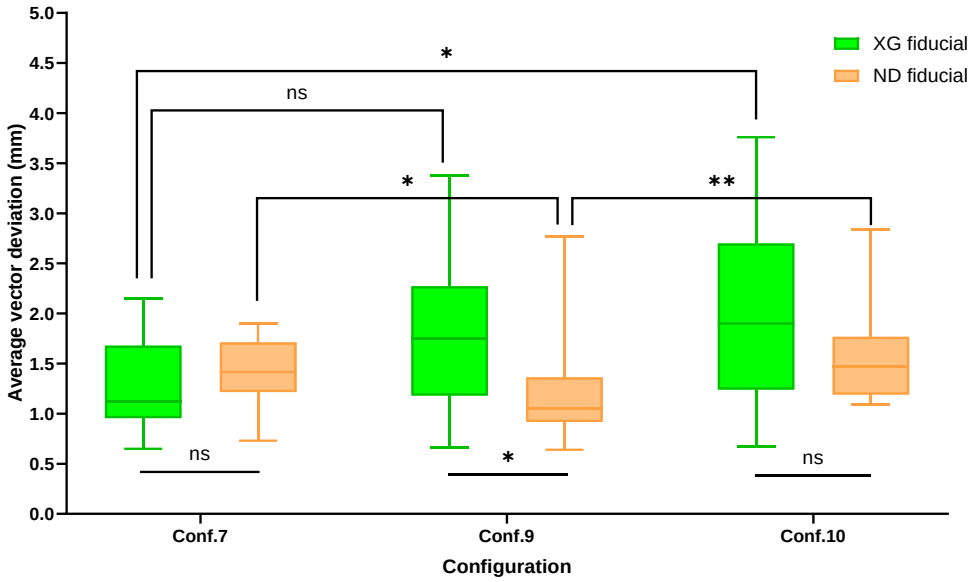

Appendix figure 2-7. A box plot of overall target registration error (average vector) for the symmetric configurations categorised by the registration modality and navigation system. The error bars represent the total ranges. Number of values in each box = 18. Independent-samples Kruskal-Wallis tests with Dunn's correction p values: ** < .01, * < .05, ns > .05. Analysis conducted in GraphPad. XG = X-Guide; ND = NaviDent.

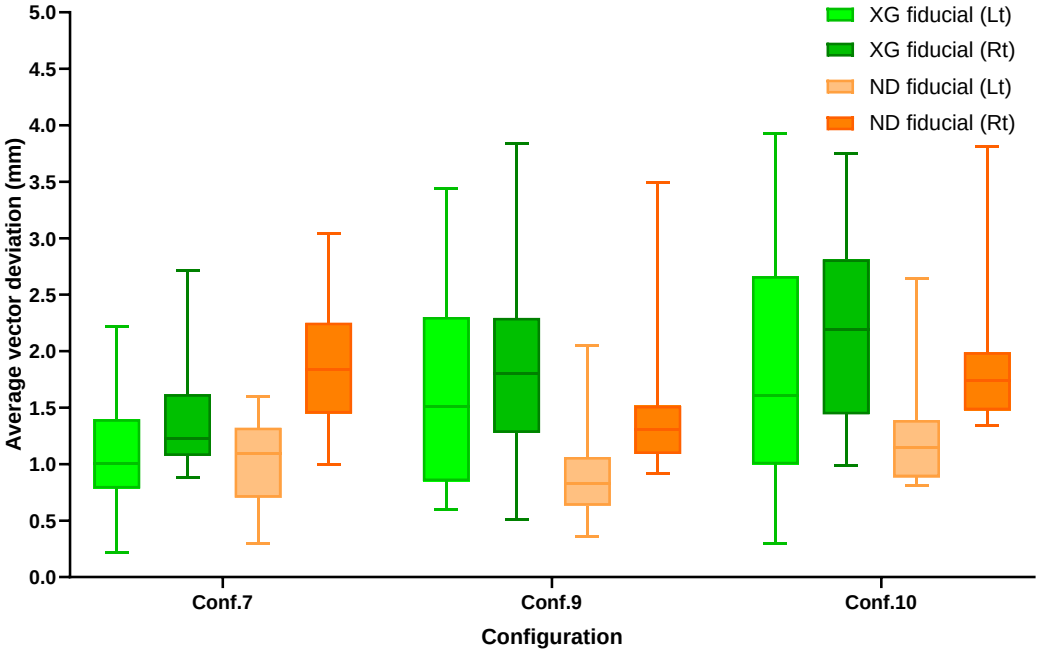

Appendix figure 2-8. A box plot demonstrating the effect of fiducial distribution among sides in the symmetric configurations on the target registration accuracy. Each modality was presented as two adjacent boxes: the left one for the left vectors and the right one for the right vectors. Number of values in each box = 18. XG = X-Guide; ND = NaviDent.

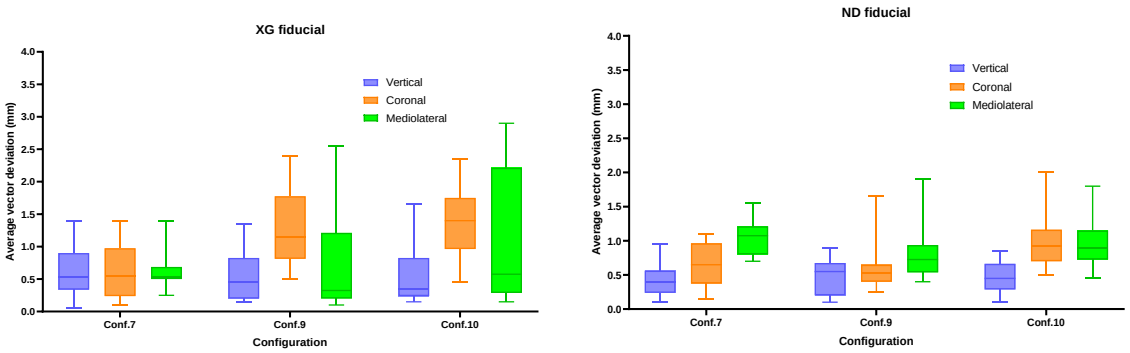

Appendix figure 2-9. Box plots showing the target registration accuracy values by deviation plane for symmetric configurations. The error bars represent the total ranges. Number of values in each box = 18. XG = X-Guide; ND = NaviDent.

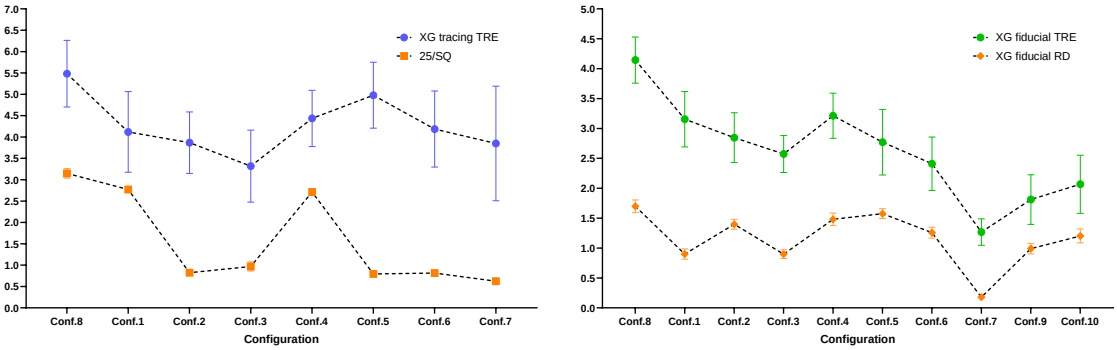

Appendix figure 2-10. Line charts showing the target registration accuracy values in relation to spread quality (SQ) and registration deviation (RD). The SQ values have inverse proportion to deviations and thus (25/SQ) were plotted for porper scaling. The error bars represent 95% confidence intervals from the means. XG = X-Guide.

Configuration	Registration Group	n	Shapiro-Wilk p value	Mean ± SD (mm)	Median (IQR) (mm)	Min. (mm)	Max. (mm)
Conf.1	XG tracing (ip.)	36	.052	4.16 ± 2.59	3.97 (4.31)	0.57	11.96
	XG tracing (cn.)	36	**.000**	4.08 ± 3.79	2.65 (3.24)	0.58	17.24
	ND tracing (ip.)	36	**.000**	2.95 ± 1.81	2.42 (2.01)	0.54	8.05
	ND tracing (cn.)	36	**.031**	3.74 ± 1.86	3.04 (2.57)	0.51	8.66
	XG fiducial (ip.)	36	**.000**	3.49 ± 1.62	3.07 (1.53)	1.50	9.81
	XG fiducial (cn.)	36	.061	2.83 ± 1.53	2.83 (1.89)	0.54	6.87
	ND fiducial (ip.)	36	**.007**	1.67 ± 0.95	1.46 (1.41)	0.46	4.28
	ND fiducial (cn.)	36	.141	3.70 ± 1.49	3.34 (2.66)	1.24	6.79
Conf.2	XG tracing (ip.)	36	**.000**	3.82 ± 2.63	3.00 (2.76)	1.10	11.54
	XG tracing (cn.)	36	**.002**	3.92 ± 2.73	3.31 (3.46)	0.46	12.10
	ND tracing (ip.)	36	**.012**	2.91 ± 1.78	2.45 (2.58)	0.14	6.63
	ND tracing (cn.)	36	**.000**	2.61 ± 1.70	2.20 (1.36)	0.55	7.77
	XG fiducial (ip.)	36	**.004**	2.66 ± 0.83	2.55 (1.14)	1.42	5.61
	XG fiducial (cn.)	36	**.000**	3.04 ± 1.76	2.45 (2.81)	0.95	8.62
	ND fiducial (ip.)	36	**.002**	1.28 ± 0.75	1.03 (1.03)	0.41	3.34
	ND fiducial (cn.)	36	**.011**	1.60 ± 0.82	1.44 (1.08)	0.33	3.86
Conf.3	XG tracing (ip.)	36	**.000**	3.86 ± 3.52	2.55 (3.47)	0.51	15.67
	XG tracing (cn.)	36	**.000**	2.93 ± 2.62	2.06 (1.88)	0.73	13.07
	ND tracing (ip.)	36	**.001**	2.23 ± 1.85	1.50 (2.56)	0.22	7.93
	ND tracing (cn.)	36	**.000**	1.64 ± 0.94	1.63 (0.99)	0.30	5.19
	XG fiducial (ip.)	36	.255	2.60 ± 1.05	2.55 (1.43)	0.77	5.66
	XG fiducial (cn.)	36	.668	2.54 ± 0.94	2.29 (1.30)	0.60	5.02
	ND fiducial (ip.)	36	**.011**	1.23 ± 0.67	1.19 (1.02)	0.17	3.61
	ND fiducial (cn.)	36	**.029**	1.69 ± 0.90	1.42 (1.42)	0.37	4.22
Conf.4	XG tracing (ip.)	36	.089	3.95 ± 2.02	3.34 (3.22)	0.96	8.34
	XG tracing (cn.)	36	**.001**	4.90 ± 2.85	4.17 (3.19)	1.36	13.46
	ND tracing (ip.)	36	**.001**	4.42 ± 2.19	4.04 (2.42)	1.28	12.11
	ND tracing (cn.)	36	.170	6.96 ± 3.47	6.90 (4.35)	1.07	17.52
	XG fiducial (ip.)	36	.943	3.14 ± 1.00	3.17 (1.23)	0.95	5.47
	XG fiducial (cn.)	36	**.001**	3.29 ± 1.47	3.25 (1.53)	1.16	7.46
	ND fiducial (ip.)	36	**.031**	2.17 ± 1.29	1.97 (1.58)	0.42	5.02
	ND fiducial (cn.)	36	.097	3.97 ± 1.93	3.51 (2.71)	0.62	8.39

Configuration	Registration Group	n	Shapiro-Wilk p value	Mean ± SD (mm)	Median (IQR) (mm)	Min. (mm)	Max. (mm)
Conf.5	XG tracing (ip.)	36	**.039**	5.18 ± 2.87	4.57 (4.69)	1.05	12.26
	XG tracing (cn.)	36	**.000**	4.91 ± 3.67	3.70 (3.40)	0.85	14.27
	ND tracing (ip.)	36	.409	3.78 ± 2.01	3.58 (2.90)	0.60	8.72
	ND tracing (cn.)	36	.219	2.37 ± 1.27	2.22 (1.40)	0.30	6.14
	XG fiducial (ip.)	36	.242	2.71 ± 1.19	2.42 (1.87)	0.80	5.50
	XG fiducial (cn.)	36	**.000**	2.83 ± 2.15	1.63 (3.47)	0.58	7.94
	ND fiducial (ip.)	36	**.000**	1.52 ± 0.79	1.22 (0.93)	0.59	4.04
	ND fiducial (cn.)	36	**.004**	1.50 ± 0.78	1.25 (1.03)	0.24	3.19
Conf.6	XG tracing (ip.)	36	**.000**	3.84 ± 3.48	2.50 (6.06)	0.32	11.44
	XG tracing (cn.)	36	**.000**	4.54 ± 3.59	3.04 (4.38)	0.79	13.74
	ND tracing (ip.)	36	**.002**	3.68 ± 2.30	3.34 (3.12)	1.05	11.63
	ND tracing (cn.)	36	.057	2.88 ± 1.32	2.65 (1.79)	1.04	5.98
	XG fiducial (ip.)	36	**.001**	2.22 ± 1.10	1.86 (1.60)	0.71	4.69
	XG fiducial (cn.)	36	**.002**	2.60 ± 1.69	2.19 (1.99)	0.55	6.92
	ND fiducial (ip.)	36	**.001**	1.56 ± 0.99	1.38 (1.16)	0.30	5.21
	ND fiducial (cn.)	36	**.013**	2.02 ± 1.03	1.84 (1.10)	0.67	5.29
Conf.7 (positive control)	XG tracing (Lt.)	18	.077	4.57 ± 3.15	4.00 (4.85)	0.79	11.06
	XG tracing (Rt.)	18	**.000**	3.13 ± 3.08	2.15 (2.27)	0.97	13.89
	ND tracing (Lt.)	18	.768	1.18 ± 0.62	1.21 (0.80)	0.22	2.62
	ND tracing (Rt.)	18	**.004**	2.09 ± 1.43	1.82 (1.23)	0.36	5.41
	XG fiducial (Lt.)	18	.595	1.09 ± 0.55	1.01 (0.61)	0.22	2.22
	XG fiducial (Rt.)	18	**.002**	1.44 ± 0.56	1.23 (0.55)	0.88	2.71
	ND fiducial (Lt.)	18	.225	1.01 ± 0.39	1.10 (0.62)	0.30	1.60
	ND fiducial (Rt.)	18	.735	1.87 ± 0.56	1.84 (0.81)	1.00	3.04
Conf.8 (negative control)	XG tracing (ip.)	36	.335	4.47 ± 2.42	4.56 (3.73)	0.95	10.26
	XG tracing (cn.)	36	**.013**	6.17 ± 3.62	5.10 (5.86)	1.47	16.01
	ND tracing (ip.)	36	.124	8.60 ± 4.01	8.20 (6.49)	2.68	17.88
	ND tracing (cn.)	36	**.042**	12.39 ± 5.05	13.51 (7.90)	3.15	21.61
	XG fiducial (ip.)	36	.641	3.75 ± 0.81	3.73 (1.15)	2.30	5.66
	XG fiducial (cn.)	36	.793	4.53 ± 1.54	4.41 (2.27)	1.39	7.89
	ND fiducial (ip.)	36	**.045**	1.75 ± 1.08	1.71 (1.80)	0.00	3.76
	ND fiducial (cn.)	36	**.032**	3.52 ± 1.72	3.17 (2.14)	0.91	8.16

Appendix table 2-7. Descriptive statistics for ipsilateral versus contralteral vector deviations (cont.). ip. = ipsilateral; cn. = contralateral; Lt. = left; Rt = right.

Configuration	Registration Group	n	Shapiro-Wilk p value	Mean ± SD (mm)	Median (IQR) (mm)	Min. (mm)	Max. (mm)
Conf.7 (8 fiducial markers)	XG fiducial	18	**.000**	1.42 ± 0.87	1.12 (0.79)	0.65	4.43
	ND fiducial	18	.496	1.45 ± 0.31	1.42 (0.50)	0.73	1.90
Conf.9 (6 fiducial markers)	XG fiducial	18	.168	1.81 ± 0.83	1.75 (1.09)	0.66	3.38
	ND fiducial	18	**.000**	1.18 ± 0.47	1.06 (0.45)	0.64	2.77
Conf.10 (4 fiducial markers)	XG fiducial	18	.251	2.07 ± 0.98	1.90 (1.46)	0.67	3.76
	ND fiducial	18	**.010**	1.56 ± 0.46	1.48 (0.58)	1.09	2.84

Appendix table 2-8. Descriptive statistics for the accuracy results (average vectors) of the symmetric configurations. Shapiro-Wilk p values < .05 indicate the lack of distribution normality.

Configuration	Comparison Group	XG fiducial	ND fiducial
Conf.9	Against Conf.10	> .999	**.006**
	Against Conf.7	**.139**	.013
Conf.10	Against Conf.7	.023	**> .999**

Appendix table 2-9. Results of multiple comparisons for average vector deviations of the symmetric configurations using independent-samples Kruskal-Wallis tests with Dunn's correction in terms of p values.

Configuration	Registration Group	n	Shapiro-Wilk p value	Mean ± SD (mm)	Median (IQR) (mm)	Min. (mm)	Max. (mm)
Conf.7 (8 fiducial markers)	XG fiducial	18	.540	0.62 ± 0.37	0.53 (0.56)	0.05	1.40
	ND fiducial	18	.600	0.42 ± 0.22	0.40 (0.33)	0.10	0.95
Conf.9 (6 fiducial markers)	XG fiducial	18	**.012**	0.56 ± 0.41	0.45 (0.63)	0.15	1.35
	ND fiducial	18	.230	0.48 ± 0.26	0.55 (0.48)	0.10	0.90
Conf.10 (4 fiducial markers)	XG fiducial	18	**.001**	0.54 ± 0.46	0.35 (0.59)	0.15	1.65
	ND fiducial	18	.668	0.46 ± 0.23	0.45 (0.38)	0.10	0.85

Appendix table 2-10. Descriptive statistics for average vertical deviations of the symmetric configurations. Shapiro-Wilk p values < .05 indicate the lack of distribution normality.

Configuration	Comparison Group	XG fiducial	ND fiducial
Conf.9	Against Conf.10	> 0.999	> 0.999
	Against Conf.7	**> 0.999**	**> 0.999**
Conf.10	Against Conf.7	**0.836**	**> 0.999**

Appendix table 2-11. Results of multiple comparisons for average vertical deviations of the symmetric configurations using independent-samples Kruskal-Wallis tests with Dunn's correction in terms of p values.

Configuration	Registration Group	n	Shapiro-Wilk p value	Mean ± SD (mm)	Median (IQR) (mm)	Min. (mm)	Max. (mm)
Conf.7 (8 fiducial markers)	XG fiducial	18	.082	0.64 ± 0.44	0.55 (0.74)	0.10	1.40
	ND fiducial	18	.132	0.63 ± 0.33	0.65 (0.59)	0.15	1.10
Conf.9 (6 fiducial markers)	XG fiducial	18	.466	1.29 ± 0.58	1.15 (0.96)	0.50	2.40
	ND fiducial	18	**.000**	0.58 ± 0.30	0.53 (0.25)	0.25	1.65
Conf.10 (4 fiducial markers)	XG fiducial	18	.985	1.38 ± 0.51	1.40 (0.79)	0.45	2.35
	ND fiducial	18	.051	1.00 ± 0.40	0.93 (0.46)	0.50	2.00

Appendix table 2-12. Descriptive statistics for average coronal deviations of the symmetric configurations. Shapiro-Wilk p values < .05 indicate the lack of distribution normality.

Configuration	Comparison Group	XG fiducial	ND fiducial
Conf.9	Against Conf.10	> 0.999	**0.001**
	Against Conf.7	0.005	**0.994**
Conf.10	Against Conf.7	0.001	0.020

Appendix table 2-13. The results of multiple comparisons for average coronal deviations of the symmetric configurations using independent-samples Kruskal-Wallis tests with Dunn's correction in terms of p values.

Configuration	Registration Group	n	Shapiro-Wilk p value	Mean ± SD (mm)	Median (IQR) (mm)	Min. (mm)	Max. (mm)
Conf.7 (8 fiducial markers)	XG fiducial	18	**.002**	0.63 ± 0.28	0.53 (0.19)	0.25	1.40
	ND fiducial	18	.321	1.06 ± 0.26	1.08 (0.41)	0.70	1.55
Conf.9 (6 fiducial markers)	XG fiducial	18	**.000**	0.72 ± 0.79	0.33 (1.01)	0.10	2.55
	ND fiducial	18	**.004**	0.79 ± 0.36	0.73 (0.40)	0.40	1.90
Conf.10 (4 fiducial markers)	XG fiducial	18	**.004**	1.14 ± 1.02	0.58 (1.92)	0.15	2.90
	ND fiducial	18	.288	0.94 ± 0.32	0.90 (0.42)	0.45	1.80

Appendix table 2-14. Descriptive statistics for average mediolateral deviations of the symmetric configurations. Shapiro-Wilk p values < .05 indicate the lack of distribution normality.

Configuration	Comparison Group	XG fiducial	ND fiducial
Conf.9	Against Conf.10	.302	.259
	Against Conf.7	**.497**	**.007**
Conf.10	Against Conf.7	**> .999**	**.547**

Appendix table 2-15. The results of multiple comparisons for average mediolateral deviations of the symmetric configurations using independent-samples Kruskal-Wallis tests with Dunn's correction in terms of p values.

Ranked by	XG tracing			ND tracing			XG fiducial			ND fiducial		
	Best	2nd	3rd	Best	2nd	3rd	Best	2nd	3rd	Best	2nd	3rd
Mean	3	7	2	7	3	2	7	6	3	7	2	3
Median	3	7	2	7	3	2	7	6	5	3	5	7

Appendix table 2-16. The best three configurations in relation to target accuracy (average vectors).

Zygomatic buttress available	P value	Zygomatic buttress in the way of surgery	P value
ND fiducial Conf.3 (ip.) against ND fiducial Conf.3 (cn.)	**.028** ip. is better	ND fiducial Conf.5 (ip.) against ND fiducial Conf.5 (cn.)	.887 Non-significant
XG fiducial Conf.6 (ip.) against XG fiducial Conf.6 (cn.)	.496 Non-significant	XG fiducial Conf.6 (ip.) against XG fiducial Conf.6 (cn.)	.496 Non-significant

Appendix table 2-17. Results of Mann-Whitney tests for the effect of the side of vector in terms of p values. The significance level was set at < .05. Analysis conducted in GraphPad. ip. = ipsilateral side where 3 of 4 fiducial markers were placed; cn. = contralateral side where one fiducial marker was placed. XG = X-Guide, ND = NaviDent.

Chapter 3

The Precision of Drill Calibration for Dynamic Navigation

3.1. Preface

In the previous chapter, we looked at one of the possible operator-related sources of error in the dynamic navigation guided protocols for ZI placement.

Other operator-related error sources include those arising from manually calibrating the drilling equipment. The process of drill calibration involves mapping the 3D structure of the drilling tool from the real-world space to the 3D space of the CBCT in the software. This tool construction should be accurate, but the level of its accuracy depends on the how well the operator applies the calibration steps and also on technical factors related to the tracking quality of the camera and the mechanical quality of the drilling tool itself. The result of the drill calibration is saved in the software as a transformation matrix (TM) between the drill tip and the handpiece tracker.

Therefore, this chapter aimed at investigating the precision of the drill calibration process using different shapes and lengths of drills and implants. The observed variation was quantified by three different operators in isolation from other sources of dynamic navigation errors via the assessment of the quality of drilling tool construction in the 3D space of the CBCT in the software. This was achieved via the calculation of the reproducibility of the transformation matrix resulting from the calibration procedure of each drill. Recognising the drill with the most reproducible transformation matrix with all points in a quad-zygoma plan had enabled the application of a single drill calibration protocol for this project (explained in section 4.8).

The most precise drill calibration was expected to produce the least drill calibration errors, as the magnitude of variation with other drills suggested that their calibration is more likely to be affected by the operator skill and the technical factors mentioned above than anything else.

This chapter is presented as a published journal article (with minor variations form the published version in order to improve clarity):

Mohammed Y. Al-Jarsha, Ashraf F. Ayoub, Mohammed M. Almgran, Chieh-Han Liu, Douglas P. Robertson, Kurt B. Naudi 2024. The precision of drill calibration for dynamic navigation. Journal of dentistry, 146, 105032.

3.2. Author declaration and contribution

Conceptualisation: The formulation of research aims and goals in this publication is totally of my own conceptualisation.

Data Curation: I completed all data processing; filtering CSV files from the total captured stream of files for all three operators and the extraction of transformation matrix data from the filtered CSV files in this publication.

Formal Analysis: I was responsible for the application of statistical analysis to synthesise all study processed data, including descriptive tests, normality tests, inter-operator agreement tests, and correlation tests in this publication.

Investigation: I participated in the practical experiment and data collection (in CSV file format) as one of the three operators in this publication.

Methodology: I designed the experiment in this publication through selection of the drills and implants to be tested, training the other operators to calibrate drills according to the manufacturer instructions and the creation of data collection sheets.

Project Administration: I participated in the management and coordination for the experiment execution in this publication.

Visualisation: I was responsible for the creation and preparation of all figures and tables for data visualisation and presentation in this publication.

Writing – original draft: I wrote the complete original draft for this publication.

Writing – review and editing: I completed the pre-publication revisions (up to version 6) based on feedback from the other co-authors. I also completed all the editing requested by the journal as well as post-acceptance proof reading.

3.3. The Precision of Drill Calibration for Dynamic Navigation

Mohammed Y. Al-Jarsha[1,2], Ashraf F. Ayoub[1,*], Mohammed M. Almgran[1], Chieh-Han Liu[1], Douglas P. Robertson[3], Kurt B. Naudi[1]

Journal of dentistry. 2024. https://doi.org/10.1016/j.jdent.2024.105032.

[1] Department of Oral Surgery, School of Medicine, Dentistry and Nursing, College of Medical, Veterinary and Life Sciences, University of Glasgow, Glasgow, United Kingdom.

[2] Department of Oral and Maxillofacial Surgery, College of Dentistry, University of Baghdad, Baghdad, Iraq.

[3] Department of Restorative Dentistry, School of Medicine, Dentistry and Nursing, College of Medical, Veterinary and Life Sciences, University of Glasgow, Glasgow, United Kingdom.

* Corresponding author (Ashraf.Ayoub@glasgow.ac.uk)

3.4. Abstract

Objectives: To quantify the reproducibility of the drill calibration process in dynamic navigation guided placement of dental implants and to identify the human factors that could affect the precision of this process in order to improve the overall implant placement accuracy.

Methods: A set of six drills and four implants were calibrated by three operators following the standard calibration process of NaviDent® (ClaroNav Inc.). The reproducibility of the position of each tip of a drill or implant was calculated in relation to the pre-planned implants' entry and apex positions. Intra- and inter-operator reliabilities were reported. The effects of the drill length and shape on the reproducibility of the calibration process were also investigated. The outcome measures for reproducibility were expressed in terms of variability range, average and maximum deviations from the mean distance.

Results: A satisfactory inter-rater reproducibility was noted. The precision of the calibration of the tip position in terms of variability range was between 0.3 and 3.7 mm. We noted a tendency towards a higher precision of the calibration process with longer drills. More calibration errors were observed when calibrating long zygomatic implants with non-locking adapters than with pointed drills. Flexible long-pointed drills had low calibration precision that was comparable to the non-flexible short-pointed drills.

Conclusions: Clinicians should be aware of the calibration error associated with the dynamic navigation placement of dental and zygomatic implants. This should be taken into consideration especially for long implants, short drills, and long drills that have some degree of flexibility.

Clinical Significance: Dynamic navigation procedures are associated with an inherent drill calibration error. The manual stability during the calibration process is crucial in minimising this error. In addition, the clinician must never ignore the prescribed accuracy checking procedures after each calibration process.

Keywords: Dynamic Navigation, Calibration, Precision, Human Error, Reproducibility, Implants, Zygomatic.

3.5. Introduction

Dynamic surgical navigation is one of the computer-guided approaches used to guide the positioning of dental implants (Yu et al., 2023, Jorba-García et al., 2023). In comparison with static surgical guides, it offers the advantages of surgical flexibility and facilitates dental implant placement in situations of restricted mouth opening and/or limited horizontal space (Jorba-García et al., 2019, Battista et al., 2022). It is also more convenient when flapless zygomatic implant placement is required (Bhalerao et al., 2022, Bhalerao et al., 2023, Bhalerao et al., 2024). Recently published meta-analyses have shown that its accuracy is comparable to that of the static guided approach (Wang et al., 2021b, Marques-Guasch et al., 2023, Fan et al., 2023), and could be even higher in relation to angular deviations (Yu et al., 2023).

A randomised controlled trial by Engkawong and colleagues demonstrated that both of these guided approaches had similar levels of patient satisfaction and patient reported outcomes as the free-hand approach when it comes to short dental implants with a two-week follow-up period (Engkawong et al., 2021).

The literature has highlighted the steep learning curve for the routine use of dynamic navigation for placement of dental implants (Battista et al., 2022, Golob Deeb et al., 2019). Included in this procedure is the calibration process to record and transfer the accurate spatial relationship between the optical pattern (the handpiece tracker) and the cutting tip of the drill or implant being used to the navigation software (Al-Jarsha et al., 2024a, ClaroNavInc., 2021, X-NavTechnologiesLLC, 2020). Technical errors or system malfunctions can occur during the calibration process which impact on the accuracy of the real-time tracking of the drills and implants (Edelmann et al., 2021, Liu et al., 2022, Mai et al., 2023).

Another source of error in dynamic navigation procedures is the registration process for mapping of the patient skull anatomy to the pre-planned position of the dental implant (Al-Jarsha et al., 2024a, Shen et al., 2023, Wei et al., 2023, Zhu et al., 2023). The accuracy of the calibration, registration, and tracking processes are essential to establish the spatial relationship between the drills and the jaw bones via the reference devices. It is then essential for the operator to monitor this spatial relationship in real-time to guide the placement of the implants in relation to the virtual plan on the CBCT during the surgical procedure (ClaroNavInc., 2021, X-NavTechnologiesLLC, 2020, Wu and Sun, 2022).

The three main operator-related sources of error associated with the use of dynamic navigation include inaccuracies in the instrument calibration, inaccuracies in the jaw registration, in addition to application errors (Al-Jarsha et al., 2024a, Widmann et al., 2009). These cumulative errors impact on the overall accuracy of the dynamic navigation procedure (Al-Jarsha et al., 2024a, Zhu et al., 2023). In the current literature, the final implant placement accuracy is often used to show the effect of variation in each of these three sources of error (Ma et al., 2022, Wu and Sun, 2024). Current dynamic navigation systems allow a calibration accuracy check which is dependent on the previous registration step (ClaroNavInc., 2021, X-NavTechnologiesLLC, 2020). Therefore, it is impossible for the clinician to check the magnitude of error resulting solely from the calibration process without quantifying the registration errors concealed within the navigation software (ClaroNavInc., 2021, X-NavTechnologiesLLC, 2020).

The calibration process of the drills or implants records the relationship of their tips and long axes in relation to the mathematical centre “centroid” of the handpiece tracker and generates a 4x4 rigid transformation matrix (TM). The rigid transformation matrix or what is also known as “the Homogenous Transform” is a common way of representing the spatial relationship between two objects in three dimensions (Walker et al., 1991). It includes the rotation angles along the x, y, and z axes of the calibrated object in addition to the translation vector, scale vector, and global scale.

When the TM is termed "rigid", this implies that there is no scaling to be applied to the unit of measurement in that space (Szauer, 2017, Trucco and Verri, 1998).

It is therefore possible to record this TM after each calibration process for the same drill to quantify the reproducibility of this procedure and the precision of the drill tip position in 3-dimensional space independent of any other confounding factors (Walker et al., 1991).

The main aim of the study was the independent assessment of the reproducibility of the calibration process for various zygomatic implants and implant drills. The word “independent” denotes that the resulting outcome measures from this assessment must be isolated from all other sources of error implicated in dynamic navigation procedures. The null hypotheses were: (1): No difference in the calibration precision between the bone-cutting drills and implants. (2): The addition of drill extensions does not impact on the calibration precision.

3.6. Materials and Methods:

3.6.1. Materials

This *in vitro* investigation was carried out using a dynamic navigation system (NaviDent®; ClaroNav Inc., Toronto, Canada). The trackers were the standard single use ones (handpiece tracker 0C482 and jaw tracker type S) in conjunction with the standard drill calibrator tool (figure 3-1).

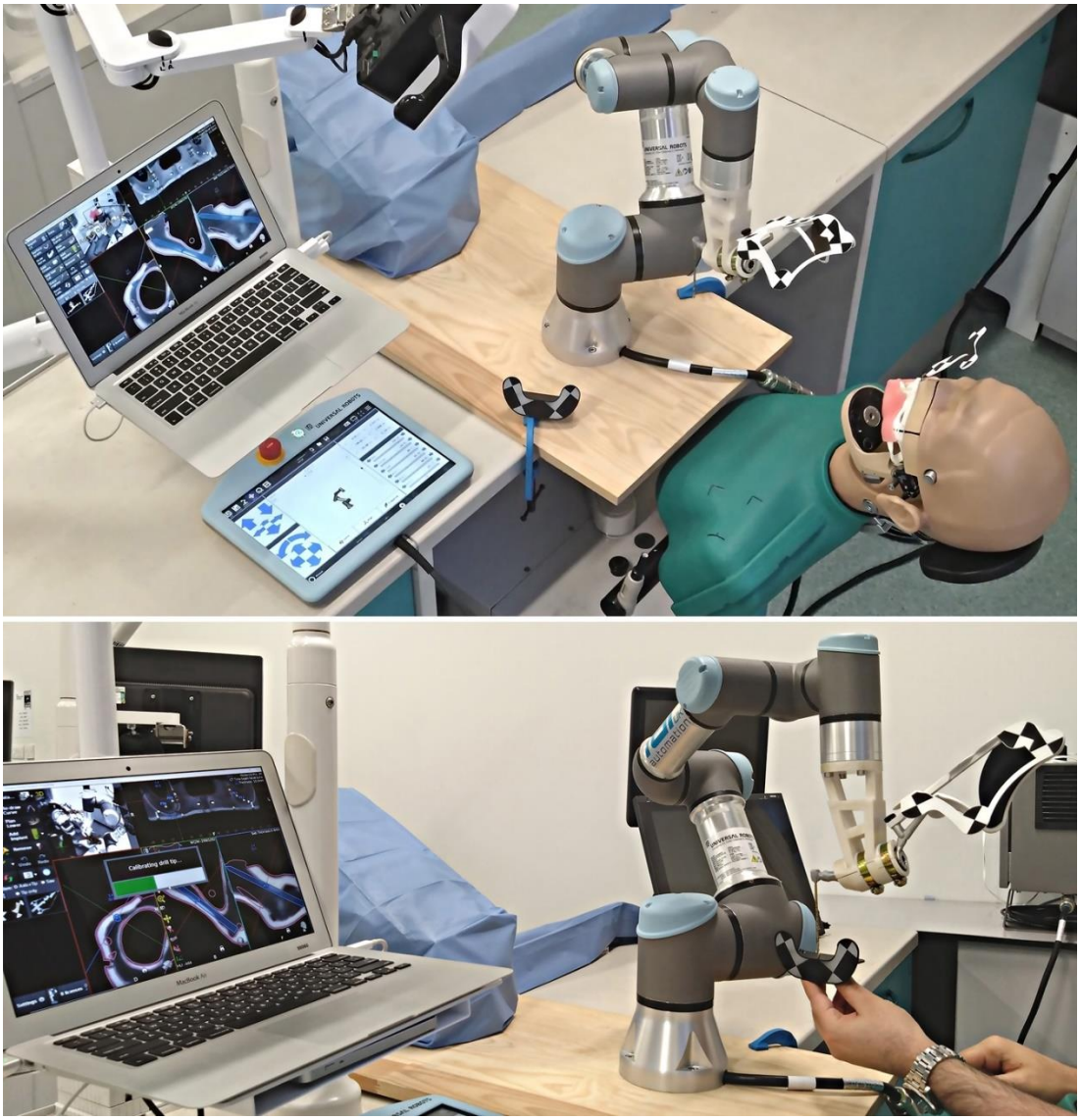

Figure 3-1. Photographs showing the experimental set-up for the assessment of drill calibration reproducibility. The robotic arm here only serves to fix the spatial relationship of the handpiece tracker and the jaw tracker in relation to the tracking camera through the entire experiment.

We tested two drills (the long spade and the zygomatic twist) of the zygomatic drilling set (Southern Implants®, Irene, RSA) and the short spade drill of the NobelReplace® kit (Nobel Biocare®, Zurich, Switzerland). We also assessed the calibration precision of a 6 mm diameter trephine drill of a commercial trephine kit. The tested implants were ZYGAN implants (Southern Implants®, Irene, RSA) (figure 3-2).

Figure 3-2. A photograph of the four drills, four implants and their connections used in the experiment. SpShort = short spade drill; SpLong = long spade drill; Implant35 = Zygomatic implant 35 mm long; Implant40 = Zygomatic implant 40 mm long; Implant45 = Zygomatic implant 45 mm long; Implant50 = zygomatic implant 50 mm long; Trephine = trephine drill; TwLong = zygomatic twist drill (2.9Φ); +Ext = with added drill extension.

To minimise machine-related variations arising from the location of the tracking camera, a robotic arm (UR3e; Universal Robots®, Odense, Denmark) with a custom-printed connection was used to maintain a fixed spatial relationship between the implant handpiece (contra-angle WS-75; W&H®, Bürmoos, Austria) and the tracking camera through the entire experiment. The connecting part was printed using a Rigid 10K resin and a FormLabs 3D printer (Form 3B; FormLabs®, Somerville, USA) (figure 3-1).

3.6.2. Variables and outcome measures

To simplify the assessment of drill calibration precision, it was necessary to identify an outcome measure that is unaffected by any other source of errors. Therefore, frequently utilised parameters like implant final deviations were avoided (Al-Jarsha et al., 2024a, Wu and Sun, 2024).

Figure 3-3 illustrates the concept of transforming a certain point between two frames of reference (Walker et al., 1991). The distance between the pre- and post- transformed point coordinates (denoted as "d" in figure 3-3) is calculated after every drill calibration process. The magnitude of this distance is of no relevance, however, the reproducibility of obtaining the same magnitude with repeated calibrations is an indication of the level of calibration precision associated with each drill or implant. It is directly related to the overall reproducibility of the transformation matrix obtained after each drill calibration process. This is a simplification of dealing with 16 numbers of every 4 x 4 transformation matrix resulting from each calibration process.

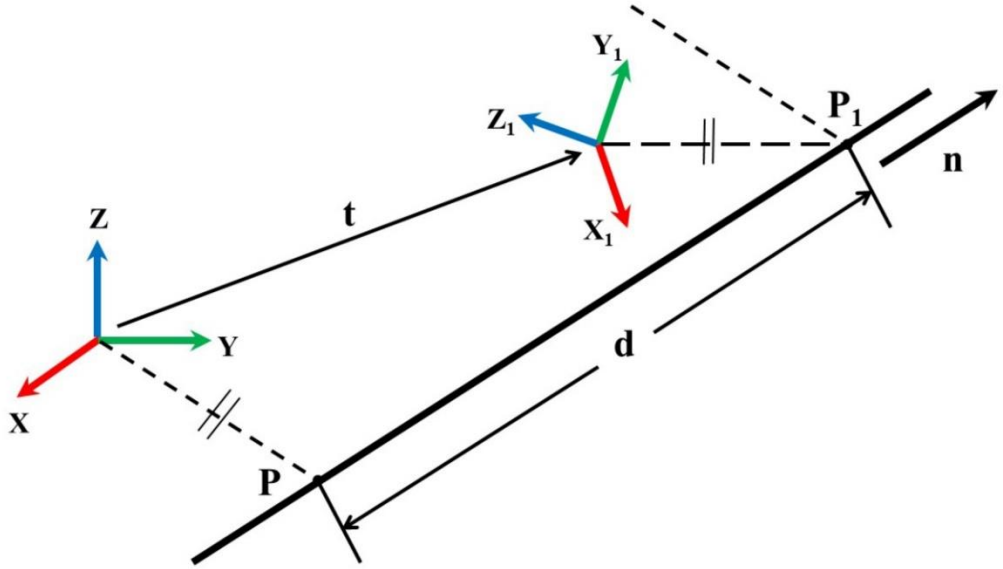

Figure 3-3. An illustration of the transformation of a point coordinate frame. t = the transformation movement between the two reference frames; XYZ represent the original frame; $X_1Y_1Z_1$ represents the new frame; P = the original point pre-transformation; P_1 = the transformed point. d = the distance between the pre- and post- transformed points. n = the direction vector of point P transformation (this figure was adapted from (Walker et al., 1991)).

Therefore, the outcome measures in this study were:

(1) Variability range (Var. range): This is the difference between the maximum and minimum values of "d" associated with each drill or implant. The range is affected by both machine- and human- related factors.

(2) Average deviation from mean (AvDevM): The mean value of "d" was calculated first, then the average of absolute deviations from that mean is calculated. It reflects the average contribution of human variations to the overall calibration precision.

(3) Maximum deviation from mean (MaxDevM): The mean value of "d" was calculated first, then the maximum value of absolute deviation from that mean was highlighted. It reflects the maximum contribution of human variations to the overall precision of the calibration process.

3.6.3. Sample size calculation

Based on a previous pilot study performed by one operator with 2 drills (the long spade drill and the zygomatic twist drill), an effect size of 0.48 was calculated from the variability ranges of 0.516 ± 0.14 mm and 0.447 ± 0.145 mm (variability range ± SD) using G*Power software v. 3.1.9.7. Incorporating this effect size to calculate the required sample size for 10 groups (assuming normal distribution, alpha was set at <0.05 and sample power set at 0.8), a total sample size of 80 was obtained (8 per group). We decided to set the sample size at 9 calibrations per drill per operator to account for further variations due to operator factors. Three operators carried out the calibration processes. Each operator received basic training to ensure standardisation of the calibration protocol prior to commencing the experiment.

3.6.4. Virtual planning stage

Four zygomatic implants were virtually planned on the model CBCT scan of an edentulous maxilla (ZYG NM01; SelModels®, Barcelona, Spain) using NaviDent® software (v.3.0.3); two anterior implants 50 mm long (one on each side) and two posterior implants (one 40 mm long on the right side and the other 35 mm long on the left side). The planning was performed according to the anatomical radiographic features of the zygomatic and maxillary bones derived from the CBCT scan (Pellegrino et al., 2020c, Aparicio et al., 2021b, Aparicio et al., 2021a).

3.6.5. Registration and calibration stages

Six fiducial screws distributed in the anterior maxilla and both tuberosity areas were used for the registration process (Al-Jarsha et al., 2024a), which was performed one time only. This was followed by the calibration of the handpiece drill axis (also one time) and then the drill length was calibrated multiple times according to the manufacturer instructions, as the clinician would do in the real clinical scenario involving a stepwise drilling process (ClaroNavInc., 2021). Based on a sample size calculation relying on results derived from an earlier pilot experiment, the length calibration step was repeated 27 times (9 repetitions for each of the three operators) to assess the reproducibility and identify the margin of error associated with this process.

3.6.6. Data collection

NaviDent® modified the software version 3.0.3 for us to provide the required transformation matrices resulting from the calibration in the form of Comma Separated Values (CSV) files. These files also included the x, y, z coordinates of the collar (entry) and apex points for each planned implant (i.e., 8 points of the 4 planned implants) in relation to the external frame of reference of the jaw tracker (Kovalevsky et al., 1989).

After a basic calibration training session, six drill variations and four implant variations (see figure 3-2) were calibrated 9 times by each of the three operators using the same 3D positional relationship between the trackers and camera. All operators had a previous experience in oral surgery (ranging from 2 to 5 years). Their ages ranged from 30 to 36 years.

Utilising the video screen capture feature in the NaviDent® software, the generated time-stamped CSV files were synchronised (i.e., matched) to the specific calibration instance executed and repeated by each operator.

The position of the dynamic navigation camera was maintained throughout the procedure, the handpiece position was firmly connected to the stationary robotic arm, and the jaw position was fixed in the dental simulator. The CSV files produced during the process were used for the analysis. This resulted in 9 CSV files per drill per operator providing 9 different TMs of every drill tip.

The reproducibility of the calibration TM was measured via the calculation of the distance between pre- and post-transformed points according to the following equation:

$$\text{Distance}_1 = \sqrt{(X_1 - X)^2 + (Y_1 - Y)^2 + (Z_1 - Z)^2}$$

where:

X,Y,Z represents point coordinates on the plan pre-transformation.

X_1,Y_1,Z_1 represents the point coordinates on the plan after transformation.

Distance_1 is the calculated distance for the 1st calibration process out of 27 per drill.

The results of these calculations were 9 distances per drill per operator for each of the entry and apex points of the 4 implants (8 points in the virtual plan).

The main outcome parameters were the range of variability in the calculated 3D distance (maximum distance minus minimum distance) and the absolute deviations from the mean value of that distance (assuming that this mean value represents the true drill tip or implant tip position).

3.6.7. Statistical Analysis

SPSS statistics (IBM SPSS, v.26) was used for statistical analysis. For each subset of data, distribution normality testing was carried out using the Shapiro-Wilk normality test. Intra- and inter-operator reliability in each calibration group was reported in terms of intra-class correlation coefficient (Koo and Li, 2016). Intra-operator reliability statistics were based on the 9 values per point (72 deviation values from 8 different means) per operator per drill. Inter-operator reliability statistics were based on the median values of both the deviations from the means as well as the variability ranges.

Correlation analysis was also performed with SPSS statistics software. GraphPad (Prism, v.9) was used to create the graphical representations.

3.7. Results

3.7.1. Descriptive statistics and normality testing

Shapiro-Wilk normality testing revealed non-normal distribution of the variability range and deviations from mean data from the 8 points on the plan per operator for each drill (n = 8). However, upon grouping all the values from drill calibrations of all the 3 operators, the variability of the data did follow the normal distribution. The outcome data derived from all of the three operators is shown in table 3-1.

Outcome (mm)	Tr. +Ext	SpSh.	SpSh. +Ext	SpL.	SpL. +Ext	TwL.	Im50	Im35 +Ext	Im40 +Ext	Im45 +Ext
All Op. Var. range (mean of 8 points)	1.620	1.758	0.875	0.695	**0.830**	0.915	2.776	2.740	2.246	2.223
All Op. AvDevM (mean of 8 points)	0.310	0.228	0.231	0.118	0.171	0.211	0.561	0.576	0.525	0.468
All Op. MaxDevM	1.894	2.255	0.767	0.670	0.494	0.635	2.066	2.080	1.592	1.612
Op.1 Var. range (med. of 8 points)	0.637	0.217	0.180	0.388	0.346	0.605	1.489	1.296	1.511	0.959
Op.1 AvDevM (med. of 8 points)	0.253	0.111	0.083	0.070	0.071	0.107	0.343	0.721	0.799	0.340
Op.1 MaxDevM	0.868	0.363	0.276	0.383	0.486	0.413	1.700	2.080	1.592	0.793
Op.2 Var. range (med. of 8 points)	1.440	1.744	0.567	0.612	0.444	0.422	1.966	1.705	1.073	1.949
Op.2 AvDevM (med. of 8 points)	0.465	0.321	0.364	0.117	0.094	0.138	0.675	0.433	0.745	0.697
Op.2 MaxDevM	1.894	2.255	0.767	0.670	0.494	0.553	2.066	1.628	1.519	1.612
Op.3 Var. range (med. of 8 points)	0.528	0.156	0.194	0.321	0.316	0.445	1.078	1.139	1.090	1.144
Op.3 AvDevM (med. of 8 points)	0.142	0.088	0.283	0.075	0.190	0.258	0.389	0.284	0.226	0.387
Op.3 MaxDevM	0.687	0.313	0.493	0.363	0.463	0.635	0.931	1.477	0.839	1.241

Table 3-1. Summary outcome data derived from drill calibration processes performed by all operators. med. = median; Op. = operator; Var. = variability; AvDevM = average deviation from mean; MaxDevM = maximum deviation from mean; Tr.+Ext = trephine drill with drill extension; SpSh. = short spade drill; SpSh.+Ext = short spade drill with drill extension; SpL. = long spade drill; SpL.+Ext = long spade drill with drill extension; TwL. = long twist drill; Im50 = 50 mm long implant; Im35+Ext = 35 mm long implant with drill extension; Im40+Ext = 40 mm long implant with drill extension; Im45+Ext = 45 mm long implant with drill extension.

In table 3-1, the discrepancies in the three precision parameters can be observed within each row affected by the drill being calibrated. The discrepancies between the three operators can also be noted via comparing the values of the same precision parameter in each column.

3.7.2. Reliability of the calibration method

The results of intra- and inter-operator reliability for the average of absolute deviations from the mean measurements are presented in table 3-2. There was a good inter-operator reliability in relation to variability range (ICC 0.755; $p < 0.0005$) and moderate reliabilities in relation to maximum deviations from means (ICC 0.665; $p = 0.007$) and average deviations from mean (ICC 0.711; $p = 0.006$). The intra-operator reliability values ranged from good to excellent ($p < 0.0005$).

Deviations from mean ICC within each operator (9 readings/operator)			ICC between all operators
Operator.1 (M.A.1)	Operator.2 (M.A.2)	Operator.3 (C.L.)	
0.931	0.796	0.758	0.711

Table 3-2. Intra- and inter-rater reliability in terms of inter class correlation coefficient (ICC) of the average of absolute deviations from the mean measurements (average from the 8 points).

3.7.3. The precision of the calibration process in relation to the measured variability range

Figure 3-4 shows the overall calibration reproducibility (attributed to machine and human sources). The apices of the planned left side zygomatic implants (points ALtA and PLtA) showed markedly higher variability. Also, with the exception of the short spade drill, all pointed drills variability ranges were < 1.0 mm while all implants variability ranges were > 2.0 mm.

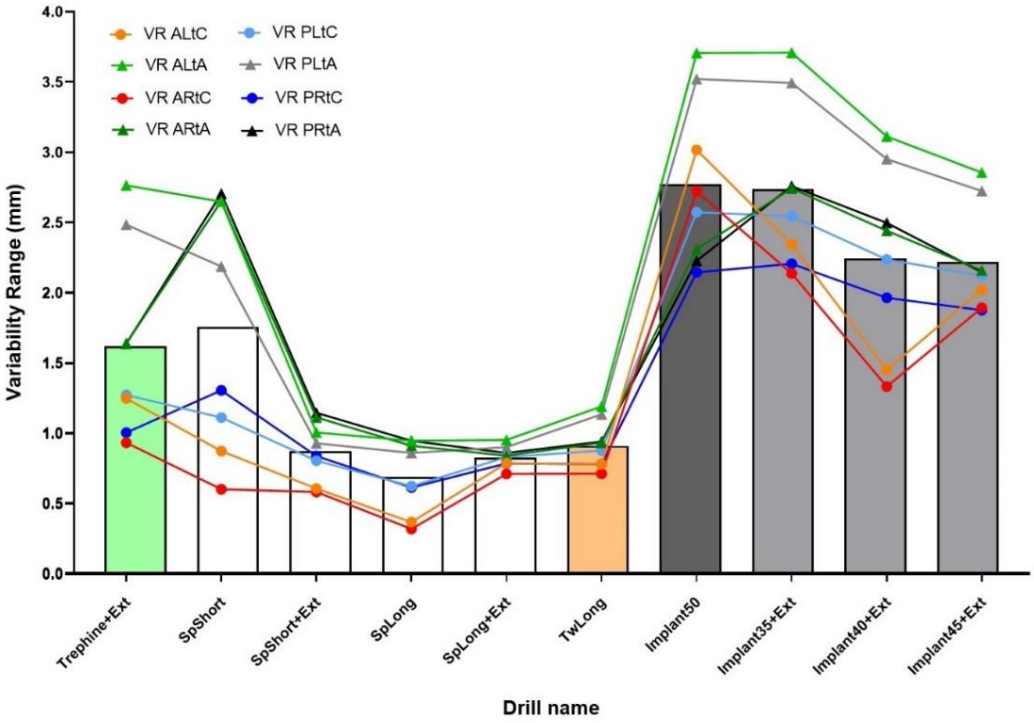

Figure 3-4. A combined line and bar graph showing the variability range of the 27 readings for each drill. Each line represents different point coordinates that were used for testing the reproducibility of the transformation matrix. Each bar represents the average of variability ranges from the 8 points. Trephine = trephine drill; SpShort = short spade drill; SpLong = long spade drill; TwLong = zygomatic twist drill (2.9Φ); Implant35 = zygomatic implant 35 mm long; +Ext = with added drill extension; VR = variability range; ALtC = anterior left implant collar point; PRtA = posterior right implant apex point.

3.7.4. Deviations from mean representing human calibration reproducibility

The data related to the human contribution to calibration precision are shown in figure 3-5. The 50 mm long zygomatic implant as well as the 35 mm long implant with added extensions showed maximum deviations > 2.0 mm. The unexpectedly high maximum deviation of the short spade drill could be an outlier value as it does not follow the same pattern of the average deviations line.

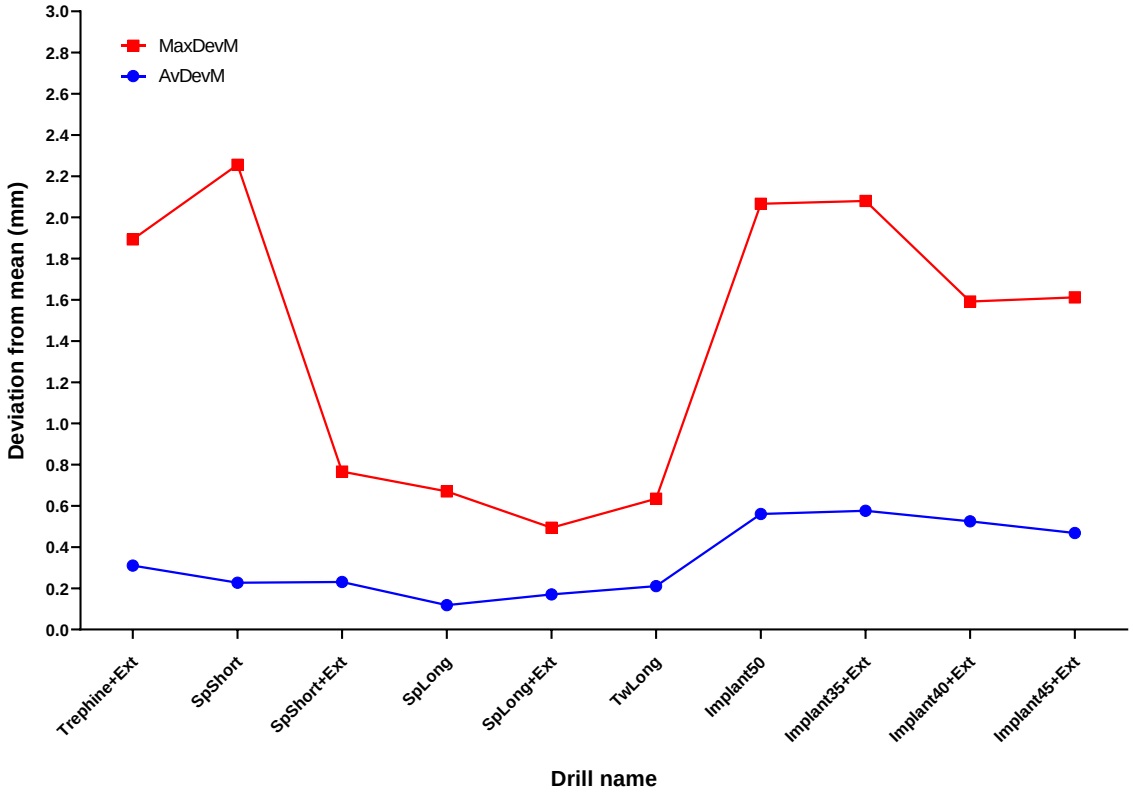

Figure 3-5. A line graph showing the deviations from mean obtained from the 27 readings for each drill. MaxDevM = Maximum deviation from mean; AvDevM = Average deviation from mean (average from 27 readings per point then mean of the 8 points). Trephine = trephine drill; SpShort = short spade drill; SpLong = long spade drill; TwLong = zygomatic twist drill (2.9Φ); Implant35 = zygomatic implant 35 mm long; +Ext = with added drill extension.

3.7.5. Relationship to drill length and shape

The results of the Pearson's correlation analysis in relation to variability range, maximum deviation from mean and average deviation from mean demonstrated no significant correlation except the strong correlation between the implant length and the reproducibility in terms of average deviations from the mean ($p < 0.05$). These are presented in table 3-3.

Drill Type	Variability Range		MaxDevM		AvDevM	
	Coefficient	P value	Coefficient	P value	Coefficient	P value
Pointed drill	-0.608491	0.276143	-0.734819	0.157242	-0.214022	0.729593
Implant	-0.919357	0.080643	-0.892595	0.107405	-0.986725	**0.013275**

Table 3-3. Correlation coefficients to test the presence of linear correlation between the drill or implant length and the resulting reproducibility parameter. The tests included the five pointed drill variations and the four implant variations. MaxDevM = Maximum deviation from mean; AvDevM = Average deviation from mean.

Figure 3-6 shows the negative linear trends of the three tested reproducibility parameters against the implant length as well as the pointed drill length. In other words, the longer the drill, the less is the error. Therefore, the longer the drill the higher is the precision.

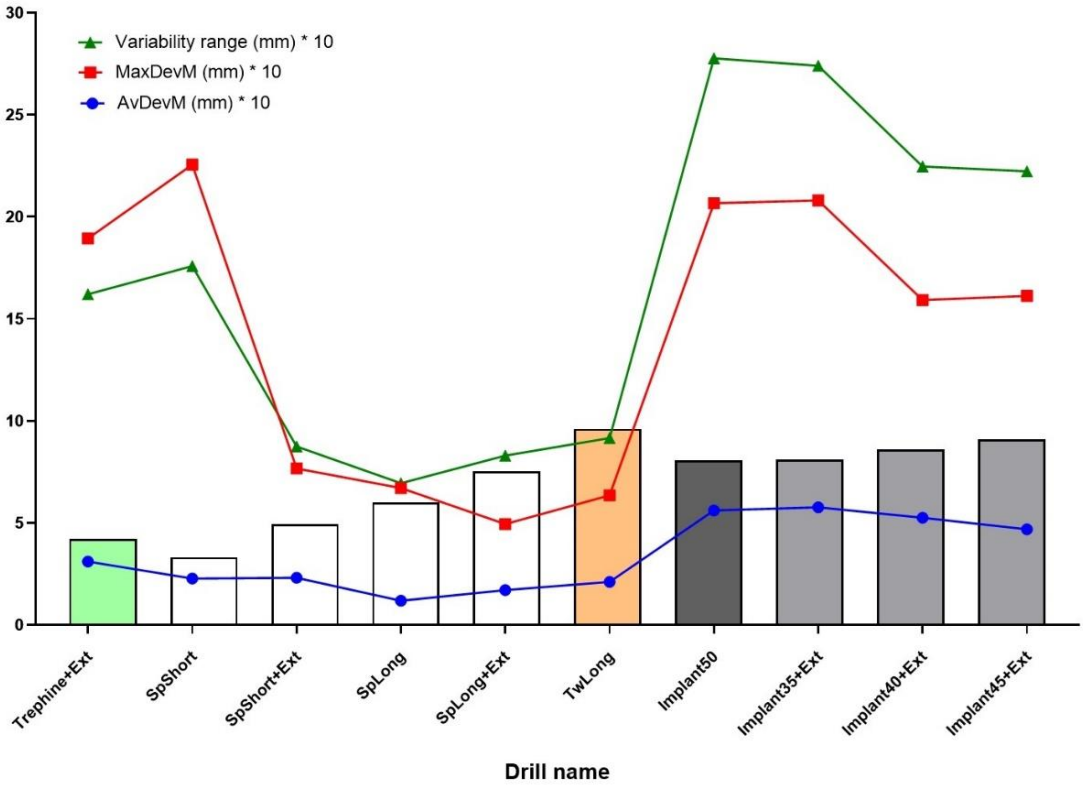

Figure 3-6. A combined line and bar graph depicting the association between drill or implant length (in cm) (the height of each bar) and the 3 reproducibility parameters (the 3 parameters were scaled to match the length bars). AvDevM = Average deviation from mean; MaxDevM = Maximum deviation from mean; Trephine = trephine drill; SpShort = short spade drill; SpLong = long spade drill; TwLong = zygomatic twist drill (2.9Φ); Implant35 = zygomatic implant 35 mm long; +Ext = with added drill extension.

3.8. Discussion

Dynamic navigation systems offer an alternative to surgical guides for implant placement with clinically acceptable outcomes (Bhalerao et al., 2023, Fan et al., 2023, Bhalerao et al., 2024). As with all other guiding techniques, they have inherent sources of positional errors which may detrimentally affect the final results (Al-Jarsha et al., 2024a, Widmann et al., 2009), particularly if the total error exceeds the accepted 2 mm safety margin (Bagheri et al., 2020).

Accurate calibration to record the relationship between the drill and the centroid of the handpiece tracker is directly dependant on the degree of the operator's precision (human factor) (ClaroNavInc., 2021). It may also depend, to a lesser extent, on the factors affecting the machine capture of this mathematic spatial relationship as well as the integrity of the handpiece-drill griping mechanism. The accuracy of the machine capture depends on the surrounding light conditions, the quality of the tracking camera, and the calibration algorithm (Wiles et al., 2004).

With all dental navigation systems, clinicians perform drill calibration in two steps; initial drill axis calibration and subsequent drill length calibration. The length calibration step is readopted with each drill used for bone cutting and for placement of the implants (ClaroNavInc., 2021, X-NavTechnologiesLLC, 2020, Stefanelli et al., 2020a). In NaviDent®, the drill length calibration step also applies a minor correction to the initially recorded axis to compensate for the play in the chuck of the handpiece (ClaroNavInc., 2021).

Having performed a jaw registration process, the clinicians are subsequently required to check the accuracy of drill calibration depending on that registration (ClaroNavInc., 2021, X-NavTechnologiesLLC, 2020, Stefanelli et al., 2020a, Wu and Sun, 2024). Therefore, the only way for the operator to check the calibration accuracy separately (from registration accuracy) is to have access to the internally generated data by the tracking equipment. NaviDent® provided our research team with a modified software version in which this data can be exported as time-stamped CSV files. This enabled the authors to assess the reproducibility of the drill calibration process independently. However, to be able to objectively quantify the magnitude of error arising from this source, one would require a gold standard measurement (e.g., with a laser tracker) to be used as a yardstick for comparison, which was not technically possible in this study (Sin et al., 2023, Nasab, 2019). As an available simple alternative, we calculated the reproducibility variables of the repeated calibration process as references to assess the relative precision of this procedure (Gallagher, 1990, Snijders et al., 2017).

We fixed the spatial relationship between the trackers and the camera in a rigid manner according to the recommended optimal distance (about 50 cm) to minimise the effect of machine factors on the calibration process (ClaroNavInc., 2021). Subsequently, the operator held the calibrator tool against the drill tip using the non-dominant hand to simulate the clinical scenario (ClaroNavInc., 2021).

The mean of the calculated distances derived from the TMs of the repeated calibrations of each specific drill has no meaningful value in itself. However, the absolute deviations from the mean distances were interpreted as the human error in the reproducibility of the calibration process.

The good intra- and inter-operator reliability figures support the stability of the tracking system and the adequate training of the three operators in performing this step. However, the wide range of the reliabilities (from good to excellent) can be explained by the difference in the level of experience in performing this step specifically. Operator no.1 (M.A.1) showed excellent intra-operator reliability due to his longer experience in using dynamic navigation.

The variations observed with the calibration of the same drill or implant group are attributed to mathematical error during the application of the transformation matrix to the coordinates of the points. These wide ranges of variability also highlight the importance of the accuracy checking process after calibration and prior to commencing the surgical procedure (Stefanelli et al., 2020a).

In contrary to the good level of inter-operator reliability associated with the variability range, the moderate level of reliability observed in the magnitude and pattern of deviations from the mean values supports that this latter outcome measure is more related to the human contribution rather than any other confounding factors. The degree of precision and focus in placing the tip in its accurate position on the calibrator tool could well be different for another operator performing the same repetitive procedure.

This is also supported by the migration from the normal distribution when the outcome measures from all 3 operators were combined, as opposed to looking at the same outcome measures for each operator separately. The same reasoning could explain the high outlier value of the short spade drill with operator no.2., as it was the first drill to be calibrated after the training session. The drill might have been loose inside the handpiece or the tip of the drill might have not been stable inside the designated calibration point on the calibrator tool.

Increasing the length of the drill or implant can improve the reproducibility of the calibration transformation matrix. This could be due to the rotation component of the matrix, as longer drills have more chance of reproducing the same rotational transformation relationship between the two frames of reference. In addition, the capture of the calibration spatial relationship is more accurate if recorded over longer distances. The flat tips of the implants and their susceptibility to "wobble" due to their loose non-locking connection within the implant adapter produced larger error ranges and deviations from the mean values.

In summary, calibration reproducibility error is small on average (< 0.6 mm). However, its maximum value could exceed the 2 mm safety margin that is usually included in the implant planning process. It could thus be implicated in causing damage to the vital structures surrounding the apex of a drill and/or implant. The secure connection of a drill extension does not seem to compromise the calibration process. However, non-locking implant adapters present serious calibration accuracy issues. Increasing the length of the drill or implant (as long as it remains relatively non-flexible) appear to enhance the reproducibility of the calibration transformation matrix.

Future studies may include wider variations of drills and implants to detect statistically significant linear correlation with the drill length and shape.

The main limitation of this study is the lack of a gold standard yardstick to locate the true drill tip position to identify the accuracy of the calibration rather than just its precision (Gallagher, 1990). It was difficult to compare our results with previously published studies because none of them had assessed the precision or accuracy of the calibration step on its own. They all measured deviations in implant placement which combines application error, registration error as well as the tracking errors of the dynamic navigation system (Widmann et al., 2009, Wu and Sun, 2024).

3.9. Conclusions

The positional variation arising from the drill calibration step is expected to be small in general (< 0.6 mm), but it could be up to 3.7 mm. Therefore, we emphasise the importance of following the standard accuracy checks as described by the manufacturer.

The precision of calibration is affected by the shape of the drill tip (i.e., whether it is pointed or flat) and whether the drill is composed of loosely connected pieces or not. Therefore, the operator needs to carefully perform this step especially for long implants and short drills that don't have sharp tips. Hand stability during calibration capture by the optical camera has a crucial effect on minimising this source of error. Consistently unacceptable results of the standard accuracy checks could be related to insufficient operator training or disfunction of the handpiece chuck that necessitates maintenance or replacement.

3.10. Chapter Appendix

The key concept of this chapter was the assessment of the precision (or reproducibility) of a particular drill tip position without knowing the true position of that tip using another more accurate method. The drill calibration algorithm incorporated in the dynamic navigation system is expected to be reproducible within a particular margin of error from the true tip position, and that the 3D volume of positions resulting from the tip calibration algorithm must contain the true position of the tip. Otherwise, the quality control measures applied by the manufacturer for selecting their drill calibration algorithm and method would have to be questioned.

The drill calibration algorithm produces a spatial relationship between the frames of references of the drill and the handpiece tracker in the form of a transformation matrix (TM). This allows the dynamic navigation camera to infer the orientation of the drill and its tip position from the position and orientation of the handpiece tracker. TM can also be looked at as seeing the same point from two different perspectives. The drill tip will have the coordinates of (0,0,0) form the perspective of the drill tip frame and that same point will have (x,y,z) coordinates from the perspective of the handpiece tracker frame. Therefore, one would expect that repeating the calibration process for the same drill would produce x,y,z coordinates that have smaller range of variability as the process becomes more precise.

We elected to test the variability range and the other two reproducibility parameters based on the distance between the pre- and post- transformed points. That is $\sqrt{(x-0)^2+(y-0)^2+(z-0)^2}$ in the above example point.

However, selecting the (0,0,0) point would have ignored testing the rotation component of the TM (the outcome of that component will always equal to zero when selecting the 0,0,0 point). The alterative was selecting the coordinates of the target points of interest, which were represented by the entry and exit points of the implants in the frame of reference of the jaw tracker.

Chapter 4

Development of the integrated robotic system

4.1. Preface

This chapter describes the series of processes involved in methods optimisation and development of components necessary for the integration between the robotic system and the dynamic navigation system.

The testing of the possible methods for optimisation was mostly conducted in a sequence of one-time experiments. Therefore, it was not possible to present detailed statistical analyses for the results of these tests.

Section 4.2 provides the justification and optimisation of using software to extract coordinates from the STL files of the implant plan, and also for the purpose of evaluation of deviation directionality after the placement of the actual implants. This section also presents a basic definition of the rigid transformation matrix and explains the need for planning more than the required number of implants in the plan in order to get a more accurate transformation matrix necessary for the subsequent steps.

Section 4.3 describes the details of developing the link between the robotic system coordinates and the dynamic navigation system coordinates. The first two methods had inaccurate results while the last two methods achieved acceptable accuracy. The hand-eye calibration method was the most straightforward as it did not require to disconnect and reconnect components to the robotic arm after establishing the link, which further contributed to its accuracy.

Section 4.4 demonstrates the requirement for the design and fabrication of custom hardware components via 3D printing which were necessary for the integration of the two systems.

Section 4.5 explains the steps involved in establishing the optimum spatial relationship between the robotic arm and the dental simulator so that the arm can reach the operative site without compromising the line-of-sight of the dynamic navigation camera.

Section 4.6 highlights the difficulty behind achieving a precise robotic procedure if the site of the operation was in a state of non-trackable movement. Therefore, it justifies performing all of subsequent development testing while the dental simulator containing the jaw model is in a stationary position in relation to the robotic arm.

Section 4.7 describes the necessity and the hardware components of an automatic switch off mechanism that was used during the robotic procedure.

Section 4.8 explains the rationale behind electing to choose an alternative simplified process for drill calibration in the dynamic navigation system.

Finally, section 4.9 describes the optimisation process for the drilling protocol in the zygomatic implant placement procedure. A trial was made in an effort to reduce the total operative time via omitting five out of the ten drilling steps. However, that did not result in better accuracy and unduly overloaded the hardware of the implant handpiece. A slight modification was therefore applied to the manufacturer-outlined drilling protocol and the same conventional number of stages were implemented to protect the implant handpiece. This modification was through preparing the alveolar part in full before advancing to the deeper portion of the zygomatic implant osteotomy.

4.2. Optimisation of coordinate extraction

4.2.1. Extraction of the entry and exit points coordinates from the exported dental implant plan (from the STL files)

The plan for any dental implant trajectory is calculated based on the 3D coordinates of two points only; entry and exit (also known as collar and apex, respectively). The vector (line) connecting these two points in space represents the direction of insertion and is an important parameter for the drilling and implant placement processes.

Several clinician-oriented commercial software packages are available on the market for the evaluation of any deviation of the placed implant from the planned implant trajectory (figure 4-1). The evaluation feature is usually incorporated in the implant planning software (e.g., the treatment evaluation component of coDiagnostiX® and the EvaluNav component of NaviDent® software).

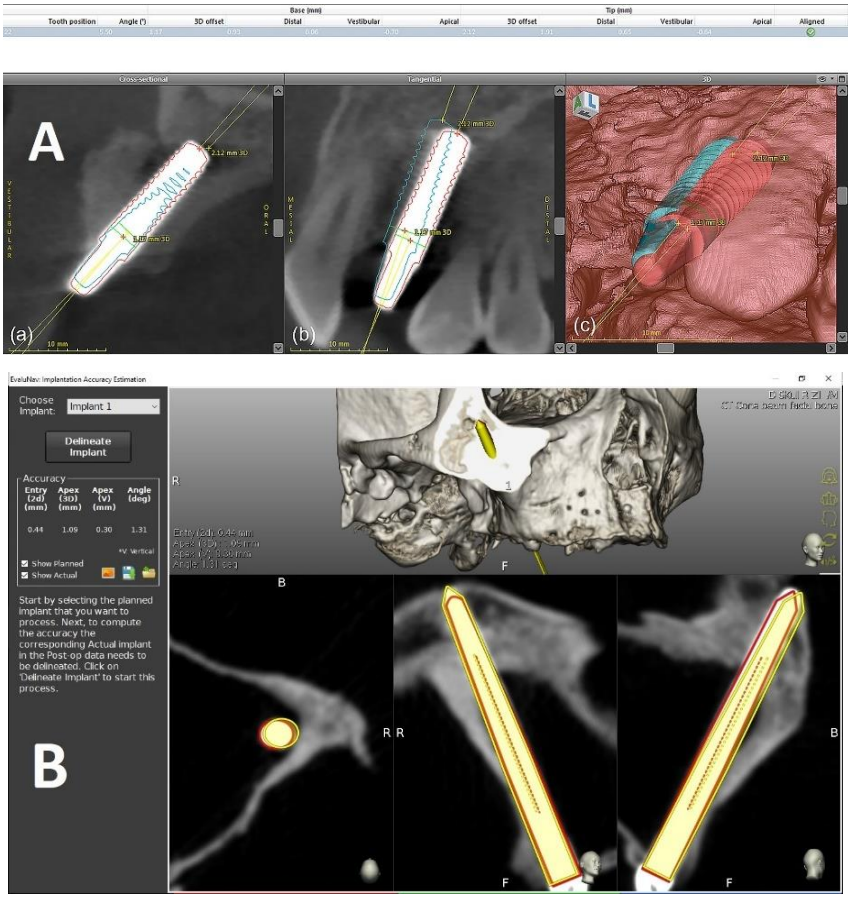

Figure 4-1. Commercial implant accuracy evaluation software. (A) coDiagnostiX® - treatment evaluation feature (Suksod et al., 2020) © 2020 Suksod et al. CCAL license (B) NaviDent®, EvaluNav software package. Both look mainly at 3D deviations, with the other 2D deviations related to either the CBCT axes or the axes of the specific implant being evaluated.

The axes' orientation of the imported CBCT into the planning software will solely depend on the orientation of the jaw during the CBCT scan. Therefore, different cases would have slightly different axes' orientation, even with careful positioning at the time of CBCT scan. CoDiagnostiX® planning software provides detailed information for deviations and has been utilised in previous studies (Kaewsiri et al., 2019, Smitkarn et al., 2019). However, the user is unable to modify the axes' orientation that was locked during the CBCT scan (also known as the coordinates frame of the CBCT). Therefore, it difficult to standardise accuracy comparisons between different cases in relation to deviation directions. EvaluNav - in version 3.0.3 - provides overall 3D deviation parameters and has the same issue of inability to standardise the position of the axes for matched comparisons of deviation directions.

As a result, recent literature is relying on more generalist but sophisticated software (e.g., Mimics® and Geomagic®) to enable the user to unify the axes (position/orientation) of different CBCT scans. After superimposing the postoperative over the preoperative CBCT scan, the planned and actual implant trajectories can be exported in the form of STL files (a common file format to represent 3D objects). The STL files for a particular case can then be moved together in the 3D space to have the axes' position and orientation in relation to its anatomical features rather than in relation to the CBCT scanning orientation. This is then followed by the extraction of the 3D coordinates for entry and exit points from the STL files (Lin et al., 2021, Vinci et al., 2020). Distance and angular deviation calculation equations are then executed upon these coordinates to have detailed 3D and 2D deviation figures with identical meaningful comparisons (Pellegrino et al., 2020b, Sittikornpaiboon et al., 2021, Abduo and Lau, 2021).

In this section, the reliability and reproducibility of Geomagic® software in extracting coordinates were tested against a general-purpose STL manipulation software. The software, Autodesk MeshMixer (v. 3.5.474 available from https://www.meshmixer.com), served as a control in testing Geomagic Design X® (v. 2020.0.3), which has previously been used in the literature for this purpose (Vinci et al., 2020, Abduo and Lau, 2021).

Extraction reliability checks were possible through comparisons between the expected 3D lengths of the implants (from the planning process) against those which were calculated from the extracted coordinates in the tested software (table 4-1).

The reproducibility of 3D lengths was tested via changing the planned implant diameter in the original plan (without moving its position) plus changing the position/orientation of the axes to a standardised position, in which each axis had a meaningful direction in relation to the anatomy (table 4-1).

Software + settings	Calculated 3D length from extracted coordinates of the centre of the circle of the collar (x_1, y_1, z_1) and the apex point (x_2, y_2, z_2)	Planned (expected) 3D length
Planned implant cone (4.3 mm) **+ MeshMixer**	44.99999222	45
Planned implant cone (4.3 mm) **+ GeoMagic (no removal of outliers)**	45.00002694	45
Planned implant cone (4.3 mm) **+ GeoMagic (fixed radius 2.15 mm)**	44.99999830	45
Planned implant cone (1 mm) + adjusted axes **+ MeshMixer**	45.00000440	45
Planned implant cone (1 mm) + adjusted axes **+ GeoMagic (no removal of outliers)**	45.00000521	45
Planned implant cone (1 mm) + adjusted axes **+ GeoMagic (fixed radius 0.5 mm)**	45.00000190	45

Table 4-1. Coordinate extraction optimisation. Top 3 rows: comparing 3 methods using the default implant diameter. Bottom 3 rows: comparing the same 3 methods after adjusting the implant diameter to 1 mm and changing the position/orientation of the axes to a standardised position. The 3D length = $\sqrt{(x_1 - x_2)^2 + (y_1 - y_2)^2 + (z_1 - z_2)^2}$.

Table 4-1 demonstrates that reducing the implant diameter from 4.3 to 1 mm had improve the accuracy of manually landmarking the centre of the circle in the implant collar (7.78×10^{-6} mm versus 4.40×10^{-6} mm difference form the expected implant length). The best settings for extracting coordinates are GeoMagic, 4.3 mm diameter, fixed radius 2.15 mm (1.70×10^{-6} mm difference from the expected implant length).

In MeshMixer, the coordinates were determined through a repeated manual landmarking technique - checking the calculated implant length each time until lengths close to the expected were obtained – table 4-1 and figure 4-2. Four to five attempts (i.e., mouse clicks) were required for each point.

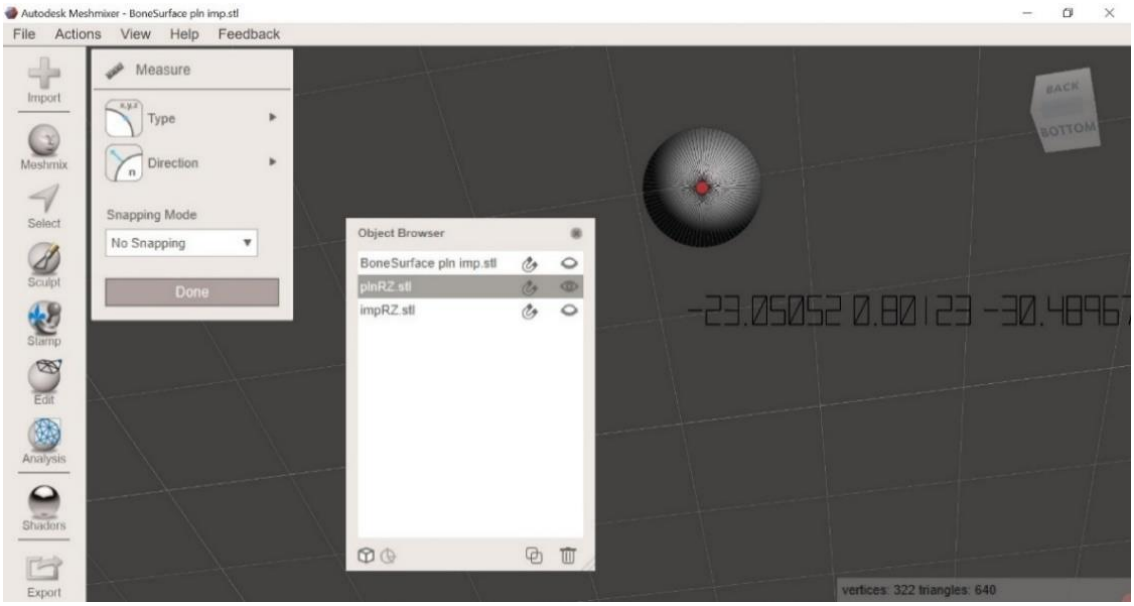

Figure 4-2. Coordinate extraction using MeshMixer. The coordinates for the centre of the implant collar (entry point) as well as those for the apex (exit point) were never 100% reproducible due to manual landmarking on the screen. The smaller the diameter of the implant, the less was the error margin in reproducing the coordinates. The software displays measurement data until the 5th decimal place of a mm.

In GeoMagic®, a built-in algorithm is available for the automatic determination of a centre of a circle. This algorithm was tested with four different settings (with and without removal of outliers, with and without activating a fixed radius) and the extraction was 100% reproducible within each setting (figure 4-3).

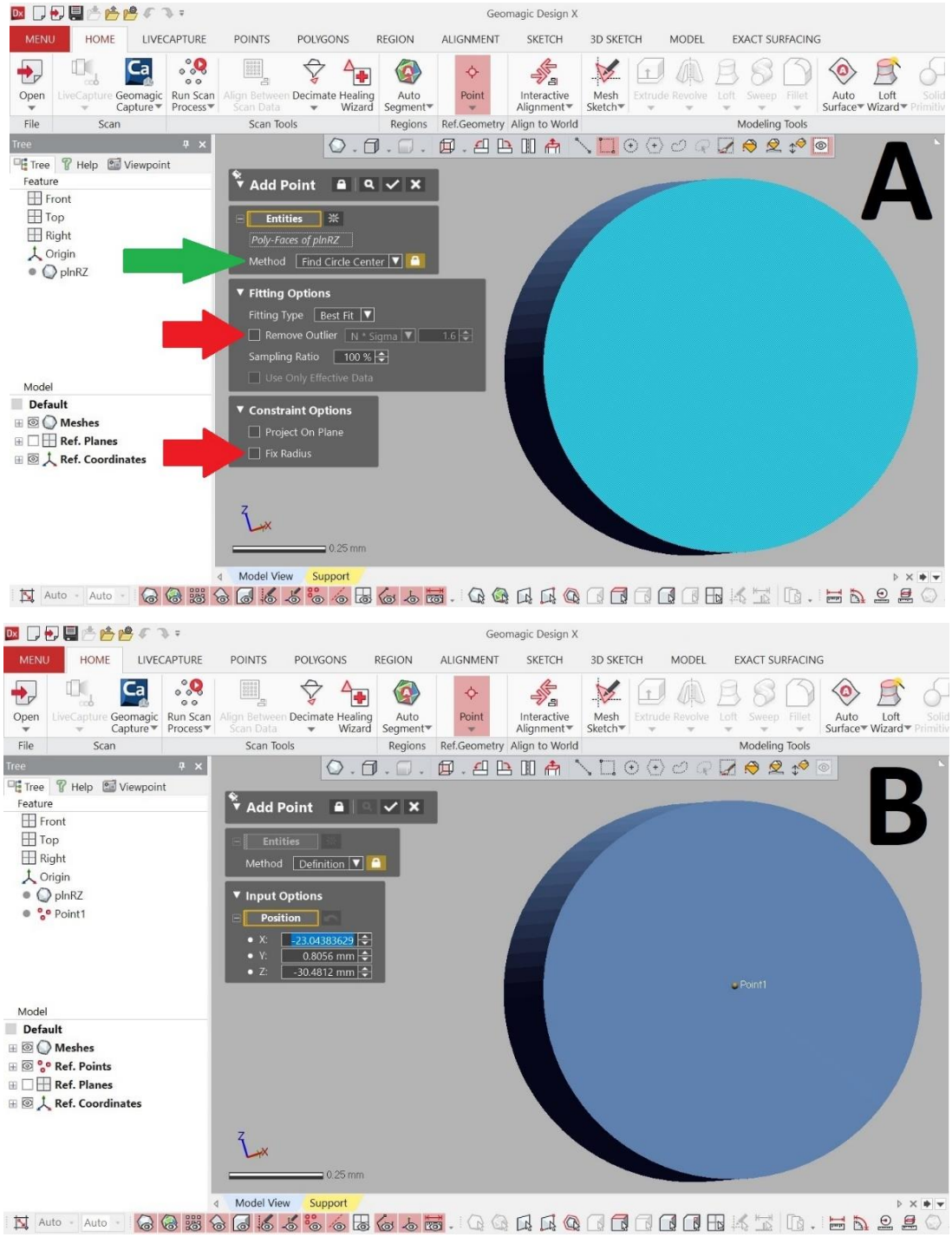

Figure 4-3. Coordinate extraction using GeoMagic. (A): Find Circle Center algorithm settings. After settings selection (arrows), the user selects any area on the flat circle surface and the algorithm will automatically detects the edge of the entire circle and calculates the coordinates of its centre based on the selected settings. (B): Definition of point coordinates for extraction. The coordinates for the centre of the implant collar (entry point) were 100% reproducible up to 12 decimal places of a mm (when using copy/paste function, the displayed number of decimals becomes 12).

The comparison results between 1 mm against the 3.4 mm implant diameter extraction using GeoMagic® software were further confirmed with another test for a ZI plan containing 8 implants (4 ZIs and 4 registration implants). The results are shown in table 4-2.

GeoMagic Software settings	Mean Error (mm)	Minimum Error (mm)	Maximum Error (mm)
Planned implant cone (3.4 mm) **+ no removal of outliers + no fixed radius**	2.60135E-05	1.77823E-05	3.05255E-05
Planned implant cone (3.4 mm) **+ removal of outliers + no fixed radius**	6.79794E-06	**8.31553E-07**	1.42536E-05
Planned implant cone (3.4 mm) **+ removal of outliers + fixed radius (1.7 mm)**	**6.66734E-06**	9.33975E-07	**1.40465E-05**
Planned implant cone (3.4 mm) **+ no removal of outliers + fixed radius (1.7 mm)**	0.001646788	0.000158427	0.002279765
Planned implant cone (1.0 mm) **+ no removal of outliers + no fixed radius**	**3.56432E-06**	**9.12282E-07**	**7.27053E-06**
Planned implant cone (1.0 mm) **+ removal of outliers + no fixed radius**	4.95043E-06	2.08915E-06	8.59243E-06
Planned implant cone (1.0 mm) **+ removal of outliers + fixed radius (0.5 mm)**	5.03645E-06	2.22981E-06	8.74423E-06
Planned implant cone (1.0 mm) **+ no removal of outliers + fixed radius (0.5 mm)**	0.000457884	2.8656E-05	0.001382211

Table 4-2. Error margin for coordinate extraction using GeoMagic® software (based on expected implant lengths). The margin is small for both the 1 mm and the 3.4 mm plans. The selected optimum settings are in the 3rd row, which is highlighted in light green colour.

Based on the results described above, the following steps were finally implemented to get the coordinates of the entry and exit points from the exported STL files:

1. The plan data were exported from the NaviDent® software as STL files which all had a common coordinates frame (software default based on the pre-operative CBCT). The STL files representing the implant cones and the external anatomy were then merged into a single STL file using MeshMixer software (https://www.meshmixer.com).

2. The coordinates of the plan were extracted using GeoMagic Design X® software from all the separated STL files of implant cones, with settings to remove outliers and a fixed radius (the apex was presented as a single point while the platform was a 3.4 mm diameter circle).

These coordinates were used as input to calculate the transformation matrix between the frame of reference of the pre-operative CBCT and that of NaviDent® jaw tracker after the registration process.

3. After obtaining the post-operative scan, this was imported into the NaviDent® software. EvaluNav was then used to superimpose the post-operative scan over the pre-operative scan containing the plan, following the software user manual instructions (figure 4-4).

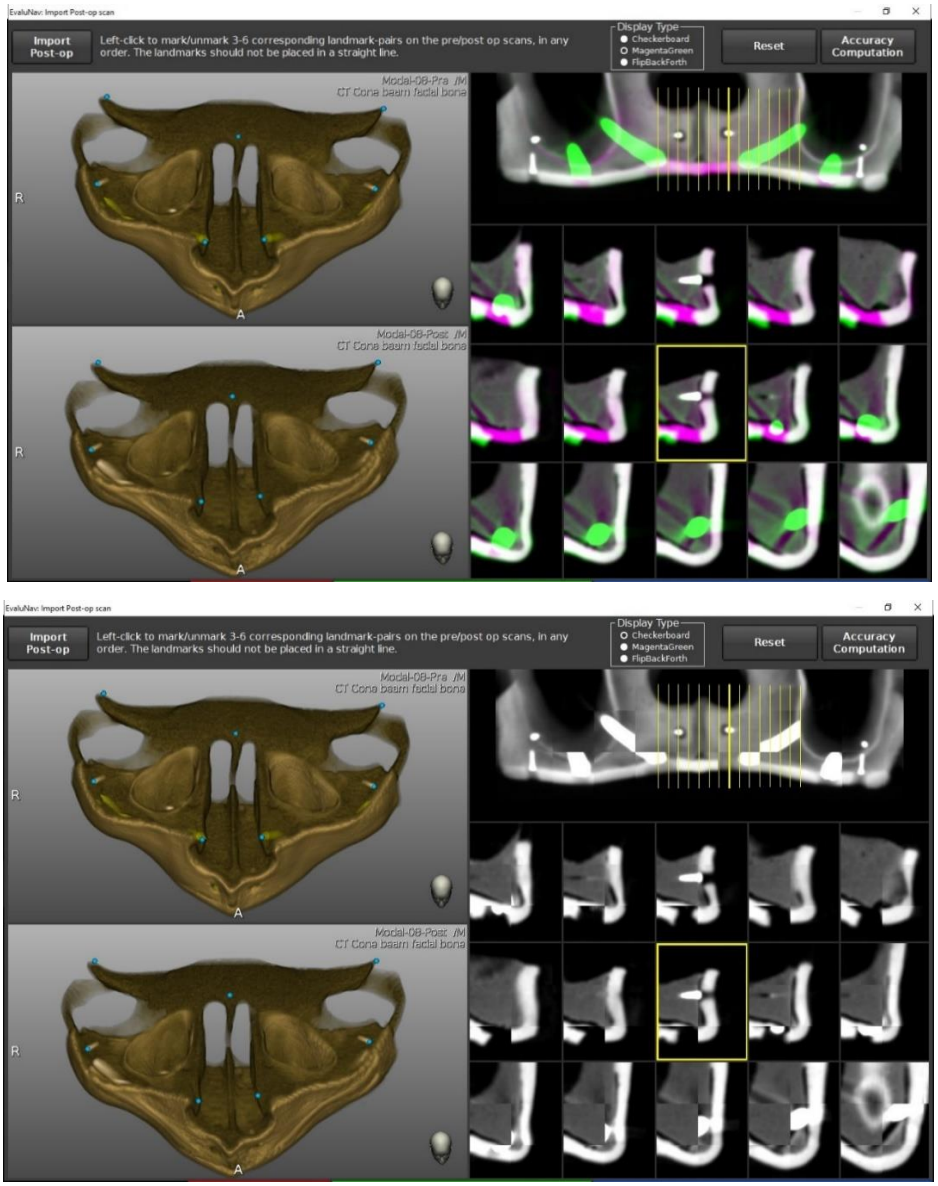

Figure 4-4. Using EvaluNav CBCT superimposition after matching the maximum number of 8 well-distributed points between the two scans. The quality of this superimposition had to be judged visually via using the MagentaGreen colour contrast theme and the checkerboard view shown in the figure. According to the manufacturer, the iterative closest point algorithm in EvaluNav is based on voxel-to-voxel matching (i.e., volume-based rather than surface-based superimposition algorithm).

4. EvaluNav automatically detected the margins of the real implant in the post-operative scan through an algorithm based on the abrupt contrast change at the implant borders with the surrounding material, and according to the shape and dimensions of that implant as provided in the pre-operative plan. This detection of actual implant borders is highly reproducible (figure 4-5). The reproducibility ranges were ± 0.06 mm and ± 0.11° for the distance and angular deviations, respectively.

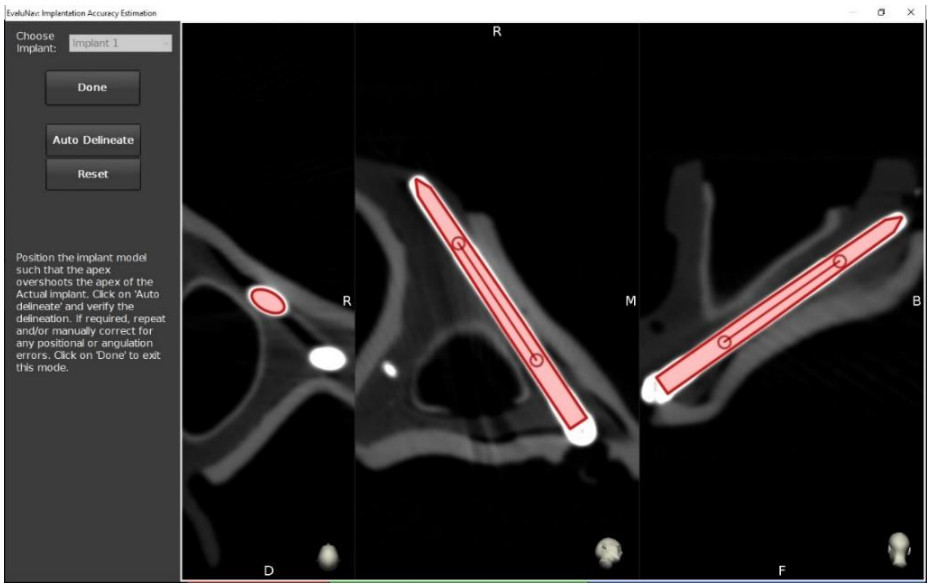

Figure 4-5. EvaluNav contrast-based superimposition of an implant cone over the real implant in the post-operative scan. The reproducibility of this superimposition was tested by delineating the red implant cone to the real implant using the automatic function five times and recording the implant deviations each time, followed by calculations of ranges in these distance and angular deviation values.

5. Initial 3D deviation data was then obtained in EvaluNav (figure 4-6).

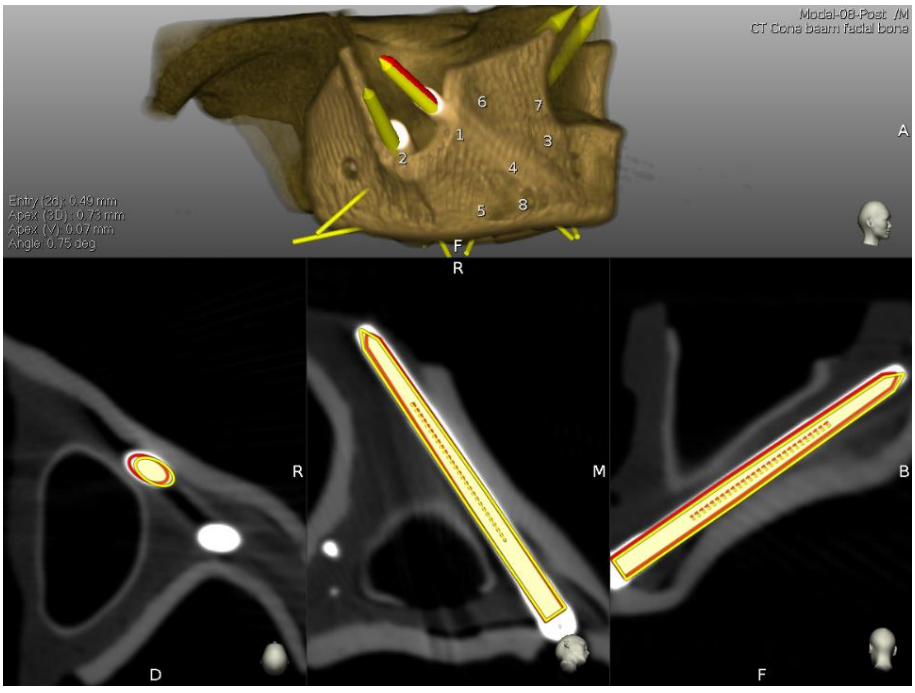

Figure 4-6. EvaluNav provides summary deviation data (mainly 3D deviations).

The 2D deviations provided by EvaluNav are in the coordinates frame of the actual implant cone (EvaluNav uses the actual implant long axis as the z axis so as to measure the vertical apex deviation and uses the x/y plane in the same frame to measure the entry 2D deviation).

6. To obtain more information regarding the direction of the deviations, the separated STL files representing the real post-operative implant positions were exported in the pre-operative coordinate frame. This allows coordinate extraction from these cones using the favourable settings highlighted in table 4-2 on page 111.

7. The exported and merged copy of the STL file was adjusted to a standardised coordinate frame for future comparisons of deviation directions. This adjustment was achieved with the MeshLab software (https://www.meshlab.net) for the first model STL file. MeshMixer software (https://www.meshmixer.com) was subsequently used to superimpose the other exported models over the outer shell of the first standardised model (figure 4-7).

   The merged file was then separated into shells to isolate the implant shapes only, now having the new standardised coordinate frame (figure 4-7).

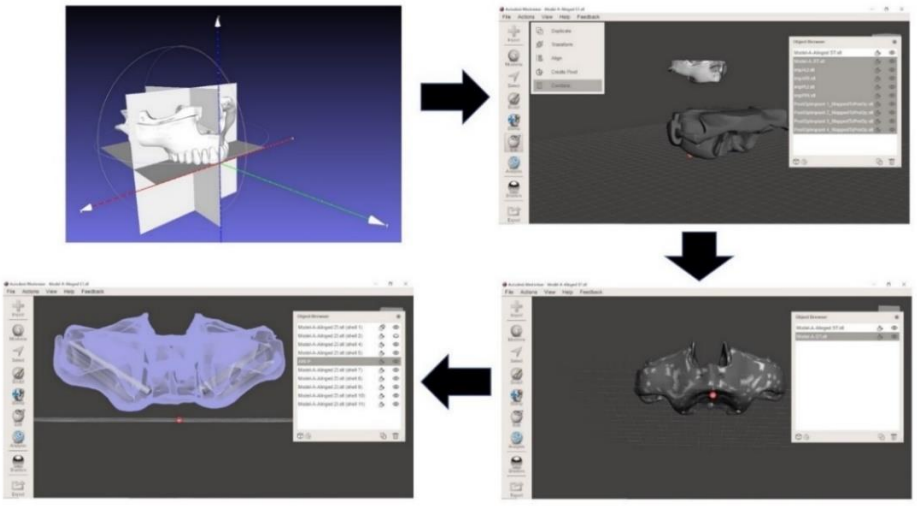

Figure 4-7. Adjusting the position/orientation of the axes with MeshLab based on the occlusal plane to create the standardised coordinates frame of reference (top left). The standardised position and orientation of axes after adjustment have identical directions for all study models and allow meaningful interpretation of the x, y and z dimensions (x = right direction, y = anterior direction, z = superior direction). The other three screenshots show the superimposition steps with Autodesk MeshMixer to bring the exported planned and post-operative implant cones to the standardised frame of reference without changing their spatial relationships to each other.

8. The coordinates were then extracted from each implant cone using GeoMagic® software (figure 4-3), using the optimised favourable settings provided in table 4-2 (removal of outliers and a fixed radius of 1.7 mm).

4.2.2. Optimising the minimum number of implants to achieve an acceptable transformation matrix for implant coordinates

A transformation matrix (TM) is a method used to express the relationship between two coordinates frames. It includes the required information to translate and rotate any particular point from one frame to the other (Gentle, 2024). One method for calculating a TM involves the input of at least three points' coordinates that have matched movements in the two frames (https://github.com/nghiaho12/rigid_transform_3D).

Testing a variable number of matching points for the implant coordinates transformation process revealed that a geometric margin of error is always present. This margin of error was reduced by increasing the number of matching points (between the STL coordinates frame and the NaviDent®-derived coordinates frame obtained after the registration process). The accuracy of reproducing the implant 3D coordinates was used to reflect this geometric error margin (figure 4-8).

NaviDent® coordinates with matched extracted STL coordinates produce a transformation matrix. The TM was produced four different times from 8, 12, 16 and 24 matching points.

These TMs were then tested individually to re-produce new NaviDent® coordinates:

Extracted STL coordinates $\xrightarrow{TM}$ New NaviDent® coordinates.

The margin of error was subsequently calculated as follows:

Margin of error = Absolute difference between the new NaviDent® coordinates and those original Navident® coordinates of the same 8 points representing the 4 zygomatic implants.

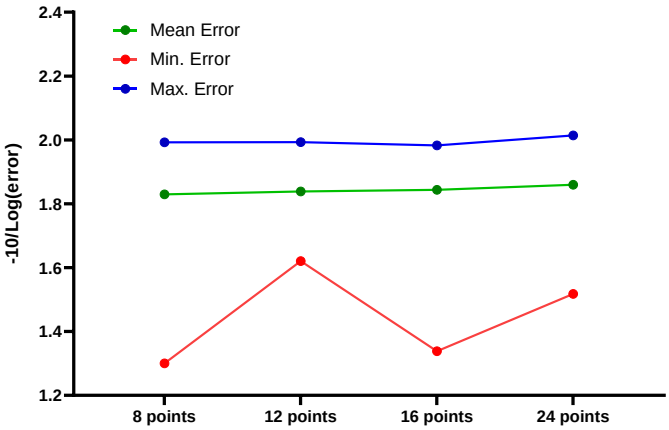

Figure 4-8. Geometric error margin (in terms of -10/Log) arising from the algorithm calculating the rigid transformation given a set of matching points in the two coordinates frames (https://github.com/nghiaho12/rigid_transform_3D). Using 12, 8, 6 and 4 planned implants (the x axis). The lowest minimum and maximum errors were associated with 8 implants (i.e., 16 points).

An optimum number of 16 points (8 implants) distributed in the model volume were enough to have a low maximum error of 7.36324 x 10^{-6} mm (-10/Log = 1.95). This means that additional planned implants that would only be required for registration purposes should be included in the plan STL file until the final number of implants reaches 8 (i.e., 16 matching points).

4.3. Transforming to robotic coordinates

The basic compontents of the robotic arm used in this study are depicted in figure 4-9. It is a 6 DOF robotic arm with 6 rotating joints, with a reach of 500 mm and pose repeatability of ± 0.03 mm. The jonits of the base, shoulder, elbow, and the three wrist joints all have ± 360° ranges.

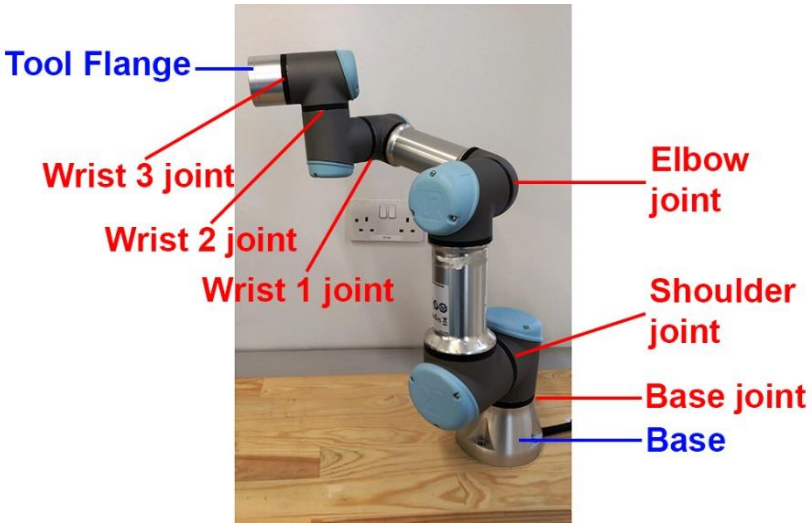

Figure 4-9. The robotic arm (UR3e) used in the project. The six joints marked with red link the base to the tool flange. The end effector is the free end that has the tool flange.

4.3.1. Transforming to robotic coordinates via OptiTrack

The initial testing stages involved establishing a TM between the dental plan coordinates (extracted from the plan STL file) and the robotic system coordinates frame. The optical tracking system OptiTrack Prime^{x} 13 with 5 tracking cameras was utilised to be an intermediate transfer component.

The calibration of OptiTrack to robotic coordinates relied on a 2-step process (figure 4-10; B and C). Dental plan (STL) to Optitrack coordinates transformation followed a “tactile registration” process. It involved securing the dental model position in relation to the base of the robotic arm and then passively moving the previously calibrated assembly of the robotic arm-drill tip to touch surface points on the model.

The software interface would then record the coordinates of the drill tip from the OptiTrack calibrated robotic system as a matching point to the touched surface point coordinates in the STL file of the dental plan. The tactile registration process was tested using 3 to 14 matching surface points (figure 4-10; D-F).

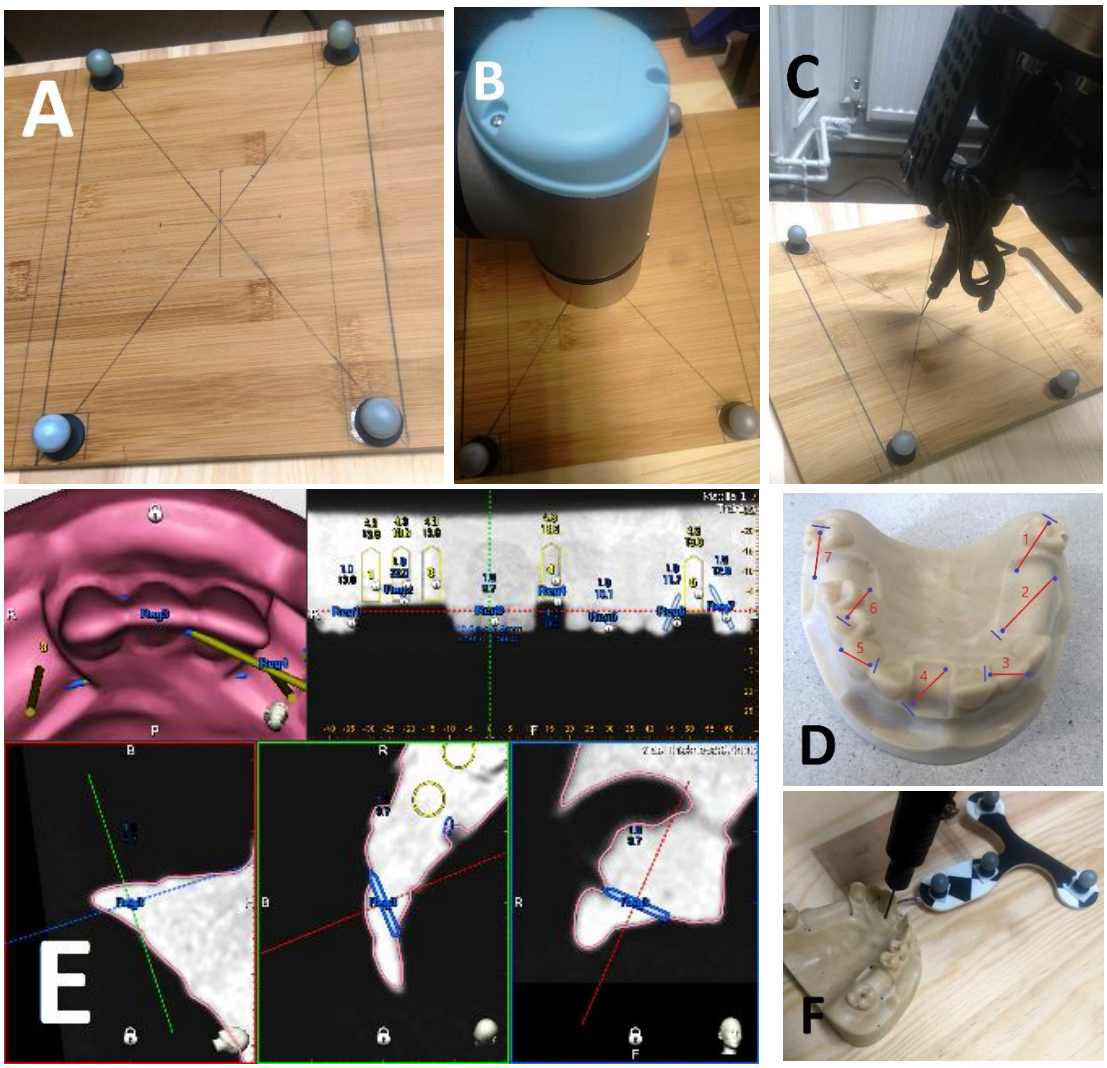

Figure 4-10. Transferring the dental plan coordinates into the robotic coordinates frame via OptiTrack. (A) A custom flat wooden calibration board (B) The first step of correlating the OptiTrack and robotic coordinates frames – relying on the real-life spatial relations between the optical tracking reflectors plus physically setting the face of the robotic end effector on the centre of the board surface. (C) The second step of OptiTrack to robotic transformation after securing a straight handpiece drill perpendicular to the end effector face. (D) Surface "tactile registration" points were marked on the dental model. (E) Registration implants were placed with the dental planning software to match the position of the registration surface points in real-life to their extracted STL coordinates. (F) The previously calibrated drill tip position touching one of the registration points (out of 3 minimum) to calculate the TM between the OptiTrack coordinate frame and the dental plan (STL) coordinate frame.

It is worth mentioning that this process was very time-consuming (about 60 minutes) and did not result in acceptable levels of accuracy (figure 4-11). This is due to the arbitrary dimensions of the custom calibrator itself (figure 4-10; A) together with the cumulative positional errors arising from human involvement during the steps described above (figure 4-10; B, C and F).

Figure 4-11. An accuracy check for OptiTrack-mediated transformation between the dental plan and the robotic coordinate frames. A shifting error of 7 to 10 mm systematically occurred in a random direction from the target point.

4.3.2. Transforming to robotic coordinates via NaviDent®

A custom 3D-printed calibrator was required to avoid inaccuracies of the tactile registration process (section 4.4.2). A custom 3D-printed grip was also created to hold a contra-angled implant handpiece (section 4.4.1) instead of the straight drilling handpiece.

The prinitng accuracy of the custom calibrator was checked with a digital vernier to ensure a 10 mm vertical distance between the calibration point (where the drill tip is held) and the point of origin of the robotic end effector. After securing the implant handpiece in its grip, the calibration processs started with the registration of the the model and drill calibration according to the standard NaviDent® instructions (figure 4-12; A).

Next, the custom calibrator was connected to the robotic arm (figure 4-12; B) and the drill tip transformation in relation to the handpiece tracker as well as the dental plan coordinates in the NaviDent® coordinates frame (for that specific session) were obtained from NaviDent® and transferred to the software interface via a USB memory drive. Finally, the known location of the calibration point in the robotic coordinates frame was recorded in 10 different robotic poses to sample these locations in the NaviDent® coordinates frame (figure 4-12; C).

The sampling process relied on the calibrated drill tip being manually held in the calibration point of the custom calibrator while the TM between the handpice tracker and the jaw tracker was being transferred to the software interface via a wireless network. Therefore, the TM between the robotic coordinates frame and the NaviDent® coordinates frame (i.e., the jaw tracker) could be calcuated by applying a rigid transformation code (https://github.com/nghiaho12/rigid_transform_3D).

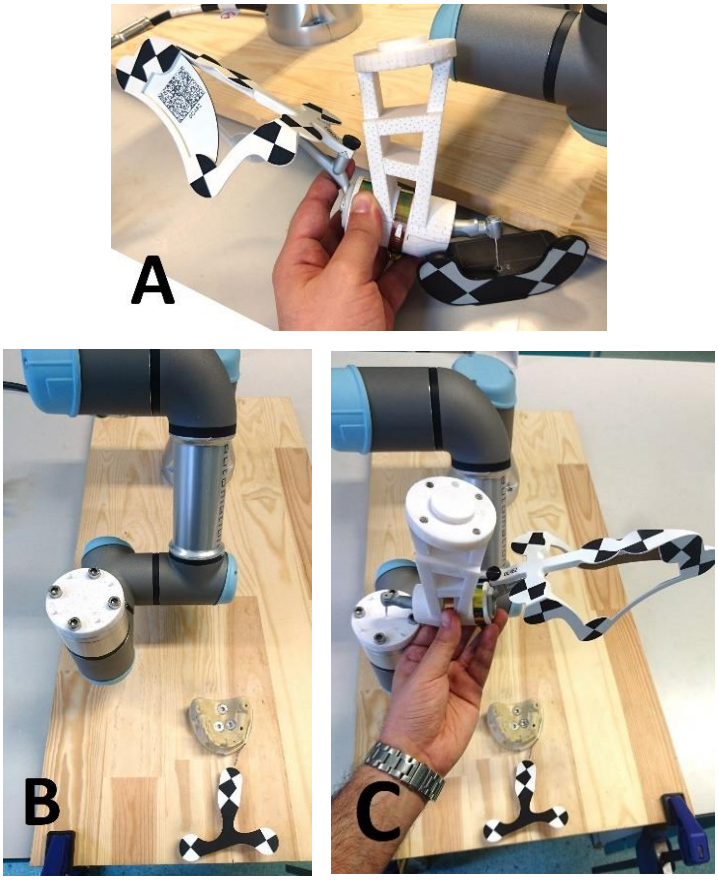

Figure 4-12. The initial attempt of transforming the dental plan coordinates into the robotic coordinates frame via NaviDent® relying on the drill tip location only. (A) Drill calibration to save tip location in relation to the handpiece tracker in NaviDent®. This was preceded by a model registration process to have the planned implants coordinates in the NaviDent® frame for the current registration session. (B) Connecting the custom calibrator and transferring the data obtained in the first step to the master computer through a USB memory drive. The TM of the dental plan STL to NaviDent® was calculated by the computer at this stage (see section 4.2.2). (C) Using the location of the calibration point at the centre of the custom calibrator (in 10 different poses), the relation of the NaviDent® (jaw tracker) to the robotic coordinate frames was established via a wireless transfer of the 10 tip locations, followed by a TM calculation (https://github.com/nghiaho12/rigid_transform_3D).

The process was further updated later by printing a new version of the custom calibrator (section 4.4.2). The drill tip was fixed in the correct, accurate position during the recording of the 10 poses, thus avoiding the possibility of introducing a source of variation in the location of the drill tip between the 10 poses (figure 4-13).

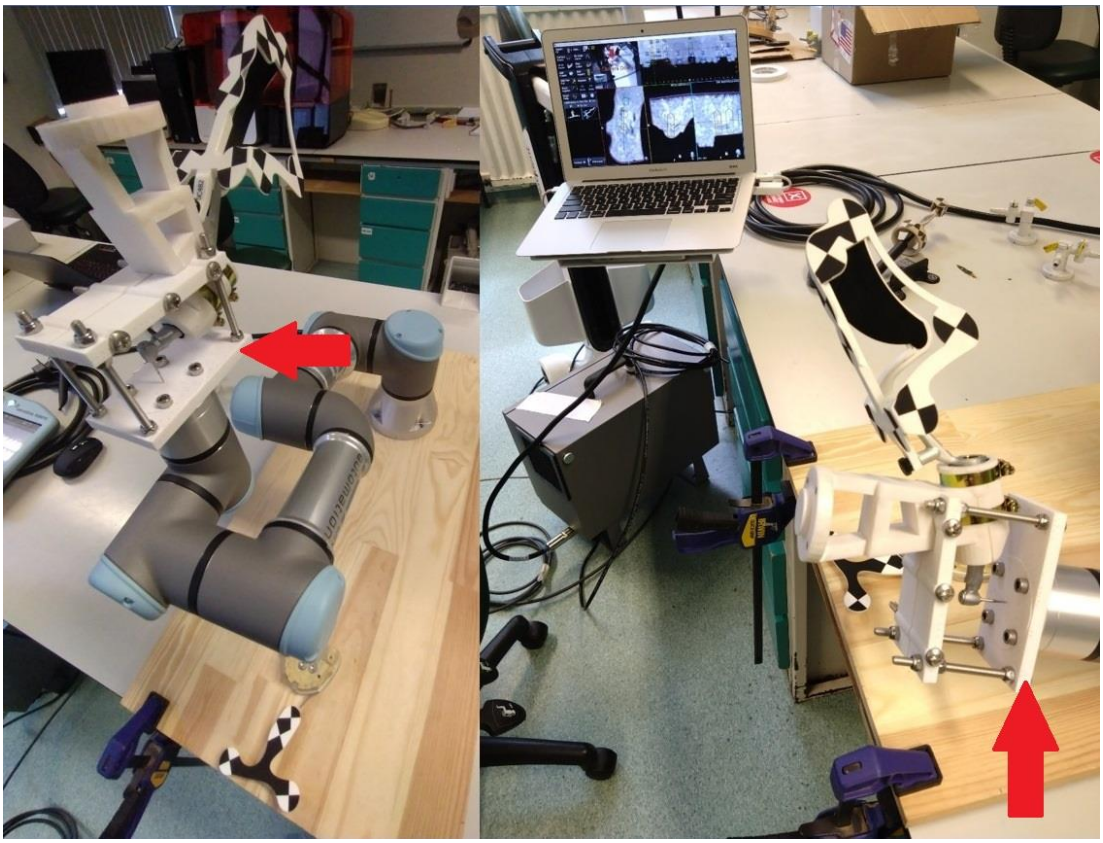

Figure 4-13. The second attempt of transforming the dental plan coordinates to the robotic coordinates frame via NaviDent® using the updated version of the custom calibrator (the rectangular piece attached to the end effector of the robotic arm – red arrow). The rigid fixation (through bolts and nuts) of the custom grip to the custom calibrator ensures reproducible drill tip location in relation to the robotic end effector throughout the 10 robotic poses.

This newly proposed calibration method took 20 to 30 minutes to achieve and its accuracy for transformation is shown in figure 4-14 below.

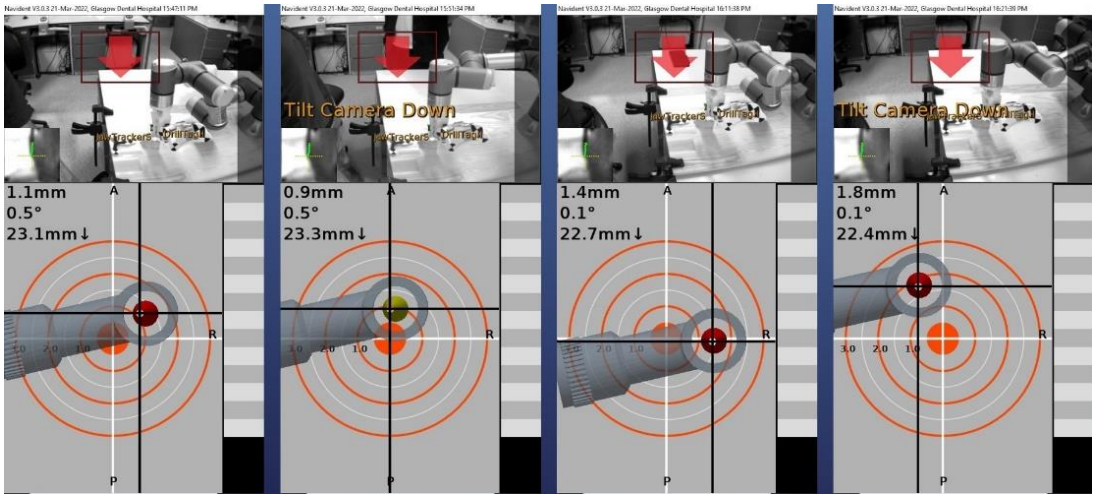

Figure 4-14. Four accuracy checks for NaviDent®-mediated transformation between dental plan and robotic coordinate frames. A shifting error of 0.9 to 1.8 mm systematically occurred in random directions from the target point. The coordinates matching error seen in this figure is independent of the model registration error.

Possible causes for the persisting coordinate matching error at this stage included residual positional error of the calibration point in the custom calibrator (i.e., the point was not located exactly 10 mm above the centre of the robotic end effector), noise incorporated in the 10 samples captured from the NaviDent® system for the drill tip locations, and noise incorporated in the 10 samples recorded by the robotic arm for the end effector locations. The term "noise" refers to the continuous fluctuations in the point coordinates during the sampling process. The causes of noise are likely to be related to the light conditions at the time of capture for the NaviDent® samples and to mechanical factors in the robotic arm samples.

The noise in NaviDent® samples was subsequently measured by obtaining 30 samples of the TM between the handpiece tracker and the jaw tracker over eight minutes while both were being fixed in static positions. The reproducibility of the TM was measured using variability range, maximum deviation from the mean, and average deviation from the mean in relation to 8 points on a ZI plan (Al-Jarsha et al., 2024b) (figure 4-15).

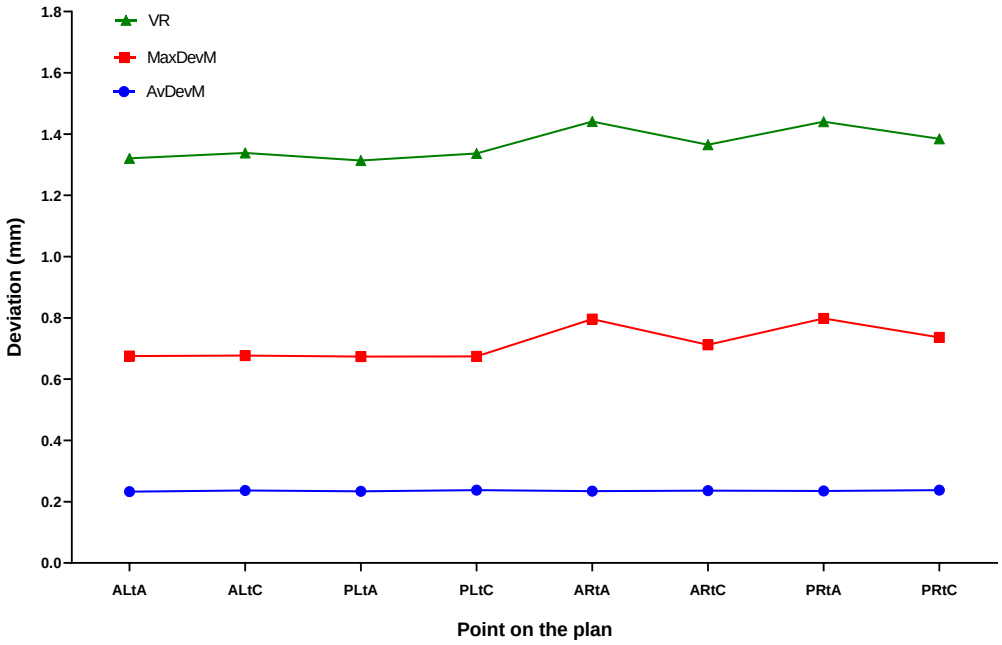

Figure 4-15. The noise arising in the TM between the handpiece tracker and the jaw tracker in NaviDent® expressed in terms of TM reproducibility parameters. VR = variability range; MaxDevM = maximum deviation from mean; AvDevM = average deviation from mean; ALtA = anterior left implant apex point; ALtC = anterior left implant collar point; PLtA = posterior left implant apex point; PLtC = posterior left implant collar point; ARtA = anterior right implant apex point; ARtC = anterior right implant collar point; PRtA = posterior right implant apex point; PRtC = posterior right implant collar point.

Most of the residual coordinate matching error appeared to be related to the variability range (VR) values as seen in figures 4-14 and 4-15.

The next method of transforming the coordinates relied on what is known as “Hand-Eye Calibration” (Daniilidis, 1999, Shah et al., 2012). The principle is to get the data from at least one motion (two poses) and solve the equation described in figure 4-16 to get the TM between the robotic arm base and the NaviDent® jaw tracker coordinates frames.

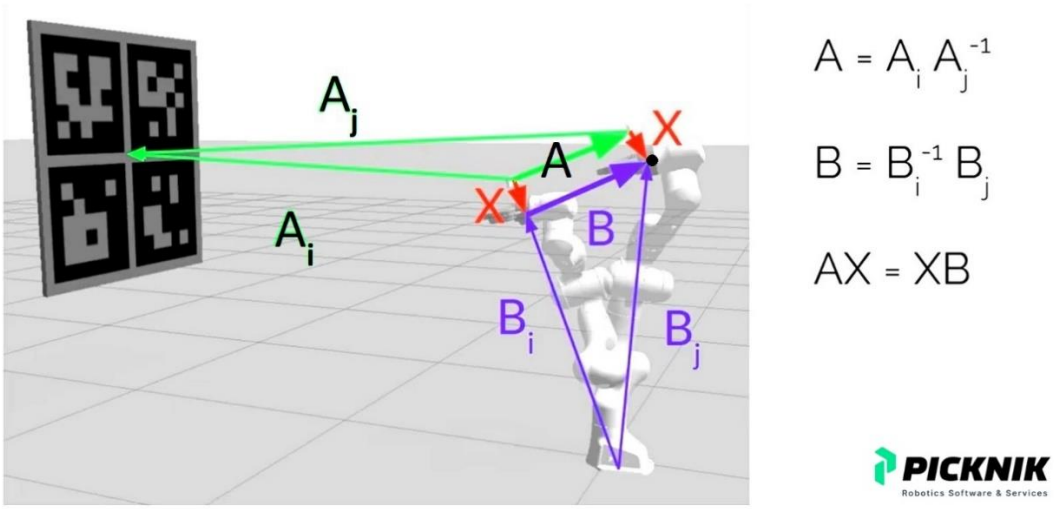

Figure 4-16. The principle of the hand-eye calibration method to get the transformation matrix (X) between an optical tracking system (A) and a robotic mechanical coordinate system (B). The 3 equations on the right side of the figure are related to the input and output of this process. The (A) transformation (bold green arrow) is the result of multiplying the (A_i) and the reverse of the (A_j) transformations. The (B) transformation (bold violet arrow) is the result of multiplying the reverse of (B_i) and the (B_j) transformations. The black point in the figure can be reached in two ways; (A) motion then (X) motion (the bold green then the right red arrow), or (X) motion then (B) motion (the left red then the bold violet arrows). © 2020 PickNik Robotics, a YouTube presentation by Dr John Stechschulte and Dr Yu Yan, with permission.

Among the multiple 3D rigid body transformation algorithms, the dual quaternion method was found to be the least affected by noise and produced the lowest rotation and translation errors (Eggert et al., 1997, Daniilidis, 1999). However, the required number of motions to produce predictably low error margins was 12 to 18, not just one (Daniilidis, 1999).

In our project, we performed 14 motions (15 pose samples) to get an acceptable matching accuracy. The ParkBryan1994 solver was selected, which used the dual quaternion algorithm to solve X, but with a closed-form least squares solution to reduce the effect of noise when obtaining A and B in the AX=XB equation (Park and Martin, 1994) (figure 4-17).

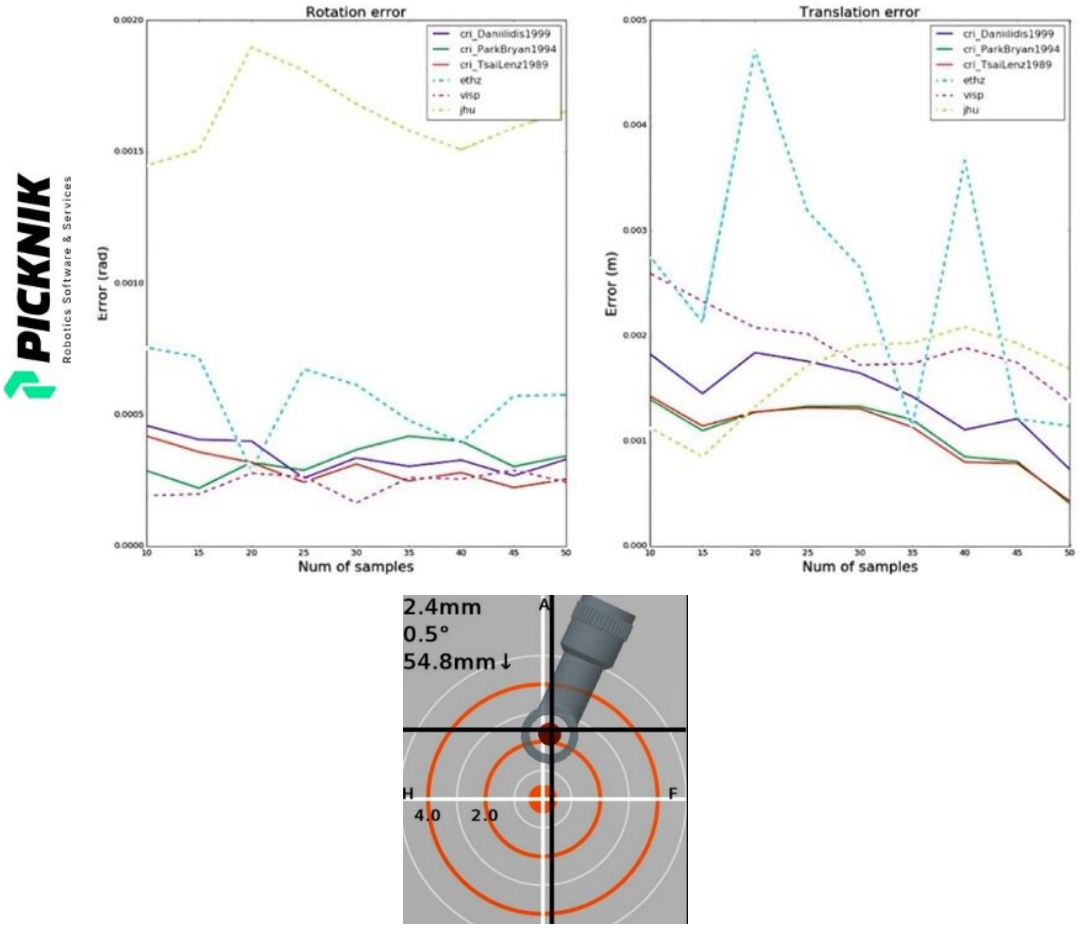

Figure 4-17. Top: the rotation and translation error associated with different hand-eye calibration solvers. ParkBryan1994 solver (the green solid line) at 15 samples was selected to achieve the best results. Bottom: the resulting deviations from the process as recorded by the Navident® optical tracking system (2.4 mm lateral shift, 0.5° angle and 0.2 mm in depth). The line graphs on the left side are from a YouTube presentation by Dr John Stechschulte and Dr Yu Yan. © 2020 PickNik Robotics, with permission.

The residual shifting error was then corrected via a supplementary refinement process that automatically collects tracking samples near the site of interest for 3 seconds with a set sensitivity limit for tracking noise (0.07 mm). This refinement step was applied to perfect the matching at that particular site (figure 4-18).

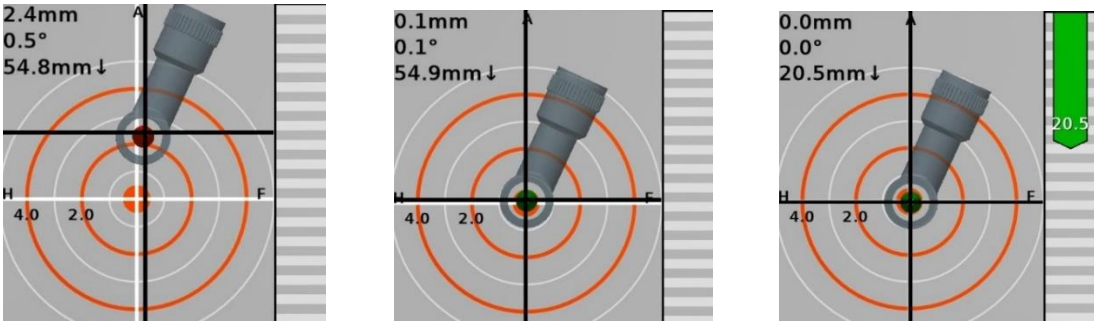

Figure 4-18. The result of the coordinates matching process using the hand-eye calibration method. Left: the initial result without refinement step. Middle: after refinement at the entry point, the deviations were reduced to 0.1 mm and 0.1°. Right: the final result that is acceptable for the coordinate matching process with zero deviations in the 3 parameters at the end point of the final zygomatic twist drill.

To standardise the procedure, the 15 sample poses were selected so that they are equally distributed around the operative site while the trackers are always in the view of the tracking camera. This work was done based on the robotic system simulation software and then the poses were recorded so that the robotic arm automatically reproduced these poses prior to all drilling experiments (figure 4-19). In fact, it was necessary to record 15 poses for the left-side trajectories and another 15 for the right-side trajectories because the camera position is different between these two sides, this is due to the camera line-of-sight limitation (figure 4-20).

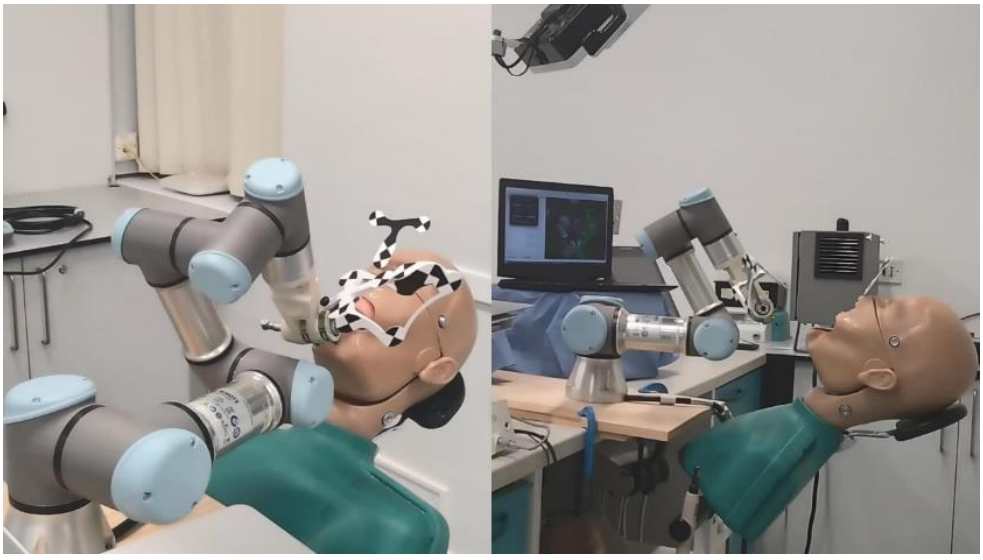

Figure 4-19. Photographs of a recorded robotic arm pose for the left-side ZI trajectories taken from two angles. The most important two requirements for recording the standard poses are: (1) both markers can be seen by the NaviDent® tracking camera (top left corner of the right photo) without having to move it between poses, and (2) the movement from one pose to the next (or previous) should not cause the robotic arm or any of its connected parts to physically collide with the surrounding environment (i.e., the movement between poses should be smooth and safe).

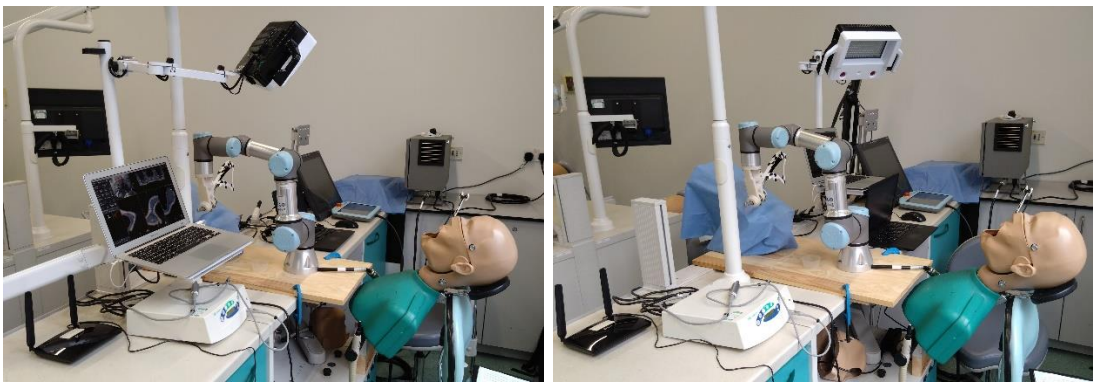

Figure 4-20. The standardised spatial setups before commencing the coordinate matching process. Left: the standardised camera position for the left-side trajectories. Right: the standardised camera position for the right-side trajectories. The dental simulator is rigidly fixed in place during all the experimental procedure from the registration step to the end of the implant placement step.

4.4. 3D printing of custom components

4.4.1. Designing the custom grip for the implant handpiece

The design process was initiated using the STL files for the shape of the handpiece tracker (provided by NaviDent®), the shape of the handpiece adapter, which connects the tracker to the handpiece (obtained by an intra-oral scanner; 3Shape® TRIOS 3 Battery Cart), and a basic shape of a handpiece (downloaded from https://grabcad.com)(figure 4-21). The goal was to achieve a grip design so that the final drill is robustly fixed in a perpendicular relationship to the end effector of the robotic arm, without obstructing the handpeice tracker from the camera view (figures 4-9 and 4-22).

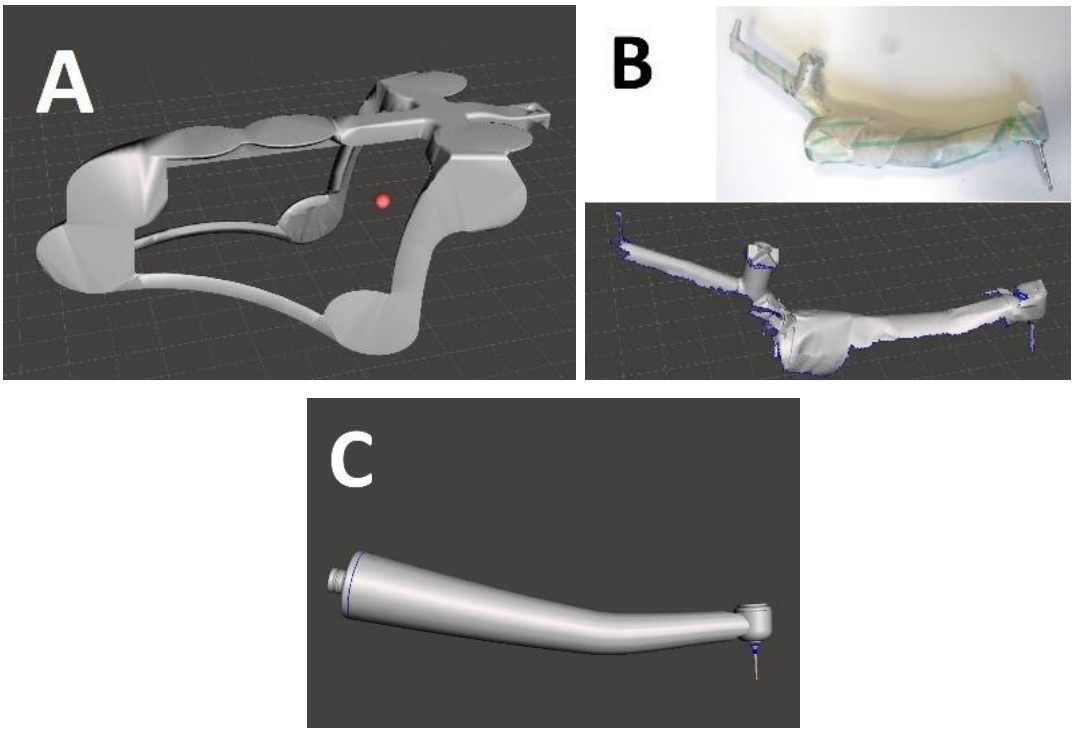

Figure 4-21. The basic 3 components for the custom grip design. (A) The handpiece tracker shape was kindly provided by NaviDent®. (B) Adapter relationship to the drill axis was obtained with an intra-oral scanner after wrapping the shiny surface of the handpiece to avoid distorting the STL file due to light reflection artifacts. (C) A basic shape of a contra-angle dental handpiece from (https://grabcad.com/library/contra-angle-dental-handpiece-1/files).

These 3 components in addition to basic geometric shapes were utilised to construct and upgrade the design of the handpiece grip using Autodesk MeshMixer (v.3.5.474).

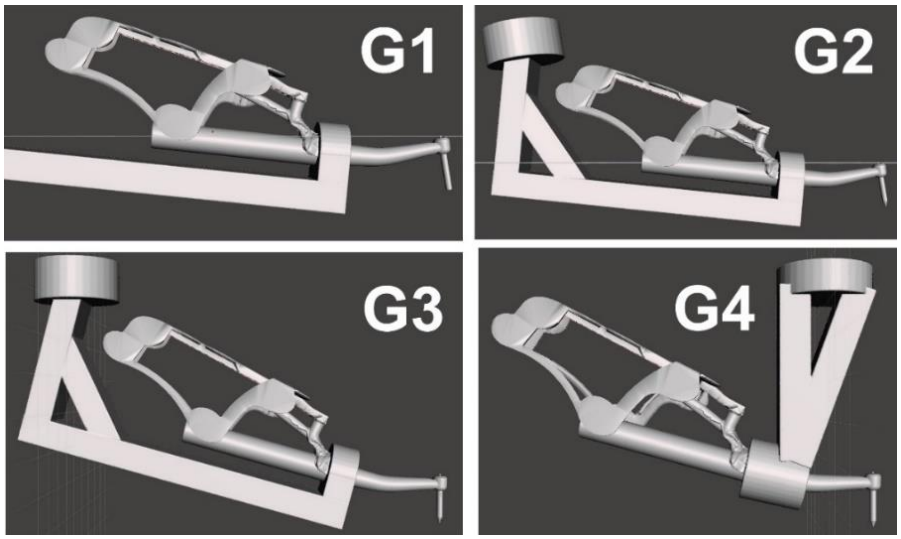

Figure 4-22. The initial stages in the grip designing process. G1 to G3 represent 3 phases of the same basic design aiming to show as much of the handpiece tracker as possible to the camera to avoid interrupted tracking. G4 represent a shift to a direct superior connection (avoids deformation due to the physical forces during drilling plus more economic in printing resin cost).

The next stage invovled adding a more exact negative replica of the end effector tool flange based on the robotic arm 3D file (downloaded from https://www.universal-robots.com/). The result was getting the first version (G5) which was the basic reference being updated in the following stages (figure 4-23).

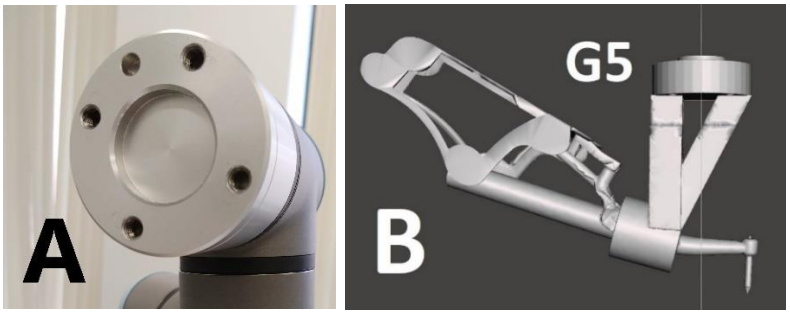

Figure 4-23. The 2nd phase of grip design involved adding an accurate negative replica of the robotic end effector tool flange. (A) The positive replica of the end effector. (B) G5-v1 grip design including a negative fitting replica for the end effector's tool flange.

The grip cylinder was divided into halves across a plane parallel to the long axis of the handpiece. Then, the shapes of the connecting arms and the outer surface of the grip cylinder were modified in v2 and v3 of the G5 design. The handpiece subtraction volume was iterated in v4 to v6. Finally, an anti-rotation forward extension of the grip cylinder was added in v7 (figure 4-24).

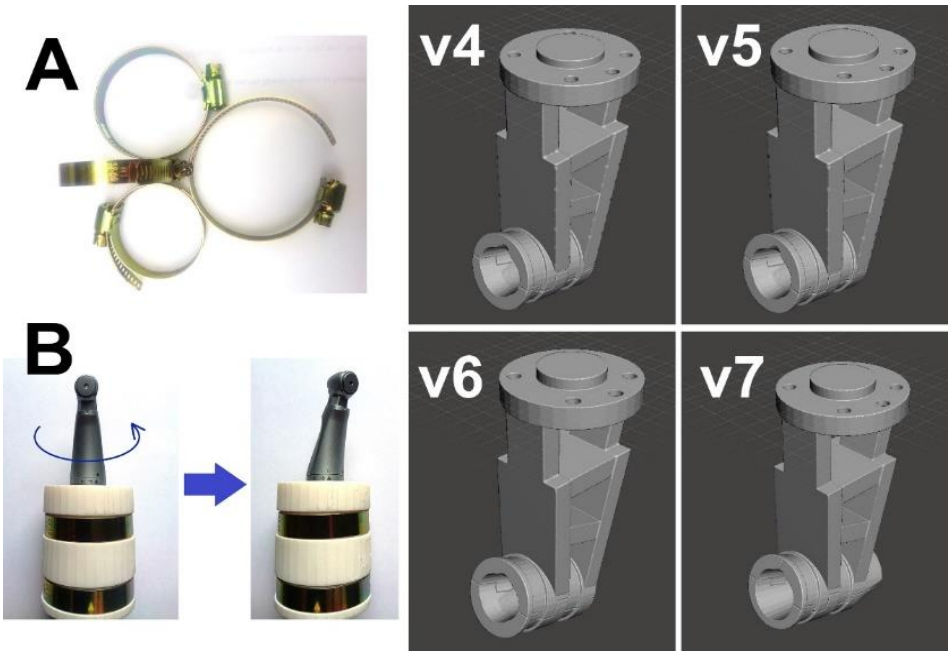

Figure 4-24. The 3rd phase of the designing process involved perfecting the design to maximise surface contacts and mechanical properties while reducing the overall bulk. (A) 5 cm clamps were to be used to connect the two halves of the grip, which were laid out separately in the printing volume. The exact shapes of the clamps were subtracted from the outer surface to ensure stable positions. (B) The possibility of rotation and/or dismantling of the handpiece with a simple cylinder design (v6). This was rectified by adding an anti-rotation forward extension before printing the complete grip design (v7).

The designing and 3D printing process of the implant handpiece grip was not without an element of trial and error. This is mainly because of the need to involve the complex shape of the outer surface of the handpiece without having its exact replica as an STL file. Printing material-associated dimensional changes also played a role in the modification of the STL design file during the time between printing the parts in the trial phase and printing the complete grip (figure 4-25).

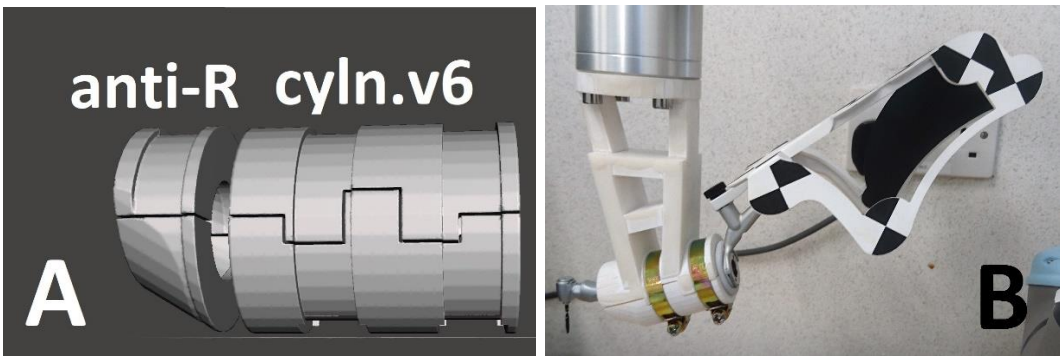

Figure 4-25. (A) Parts which were printed separately to check their critical fit; the grip cylinder v6 and the forward anti-rotation extension. (B) The complete grip (v7) that was printed (the same one used in all the experiments in this research project).

4.4.2. Designing the custom robotic calibrator

The rationale behind designing this part was explained in section 4.3.2.

The very first version exhibited printing dimentional changes which were rectified in version 2. This was achieved by modifiying the STL file dimentions prior to re-printing with correction factors (figure 4-26). A 3rd version was printed to avoid having to hold the grip assembly statically multiple times during the calibration step mentioned in section 4.3.2. (figure 4-27).

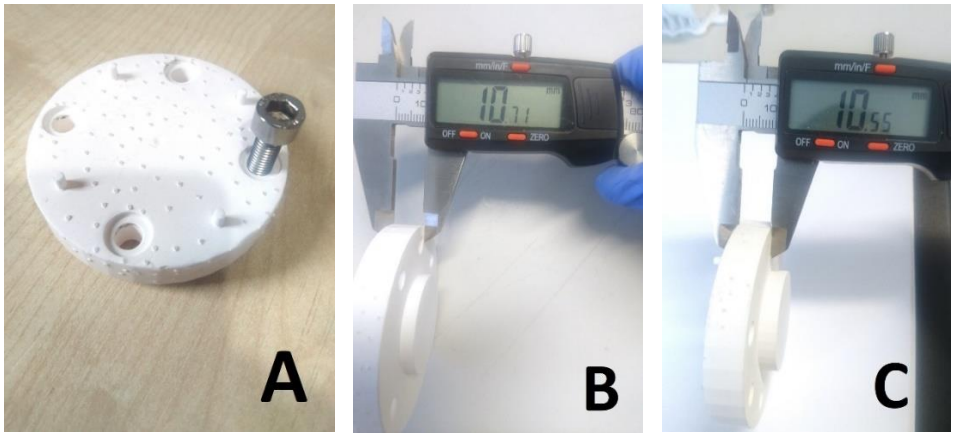

Figure 4-26. The first 2 versions of the custom calibrator. (A and B) v1 in which the STL dimensions were identical to the intended target not accounting for printing dimensional changes. (C) The exact intended dimensions were achieved after changing the STL dimensions in v2 (the depth of the calibration point is 0.55 mm).

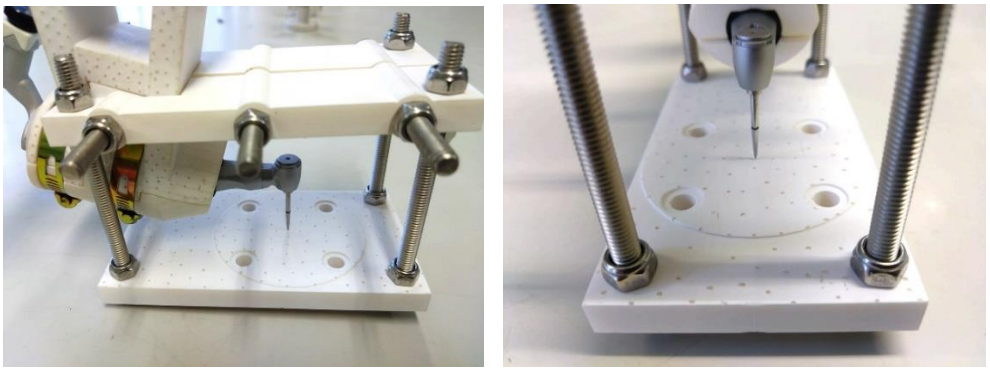

Figure 4-27. Custom calibrator v3. The design includes 3 resin parts assembled together around the implant handpiece grip via 7 bolts and 15 nuts to control and secure the position of the drill tip on the intended calibration point in the lower plate. The distance between the calibration point and the point of origin of the robotic end effector is 10 mm.

4.4.3. Designing the custom model connection

This component was necessary to rigidly link the commercially available models to the dental simulator jaw.

An STL file was extracted from the CBCT scan of one of the models to be used for the main experiment. In addition, the real-world measurements from the jaw fitting area in the dental simulator were obtained. Using a similar technique to that described in section 4.4.1, a basic shape model connection was designed and then the top 3 mm of the model STL was subtracted to create a rigid lock-and-key connection between the models and the dental simulator unit (figure 4-28).

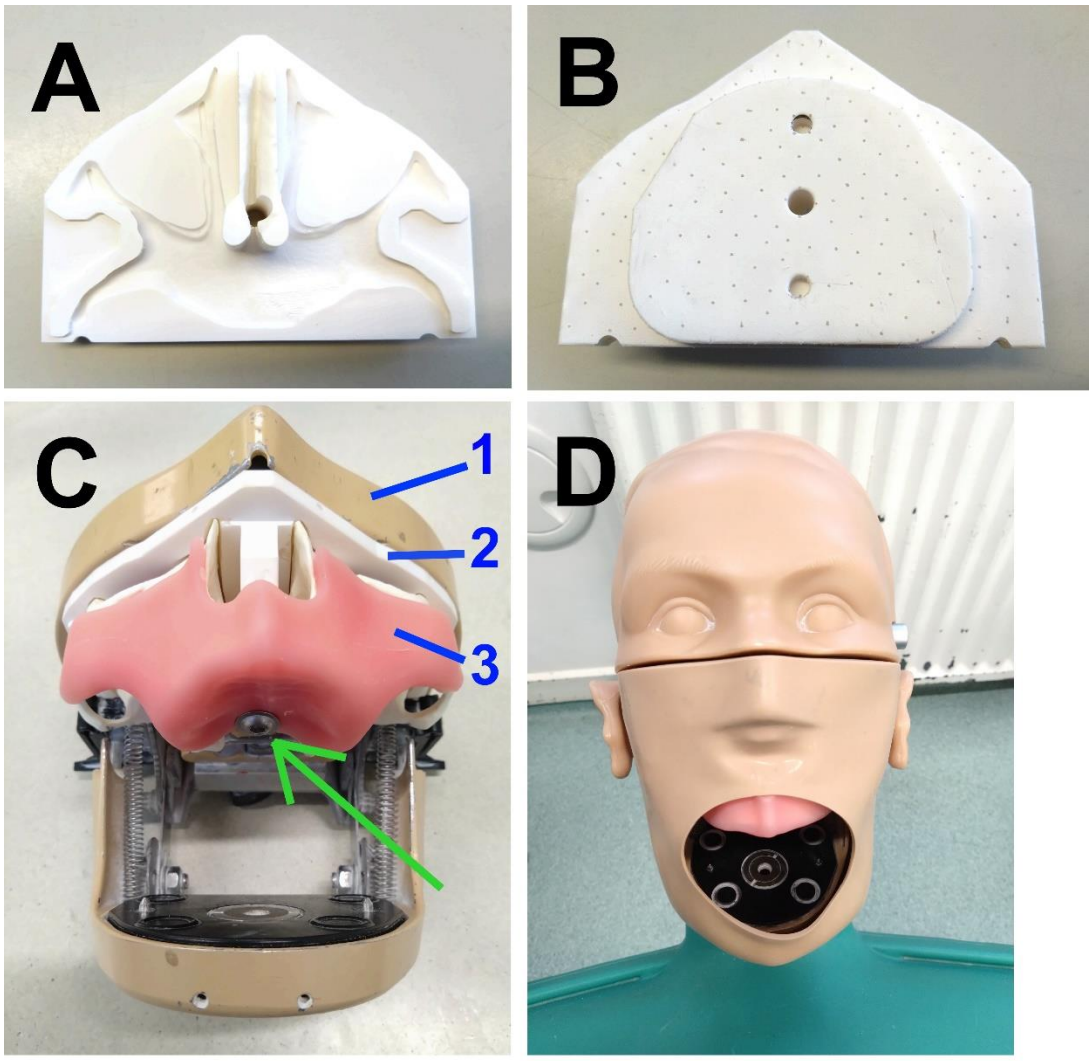

Figure 4-28. The custom connection between the model and the dental simulator jaw. This connection serves to ensure a rigid friction fit connection to avoid any movement. (A) The model fitting side. (B) The dental simulator fitting side. (C) The connected model assembly before incorporating a silicone mask. The 6 mm diameter vertical long bolt (green arrow) transverses the 3 compnents (blue numbers) and holds them tightly in place. (D) The assembly during the experiment also included a silcone mask to simulate the skin.

4.5. Optimisation of the work volume and approaching path (to avoid collisions with the environment)

ROS (Robot Operating System https://ros.org) is a simulation software for robotic arm movements and is also able to communicate commands controlling these movements within the real world. The 3D visualisation component of the software (RViz) is the interactive user interface of ROS (figure 4-29).

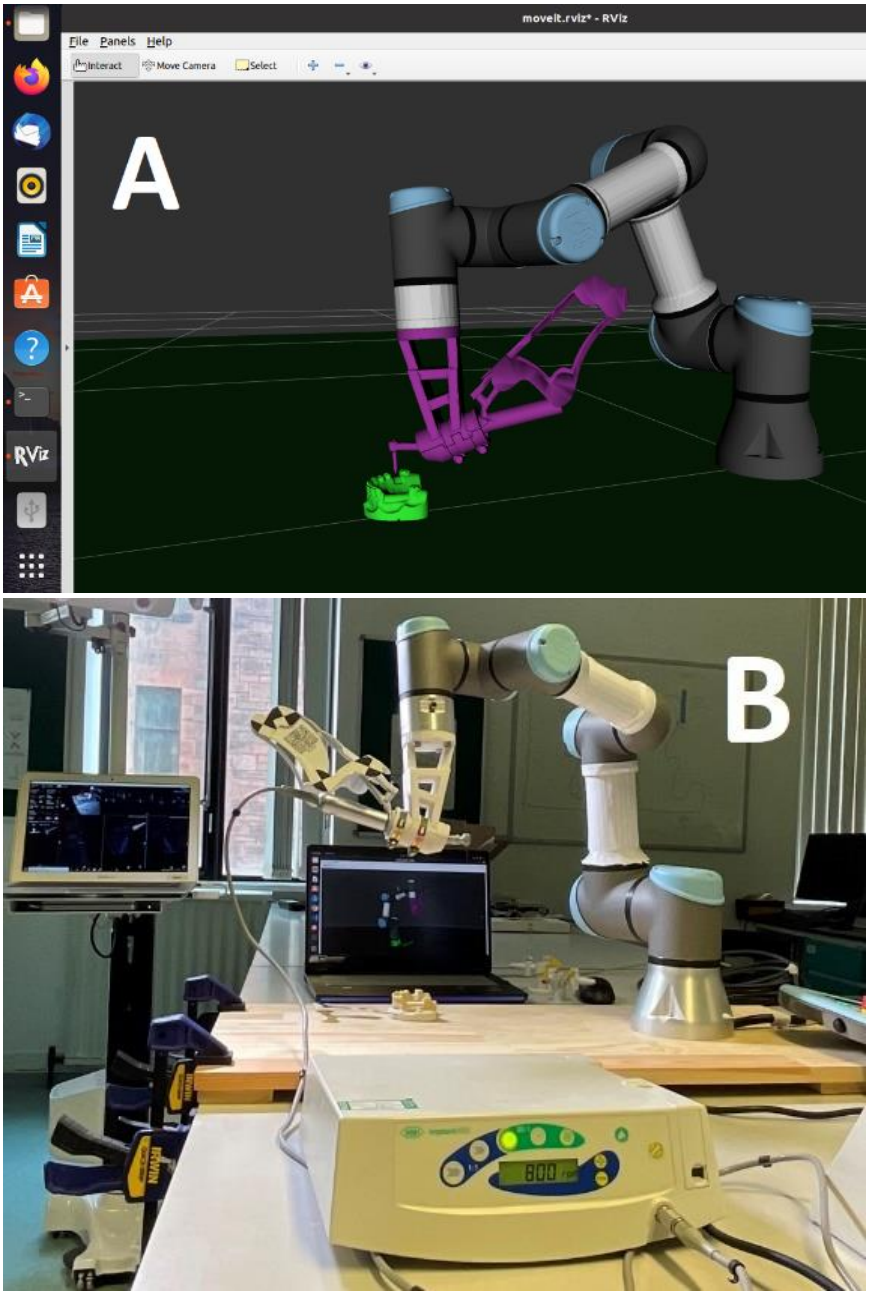

Figure 4-29. RViz interface of ROS. (A) Simulation for approaching a target point offline (with no connection to the robotic arm). (B) Communicating the desired target position to the robotic arm in reality.

The custom design of the handpiece grip discussed in section 4.4.1. was transferred to RViz after re-orienting its axes to match those of the virtual robotic arm in ROS using MeshLab (https://www.meshlab.net)(figure 4-30).

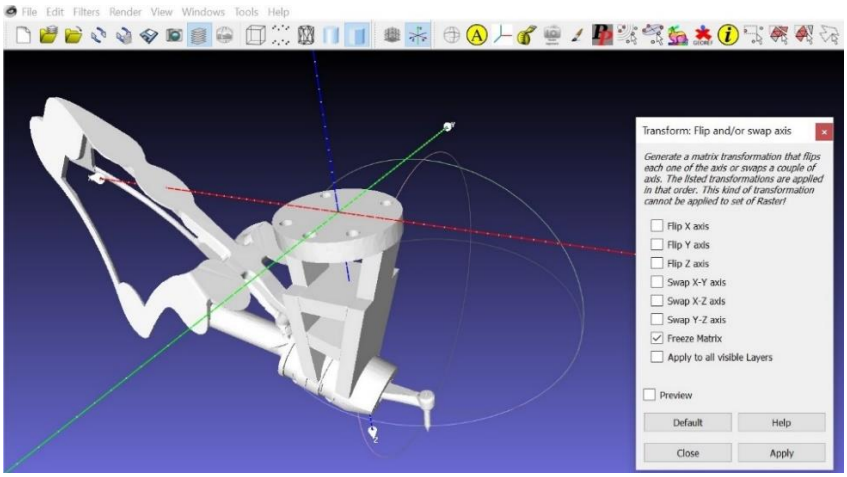

Figure 4-30. Re-orienting the axes of the grip assembly to match those of the robotic end effector in RViz.

Next, the dental simulator was converted to a 3D model through stereophotogrammetry. The process included capturing 150 high resolution 2D photos of the model from 5 directions with variable angles, followed by the use of a computer application to stitch these photos into a 3D object. (The method is explained here: https://github.com/NVlabs/instant-ngp). Since the purpose of recreating the environment was simple collision avoidance, the original large sized file (around 470 MB) was simplified as a combination of regular shapes available in MeshMixer (3.3 MB) (figure 4-31).

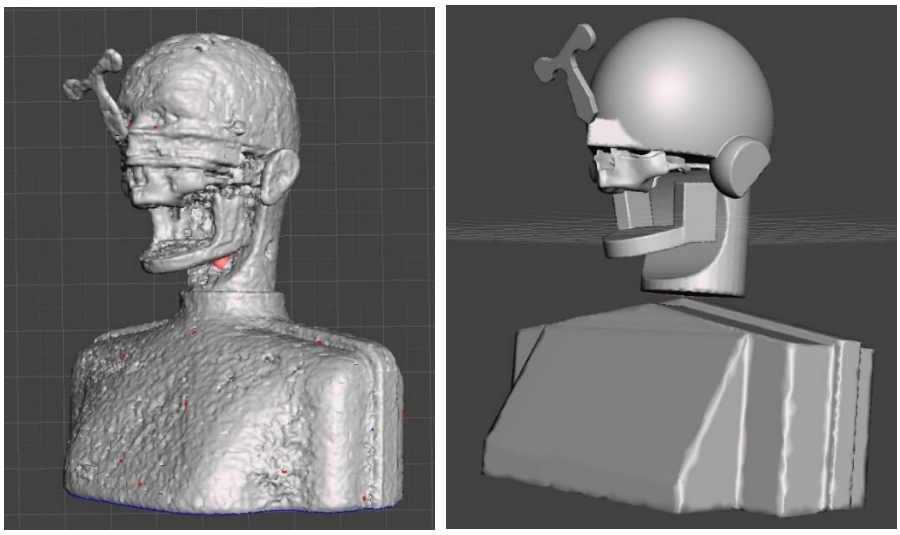

Figure 4-31. Left: the 3D representation of the dental simulator that was obtained using stereophotogrammetry. Right: a simplified representation was created and then aligned to the frame of reference of the implant plan.

After importing the 3D representations of all the involved structures into the virtual environment (RViz), a simulation interface was developed to find out the best position of the dental simulator in relation to the base of the robotic arm so that all 4 trajectories can be executed safely without risk of collisions (figure 4-32). This version of the software interface was then upgraded multiple times to be more user-friendly through the addition of interactive labels and shortcut buttons for the required functions (figure 4-33).

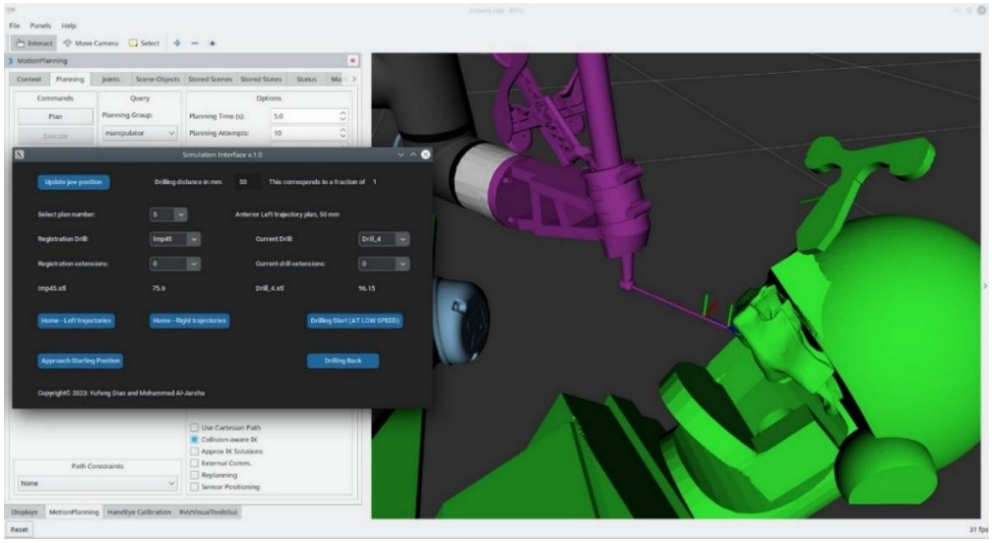

Figure 4-32. The simulated experimental environment for robotic-guided zygomatic implant placement. The environment was developed via designing and positioning all invloved componets identical to their real dimensinos (the dental simulator, the handpeice grip, the implant drills ,... etc.). The user interface simplifies dealing with the underlying code which has already been tested and refined in earlier steps.

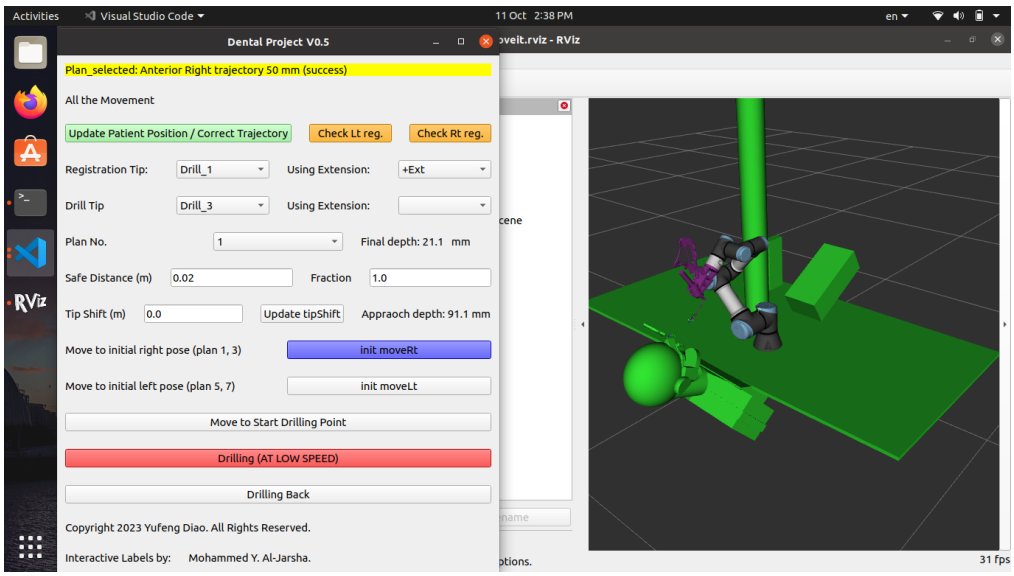

Figure 4-33. A screenshot for the latest version of the user interface used for robotic-guided zygomatic implant placement in this project. The colour indicators help to smooth the practical steps in the protocol. The top label also refreshes in real time to mointor the depth during the implant placement step, which is required to activate an automatic cut-off switch at the desired depth.

4.6. Real-time communication on movement

When the operating site (the jaw) moves during the procedure (as can happen in real patients), this movement needs to be quantified in relation to the base of the robotic arm and then relayed to the tracking system so that the communicated transformation matrix is adjusted accordingly.

A third optically tracked pattern is required to be affixed to the base of the robotic arm as a reference for the jaw movement. The pattern attached to the end effector can be in a state of movement itself while the jaw moves and is therefore not of use for this purpose. The optical tracking system is then required to track all 3 patterns, or alternatively, a second tracking camera has to track and relay the jaw position in relation to the robotic base.

The current communication protocol (assuming a stationary jaw) is carried out via a Transmission Control Protocol (TCP) over a wireless network. The TM of the NaviDent® handpiece to jaw tracker is streamed to the network at the rate of 5 Hz (i.e., 5 files containing the momentary TM per second). The computer with Robotc Operating System (ROS) receives these data and implements them in the registration process described at the end of section 4.3.

4.7. The auto-switch function for implant placement

A potential human error could have arisen in implant placement depth during the experiments if the implant engine was merely controlled with a footswitch. To exclude this potential error, an automated switch mechanism was deemed necessary so that the implant engine would stop without the need for human intervention when reaching the final planned depth.

A simple prototype was designed and assembled to cut-off the main power to the implant engine when the software sends the appropriate signal. Initially, the robotic coordinates were used to define that signal. However, due to the persistent minor variations in the form of premature stops, the code was modified so that the cut-off signal was dependent on the coordinates provided by the navigation system via the real-time wirelessly streamed TM during the implant placement step.

The premature stops occurred due to the physical resisting forces acting against the direction of implant advancement causing the robotic system to recognise reaching the end point of the trajectory before actually reaching that position in the real environment. In contrast, relying on the wirelessly streamed TM provided by NaviDent® to cut off the power meant that the cut-off signal would only be generated if the handpiece tracker reaches a position in the real environment corresponding to the end point of the planned implant trajectory.

The auto-switch prototype consisted of the following components:

- STMicroelectronics STM32 Nucleo-32 MCU Development Board (NUCLEO-L432KC) mounted on a breadboard: This development board is the central processing unit of the prototype. It is responsible for receiving and interpreting commands from a laptop, then directing these instructions to the other components. It also converts USB signals into TTL (Transistor-Transistor Logic) serial signals, facilitating communication with the laptop. The STM32 Nucleo board was chosen for its high-speed performance (figure 4-34 A). The boards can be easily purchased online as they are used for teaching in electronic circuit creation.

- USB DC Buck PSU Step UP/Down 5V to 1.2V-24V Power Supply: This power supply module ensures that the SG90 servo motor has the necessary power to operate. It converts a USB power source (5V) into the appropriate voltage (4.8V) required by the servo (figure 4-34 B).

- SG90 Micro Servo Motor: This servo motor was used to operate a small mechanical arm that rotates for a certain angle then returns back to its starting position. Under the control of the STM32 Nucleo board, it can physically toggle a power switch on a plug through this small rotational movement (figure 4-34 C).

- Amazon Smart Plug HD34UK: This is an AC power plug with a side button to control the electricity flow (on/off). The mechanical arm of the SG90 servo motor was aligned to this button so that the plug will be controlled by the mechanical action of the SG90 servo arm (figure 4-34 D).

The delay between receiving the signal and turning off the power was compensated via triggering the cut-off signal 0.3 mm short of the desired final depth, which corresponded to about 0.3 second (advancing speed of the robotic arm during implant placement was ~ 1 mm/second).

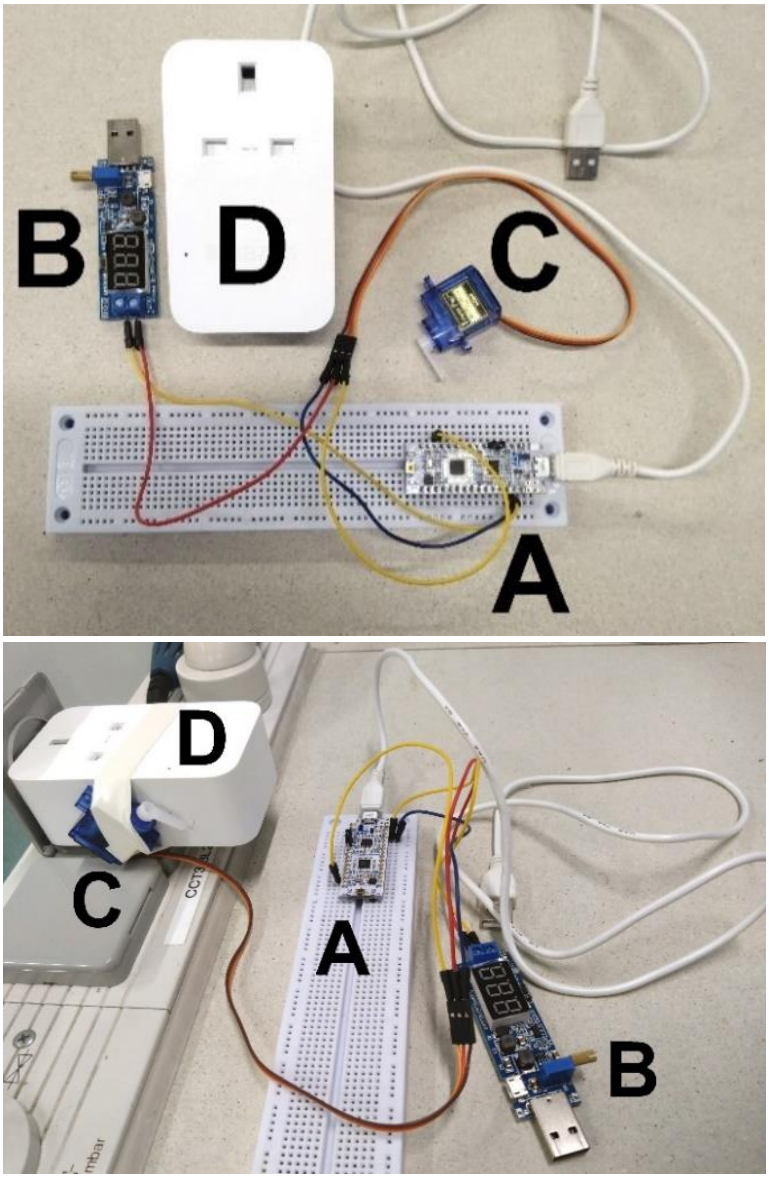

Figure 4-34. The physical components of the auto-switch prototype. (A) NUCLEO-L432KC Development Board on a breadboard. (B) PSU Step UP/Down 5V to 1.2V-24V Power Supply. (C) SG90 Micro Servo Motor. (D) Amazon Smart Plug HD34UK.

4.8. Drill calibration method selection

The drill calibration process requires that both the handpiece tracker as well as the calibrator tool be in the view of the tracking camera during the 3 seconds required for drill length calibration (figure 4-35).

Figure 4-35. The process of drill length calibration while the handpeice and the attached tracker are connected to the robotic arm. Note the need to set-up the robotic arm joints in a specific manner that do not block the camera line-of-sight to the optical patterns of the calibrator and the handpiece tracker. The camera is located far ouside the top left corner of this photograph.

In the manual procedure, it would be easy to repeat this step with every drill change during the stepwise implant osteotomy. However, while the handpiece is connected to the robotic arm, there is a need to manually use the robotic arm controller and re-adjust its pose to ensure a clear line-of-sight for the tracking camera. This means that every re-calibration step would take a couple of minutes rather than few seconds.

It was also noted that following the standard drill re-calibration process and then instructing the robotic arm to reproduce the same pose resulted in angular and translational discrepancies on the monitoring screen (figure 4-36). Therefore, it was deemed more practical (timewise) and more logical to only do a single drill calibration during the robotic implant placement procedure. The logical reasoning pertains to the fact that the robotic arm's reported pose repeatability (by the manufacturer) is ± 0.03 mm, so the discrepancy in the pose was attributed to the re-calibration step itself rather than any changes happening in the real world. This is especially true with the tracking camera and the resin model both fixed in place and the approach being tested in air without any physical resistance, so as to reproduce the exact same pose.

The discrepancies in the deviations on single- versus multiple- drill calibration protocols were confirmed with simulations in air for two trajectories; one on the left side and the other on the right side (table 4-3).

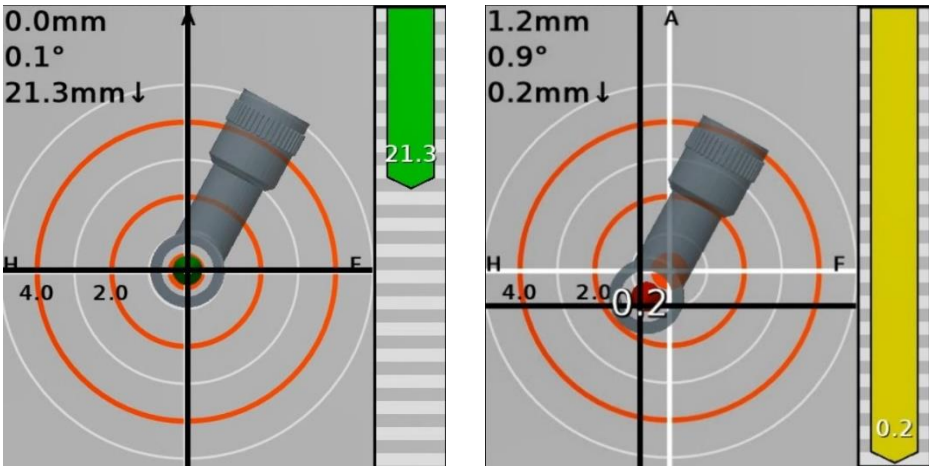

Figure 4-36. The drill tip deviations as displayed by the optical tracking system when a particular drill is calibrated and then the robotic arm is instructed to simulate a drilling movement (in air). (Left): 0.0 mm, 0.2 mm and 0.1° deviations when a single calibration protocol is used. (Right): 1.2 mm, 0.2 mm and 0.9° deviations when a multiple calibration protocol is used. The testing drill is a zygomatic twist drill 2.7Φ. The calibration drill used for the single drill calibration in the left-side picture is 21.1 mm shorter than the testing drill.

Protocol	Single Drill Calibration						Multiple Drill Calibration					
Trajectory	Posterior Left			Posterior Right			Posterior Left			Posterior Right		
Deviation / Testing drill	2D (mm)	Depth (mm)	Angle (°)	2D (mm)	Depth (mm)	Angle (°)	2D (mm)	Depth (mm)	Angle (°)	2D (mm)	Depth (mm)	Angle (°)
Short Needle	0.1	0.3	0.0	0.2	0.1	0.0	0.4	1.9	0.5	1.0	1.6	1.7
Short Final	0.1	0.2	0.0	0.0	0.0	0.0	0.7	0.0	0.9	0.9	0.4	1.4
Zygomatic Round	0.3	0.2	0.1	0.0	0.0	0.0	0.8	0.0	0.7	0.4	0.0	0.4
Zygomatic Needle	0.2	0.1	0.0	0.1	0.1	0.0	0.7	-0.1	0.8	1.0	0.3	1.0
Zygomatic Twist	0.0	0.2	0.1	0.2	-0.1	0.0	1.2	0.2	0.9	0.9	0.2	0.6
Zygomatic Final	0.1	0.1	0.0	0.1	-0.1	0.0	0.6	-0.1	0.5	1.1	0.1	0.8
Zygomatic Side-cutting	0.1	0.1	0.0	0.1	0.1	0.1	1.4	-0.2	1.1	1.2	0.2	1.1
Zygomatic Counter-sink	0.1	0.0	0.0	0.1	0.0	0.0	0.4	0.0	0.1	1.3	0.5	1.0
Mean	0.13	0.15	0.03	0.10	0.01	0.01	0.78	0.21	0.69	0.98	0.41	1.00
Standard Deviation	0.09	0.09	0.05	0.08	0.08	0.04	0.36	0.69	0.31	0.27	0.51	0.42
Range	0.30	0.30	0.10	0.20	0.20	0.10	1.00	2.10	1.00	0.90	1.60	1.30

Table 4-3. Simulation observed deviations comparing single- versus mutiple- drill calibration protocols. The maximum observed summary deviation data are highlighted in the bottom three rows (e.g., single drill calibration deviation ranges were 0.3 mm and 0.1°, while they were 2.1 mm and 1.3° for the multiple drill calibration protocol).

Utilising a single drill calibration protocol also has the advantage of being able to track any possible physical movement of the resin model and/or the base of the robotic arm in between the drilling steps. This is achieved via re-simulating the approach to the yardstick point in air (the end point of the final zygomatic drill). It should not change throughout the entire osteotomy procedure to indicate no changes to the spatial relationship between the resin model and the base of the robotic arm. On the other hand, with the multiple calibration protocol, this advantage would be lost because the yardstick point deviations could not be replicated again even if the same drill was re-calibrated (see chapter 3 for more details about drill calibration optimisation experiments).

The only practical disadvantage of the single drill calibration protocol is the incorrect displayed depth value when compared to the real world (figure 4-36). The user interface shown in section 4.5 provides a user-friendly solution to this issue by displaying the expected approach depth and final depth in millimetres whenever the selected drills or the drilling fraction are changed by the user (figure 4-33 on page 133).

4.9. Drilling protocol adjustments

The drilling protocol followed the manufacturer instructions with respect to the recommended speed of rotation (rpm between 1000 and 1500 for the zygomatic drills and 2000 for the short alveolar osteotomy drills). The anterior trajectories were ZAGA type 1 whereas the posterior trajectories were ZAGA type 2 (Aparicio, 2011). (See figure 5-7 on page 153 in section 5.2.2 for an illustration of the plan).

4.9.1. The default 10 stages protocol used for initial testing

After ensuring good coordinate matching (see figure 4-18 on page 124 in section 4.3.2), the drilling started with a 6 mm diameter trephine drill to remove the thick layer of silicone representing the gingival tissues covering the resin model.

This step was unreliable and often caused the drill to be deflected by the thick silicone layer on initial contact, probably due to the physical properties of the silicone. This was rectified by removing a circular area of silicone in the osteotomy site with a manual biopsy punch tool (6 mm in diameter) instead of the trephine drill. This also had the benefit of replicating what would be done in actual clinical cases.

Next, the entry site was marked with a short round bur (2 mm deeper than the implant entry point). Then a short spade (needle) drill was used to reach about 7 to 10 mm (fifth of the trajectory length). The alveolar preparation was paused here to follow the manufacturer recommendation of using the precision and twist zygomatic drills before completing the alveolar preparation step. So, the sequence after the short spade drill was; zygomatic spade drill, zygomatic round drill (to mark zygomatic bone entry), zygomatic initial twist drill (2.7 mm in diameter), zygomatic final twist drill (2.9 mm in diameter), zygomatic counter-sink drill, alveolar final drill (3.5 mm in diameter) and finally the implant placement step.

Another early modification was to complete the preparation of the alveolar part with a 5 mm diameter drill (Nobel Replace®, WP) before the use of any zygomatic drill. The main reason was to enable the use of the drill extender (4.5 mm in diameter) with the subsequent zygomatic drilling steps allowing the extender to go into the alveolar osteotomy site without interference.

4.9.2. Testing a 5 stages protocol to increase time efficiency

This protocol was tried with the robotic drilling procedure driven by the fact that it should not be more difficult for the robotic arm to control a long drill to prepare both the alveolar as well as the zygomatic osteotomy sites.

The included steps were; manual biopsy punch, zygomatic round drill, zygomatic final twist drill, zygomatic counter-sink drill and finally the implant placement step. The accuracy results from this protocol were still comparable to the 10 stages protocol. However, the effect of high frictional and flexural forces could be clearly observed during all the drilling steps (except counter-sinking).

Assuming that such high frictional forces for a long distance will most likely prohibit the transfer of this protocol to the clinical environment (due to potential bone damage), further experimentation with this protocol was terminated. This decision also contributed to protecting the implant handpiece from further damage due to the flexural forces applied to the drills. The 4 drills used in this protocol are shown in figure 4-37.

Figure 4-37. The tools involved in the 5 stages drilling protocol ordered from left to right: biopsy punch tool (6.0Φ) that was shortend to enhance access, round drill, final twist drill (2.9Φ), counter-sink drill, implant placement.

4.9.3. The modified 10 stages protocol used as the final protocol

The drilling protocol was further optimised via the addition of a side-cutting drill before counter-sinking. This modification reduced the possibility of the ZI to deflect away from the zygomatic bone entry site upon insertion. The drills involved are shown in figure 4-38.

Figure 4-38. The 9 drills involved in the 10 stages drilling protocol ordered from left to right: short spade drill, short final alveolar drill, zygomatic round drill, zygomatic spade drill, zygomatic initial twist drill (2.7Φ), zygomatic final twist drill (2.9Φ), zygomatic side-cutting drill, zygomatic counter-sink drill, zygomatic implant placement. The 1st stage was removing the silicone layer covering the entry position with a biopsy punch tool, which is shown in the previous figure.

The implant placement step was also divided into stages to reduce the chance of damage to the handpiece from the excessive torque required during this stage. The 15 mm long apical threads were segmented into 7 mm for initial robotic handpiece advancement, followed by manual rotation of the implant (without apical pressure) for about 10 complete turns (~5 mm) and thus leaving the final 3 mm to be finalised by the robotic arm again with the activation of the automatic cut-off function explained in section 4.7.

Chapter 5

The Accuracy of Dynamic Navigation-Guided Robotic Placement of Zygomatic Implants – a comparative in vitro study

This chapter describes an *in vitro* experiment to compare the accuracy of the zygomatic implant placement using robotic versus traditional dynamic navigation techniques. The aim was to investigate the application error with the expectation that the robotic technique would achieve a higher accuracy.

5.1. Introduction

One of the effective rehabilitation treatment options for the edentulous maxillae is the placement of zygomatic implants (ZIs) (Pellegrino et al., 2020a, Testori et al., 2024). This approach is not without associated surgical complications, particularly those caused by the need for flap reflection, such as swelling, postoperative pain and hematoma (Kämmerer et al., 2023). The flapless approach for dynamic navigation guided placement of ZIs under local anaesthetic has been proven to be successful in reducing these complications (Bhalerao et al., 2023, Bhalerao et al., 2024). Rehabilitation of these cases usually involves the placement of four ZIs or two posterior ZIs with conventional anterior dental implants (Varghese et al., 2021, Wadde et al., 2024). The decision-making process depends on the availability of bone in three zones of the maxilla; the anterior, middle, and posterior zones, I, II, and III, respectively (Aparicio et al., 2014, Aalam et al., 2023). If zones II and III do not have enough bone, rehabilitation with ZIs would be the only fixed prosthetic option that does not include complicated bone augmentation and sinus-grafting procedures (Aparicio et al., 2014) (see figure 1-13 in section 1.5 on page 22). Bone availability in zone III would add the option of supplementing the rehabilitation plan with pterygoid implants (Aalam et al., 2023).

5.1.1. Static guided ZI placement

Static guidance using surgical templates is the most commonly used method when guiding the placement of ZIs, but it has its limitations (Chrcanovic et al., 2010). The initial versions of these templates were associated with high error values due to the fact that the implant placement step could only be achieved after the removal of the template (Chrcanovic et al., 2010).

Schiroli's research team proposed a flapless approach for ZI placement using static guides (Schiroli et al., 2011). They reported the challenging nature of this approach both *in vitro* and on cadavers, especially in relation to implant angulation (Schiroli et al., 2011, Schiroli et al., 2016).

J. Chow proposed a specially designed ZI drilling guide to supplement the conventional static surgical template. It consisted of two metallic pieces that ensured a straight trajectory between the entry and exit points which enhanced the optimal implant positioning (Chow, 2016).

Bedrossian and colleagues published some surgical principles that highlighted the prevention and management of complications associated with ZI placement. They stressed the importance of understanding the anatomy and physiology of the surgical site in addition to the direct visualisation of the penetration site of the final twist drill into the lateral cortex of the zygomatic bone during the osteotomy. They also presented the management of ZI fracture, ZI over-extension and post-placement maxillary sinus blockage. They advised copious irrigation and cross-arch splinting as preventative measures to reduce the possibility of these complications (Bedrossian, 2021).

Jayanetti and colleagues suggested the use of double sleeves when the anatomy allows it (in ZAGA-3 and 4 cases) (Jayanetti et al., 2021). Rigo and colleagues advocated a fully guided ZI placement approach to simplify the conventional surgical procedure by using metallic surgical templates. This technique is still dependant on the presence of sufficient supporting bone on which to fix the template (Rigo et al., 2021).

Gallo and colleagues have reported on the accuracy of static-guided ZIs with the detailed directionality of the deviations. The differences in the accuracy between the anterior and posterior ZI and between the right and left sides were statistically non-significant (Gallo et al., 2023). Further research is ongoing in relation to the refinement of these guides (Hernández-Alfaro et al., 2023, Mao et al., 2023).

5.1.2. Dynamic navigation guided ZI placement

Watzinger and colleagues were among the first research teams to attempt ZI placement based on a surgical navigation system (Watzinger et al., 2001). Their study on cadavers resulted in 1.7 ± 1.3 mm deviations at the implant entry point and 1.3 ± 0.8 mm deviations at the exit point (Watzinger et al., 2001). The technique of ZI placement under dynamic navigation has been heavily investigated since that time (Hung et al., 2017, Fan et al., 2023, Wang et al., 2024c). Due to the increased confidence in the refined dynamic navigation techniques, Bhalerao and colleagues recently implemented a flapless approach for ZI placement using dynamic navigation (Bhalerao et al., 2023, Bhalerao et al., 2024). González-Rueda and colleagues added the mixed-reality dimension using HoloLens glasses (González-Rueda et al., 2023). Optimising the registration of patient space and enhancing the drill calibration process are crucial to improve the accuracy of the placement of dental and zygomatic implants under dynamic navigation guidance (Al-Jarsha et al., 2024a, Al-Jarsha et al., 2024b).

5.1.3. Robotic guided ZI placement

Despite the fact that dynamic navigation has improved the accuracy of placement of ZIs and reduced the associated morbidity, the method is dependent on the operator's manual dexterity and requires extensive training to maximise the visual-manual coordination (Xu et al., 2023b, Wang et al., 2024c). These limitations inspired the development of the robotic placement of ZIs, which could eliminate the operator error arising from the level of their manual dexterity and coordination (Shengchi et al., 2018, Cao et al., 2020).

Yang and colleagues have divided the robotic systems into 5 levels of autonomy; level 1 being robotic assistance (i.e., passive robotics such as DentRobot®, Cobot®, and Yomi® systems), level 2 being task autonomy (i.e., semi-active and active robotics such as Remebot® and Yakebot® systems), and levels 3 to 5 being the target for future development (conditional autonomy, high autonomy, and full automation) (Yang et al., 2017).

In level 1 of autonomy, the human controls the tool attached to the robotic arm while the arm restricts certain movements physically to provide assistance in localisation. Level 2 robotic systems are able to perform pre-programmed tasks irrespective of feedback received from the robotic arm sensors. Level 3 systems rely on information feedback from the robotic arm to modify the pre-programmed tasks based on pre-programmed conditions. Level 4 and 5 autonomies require the inclusion of artificial intelligence to make decisions that are too complicated to program in a prescribed number of conditions with simple programming (Yang et al., 2017).

Shengchi, Cao and colleagues were among the first investigators of the use of robotic systems for the placement of ZIs *in vitro* (Shengchi et al., 2018, Cao et al., 2020). This was followed by Li, Deng and colleagues who tried their two-stage protocol *in vitro* and then in clinical cases (Deng et al., 2023c, Li et al., 2023a). Their protocol involved the use of the semi-active Remebot® system to prepare the alveolar ridge in the first stage, followed by the manual insertion of the zygomatic drills in the prepared socket and the manual installation of these drills on the handpiece. In the second stage, the robotic drilling of the zygomatic bone was completed (Deng et al., 2023b, Deng et al., 2023c, Deng et al., 2023a). These papers were followed by other studies which investigated challenging clinical cases involving ZI implant placement, such as flapless cases with immediate loading (Li et al., 2023a, Olivetto et al., 2023). To provide a more robust robotic supervision, implementing the HoloLens glasses can achieve a mixed-reality environment for monitoring the robotic drilling procedure, and constitutes a novel “hybrid” ZI placement robotic protocol (Fan et al., 2024).

Robotic technology has been shown to be successful in the placement of dental and ZIs (Olivetto et al., 2023, Tian et al., 2023, Fan et al., 2024). It has the advantages of efficiency and precision, as well as allowing the flapless placement of dental implants, in addition to overcoming the difficulties of the limited surgical access (Tian et al., 2023). Several research teams have attempted to use robotic implant technology to perform supplemental procedures such as sinus floor elevation (Su et al., 2024) and endodontic surgery (Liu et al., 2024).

Xu and colleagues have evaluated active (Yakebot®), semi-active (Remebot®), and passive (DentRobot®) optically tracked commercial implant robotic systems (Xu et al., 2023a). They reported better accuracy of implant position with active and semi-active systems that required less human-robot interaction during surgery than passive systems (Xu et al., 2023a). Passive and semi-active robotic systems require the operator to handle the robotic arm while entering and exiting the patient's mouth. Therefore, these steps took less time than with active robotic systems which require extensive calibration-registration-verification processes that are time-consuming (Xu et al., 2023a, Bolding and Reebye, 2021). Studies on the accuracy of, Yomi®, a passive robotic system that depends on mechanical rather than optical tracking, reported higher errors in the placement of implants, both *in vitro* (Mozer and Guentsch, 2024) and in a clinical series (Neugarten, 2024).

Huang and colleagues have promoted the use of a dual robotic arm system in order to overcome the issue of the obstructed field of vision of the tracking camera. In addition to tracking the marker attached to the jaw, the camera also contributed to their monocular optical positioning system, in which the fact of keeping a fixed spatial relationship between the bases of the two robotic arms reduced the operative preparation time (Huang et al., 2023). Tang and colleagues have also suggested the same idea (Tang et al., 2024). The workflow for rehabilitating full arches with immediate dental implants is currently being established (Wang et al., 2024b, Shu et al., 2024). Therefore, the robotic intervention protocols are still under research, and further work is needed with the aim of improving the robotic systems and their associated protocols.

In this chapter, the accuracy of the robotic drilling and ZI placement using a newly developed task-autonomous active robotic system was tested against manual drilling and placement under dynamic navigation guidance. The robotic prototype system was composed of a 6 degrees of freedom robotic arm (UR3e) and an optical dynamic navigation system (NaviDent®).

The aim was to compare the dimensional accuracy of the robotic zygomatic implant placement protocol against two different dynamic navigation systems; X-Guide® and NaviDent®. The results would establish an evaluation of the magnitude of application error, with minimisation of confounding errors arising from other sources such as registration error and drill calibration error as they are being minimised and standardised across the three groups.

5.2. Materials and Methods

This experiment was conducted on 12 plastic models with 8 ZIs implants that were re-inserted into 48 ZI locations in three groups; robotic group (16 ZI locations), NaviDent® DN group (16 ZI locations), and X-Guide® group (16 ZI locations). The sample size calculation and the distribution of these locations are described in the study design section 5.2.3. The outcome measures were ZI deviations in terms of 3D entry point, 3D exit point, 2D directional, in addition to angular deviations. Procedure time was recorded for the 3 groups and the force feedback data were also collected from the robotic group.

5.2.1. Materials

The NaviDent® (ClaroNav, Canada) and X-Guide® (X-Nav Technologies, USA) dynamic navigation systems were used for this experiment. Software versions were NaviDent® 3.0.3 and X-Guide® 3.1.1.11, respectively.

The UR3e robotic arm (Universal Robots®, Denmark) that had been integrated with one of the dynamic navigation systems was used to place the implants in the study group (figure 4-9 in section 4.3 on page 116).

The anatomically accurate plastic models used in this experiment were ZYG NM 01 (SelModels®, Spain). They resemble the human anatomy and simulate the usual force feedback felt during drilling and implant placement in real bone of D2 type density (Figure 5-1). The selection of D2 bone density was based on the published literature regarding the architecture of the zygomatic bone (Nkenke et al., 2003, Pryor McIntosh et al., 2016).

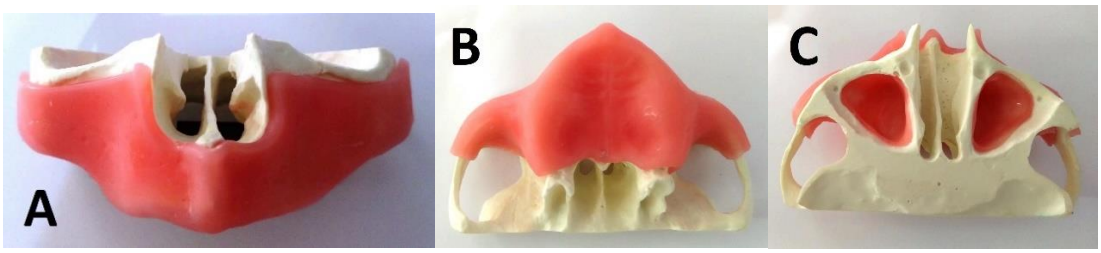

Figure 5-1. The zygomatic implant placement model (Ref. ZYG NM 01) from SelModels®. (A) Frontal view. (B) Occlusal (inferior) view. (C) Superior view.

The fiducial markers were the same as those used for the previous experiments (1.2x6 mm, Stryker Leibinger). This specific size was selected so that both dynamic navigation systems included in the experiment could recognise them. They are also depicted in figure 5-2.

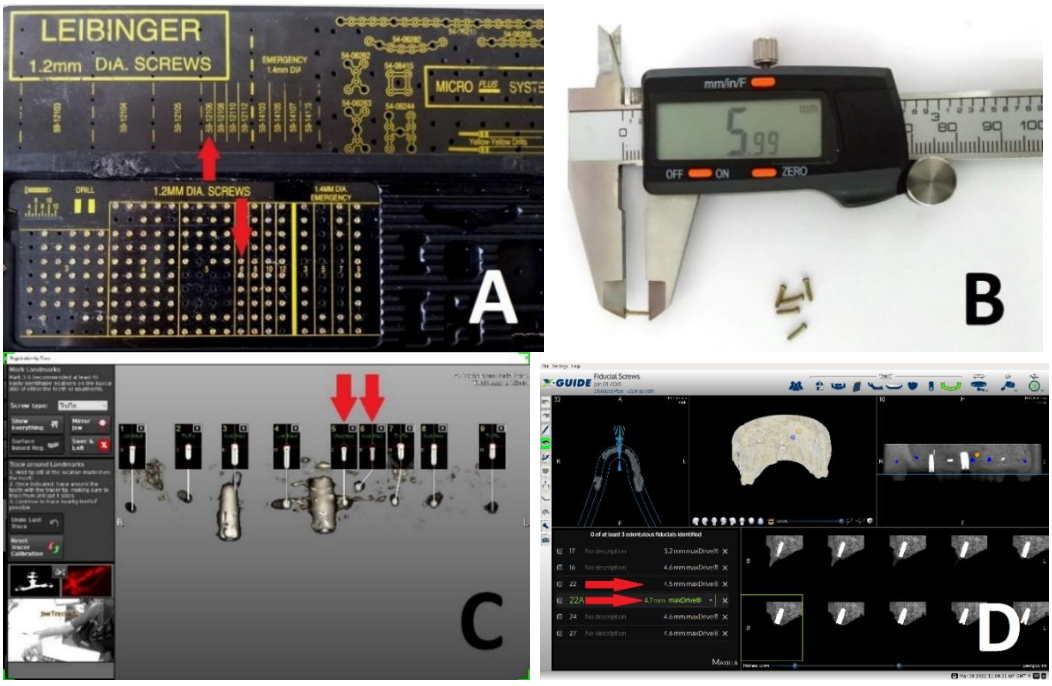

Figure 5-2. The fixation screws used as fiducial makers. (A) The surgical kit – the selected size is marked with red arrows. (B) Caliper vernier real-life dimension check prior to placement in the models. (C) A screenshot from NaviDent® fiducial registration screen – screws were recognised as Ustomed® 1.2x6mm bone fixation screws. (D) A screenshot from X-Guide® fiducial detection screen – screws were recognised as KLS martin maxDrive® 1.5x5mm bone fixation screws. (E) Fiducial markers recommended by NaviDent® and X-Guide® navigation systems. The screen captures from the user manuals are with permissions.

A dental imaging system (KaVo OP 3D Vision; KaVo Dental GmbH, Germany) was utilised to obtain the CBCT scans for the study. Scans were carried out pre- and post- implant placement. The settings were FOV 6x16 cm, voxel size 0.4 mm, 120 KVP, 5 mA and exposure time of 3.7 seconds. Figure 5-3 shows the alignment of the model during the CBCT scanning procedure. The pre- and post-operative scans were superimposed based on the entire shape of the surface (figure 4-4 on page 112; section 4.2.1). Therefore, precision in positioning on the CBCT table was not critical, as long as the entire model was within the field of view.

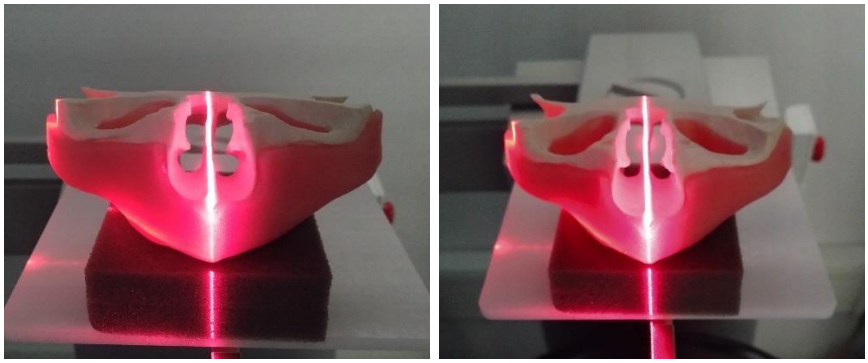

Figure 5-3. The positioning of the model during a preoperative and postoperative CBCT scans. The laser guidance position was observed but a high-level of precision was not required.

Zygomatic implants (ZYGAN™ ; Southern Implants® , RSA) were placed using the specific manufacturer drill set. The W&H Implantmed® motor (SI-95 230) and the W&H WS-75 surgical contra-angle handpiece were used to place the ZIs in all tested groups.

5.2.2. Planning procedure

Preoperative CBCTs were obtained to plan 4 zygomatic implants per model (QZP design). The specific length and trajectory in each of the 4 sites were dependant on the anatomy of that area according in the model (Pellegrino et al., 2020c, Aparicio et al., 2021b, Aparicio et al., 2021c).

The planning process was carried out to determine the appropriate implant lengths for the particular anatomy of the zygomatic model that is shown in figure 5-1. Therefore, these steps including three rather than one pre-operative CBCT scan were only performed one time (for the first model).

A set of radio-opaque teeth was arranged in the prosthodontic laboratory to fit the edentulous arch of the model (figure 5-4; A). Next, the model was scanned together with the teeth wax-up (figure 5-4; B).

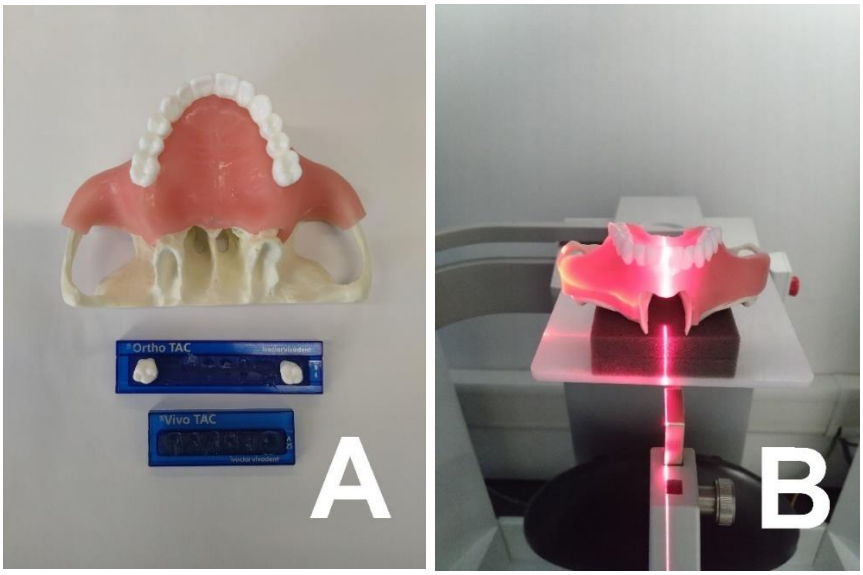

Figure 5-4. (A) The arrangement of radio-opaque teeth to get the information needed for an optimal prosthodontically-driven implant plan. (B) The setup for the CBCT scan of the model with the radio-opaque teeth.

STL files were segmented and then extracted from the scan to represent the outer surface (silicone layer), the teeth, and the bone surface (i.e., the resin surface under the silicone layer). The segmentation process was carried out in 3D Slicer software (v. 5.1.0). All resulting STLs were then aligned so that the occlusal plane was horizontal, and the model was centred according to the dental midline (figure 5-5).

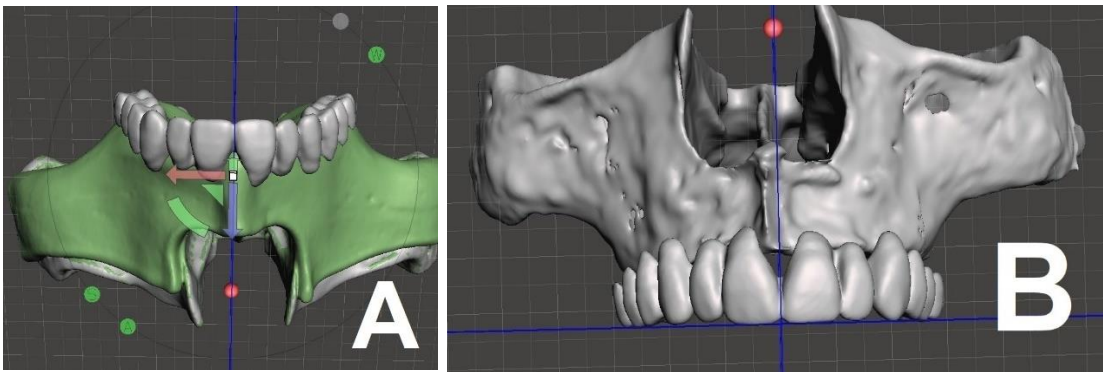

Figure 5-5. (A) The alignment of the STL without the teeth to the one with the teeth relying on the outer surface (to get a smooth surface representation of the silicone under the teeth). (B) Confirming the alignment after setting occlusal plane, the dental midline, and the removal of the soft tissue layer so that the STL is ready for the next step in the planning process. The software used to carry out these steps was MeshMixer.

An STL library was created to represent the shapes of the implants based on the dimensions provided in the user manual and those obtained by direct caliper vernier measurement of the real implants (figure 5-6).

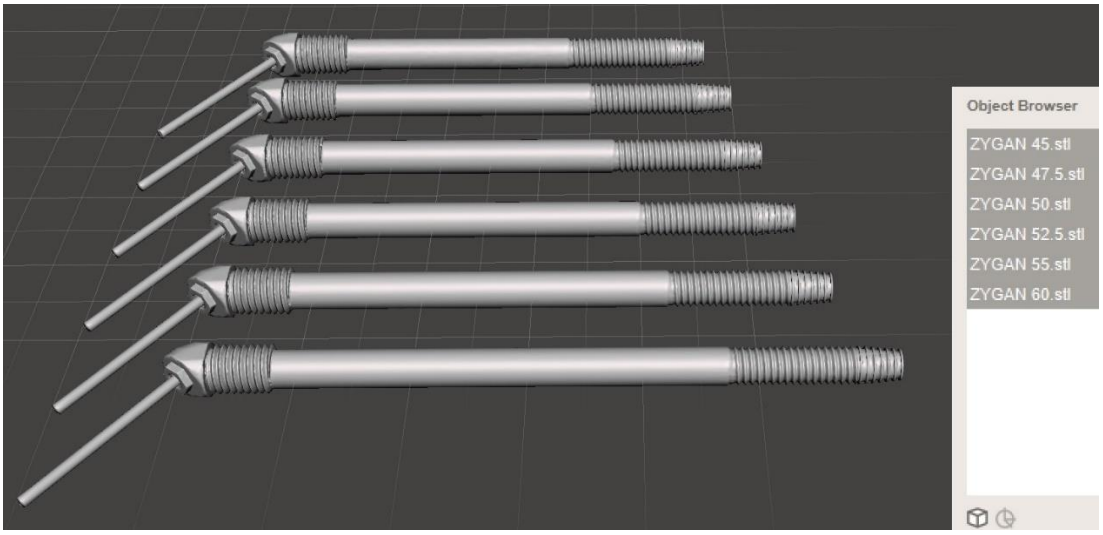

Figure 5-6. A custom library of zygomatic implants was created in MeshMixer with an added small cylinder (1x20 mm) on the coronal portion, to represent the prosthodontic axis which is always at 55° from the long axis of the implant (this implant had a 55° angle built-in its design). This step was necessary to directly reflect the changes in the prosthodontic axis when the 3D position of the implant is modified during the planning process.

Next, the trajectories of the implants were planned in MeshMixer depending on the STL representations mentioned above, rather than in any CBCT planning software. This allows easier and faster determination of the final position and angulation of the trajectories as the prosthodontic axis cylinders could be easily re-aligned to the desired positions and angulation in relation to the occlusal plane (figure 5-7).

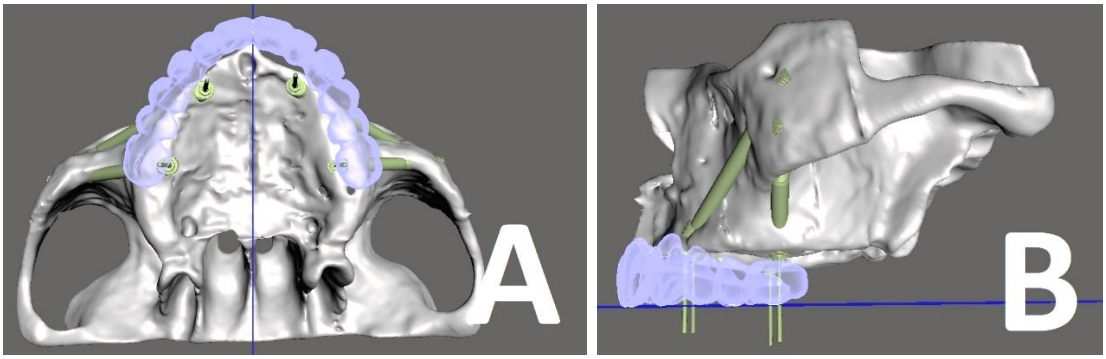

Figure 5-7. The final zygomatic implant plan as designed in MeshMixer. This plan is ready to be exported with the outer soft tissue so that it can be imported into the dynamic navigation systems. (A) Occlusal view to show alignment to the dental midline (blue line). (B) Lateral view to show the alignment to the occlusal plane (blue line) and the four prosthodontic axes of the zygomatic implants (green) perpendicular to the occlusal plane.

According to the planning procedure described above, the selected implant lengths were as follows:

- 50 mm for the anterior right trajectory (ZAGA-1).
- 40 mm for the posterior right trajectory (ZAGA-2).
- 50 mm for the anterior left trajectory (ZAGA-1).
- 35 mm for the posterior left trajectory (ZAGA-2).

The ZAGA classification was based the publication of Aparicio's team (Aparicio, 2011, Aparicio et al., 2021a) (see section 1.5). The selection of these classes was based on the anatomy of the model. They are also the most common classes in these locations (Wang et al., 2021a).

After the extraction of an STL surface file representing the outer anatomy from every pre-operative CBCT DICOM using InVesalius software (v.3.1.1), this ZI plan was superimposed over each pre-operative STL surface file to produce model-specific STL plan files. This was followed by importing each model-specific STL plan over its corresponding pre-operative scan as a surface scan in STL file format (figures 5-8 and 5-9).

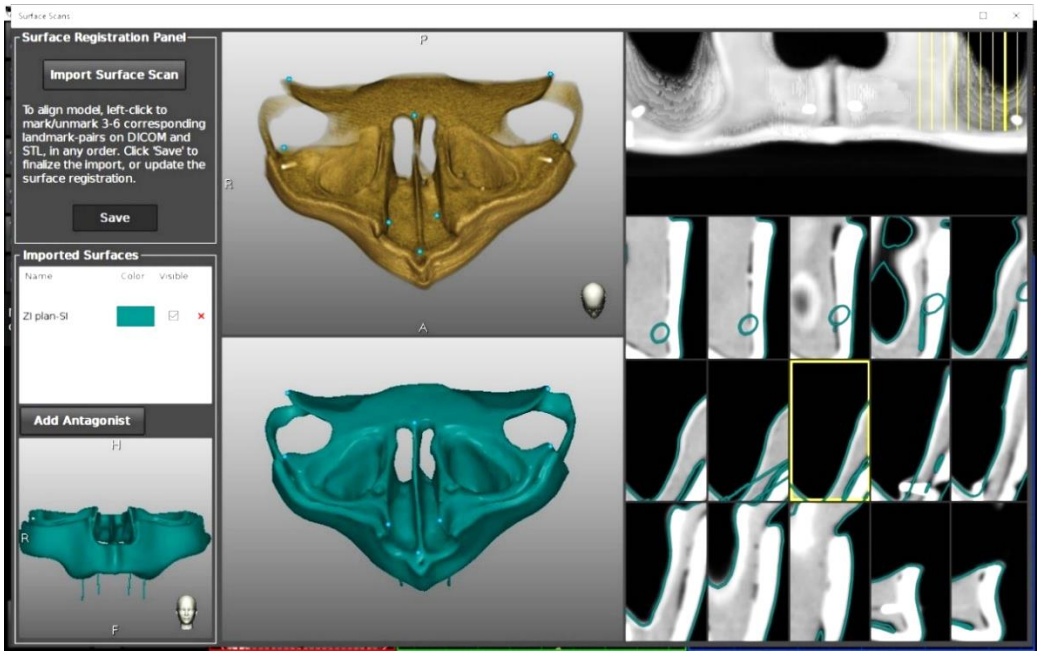

Figure 5-8. Importing the unified plan (as STL) into the NaviDent® software and aligning it to the preoperative models containing the fiducial screws. The light brown-coloured model is a representation of the preoperative CBCT scan. The dark turquoise-coloured model is the STL file of the final ZI plan. The right section of the screenshot is used to judge the accuracy of the 3D superimposition of the STL file over the CBCT.

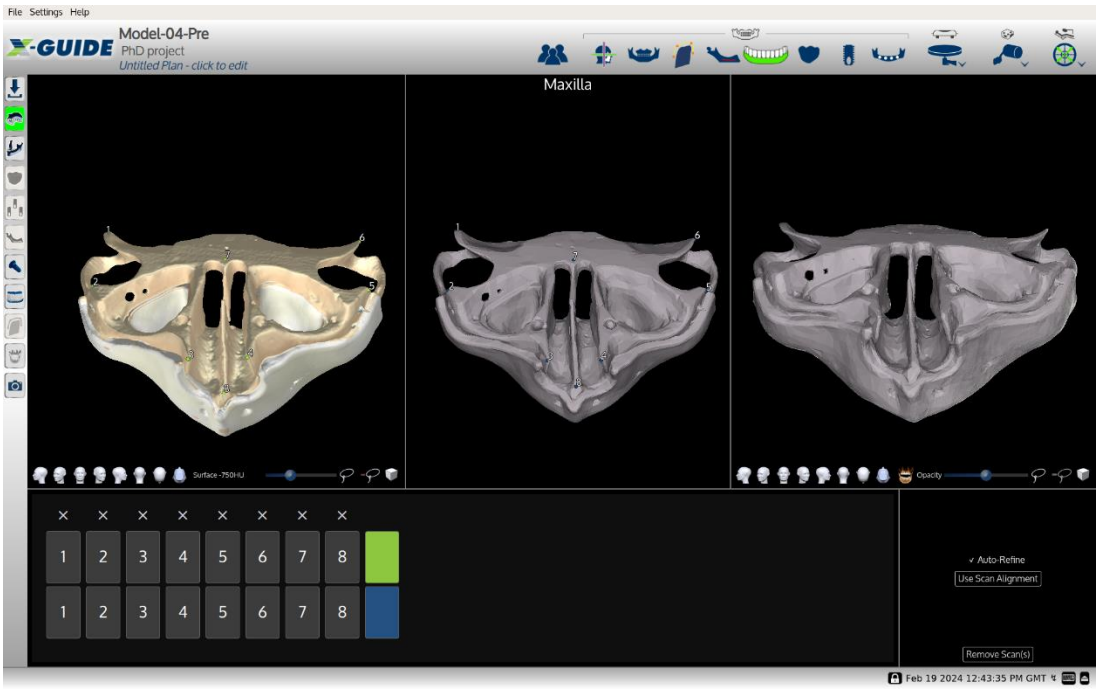

Figure 5-9. Importing the unified plan (as STL) into the X-Guide® software and aligning it to the preoperative models containing the fiducial screws. The left model is a representation of the preoperative CBCT scan. The model in the centre is the STL file of the final ZI plan. The right section of the screenshot is used to judge the accuracy of the 3D superimposition of the STL file over the CBCT.

Next, the operator aligned new NaviDent® or X-Guide® implant cones over those that were already part of the STL plan file (figures 5-10 and 5-11) and identified the fiducial markers in that import (figure 5-12).

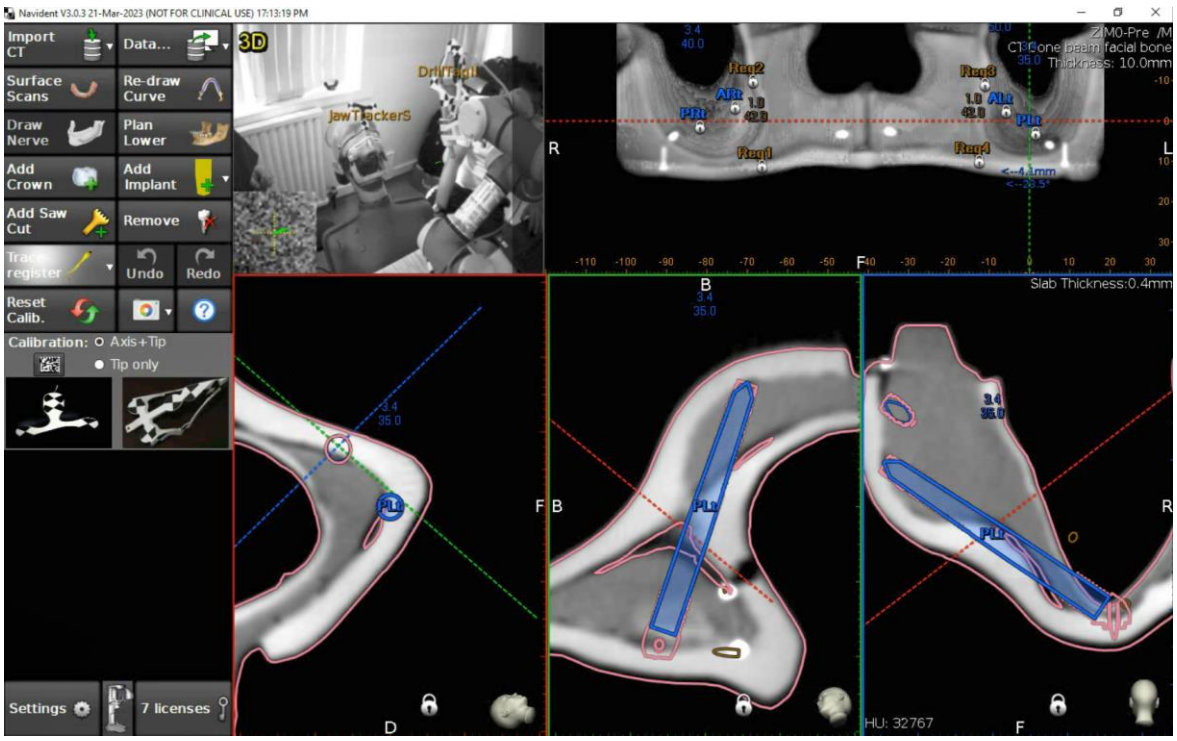

Figure 5-10. Aligning NaviDent® implant cones (the blue outline) to the STL plan (pink outline) so that the model is ready for the next steps of dynamically navigated implant placement. The top section of the screenshot includes the camera view and the panoramic view of the implant plan. The bottom 3 sections illustrate an occlusal, lateral and posterior views of the planned implant trajectory.

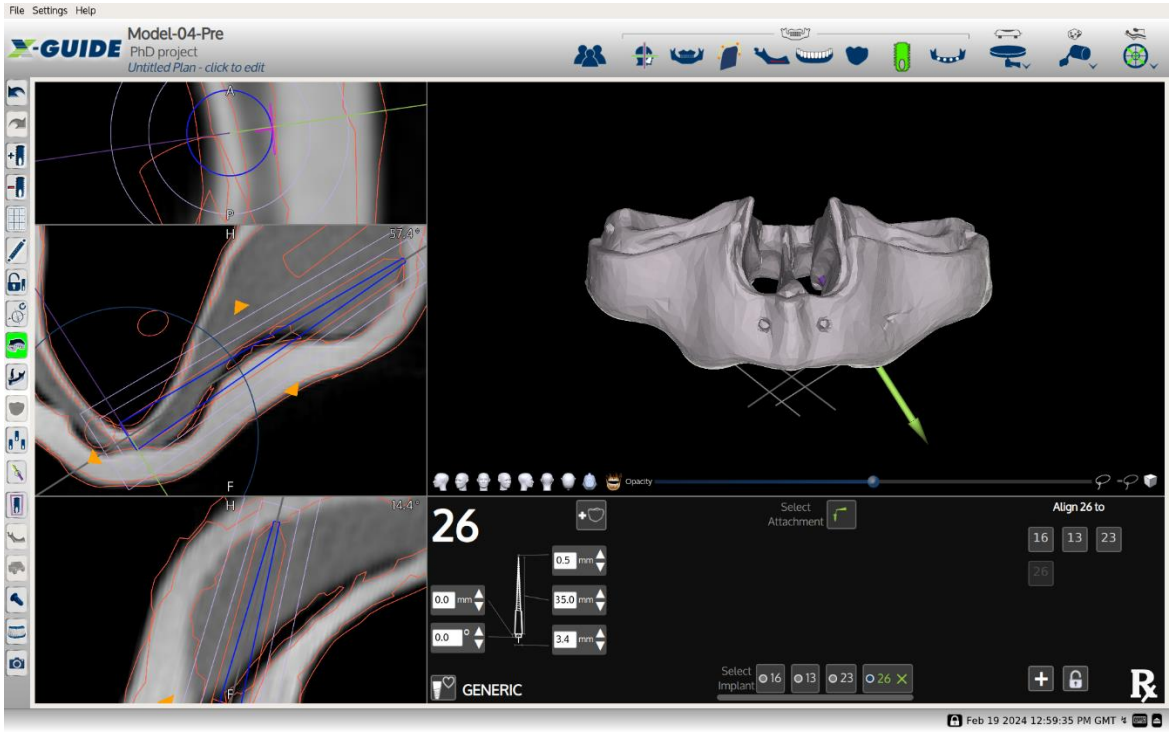

Figure 5-11. Aligning X-Guide® implant cones (the blue outline) to the STL plan (orange outline) so that the model is ready for the next steps of dynamically navigated implant placement. The right section of the screenshot includes the 3D view of the implant plan. The left 3 sections illustrate an occlusal, posterior, and lateral views of the planned implant trajectory.

Figure 5-12. The distribution of fiducial makers on the zygomatic model. Top: the 3 registration fiducials on the right side of the model (yellow arrows) and the target fiducial (blue arrow). Middle: A screenshot from NaviDent® software showing the registration fiducials in a panoramic view during the registration step as well as the quality of the distribution (the green circles with no.1) of the 4 planned zygomatic implant trajectories (yellow circles). Bottom: A screenshot from X-Guide® software showing the registration fiducials in a panoramic view during the registration step as well as the quality of the distribution (registration deviation value of 1.18 mm in this example).

5.2.3. Study design

Sample size calculation was based on the angular deviation figures from the study of Cao and their colleages (Cao et al., 2020) setting α at 0.05 and sample power at 0.8 (figure 5-13). The reported deviations were not specific to a single location according to the Cao et. al. study. They reported 2.07° ± 0.30° deviation from 4 manually placed ZIs under dynamic navigation, and 1.52° ± 0.58° deviation from 12 robotically placed ZIs under dynamic navigation. The resulting size calculation is therefore for the total arm rather than a specific implant position (Cao et al., 2020).

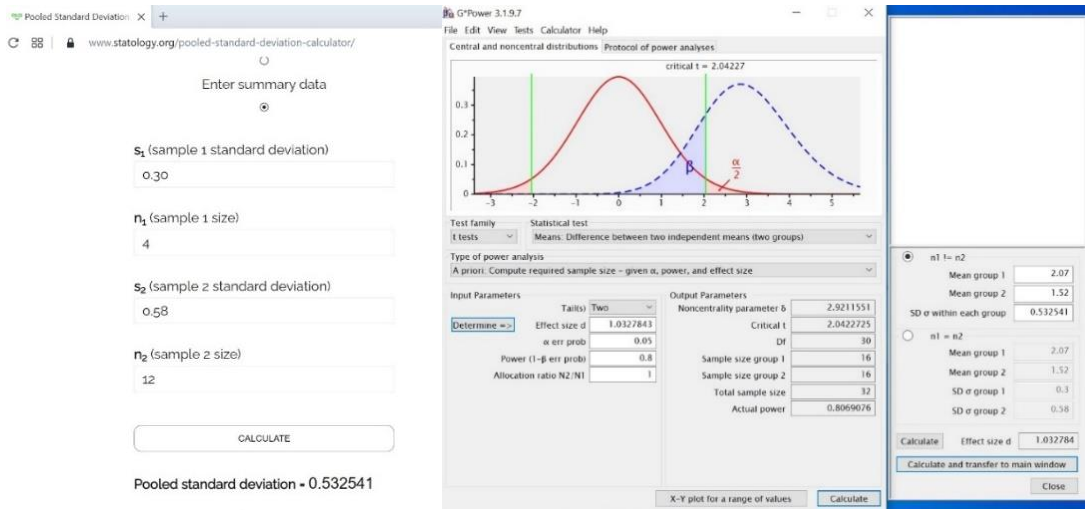

Figure 5-13. Sample size calculations for ZI placement experiment. The groups were not equal in size (Cao et al., 2020). Therefore, a pooled standard deviation was calculated ($\sqrt{\frac{(n_1-1)s_1^2+(n_2-1)s_2^2}{n_1+n_2-2}}$) as shown on the left side of the figure. G*Power software was then used to calculate the required sample size for an independent group comparison as shown on the right side of the figure. 16 implants per arm ➔ 4 models per arm.

The implants were inserted bilaterally in a systematically randomised fashion to include the 3 proposed arms of the study (figure 5-14).

Model no.	Right-Anterior	Right-Posterior	Left-Anterior	Left-Posterior
1				
2				
3				
4				
5				
6				
7				
8				
9				
10				
11				
12				
Totals	4	4	4	4
	4	4	4	4
	4	4	4	4

Key	Group/Arm
	DN - NaviDent
	DN - XGuide
	DN + Robotics

Figure 5-14. The systematic distribution for the zygomatic implants among the models based on 3 study comparative arms and 4 locations per model. The 4 implants' lengths and trajectories were identical in all models as they had identical anatomy. During results' data collection and analysis, the assessor was blinded to reduce the risk of bias (a person different from the operator assigned a different model identification key during the analysis step which was only revealed after the analysis was concluded). DN = dynamic navigation.

After concluding this experiment, a supplementary control group was necessary to isolate the effect of two confounding factors. This 4th group included 4 models where ZIs are placed manually under the guidance of NaviDent®, but using the single drill calibration protocol described in section 4.8. The two confouding factors were the tactile feedback and the calibration protocol.

5.2.4. Calibration and Registration procedures

The drill calibration processes followed the manufacturer instructions for the two dynamic navigation groups (i.e., multiple drill calibration protocol). However, a single drill calibration protocol was utilised for the robotic group and for the supplementary control group. The differences between these protocols are described in section 4.8.

In all arms of the study, the registration process for the data of each specific model CBCT in the dynamic navigation system to their real anatomy was done according to a single optimised protocol (Al-Jarsha et al., 2024a). The acceptable threshold for registration accuracy was 0.0 mm on the operative side and 0.1 mm on the contralateral side (figures 5-15 and 5-16).

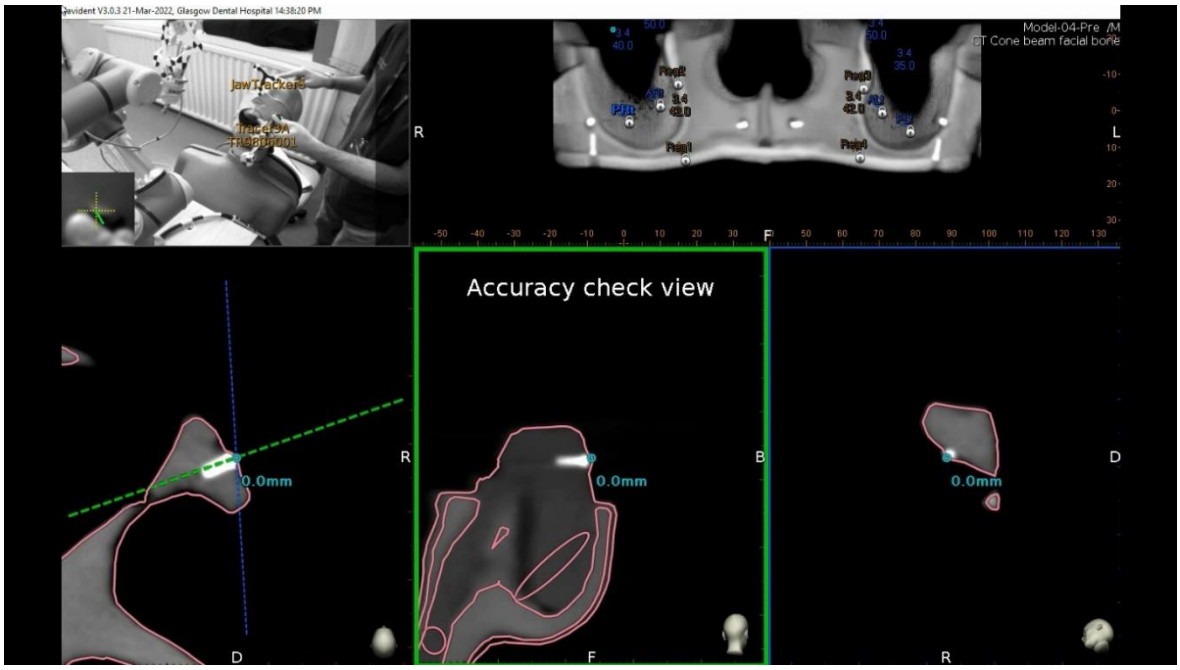

Figure 5-15. The registration accuracy check using the tracer tool at the right target fiducial shows 0.0 mm error at this point according to the NaviDent® system.

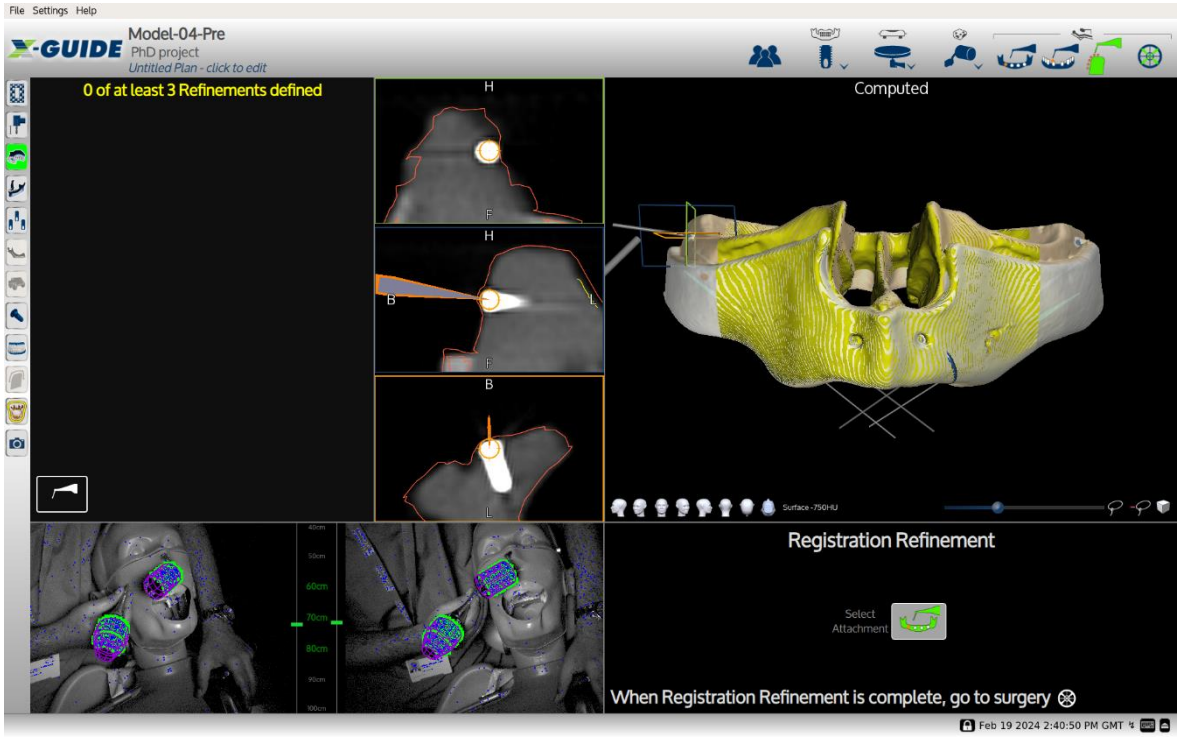

Figure 5-16. The registration accuracy check using the tracer tool at the right target fiducial according to the X-Guide® system.

One accurate registration was needed in each session. However, if movement of one or more of the critical components was suspected during the drilling process and then verified through a registration accuracy check, it would have been necessary to repeat the registration process.

Besides dynamic navigation registration, it was necessary to conduct a robotic registration process in the robotic group. This process aimed to match the coordinates between the robotic arm and the NaviDent® system. The Hand-Eye calibration protocol (described at the end of section 4.3.2) was implemented for UR3e robotic registration and its refinement. The accuracy check for this registration involved approaching the exit point of the trajectory in air, after selecting the final zygomatic twist drill in the robotic control software (see figure 4-18 on page 124).

5.2.5. Implant placement procedure

The implant drilling and placement procedure followed a slightly modified protocol of that recommended by the implant manufacturer (see section 4.9). However, no water cooling was necessary as the implants were being placed in resin models. A drill extension was added with particular drills to avoid collision of the grip used for the robotic arm with the model and the dental simulator assembly.

Registration and operative times were recorded by noting the starting time of each drilling step on a printed drilling protocol sheet produced for every trajectory in all study groups (figure 5-17).

The force feedback data were recorded for 12 trajectories in the robotic group using the built-in wrench sensor in the robotic arm.

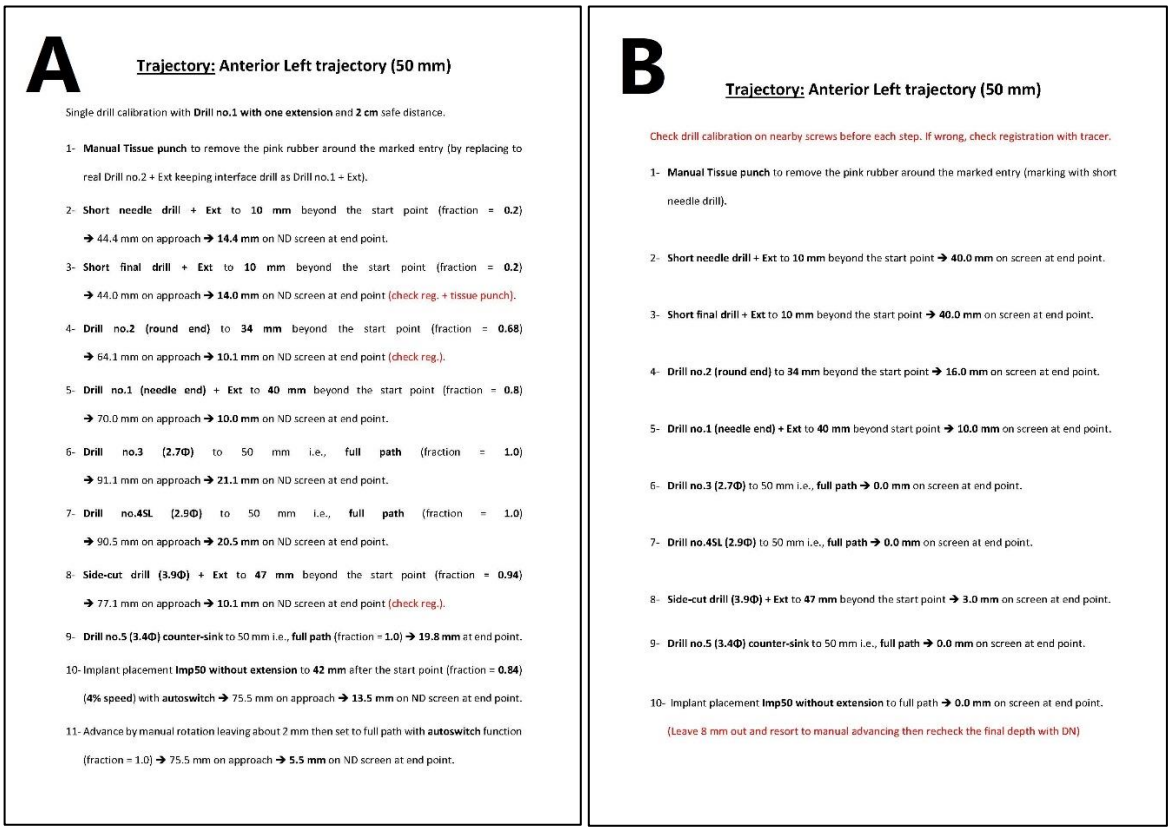

A

Trajectory: Anterior Left trajectory (50 mm)

Single drill calibration with **Drill no.1 with one extension** and **2 cm** safe distance.

1- **Manual Tissue punch** to remove the pink rubber around the marked entry (by replacing to real Drill no.2 + Ext keeping interface drill as Drill no.1 + Ext).

2- **Short needle drill + Ext** to **10 mm** beyond the start point (fraction = **0.2**) → 44.4 mm on approach → **14.4 mm** on ND screen at end point.

3- **Short final drill + Ext** to **10 mm** beyond the start point (fraction = **0.2**) → 44.0 mm on approach → **14.0 mm** on ND screen at end point (check reg. + tissue punch).

4- **Drill no.2 (round end)** to **34 mm** beyond the start point (fraction = **0.68**) → 64.1 mm on approach → **10.1 mm** on ND screen at end point (check reg.).

5- **Drill no.1 (needle end) + Ext** to **40 mm** beyond the start point (fraction = **0.8**) → 70.0 mm on approach → **10.0 mm** on ND screen at end point.

6- **Drill no.3 (2.7Φ)** to 50 mm i.e., **full path** (fraction = **1.0**) → 91.1 mm on approach → **21.1 mm** on ND screen at end point.

7- **Drill no.4SL (2.9Φ)** to 50 mm i.e., **full path** (fraction = 1.0) → 90.5 mm on approach → **20.5 mm** on ND screen at end point.

8- **Side-cut drill (3.9Φ) + Ext** to **47 mm** beyond the start point (fraction = **0.94**) → 77.1 mm on approach → **10.1 mm** on ND screen at end point (check reg.).

9- **Drill no.5 (3.4Φ) counter-sink** to 50 mm i.e., **full path** (fraction = **1.0**) → **19.8 mm** at end point.

10- Implant placement **Imp50 without extension** to **42 mm** after the start point (fraction = **0.84**) (**4% speed**) with **autoswitch** → 75.5 mm on approach → **13.5 mm** on ND screen at end point.

11- Advance by manual rotation leaving about 2 mm then set to full path with **autoswitch** function (fraction = 1.0) → 75.5 mm on approach → **5.5 mm** on ND screen at end point.

B

Trajectory: Anterior Left trajectory (50 mm)

Check drill calibration on nearby screws before each step. If wrong, check registration with tracer.

1- **Manual Tissue punch** to remove the pink rubber around the marked entry (marking with short needle drill).

2- **Short needle drill + Ext** to **10 mm** beyond the start point → **40.0 mm** on screen at end point.

3- **Short final drill + Ext** to **10 mm** beyond the start point → **40.0 mm** on screen at end point.

4- **Drill no.2 (round end)** to **34 mm** beyond the start point → **16.0 mm** on screen at end point.

5- **Drill no.1 (needle end) + Ext** to **40 mm** beyond start point → **10.0 mm** on screen at end point.

6- **Drill no.3 (2.7Φ)** to 50 mm i.e., **full path** → **0.0 mm** on screen at end point.

7- **Drill no.4SL (2.9Φ)** to 50 mm i.e., **full path** → **0.0 mm** on screen at end point.

8- **Side-cut drill (3.9Φ) + Ext** to **47 mm** beyond the start point → **3.0 mm** on screen at end point.

9- **Drill no.5 (3.4Φ) counter-sink** to 50 mm i.e., **full path** → **0.0 mm** on screen at end point.

10- Implant placement **Imp50 without extension** to full path → **0.0 mm** on screen at end point.
(Leave 8 mm out and resort to manual advancing then recheck the final depth with DN)

Figure 5-17. Example protocol sheets. (A) The single drill calibration protocol for the anterior left ZI trajectory. This protocol was applied for the robotic group and the NaviDent single calibration group. (B) The multiple drill calibration protocol for the anterior left ZI trajectory. This protocol was applied for the NaviDent group and the X-Guide group. During the experiment, the starting time of each step in the protocol was noted next to its number on the left.

5.2.6. Blinding process and accuracy analysis

The analysis was carried out blind. In order to ensure this, the following process was followed: different model keys (analysis keys, consisting of letters A to L) were randomly assigned to the models' operative keys (numbers 1 to 12). This random assignment was carried out by the principal supervisor and the deviations were extracted by the operator without knowing the operative key described in figure 5-14 (section 5.2.3).

This blinding process was applied to both pre- and post-operative CBCT scans in addition to the exported STL files from EvaluNav that were described in section 4.2.1. on page 111.

Having the axes of the exported STL files of the implant cones adjusted as described at the end of section 4.2.1 (figure 4-7 on page 114) facilitated the interpretation of deviation directions (figure 5-18).

Description	Collar - Point A			Apex - Point B			Distance (mm)	Collar	Apex
	x	y	z	x	y	z	3D	X-Shift	X-Shift
ImpPRt plan	20.574915	-34.17766	9.2058213	53.249027	-37.69085	32.010647	40.00000144	-1.07884614	-1.78298569
ImpPRt actual	19.496069	-34.25596	10.134831	51.466042	-38.57928	33.78286	39.99999307	Y-Shift	Y-Shift
Angle	1.955256							-0.07830136	-0.88843155
Collar Dev	20.574915	-34.17766	9.2058213	19.496069	-34.25596	10.134831	1.425867758	Z-Shift	Z-Shift
Apex Dev	53.249027	-37.69085	32.010647	51.466042	-38.57928	33.78286	2.6662872	0.92900956	1.772212982
							X	Mediolateral	+ve is Right
							Y	Ant.-post.	+ve is Forward
							Z	Sup.-infer.	+ve is Upward

Figure 5-18. When the axes have meaningful directional interpretation, the translational deviation information can be readily obtained (e.g., subtracting x coordinates of the apex in the plan from the x coordinates of the actual implant apex gives how much has the apex deviated mediolaterally and in what direction, because the x axis represents the mediolateral direction for all implants and in all models (Pellegrino et al., 2020b)).

The reproducibility (uncertainty) of the evaluation method was tested by extracting the deviations from one model after each of five repeated superimpositions. The 3D parameters of entry and exit deviations in addition to angular deviations were used to express the reproducibility in terms of the mean range of the 4 ZIs.

After the extraction of all deviation information, the blinding process described above was reversed so that the assignment of these deviations was related back to the operative key (figure 5-14 in section 5.2.3).

5.2.7. Statistical analysis

The null hypothesis for this experiment was that the implant placement accuracy for the robotic drilling group is not better than the manual drilling groups. The primary outcome measures were implant deviations in terms of 3D entry point, 3D exit point, 2D directional, and 3D angular deviations. The secondary outcome measures were procedure time (registration time and operative time) in addition to the robotic force feedback data.

Statistical analysis was conducted in SPSS statistics (IBM SPSS, v.26) to test the normality of distribution of the study groups and to decide on the statistical significance testing. The Shapiro-Wilk normality test was used for this purpose.

Statistical tests for normally distributed data included one-way ANOVA for multiple comparisons and Pearson's correlation coefficient for factor effects. For non-normally distributed data, non-parametric statistics were used instead (i.e., the independent sample Kruskal Wallis test for multiple comparisons and the Spearman's correlation coefficient for factor effects). The multiple comparison tests were carried out in GraphPad (Prism, v.9) with statistical significance level set at <0.05. GraphPad (Prism, v.9) was also used to create the graphical representations.

5.3. Results

The deviation data for all investigated groups had normal distribution upon Shapiro-Wilk normality testing. Therefore, the one-way ANOVA test was implemented for statistical multiple comparisons.

5.3.1. 3D deviations

The 3D deviations of the implant entry and exit points from the planned positions, in addition to the angular deviations for the main 3 comparison groups are shown in table 5-1 and figure 5-19.

ZI Placement Group	n	3D Entry deviation Mean ± SD (mm)	3D Exit deviation Mean ± SD (mm)	3D Angular deviation Mean ± SD (°)
Robotic	16	1.80 ± 0.69	2.80 ± 0.95	1.74 ± 0.92
NaviDent	16	1.21 ± 0.49	1.75 ± 0.75	1.24 ± 0.64
X-Guide	16	1.01 ± 0.37	1.50 ± 0.91	1.36 ± 0.89

Table 5-1. Descriptive statistics for the 3D deviation parameters that resulted from testing the main 3 groups.

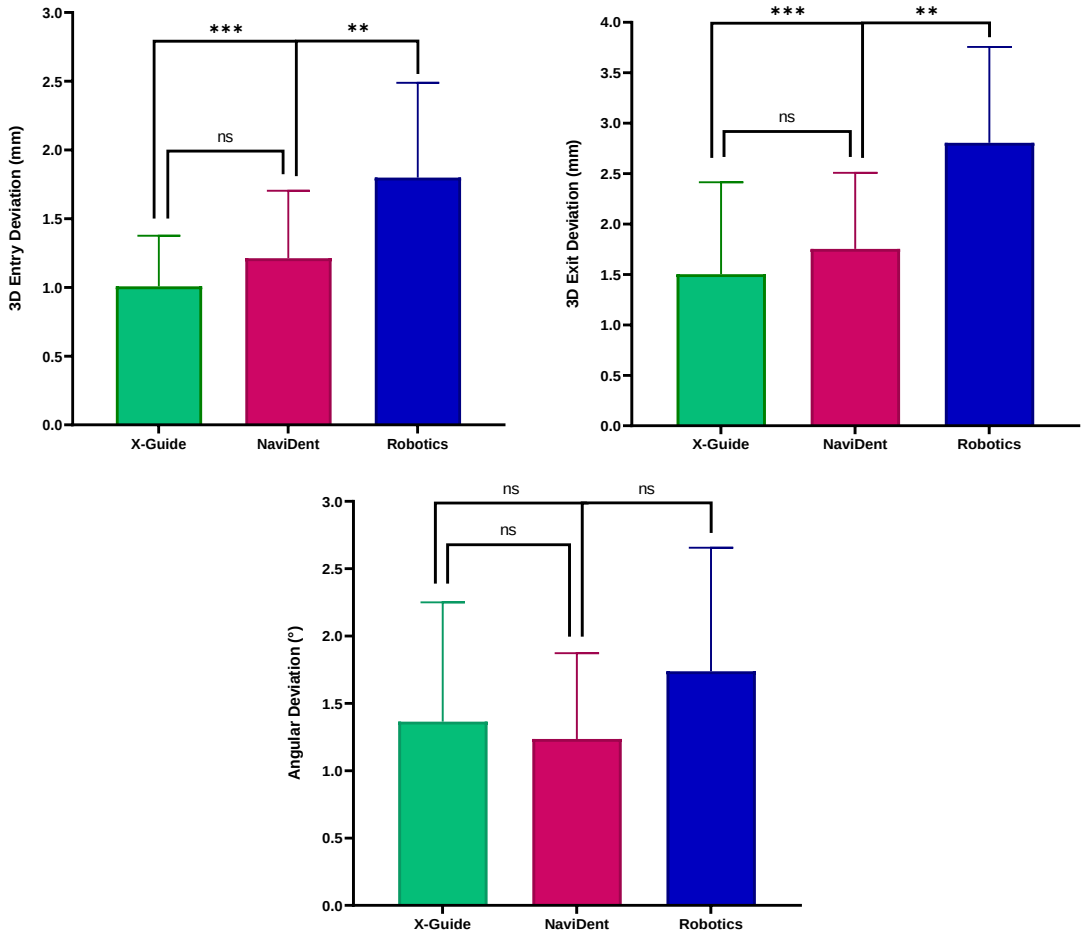

Figure 5-19. Bar charts demonstrating the 3D deviation parameters that resulted from testing the main 3 groups for ZI drilling and placement. Number of values in each bar (n = 16). The error bars represent the standard deviations from the mean values. One-way ANOVA tests with Bonferroni's correction p values: *** < 0.001, ** < 0.01, * < 0.05, ns > 0.05.

The 3D deviations of the implant entry and exit points from the planned positions, in addition to the angular deviations for the additional control group in comparison to robotic and standard NaviDent groups are shown in table 5-2 and figure 5-20.

ZI Placement Group	n	3D Entry deviation Mean ± SD (mm)	3D Exit deviation Mean ± SD (mm)	3D Angular deviation Mean ± SD (°)
Robotic	16	1.80 ± 0.69	2.80 ± 0.95	1.74 ± 0.92
NaviDent S.C.	14	1.29 ± 0.77	1.92 ± 0.93	1.57 ± 1.05
NaviDent	16	1.21 ± 0.49	1.75 ± 0.75	1.24 ± 0.64

Table 5-2. Descriptive statistics for the 3D deviation parameters that resulted from testing the additional control group for ZI drilling and placement. S.C. = single calibration.

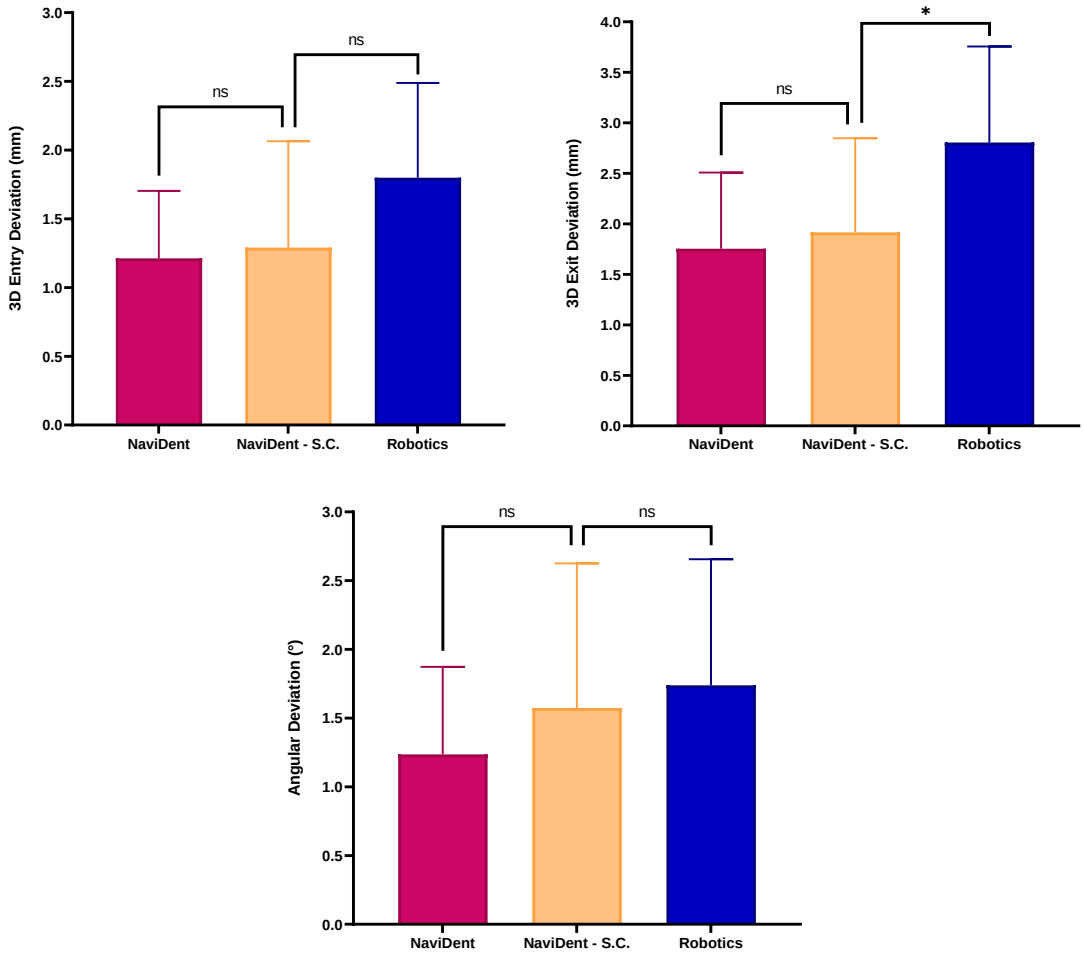

Figure 5-20. Bar charts demonstrating the 3D deviation parameters that resulted from testing the additional control group for ZI drilling and placement. Number of values in each bar (n = 16) except the NaviDent S.C. group (n = 14). S.C. = single calibration. The error bars represent the standard deviations from the mean values. One-way ANOVA tests with Bonferroni's correction p values: * < 0.05, ns > 0.05.

The uncertainty of the evaluation method in terms of mean ranges were 0.38 mm for the entry points, 0.56 mm for the exit point, and 0.41° for angular deviations.

Based on the 3D deviation results, the null hypothesis for this experiment was accepted. This means that the robotic group accuracy results were not better than the manual drilling under dynamic navigation guidance.

5.3.2. 2D directional deviations

To illustrate the directionality of deviations, one method was the utilisation of violin plots (figure 5-21). This method is an improvement over the ordinary boxplots in that they provide smoothed histogram of data density along the data points as an outer border of the violin (Hu, 2020).

The other method to illustrate the corresponding deviations of entry and exit points for each specific implant is the formation of 3D scatters from two parallel 2D scatters (figure 5-22). The advantage of this method is that one of the 2D scatters represents the entry point deviations while the other one represents the exit point deviations. Therefore, connecting lines between the corresponding points provides a good visualisation of these deviations in each single implant, in addition to providing subjective visual clues about 2D angular deviations in a particular plane (Abduo and Lau, 2021).

The detailed deviation directionality data is shown in tables 5-3 to 5-5.

ZI location/no.	Vertical Entry point deviations (mm)				Vertical Exit point deviations (mm)			
	Robotic	ND S.C.	ND	XG	Robotic	ND S.C.	ND	XG
ALt1	0.064	-0.178	-0.246	-0.317	-1.081	-0.916	0.565	-2.097
ALt2	-0.433	0.296	0.597	0.961	-0.881	-1.122	0.382	0.570
ALt3	0.026	0.283	0.760	0.362	-0.781	0.008	0.499	0.138
ALt4	0.549	-0.167	-0.382	0.288	-0.242	-0.422	-1.038	0.431
PLt1	-2.115	-1.745	-1.836	-0.594	-2.257	-1.696	-1.293	-0.723
PLt2	0.776	-0.590	-0.522	0.702	1.512	-0.281	-0.771	0.633
PLt3	-0.415	-1.612	-1.488	0.130	0.136	-2.127	-1.541	0.942
PLt4	-0.355	-2.014	-0.256	1.189	-0.427	-1.787	0.205	1.744
ARt1	-0.652	-0.816	-0.869	0.689	-1.126	-1.240	-2.211	0.387
ARt2	-0.260		-0.242	0.511	-1.543		-0.709	-0.645
ARt3	0.575	0.234	-1.073	0.039	0.946	-0.340	-1.299	-0.006
ARt4	1.892		-1.254	-0.299	2.404		-2.027	-0.382
PRt1	1.472	-0.419	-1.571	1.218	2.991	0.045	-2.534	2.616
PRt2	2.035	0.341	0.641	1.033	3.345	1.905	0.861	1.699
PRt3	1.398	0.913	0.336	0.407	2.763	1.309	1.408	0.051
PRt4	2.121	-1.244	0.929	1.222	2.492	-1.248	1.772	0.823
Median	0.306	-0.299	-0.319	0.459	-0.053	-0.669	-0.740	0.409

Table 5-3. Descriptive statistics for the vertical deviations that resulted from testing the four ZI placement groups. Negative values indicate downward direction while positive values indicate upward direction of the actual implant entry or exit point in relation to the intended plan. ALt = Anterior left; PLt = Posterior left; ARt = Anterior right; PRt = Posterior right; ND = NaviDent®; S.C. = single calibration; XG = X-Guide®.

ZI location/no.	Coronal Entry point deviations (mm)				Coronal Exit point deviations (mm)			
	Robotic	ND S.C.	ND	XG	Robotic	ND S.C.	ND	XG
ALt1	0.263	0.704	-1.312	-0.174	-1.258	1.284	-1.677	-1.315
ALt2	-1.304	-0.243	-0.812	-0.110	-1.387	0.142	-0.417	0.653
ALt3	-1.025	-0.873	-0.266	-0.343	-1.843	-0.941	0.331	-0.589
ALt4	-1.737	-0.485	-0.505	-0.060	-2.938	-0.728	-0.482	0.729
PLt1	0.501	0.183	0.206	-0.478	-0.230	-0.679	-0.350	-1.876
PLt2	-1.657	-0.142	-0.125	-0.328	-2.046	-0.485	-0.163	-0.244
PLt3	-1.959	-0.765	-0.773	-0.185	-3.285	-1.547	-1.713	-0.905
PLt4	-0.482	0.156	-0.717	-0.620	-0.816	-0.985	-1.818	-1.289
ARt1	0.981	-0.136	0.610	-0.325	2.548	-2.868	-0.758	-0.434
ARt2	-0.112		0.293	-0.452	1.557		0.166	-2.116
ARt3	0.076	-0.133	-0.306	-0.726	0.494	-1.835	-0.340	0.183
ARt4	0.123		-0.289	-0.386	0.852		-0.300	-0.414
PRt1	0.587	0.422	0.554	-0.019	0.629	-0.313	1.003	0.003
PRt2	-0.264	1.404	0.119	-0.0190	-1.698	0.194	-0.086	-1.485
PRt3	0.300	0.316	0.915	-0.019	-0.341	-0.225	1.502	-0.214
PRt4	0.002	0.980	-0.078	-0.030	-0.055	0.990	-0.888	-0.585
Median	-0.055	0.011	-0.195	-0.255	-0.579	-0.582	-0.345	-0.509

Table 5-4. Descriptive statistics for the coronal deviations that resulted from testing the four ZI placement groups. Negative values indicate backward direction while positive values indicate forward direction of the actual implant entry or exit point in relation to the intended plan. ALt = Anterior left; PLt = Posterior left; ARt = Anterior right; PRt = Posterior right; ND = NaviDent®; S.C. = single calibration; XG = X-Guide®.

ZI location/no.	Mediolateral Entry point deviations (mm)				Mediolateral Exit point deviations (mm)			
	Robotic	ND S.C.	ND	XG	Robotic	ND S.C.	ND	XG
ALt1	0.938	1.037	0.079	-1.180	0.940	1.888	-0.673	-0.581
ALt2	-0.059	-0.194	-1.465	0.391	0.211	1.039	-1.131	1.011
ALt3	-1.013	0.102	-0.191	1.189	-0.871	0.275	0.269	1.222
ALt4	1.818	0.373	0.547	-0.533	1.757	0.436	1.005	-0.266
PLt1	1.669	1.578	0.960	-0.069	1.786	1.558	0.583	0.033
PLt2	-0.539	0.288	-0.084	0.618	-1.060	0.045	0.092	0.663
PLt3	-0.240	1.400	-0.132	0.700	-0.624	1.822	-0.074	0.135
PLt4	1.484	1.940	-0.896	1.081	1.548	1.766	-1.198	0.703
ARt1	-1.224	-0.074	0.240	-0.133	-0.170	-1.376	0.382	0.010
ARt2	0.443		0.318	-0.247	2.034		0.563	-0.352
ARt3	-0.240	-0.147	0.074	-0.139	-0.279	-0.690	0.205	0.343
ARt4	-0.482		0.513	0.146	-0.471		1.004	0.187
PRt1	-1.499	1.059	1.071	-1.074	-2.618	0.591	1.770	-2.096
PRt2	-1.892	-0.431	-0.063	-0.880	-3.067	-1.898	-0.243	-1.564
PRt3	-1.295	0.037	-0.123	-0.625	-2.383	-0.343	-0.837	-0.401
PRt4	-1.204	1.037	-1.079	-0.337	-1.478	1.042	-1.783	-0.126
Median	-0.361	0.330	0.006	-0.136	-0.375	0.514	0.148	0.021

Table 5-5. Descriptive statistics for the mediolateral deviations that resulted from testing the four ZI placement groups. Negative values indicate medial direction while positive values indicate lateral direction of the actual implant entry or exit point in relation to the intended plan. ALt = Anterior left; PLt = Posterior left; ARt = Anterior right; PRt = Posterior right; ND = NaviDent®; S.C. = single calibration; XG = X-Guide®.

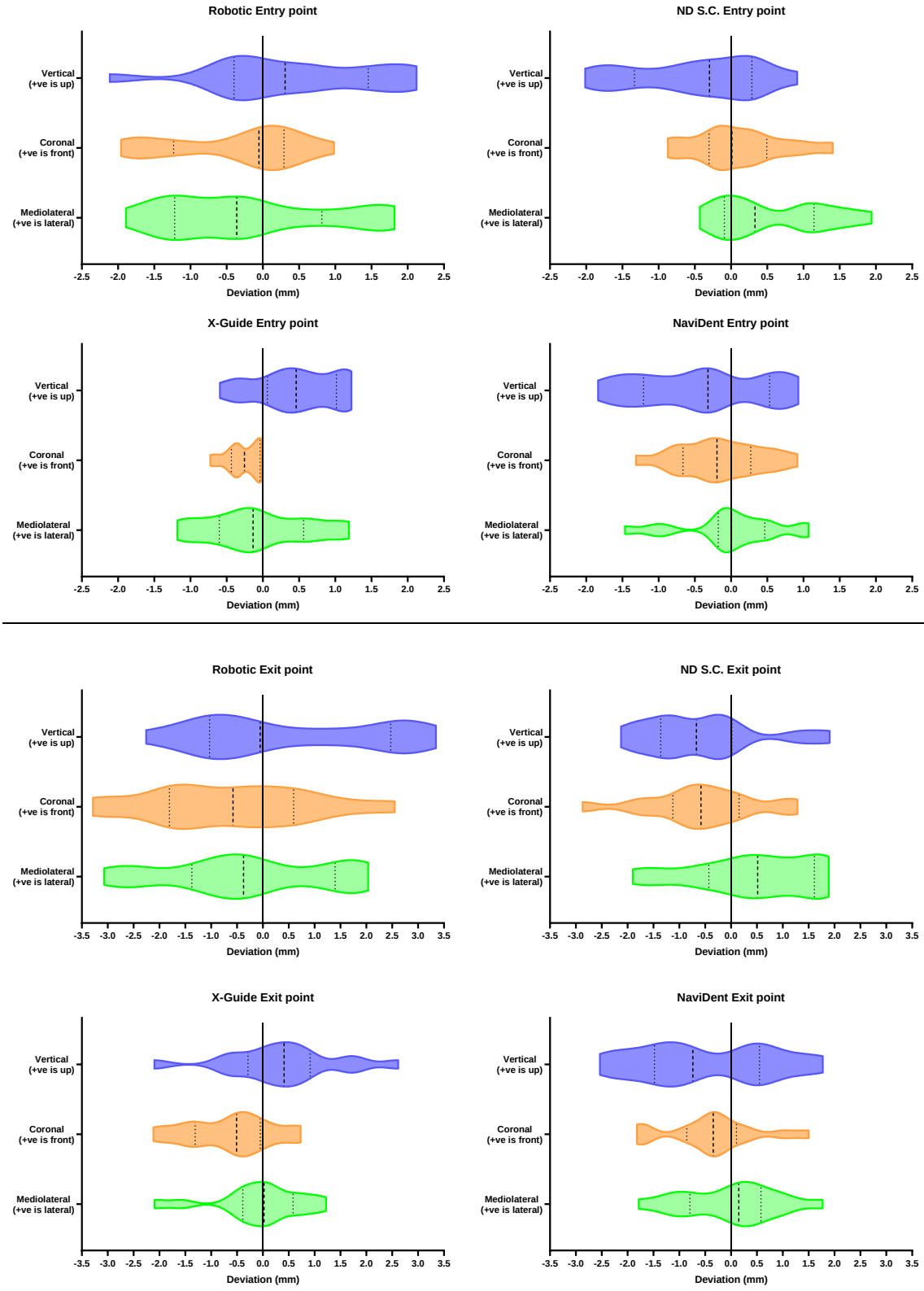

Figure 5-21. Violin plots showing the distribution of the ZI entry and exit point deviations in every direction. The top 4 sections are for entry point deviations whereas the bottom 4 sections are for exit point deviations. The dashed lines represent the medians and the interquartile range limits. S.C. = single calibration.

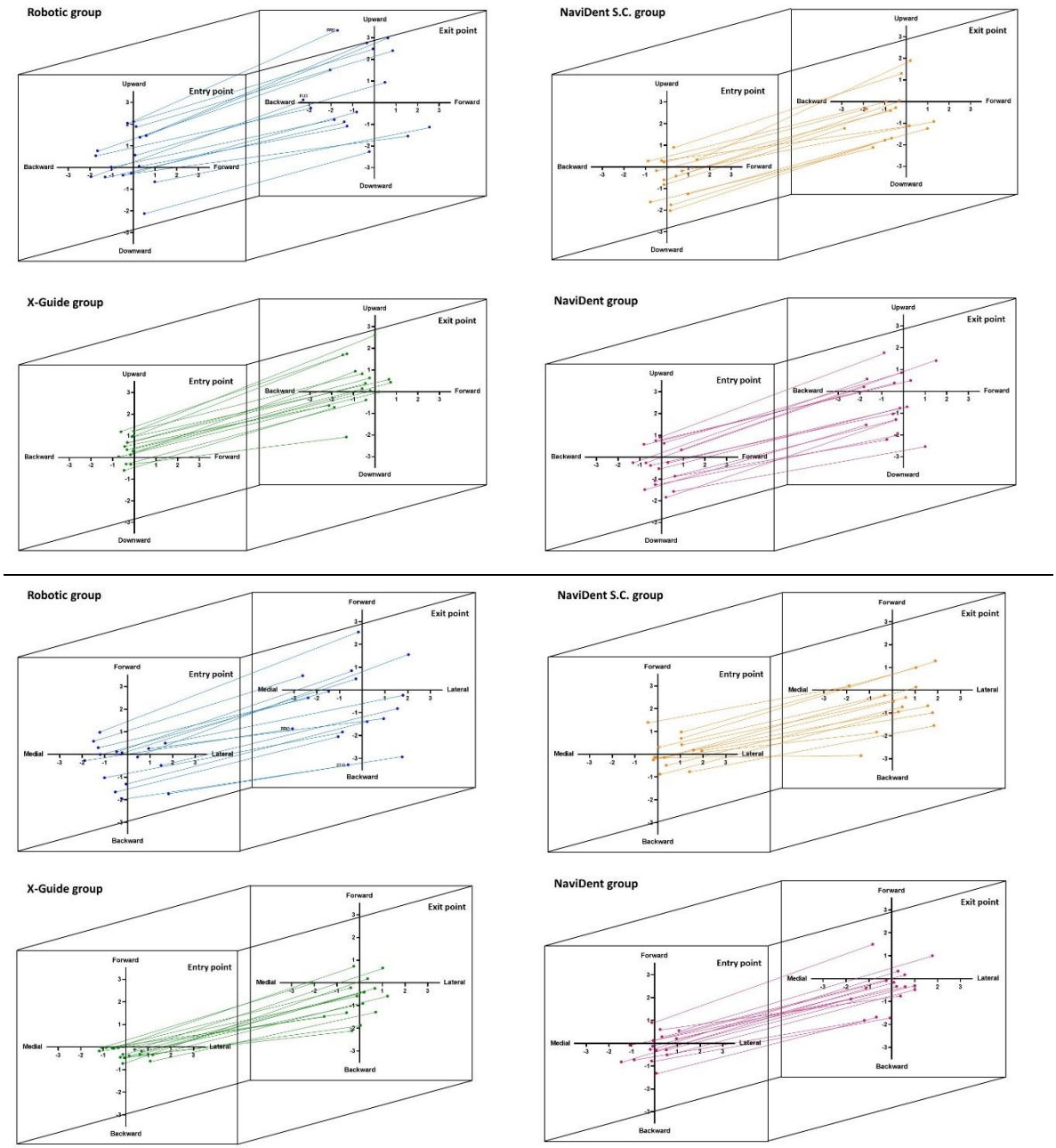

Figure 5-22. 3D Scattered diagrams depicting the distribution of the ZI entry and exit point deviations in every direction. The top 4 sections are from a sagittal view whereas the bottom 4 sections are from an occlusal view to include the mediolateral direction. The connecting lines between entry points and corresponding exit points provides a visual estimation of angular deviations, too. S.C. = single calibration.

In the robotic group, the median values of the entry deviations were 0.31 mm, -0.05 mm, and -0.36 mm for the vertical, coronal and mediolateral directions, respectively. The median values of the exit point deviations were -0.05 mm, -0.58 mm, and -0.38 mm for the vertical, coronal and mediolateral directions, respectively (figure 5-21).

In the NaviDent single calibration group, the median values of the entry deviations were -0.30 mm, 0.01 mm, and 0.33 mm for the vertical, coronal and mediolateral directions, respectively. The median values of the exit point deviations were -0.67 mm, -0.58 mm, and 0.51 mm for the vertical, coronal and mediolateral directions, respectively (figure 5-21).

In the NaviDent group, the median values of the entry deviations were -0.32 mm, -0.20 mm, and 0.01 mm for the vertical, coronal and mediolateral directions, respectively. The median values of the exit point deviations were -0.74 mm, -0.34 mm, and 0.15 mm for the vertical, coronal and mediolateral directions, respectively (figure 5-21).

In the X-Guide group, the median values of the entry deviations were 0.46 mm, -0.26 mm, and -0.14 mm for the vertical, coronal and mediolateral directions, respectively. The median values of the exit point deviations were 0.41 mm, -0.51 mm, and 0.02 mm for the vertical, coronal and mediolateral directions, respectively (figure 5-21).

Considering the exit point deviation directions; upward vertical deviations, backward coronal deviations, and medial deviations were highlighted as being clinically significant. For the robotic group, out of the 16 zygomatic implants; 8 had upward vertical deviations (50.0%, 2.07 ± 1.11 mm), 11 had backward coronal deviations (68.75%, -1.45 ± 1.06 mm), and 10 had medial deviations (62.5%, -1.30 ± 1.04 mm) (figure 5-22).

For the NaviDent single calibration group, out of the 14 zygomatic implants; 4 had upward vertical deviations (28.57%, 0.82 ± 0.94 mm), 10 had backward coronal deviations (71.43%, -1.06 ± 0.81 mm), and 4 had medial deviations (28.57%, -1.08 ± 0.70 mm) (figure 5-22). Two anterior right ZIs were excluded as outliers because they did not engage the zygomatic bone due to alveolar buccal fractures during the drilling procedure.

For the NaviDent group, out of the 16 zygomatic implants; 7 had upward vertical deviations (43.75%, 0.81 ± 0.58 mm), 12 had backward coronal deviations (75.0%, -0.75 ± 0.64 mm), and 7 had medial deviations (43.75%, -0.85 ± 0.59 mm) (figure 5-22).

For the X-Guide group, out of the 16 zygomatic implants; 11 had upward vertical deviations (68.75%, 0.91 ± 0.79 mm), 12 had backward coronal deviations (75.0%, -0.96 ± 0.65 mm), and 7 had medial deviations (43.75%, -0.77 ± 0.75 mm) (figure 5-22).

5.3.3. Procedure time

The overall registration time for the robotic group was 23.8 ± 7.0 minutes for each side of a model. Operative time excluding registration was 66.8 ± 8.8 minutes for each trajectory.

The registration time for the NaviDent single calibration group was 7.1 ± 3.3 minutes for each side of a model. Operative time was 33.8 ± 3.9 minutes for each trajectory.

For the NaviDent group, registration time was 6.9 ± 1.6 minutes and operative time was 34.6 ± 5.4 minutes. The registration time for the X-Guide group was 9.6 ± 1.9 minutes and the operative time was 38.4 ± 5.0 minutes.

The details of time cost in the robotic group are shown in figure 5-23.

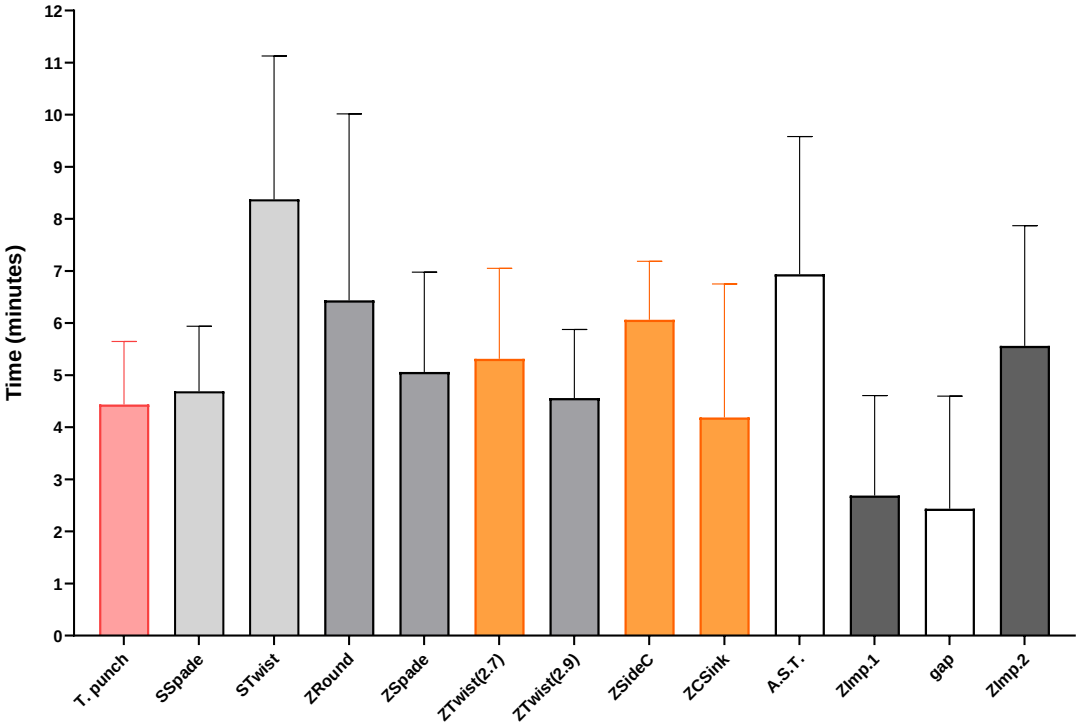

Figure 5-23: The time cost per drilling step detailing the operative time spent during the robotic ZI placement protocol. Orange coloured bars represent osteotomy with titanium drills, light grey coloured bars represent drilling with stainless steel drills. Dark grey coloured bars represent ZI insertion step, A.S.T. = automatic switch testing, gap = ZI manual advancement stage.

5.3.4. Force feedback recorded during the experiment

The relationships between actual ZI deviations and the mean drilling force in the robotic group is shown in figure 5-24. With the exception of the posterior right trajectories, it can be noted that the higher drilling forces are generally associated with less deviations. Other than this subjective observation, no substantial correlation was found between the ZI deviation and the 3D drilling forces (i.e., no statistical correlation was found between the ZI deviations and the 3D mean drilling force or the 3D force feedback from any particular drill). However, when the component force vectors were taken into consideration, the zygomatic round drill in addition to a few other drills demonstrated positive correlations with the y force vector and negative correlations with the x force vector (Table 5-6). This observation could be valuable in future experiments as the detection of high value y force and low value x force vectors with these drills would alert the operator to the possibility of higher implant deviations. This in turn may direct the operator decision in applying a drilling procedure modification to avoid these deviations.

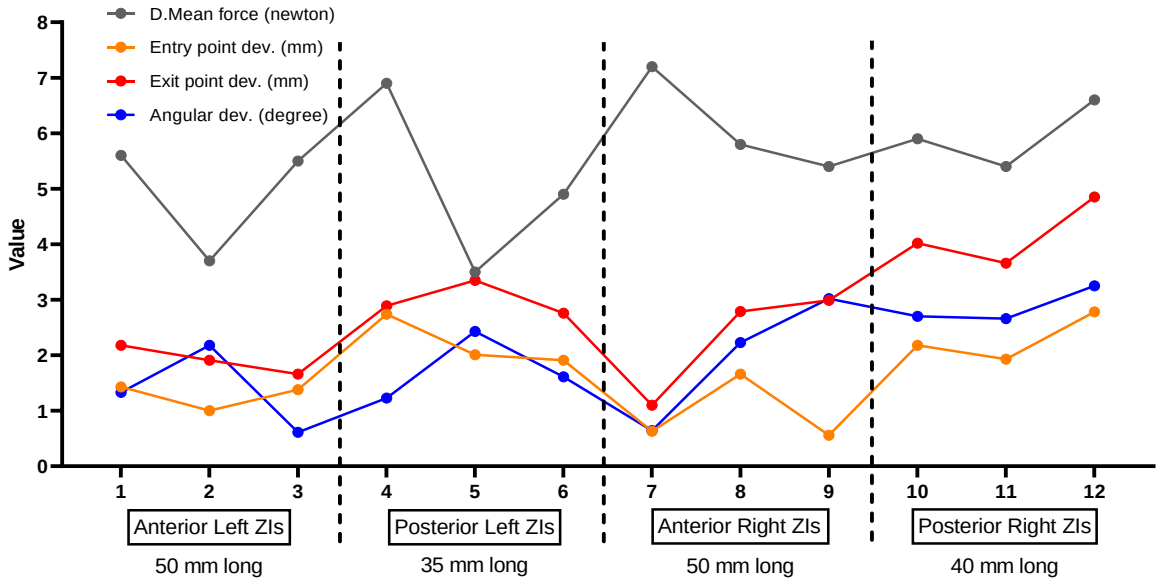

Figure 5-24. A line graph showing the trajectory-specific relationships between the mean drilling force (D.Mean force) and the 3D actual implant deviations at its entry, exit as well as angular deviation from the planned trajectory.

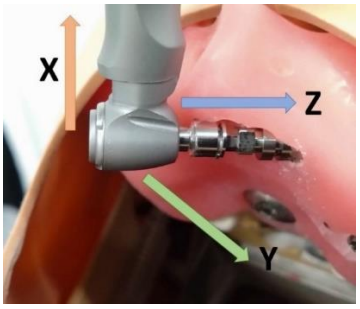

	SSpade	STwist	ZRound	ZSpade	ZTwist (2.7)	ZTwist (2.9)	ZSideC	ZCSink	ZImp.	D.Mean	D.Max
Correlation with Entry point 3D deviation											
X Force	-0.255	-0.458	-0.317	-0.313	-0.252	-0.520	-0.302	0.219	-0.154	-0.460	-0.441
Y Force	0.097	0.546	0.555	0.331	0.537	0.718	0.397	0.195	0.354	0.586	0.521
Z Force	-0.253	0.495	-0.560	-0.176	-0.256	-0.048	0.562	0.009	0.096	-0.099	-0.483
XY Force	-0.111	0.041	0.422	0.082	0.268	0.003	0.241	0.254	0.266	0.268	0.258
3D Force	-0.216	0.175	0.279	0.035	-0.095	-0.118	0.444	0.158	0.253	0.178	0.083
Correlation with Exit point 3D deviation											
X Force	-0.544	-0.845	-0.782	-0.647	0.008	-0.440	-0.560	0.026	-0.235	-0.832	-0.805
Y Force	-0.006	0.229	0.852	0.619	0.722	0.434	0.575	0.356	0.009	0.700	0.670
Z Force	-0.310	0.476	-0.122	-0.399	-0.568	-0.244	0.503	-0.033	-0.184	-0.216	-0.408
XY Force	-0.330	-0.407	0.527	0.151	0.536	0.006	0.242	0.291	-0.069	0.157	0.109
3D Force	-0.386	-0.304	0.496	0.032	-0.207	-0.180	0.446	0.132	-0.185	0.033	0.015
Correlation with Angular deviation											
X Force	-0.407	-0.761	-0.835	-0.731	0.276	-0.179	-0.531	-0.192	-0.305	-0.773	-0.750
Y Force	-0.016	-0.131	0.705	0.471	0.492	0.044	0.433	0.224	-0.184	0.443	0.421
Z Force	-0.263	0.152	0.207	-0.590	-0.782	-0.383	0.183	-0.160	-0.372	-0.431	-0.402
XY Force	-0.241	-0.546	0.322	-0.024	0.516	0.007	0.086	0.038	-0.283	-0.066	-0.109
3D Force	-0.281	-0.528	0.376	-0.165	-0.402	-0.211	0.183	-0.104	-0.466	-0.247	-0.160

Table 5-6. Pearson's correlation coefficients to appreciate the associations between the force feedback recorded by the robotic arm (at the end point of the drilling path) and the actual ZI deviations. Highlighted cells indicate statistically significant correlations (p value < 0.05). SSpade = short spade drill; STwist = short twist drill 5.5Φ; ZRound = zygomatic round drill; ZSpade = zygomatic spade drill; ZTwist = zygomatic twist drill; ZSideC = zygomatic side-cutting drill; ZCSink = zygomatic counter-sink drill; ZImp. = zygomatic implant placement stage; D.Mean = mean drilling force; D.Max. = maximum drilling force. The photograph at the top of the table demonstrates the direction of the x, y and z force vectors: x is supero-inferior, y is mediolateral, and z is inward-outward (in relation to both the drill and the robotic end effector).

5.4. Discussion

Dynamic navigation procedures involve multiple operative steps that can influence the final outcome (Al-Jarsha et al., 2024a). Despite contributing to creating artificial scenarios, optimisation steps such as the registration of the patient space and the drill calibration are crucial for *in vitro* studies (Al-Jarsha et al., 2024a, Al-Jarsha et al., 2024b). Similarly, to test the consistency and predictability of a new method, it is wise to apply it repeatedly in one commonly encountered scenario before trying to generalise it for multiple scenarios. For this reason, we elected to use identical model anatomy and the same ZI plan for all cases in this initial testing stage.

The angular deviations were used in calculating the sample size. This is because, in addition to its anatomical implications, it has been reported that wrong angulation for dental implants may interfere with the long-term survival through its biomechanical effects on the cortical bone (Chatterjee et al., 2023, Thomková et al., 2023).

Using a silicone face mask in this study (section 4.4.3; figure 4-28 on page 130) has made the outcomes of this study more clinically relevant as most previous *in vitro* studies had been criticised for excluding it. This is because it impacts on direct visualisation with the manual drilling protocol (Fan et al., 2023).

In the test group of robotic drilling, the wireless transfer of TMs originating in the NaviDent® system (see sections 4.2.2 and 4.3.2) allowed a hand-eye calibration protocol to be conducted (Zhang et al., 2017, Sun et al., 2022, Yan et al., 2023). Multiple drill calibrations were not practical for time- and reproducibility- related reasons. The NaviDent® software (v. 3.0.3) had an automated axis adjustment algorithm with every new drill length calibration. Therefore, the yardstick for checking a reproducible robotic position would be lost with multiple drill calibration (see section 4.8 on page 137).

This prototype system also involved the use of an automatic switch-off hardware to control the implant engine (see section 4.7 on page 134). This automated control eliminates the human factor of stopping the implant advancement at the correct final depth by automatically turning off the implant engine depending on the coordinates being transmitted in real-time during the implant placement step. The standardisation of the frame of reference to explain directionality of deviations was adopted in a previous investigation (Pellegrino et al., 2020b).

Li and colleagues highlighted the importance of angular deviation control for the safe robotic placement of dental implants in edentulous jaws (Li et al., 2023b). In this investigation, there was no statistically significant difference between all tested groups with respect to angular deviations (figures 5-19 and 5-20). However, the standard deviation value in the NaviDent® group was less than that of the other 3 groups.

This observation could be attributed to the automated axis adjustment algorithm mentioned above. Prior to each drilling step, the drill length calibration step result in a slightly different angle on screen and thus contributes to the final implant angle having less variation. This is also supported by the higher values of the angular deviation and its standard deviation in the NaviDent® group where single drill calibration was used (figure 5-20).

The differences in the 3D entry and exit point deviations between the X-Guide® and the NaviDent® manual drilling groups were also statistically non-significant (figure 5-19). Nevertheless, these deviations were better in both of these manual groups than the robotic group (p values < 0.001 and < 0.01, respectively). The main null hypothesis of the study was therefore accepted.

As a follow-up to these results, the 4th group (NaviDent® with single drill calibration) was tested to investigate which of the known sources of error had the greatest impact on distance deviation in the robotic group. There were two main possible sources; the drill calibration method (single drill calibration) and the actual drilling method (robotic drilling without tactile feedback). For the 3D exit point deviations, it appears that the tactile feedback had the higher impact (p value < 0.05). For the 3D entry deviations and angular deviations, the impact of these two sources seems to be equal, with the single drill calibration protocol possibly affecting the final angle deviation as explained earlier (figure 5-20).

In the robotic group, only a few deviations exceeded the 2 mm safety limit for the entry point, whereas the range of exit point deviations was in the 3 mm boundary (figures 5-21 and 5-22). The 3 mm is considered to be the safe margin during zygomatic implant planning (Chow, 2020).

In addition to possible residual errors arising from human marker localisation issues and other sources of human-related errors (Chen and Hu, 2023, Al-Jarsha et al., 2024a, Al-Jarsha et al., 2024b, González Rueda et al., 2023), the results of this chapter support Li and colleagues' argument that the robotic implant placement deviations depend on the specific characteristics of the surgical site (Li et al., 2023b).

Interestingly, an investigation by Du and colleagues using the SinoPlan® robotic system to place electrodes in the skull showed that the trajectory-skull angle significantly influenced the placement radial error (Du et al., 2024). The similarities between the long zygomatic drills and these neurological electrodes supports the earlier argument of anatomical influences on the deviations with robotic implantations (Du et al., 2024, Li et al., 2023b). In this experiment, it can be argued that the planned posterior trajectories had a more challenging path, particularly at the point of the entry into the zygomatic bone (see figure 5-7 on page 153). This can partially explain the tendency for the posterior trajectory deviations to be higher (figure 5-24). The difference in the implant lengths between these two regions is another possibility but may be less likely to be the cause according to a previous study (Wang et al., 2024d).

The prototype active robotic system in this project produced 3D deviations of 1.80 ± 0.69 mm at the entry point, 2.80 ± 0.95 mm at the exit point, and 1.74 ± 0.92° angular deviation. The commercially available active robotic system Yakebot® was reported to achieve clinical sub-millimetre accuracy, but with regular dental implants rather than ZIs (0.65 ± 0.25 mm, 0.65 ± 0.22 mm, and 1.43 ± 1.18°)(Wang et al., 2023a). The semi-active commercial robotic system Remebot® achieved *in vitro* ZI placement accuracy of 0.57 ± 0.19 mm, 1.07 ± 0.48 mm, and 0.91 ± 0.51° for the entry, exit and angular deviations, respectively (Deng et al., 2023b). The passive commercial robotic system Yomi® produced a clinical accuracy of 1.31 ± 0.46 mm, 1.58 ± 0.61 mm, and 2.34 ± 1.71° with conventional dental implants (Klass et al., 2023). Yomi® also achieved 1.10 ± 0.69 mm , 1.12 ± 0.69 mm and 1.42 ± 1.53° in another large clinical series (Neugarten, 2024).

The method of assessment and its uncertainty level might have played a role in achieving sub-millimetre accuracy levels with commercial systems, particularly as these studies did not implement a comparative blind analysis protocol as was done in this investigation, which could have resulted in potential analysis bias within those studies (Wang et al., 2023a, Deng et al., 2023b, Klass et al., 2023).

The vertical upward, coronal backward, and medial deviations at the exit point are clinically relevant to comment on the safety of the procedure (Zielinski et al., 2023). The orbital cavity would be affected if the exit point of an anterior ZI was to deviate in upward and/or medial direction. Similarly, a backward deviation of a posterior ZI exit point may compromise the vital structures in the infra-temporal fossa. The distribution of the directional deviations in figure 5-21 suggests that for zygomatic implant placement, tactile force feedback improved the implant placement safety via reducing the number as well as the magnitude of deviations in the risky directions (i.e., when comparing between robotic and NaviDent® with single drill calibration groups). On the other hand, the impact of using the recommended multiple calibration protocol in the NaviDent® group has only slightly improved the magnitude of these deviations (figure 5-21).

However, this does not necessarily mean that it is unsafe to use this current version for other applications involving shorter trajectories. In fact, the results of our 3D angular deviations with zygomatic implant placement (1.74° ± 0.92°) agrees with previously published results concerning conventional dental implants (Yang and Li, 2024, Khaohoen et al., 2024, Wu et al., 2024). These recent meta-analyses reported 1.8° (95%CI: 1.2° to 2.5°), 1.71° (95%CI: 0.04 to 3.38), and 1.69° (95%CI: 1.25° to 2.12°) for robotic-assisted implant angular deviations (Yang and Li, 2024, Khaohoen et al., 2024, Wu et al., 2024). However, both entry and exit point deviations were found to be less than 1 mm in the mentioned meta-analyses, which contrasts with our findings (table 5-1 and figure 5-19).

The level of uncertainty due to the superimposition of CBCTs during evaluation should always be assessed when reporting implant deviation data. Shimizu and colleagues found that the specific computerised tomography protocol has an influence on the extracted implant deviations. Incorporating glass ceramic markers into a matching template when scanning the patient had improved the image matching accuracy during the superimposition and resulted in smaller implant deviation data (Shimizu et al., 2023).

In this experiment, the uncertainty in the evaluation method was less than all calculated standard deviations for the accuracy data. Aside from uncertainty in the method of evaluation, using the dynamic navigation coordinates as a yardstick for the trajectory plans could also be criticised and be the reason for not achieving < 1° or < 1 mm 3D deviation in any group (tables 5-1 and 5-2). This yardstick implicates the sources of error as potentially coming from the CBCT acquisition, registration, drill calibration, as well as the optical tracking noise itself (see figure 4-15 on page 122).

Looking at the results of the average registration and operation times, it is obvious that the time cost was too high for all groups due to the frequent accuracy checks and the insistence on achieving extremely high accuracy levels upon these checks. The registration time in the robotic group was about 15 minutes longer than in the manual groups due to the extra step of registration to record the transformation matrix of the robotic to the tracking system. In addition, the advancing speed of the robotic arm drilling was set to the minimum (~0.5 mm/second) to protect the drills and the handpiece. This has led to every step of robotic drilling taking several minutes (figure 5-23). A fully guided drilling protocol was implemented in this project. This is because it has been proven that the deviations tend to increase with each step if only the pilot drill was guided (Sharma et al., 2023). The overall surgical time for manual placement of dental implants under dynamic navigation was found to be in the range of 9.5 to 13.5 minutes (Mampilly et al., 2023, Deeb et al., 2022).

Regarding the manual placement groups, it is well documented that the accuracy of placement is expected to increase with time due to the accumulated surgical training (Wang et al., 2022a). However, because we used the same contra-angle implant handpiece for all manual placement procedures, the level of mechanical damage to this handpiece is also expected to increase with time, which may have balanced the effect of the improved dexterity due to training (see section 6.3, figure 6-1 on page 197).

For the force feedback data, figure 5-24 only shows the previously mentioned tendency of higher resulting deviations with less recorded mean drilling force. It makes sense that if the drills did not cut much of the resin, it would be expected that the implant would end up away from the planned intra-resin trajectory due to increased resistance from the material.

The correlations with the component force vectors observed in table 5-6 indicate the possibility of differential interpretation of the force feedback based on its direction. If there were high resistance forces perpendicular to the long axis of the handpiece (i.e., y force vector in table 5-6), more deviations resulted when analysing this trajectory’s deviations (i.e., positive correlation).

On the other hand, if the resistance forces were parallel to the long axis of the handpiece (i.e., x force vector in table 5-6), less deviations were expected because this resistance is evidence of cutting action (i.e., negative correlation). These force data were derived from the end effector of the robotic arm rather than the drill itself. More advanced force sensors are required to be attached to the handpiece itself and a larger sample is probably required to form conclusions regarding the association of force feedback with the final implant deviations. It appears that conventional mechanical drills might constitute a refractory issue for the robotic drilling. Sharma and colleagues investigated flexible drilling with a steering cannula to reduce the stress and strain for spinal fixation simulation (Sharma et al., 2024). Hard-tissue lasers could be another attractive option to use with robotic systems (Ganta et al., 2023, Ebeling et al., 2023).

There are some suggestions in the literature about the effect of lateral force resistance on the implant drills, whether due to the inherent anatomy of the alveolar ridge (Göçmen et al., 2023) or the design of the drill (Takács et al., 2023). Atrophic ridges and straight implant drills produced larger inaccuracies than less atrophic ridges and step drills (Göçmen et al., 2023, Takács et al., 2023). Attempts to tackle this negative effect were through the implementation of initial piezosurgery site preparation (Pellegrino et al., 2017) and via preparing the zygomatic site in a two-stage protocol whereby the alveolar part is widened before starting the implant osteotomy in the zygoma (Deng et al., 2023b).

In summary, there is a need for a custom drilling set to go with the robotic placement protocol. The required customisation is best addressed with less flexible materials for the manufacture of the osteotomy drills, as using the same current materials with increased diameters would deduct from the advantage of fitting small diameter implants suitable for areas with limited bone volume. The length of the custom drills should be enough that they would not require the addition of drill extensions that enter the osteotomy paths, as such a compromise would most probably necessitate making a wider opening than the neck of the actual zygomatic implant.

5.5. Conclusions

The drilling method under dynamic navigation contributed less to the overall error when performed by the human hand. The robotic drilling method produced clinically acceptable accuracy, but was not better than the manual drilling in this investigation. The accuracy of our prototype was less than that reported for the commercially available active robotic systems with conventional dental implants.

Registration and operation times are longer with dynamic navigation techniques than other implant guiding techniques, particularly, if frequent accuracy checks were added to the protocol to ensure a robust final accuracy. Robotic drilling may require even longer registration and operative times, especially if the registration process was not automated and more checks were added to the protocol for safety reasons.

The available drilling tools for the manual drilling protocol might not be suitable for robotic drilling. Sharper and less flexible drills are especially important to drill long trajectories like those required for ZIs. The handpiece needs to have more tolerant gears and/or have smart force sensors to withstand the drilling forces without getting damaged. These force sensors could also act as predictors for the final deviations, thus guiding the operator to modify the standard drilling protocol during the operation based on the observed force data.

5.6. Chapter Appendix

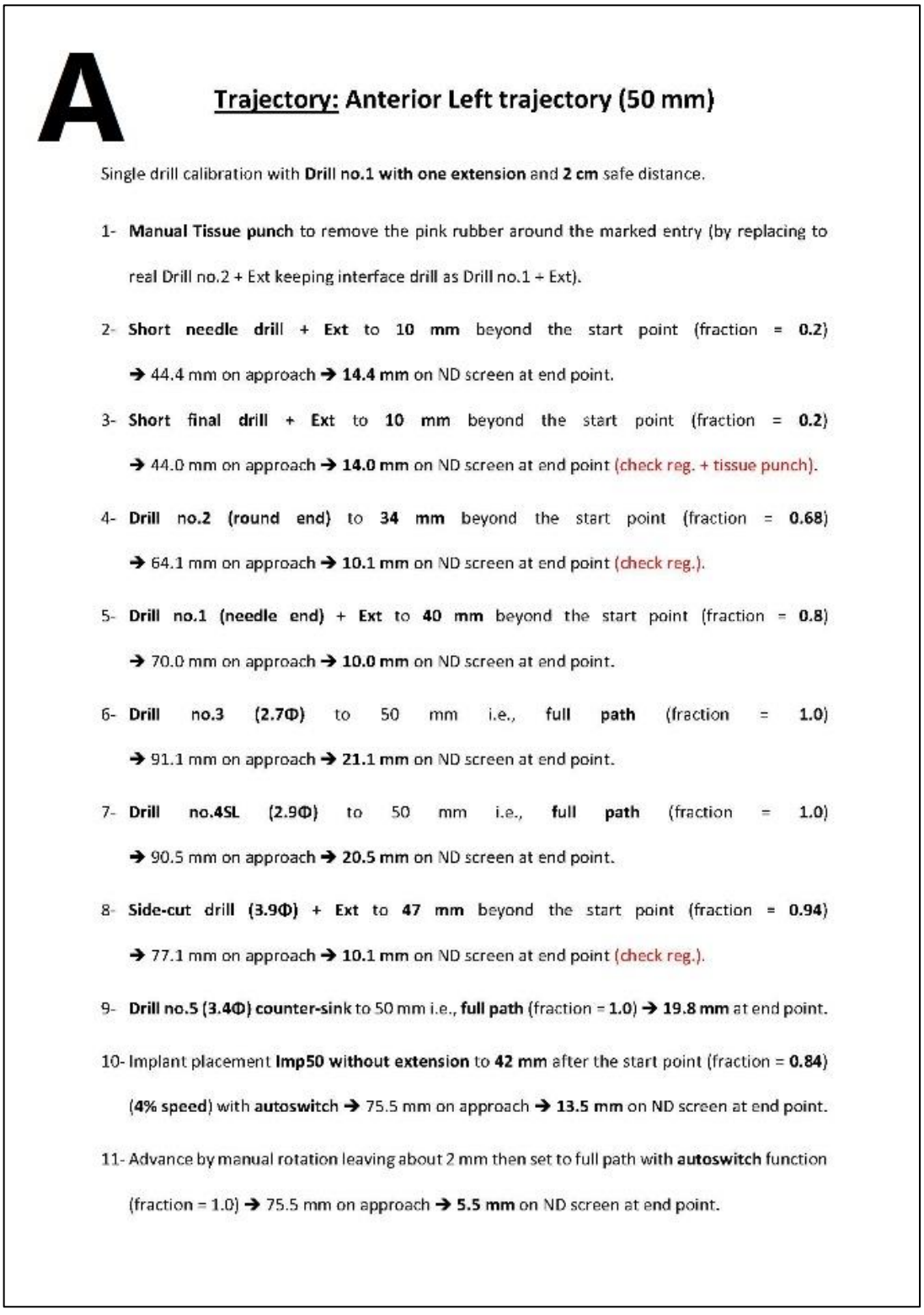

A

Trajectory: Anterior Left trajectory (50 mm)

Single drill calibration with **Drill no.1 with one extension** and **2 cm** safe distance.

1- **Manual Tissue punch** to remove the pink rubber around the marked entry (by replacing to real Drill no.2 + Ext keeping interface drill as Drill no.1 + Ext).

2- **Short needle drill + Ext to 10 mm** beyond the start point (fraction = **0.2**) → 44.4 mm on approach → **14.4 mm** on ND screen at end point.

3- **Short final drill + Ext to 10 mm** beyond the start point (fraction = **0.2**) → 44.0 mm on approach → **14.0 mm** on ND screen at end point (check reg. + tissue punch).

4- **Drill no.2 (round end) to 34 mm** beyond the start point (fraction = **0.68**) → 64.1 mm on approach → **10.1 mm** on ND screen at end point (check reg.).

5- **Drill no.1 (needle end) + Ext to 40 mm** beyond the start point (fraction = **0.8**) → 70.0 mm on approach → **10.0 mm** on ND screen at end point.

6- **Drill no.3 (2.7Φ)** to 50 mm i.e., **full path** (fraction = **1.0**) → 91.1 mm on approach → **21.1 mm** on ND screen at end point.

7- **Drill no.4SL (2.9Φ)** to 50 mm i.e., **full path** (fraction = **1.0**) → 90.5 mm on approach → **20.5 mm** on ND screen at end point.

8- **Side-cut drill (3.9Φ) + Ext to 47 mm** beyond the start point (fraction = **0.94**) → 77.1 mm on approach → **10.1 mm** on ND screen at end point (check reg.).

9- **Drill no.5 (3.4Φ) counter-sink** to 50 mm i.e., **full path** (fraction = **1.0**) → **19.8 mm** at end point.

10- Implant placement **Imp50 without extension** to **42 mm** after the start point (fraction = **0.84**) (**4% speed**) with **autoswitch** → 75.5 mm on approach → **13.5 mm** on ND screen at end point.

11- Advance by manual rotation leaving about 2 mm then set to full path with **autoswitch** function (fraction = 1.0) → 75.5 mm on approach → **5.5 mm** on ND screen at end point.

Figure 5-17. Example protocol sheets. (A) The single drill calibration protocol for the anterior left ZI trajectory. This protocol was applied for the robotic group and the NaviDent single calibration group. During the experiment, the starting time of each step in the protocol was noted next to its number on the left.

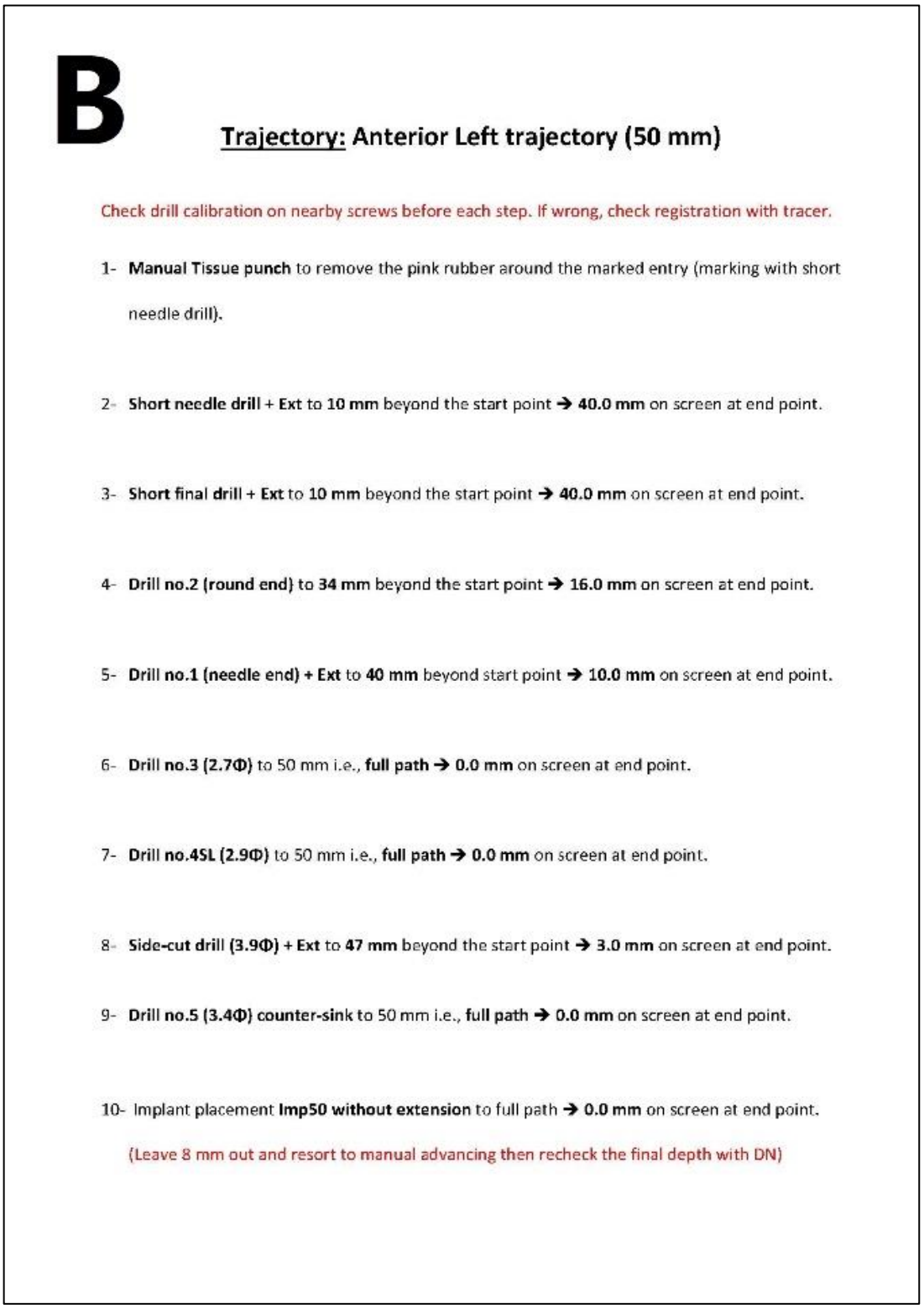

B

Trajectory: Anterior Left trajectory (50 mm)

Check drill calibration on nearby screws before each step. If wrong, check registration with tracer.

1- **Manual Tissue punch** to remove the pink rubber around the marked entry (marking with short needle drill).

2- **Short needle drill** + **Ext** to **10 mm** beyond the start point → **40.0 mm** on screen at end point.

3- **Short final drill** + **Ext** to **10 mm** beyond the start point → **40.0 mm** on screen at end point.

4- **Drill no.2 (round end)** to **34 mm** beyond the start point → **16.0 mm** on screen at end point.

5- **Drill no.1 (needle end)** + **Ext** to **40 mm** beyond start point → **10.0 mm** on screen at end point.

6- **Drill no.3 (2.7Φ)** to 50 mm i.e., **full path** → **0.0 mm** on screen at end point.

7- **Drill no.4SL (2.9Φ)** to 50 mm i.e., **full path** → **0.0 mm** on screen at end point.

8- **Side-cut drill (3.9Φ)** + **Ext** to **47 mm** beyond the start point → **3.0 mm** on screen at end point.

9- **Drill no.5 (3.4Φ) counter-sink** to 50 mm i.e., **full path** → **0.0 mm** on screen at end point.

10- Implant placement **Imp50 without extension** to full path → **0.0 mm** on screen at end point.

(Leave 8 mm out and resort to manual advancing then recheck the final depth with DN)

Figure 5-17. Example protocol sheets. (B) The multiple drill calibration protocol for the anterior left ZI trajectory. This protocol was applied for the NaviDent group and the X-Guide group. During the experiment, the starting time of each step in the protocol was noted next to its number on the left.

Clinicians are strongly advised to get an additional sample for the hand-eye calibration process near the implant trajectory of interest as a refinement step. Otherwise, residual deviations were unavoidable between the optical tracking system and the robotic system.

Chapter 6

General Discussion and Conclusions

6.1. Discussion Summary

This chapter aims to connect the results of the three investigated human sources of error in dynamic navigation placement of zygomatic implants, and also put those results into a broader context. The rationale is to rank the contribution (i.e., impact) of these sources to the overall accuracy and therefore, sets the priorities for future developments in the system hardware and operator training.

The accuracy of zygomatic implant placement is crucial for patients requiring this rehabilitation option. Accurate placement reduces the possibilities for intra- and post-operative complications and facilitates immediate provisional restorations. This is especially true with rehabilitation treatment plans based on multiple implants including the quad zygoma protocol (Bolding and Reebye, 2021, Pan et al., 2021, Wadde et al., 2024, Davó et al., 2023).

When it comes to implant placement accuracy, the primary parameters for assessment are usually entry point, exit point, and angulation deviations from the planned path (Guo et al., 2024). Both entry point and angulation deviations are mainly associated with restorative implications, while exit point deviations are predominantly associated with surgical implications (Bedrossian, 2021).

In most cases of entry and exit point deviations, it is not enough to denote the magnitude of the 3D deviation. The specific direction of the deviation becomes more significant from the clinical point of view with increased deviation magnitude (Hernández-Alfaro et al., 2023). It is well-known that the final deviations resulting from a complex procedure will accumulate the deviations contributed in each step involved in that procedure (Widmann et al., 2009).

In our project, when considering the area of the exit point of the zygomatic implant, the registration error of the selected configuration of fiducial markers (chapter 2) was 1.06 mm (median of Conf.9 – appendix table 2-8 on page 76). The drill calibration precision of the selected drill for the single calibration protocol (chapter 3) was 0.83 mm (variability range of SpL.+Ext drill – table 3-1 on page 93). Both sources arise from manual localisation errors derived from the operator and tracking errors that are related to the quality of the tracking camera and the algorithm used by the system to establish the 3D spatial relationships (Al-Jarsha et al., 2024a, Al-Jarsha et al., 2024b).

Although the variability range of the drill calibration does not imply a direct margin of error from the true position of the drill tip, this value implies that the true drill tip would have to be located within this range if the calibration algorithm was expected to perform its purpose, at least once out of the 27 repetitions applied for each drill. The variability range can thus be used as a reference to the margin of error of the drill calibration process.

It is an interesting observation that adding up the magnitude of the two human-related sources almost equals to the total error at the exit point in the manual placement group with single drill calibration protocol of 1.92 mm (chapter 5, table 5-2 on page 165). 1.06 mm + 0.83 mm = 1.89 mm.

Although this suggests an additive nature of these two sources, we have already mentioned earlier that the final deviation would depend on the specific direction of its component deviations and therefore, this observation should be looked at carefully. This is also supported by the fact that other sources of error are involved in the procedure and its assessment method (e.g., human application error, tracking camera noise, and uncertainty in the method of assessment due to the software superimposition and automatic alignment algorithms). The net collective error from all these remaining sources is unlikely to be as small as 0.03 mm (1.92 mm – 1.89 mm).

Nevertheless, given the strict procedure standardisation applied while assessing the three human sources of errors in the previous three chapters, it would be possible to comment on the estimated difference in the application error due to the use of the robotic arm over the human hand for the exit point deviations. 2.80 mm (mean 3D exit point deviation of robotic group) – 1.92 mm (mean 3D exit point of the manual group with single drill calibration) = 0.88 mm. (i.e., the trained human hand produced about 0.88 mm less deviation in the exit point than the robotic arm investigated in this project).

Therefore, the impact of the three types of human-related error investigated in this project on the overall ZI placement accuracy could be ranked from high to low as follows; registration error, drill calibration error, then application error. This ranking is supported by the previous literature that focused primarily on improving the registration protocol rather than any other error source arising from dynamic navigation procedures (Chackartchi et al., 2020, Choi et al., 2020, Stefanelli et al., 2020a, Zhou et al., 2021, Ma et al., 2022, Shen et al., 2023, Wu et al., 2023a, Wu and Sun, 2024).

This ranking could direct the development of the systems and justify training programs for ZI placement under dynamic navigation. Therefore, improving the current registration tools and training takes priority, followed by drill calibration tools and training development, followed by developing smart robotic systems that minimise the application error, even with novice operators. This ranking was also supported with a previous *in vitro* study regarding the learning curve of dynamic navigation-guided ZI placement, which reported that the previous training affected the operation time rather than the final implant accuracy (Wang et al., 2024c).

Further research should prioritise the focus on testing the impact of improving the hardware and the software of the guiding systems, with emphasis on separating each error source and detailing the directionality, as was done in this project. It should be noted, however, that involving complex hardware developments is more likely to require a steep operator learning curve in itself (to train the operator in performing the new protocols using the new hardware/software).

In addition to the above, the overall goal of future research should be improving accuracy without overdue increase of the procedure cost from the patient's point of view, as that might limit the public access to these new expensive guiding systems (Milner et al., 2020).

Static guides represent the simplest form of guiding hardware to assist the placement of ZIs. They can achieve acceptable accuracy, but a high level of surgical skills is still required because most of them require large surgical flaps. This in turn would put more risk to the anatomical vital structures around the surgical site (Chow, 2016, Jayanetti et al., 2021, Rigo et al., 2021). The development of static guides for flapless ZI placement is made more challenging by the length of the zygomatic implants which results in angulation errors (Schiroli et al., 2011, Schiroli et al., 2016).

On the other hand, dynamic navigation guidance provides more flexibility in clinical scenarios with limited intraoral space, and the flapless application is more straightforward. However, it is more technically demanding and prior training for the surgeon is required for them to accustom looking away from the surgical site to receive the visual clues from the dynamic navigation screen (Block and Emery, 2016, Golob Deeb et al., 2019, Zhan et al., 2020). Trying to solve this issue by including augmented reality to superimpose the 3D image of the surgical plan on the surgical site itself further introduced new training needs in the use of this new technology (Tao et al., 2024).

Improving the accuracy of dynamic navigation guidance also involves operator training in the steps of registration (Al-Jarsha et al., 2024a), drill calibration (Al-Jarsha et al., 2024b), and the execution of the surgery (Wang et al., 2024c). To reduce these training needs, limiting the human involvement in the registration and tool calibration processes are required, and the use of robotics with various levels of requirement for human collaboration/supervision is still underway (Xu et al., 2023a, Yang et al., 2017). Currently available robotic systems for implant placement still require a certain level of human control, which again introduces operator training needs for preoperative set-up and intra-operative collaboration and supervision (Xu et al., 2023a, Fan et al., 2024).

In this project, the development of a robotic system to achieve a relatively simple task was not without difficulties (see section 6.3). This project focused on successfully instructing the robotic arm with its connected tool to achieve a pre-planned pose and then advancing in a short movement based on the 3D location of two points in the 3D space. However, since the location of these two points had to be derived from information available in another system (the dynamic navigation optical tracking system), utmost care had to be taken to achieve an accurate transfer of these 3D locations between the two systems, and the locations had to be accurately transferred from the real environment to the first system (i.e., the optical DN system). In addition, the robotic movements had to avoid collision with extraoral structures and other physical obstacles in the environment (see section 4.5). The line-of-sight of the optical tracking camera was also considered in planning the drilling movements so that the operator is not precluded from supervising the procedure by monitoring the navigation system screen.

The results of this initial development and testing stage demonstrate that the robot was not yet as accurate as the human hand despite the robust protocol and efforts taken to achieve minimal errors in transferring the 3D locations. The difficulties encountered by the robotic system were mostly related to the suitability of the drilling hardware and the anatomy of the drilling path (see section 6.3). The time required for the procedure should be balanced against the frequency of the accuracy checking steps that would result in a reasonable overall time requirement for clinical applications. The investigated robotic procedure was slow that would prohibit its direct clinical implementation. The speed of the procedure is important for its practicality and this is something that needs further work to improve it.

During the foreseeable future, the availability of multiple surgical treatment options is expected for patients requiring the placement of ZIs, each of which would have its own level of final implant accuracy. The implementation of one option or another will depend on the availability and cost implications of newly introduced technologies, as well as on the availability of operators with the level of training required for these surgical options. The most up-to-date technological breakthroughs have not yet reached the level of full automation that would preclude the need for proper surgical skills.

6.2. Conclusions

Registration using fiducial markers resulted in higher levels of accuracy than the tracing method. Therefore, the fiducial registration method was chosen for the subsequent steps in this thesis. On the basis of the data supporting this conclusion, we can confirm the recommendation of using the fiducial registration method over the tracing registration for clinical use in cases of edentulous maxillae.

Configurations 3, 5 and 6 presented in this thesis were shown to result in higher registration accuracies. Configuration 9, which represents a mirror image of both configurations 5 and 6, was therefore used in the subsequent experiments. These fiducial marker configurations can be recommended for clinicians placing zygomatic implants under dynamic navigation.

In the edentulous maxillae, increasing the number of intraoral fiducial markers available for registration from four to six improved the registration accuracy. On the contrary, increasing the number from six to eight fiducial markers did not result in a statistically significant imporvment in the registration accuracy. We utilised a configuration that had six fiducial markers distributed in the anterior area and the tuberosity area of the maxillary alveolus for this project (Configuration 9). We recommend this configuration for use in clinical cases not only because of its resulting accuracy, but also for the expected patient comfort as it does not include placing any fiducial markers in the palatal area.

Long drills with pointed tips that are made of stainless steel had better precision than drills made of a more flexible material (e.g. titanium), or those which were shorter in length or had non-pointed tips. In this thesis, we optimised the drill calibration in the robotic protocol by calibrating a single long pointed drill made of stainless steel instead of performing multiple drill calibrations which would have introduced variations (see table 4-3 on page 138). We still recommend multiple drill calibrations for the manual drilling protocol to acheive higher final accuracy. However, we advise clinicians to perform all drill calibrations carefully with a stable hand and always perform the recommended calibration accuracy checks prior to every drilling step.

Under *in vitro* conditions, where other sources of error implicated in optical tracking are reduced to a minimum, robotic drilling in simulated high density bone areas (D2) with long zygomatic drills subjected to heavy lateral forces did not perform better than manual drilling using the same optical tracking system for dynamic navigation. The robotic arm drilling did not produce better accuracy than the manual drilling in this project.

Merely matching the coordinates for the drilling procedure was not engough to obtain higher accuracy than the manual procedure. There is a need to make the robotic arm smarter to adjust for the resisting lateral forces and/or design more rigid drill bits held by custom heavy duty handpieces for the robotic arm implant procedures. We acheived the coordinate matching between the robotic and the dynamic navigation system, but it appears that there are residual sources of error not detected by the operator monitoring the dynamic navigation screen during robotic drilling. Therefore, the potential suitability of the prototype presented in this project for clinical zygomatic implant placement is dependant on further develping the associated drilling hardware so that the final system can avoid or account for this residual source of error. Further impromvents to the quality of dynamic navigation registration, drill calibration and tracking would reduce the variation between the real position of the implant and its representation on the dynamic navigation screen, which is the yardstick for the robotic protocol.

6.3. Limitations of the study

6.3.1. Time requirement

The main limitation of the current system is the prolonged time required to perform the implant placement. The current preoperative time includes the steps of implant plan coordinate extraction before transferring the coordinates to the robotic arm software. The preparation time is longer than that required for human-operated dynamic navigation because of the steps required to setup the device in a suitable place for its working volume, in addition to the process of robotic registration. Each manual implant placement procedure in this study required about 40 minutes due to the rigorous and continued checks and refinements to the original registration and drill calibration stages. This would be impractical to replicate in the clinical setting. Previous *in vitro* studies investigating commercial robotic systems reported preparation times between 5 and 7 minutes, and similar operation surgical times per dental implant trajectory (Xu et al., 2023a, Xi et al., 2024). However, the long preoperative preparation time is recognised as a limitation in the clinical studies (Wang et al., 2024b). Investigations of the robotic zygomatic implant placement procedures did not report on preparation or surgical times (Cao et al., 2020, Deng et al., 2023b, Deng et al., 2023c, Li et al., 2023a, Guo et al., 2024, Fan et al., 2024).

6.3.2. Interpretation of the final results and the fixed head position

Utmost care must be taken while trying to generalise the absolute accuracy results of our manual procedure groups to the clinical scenario. This is mainly because the level of meticulous care taken in this project for the manual placement groups to minimise the sources of errors prior to every drilling step, would not be practical or achievable in the clinical setting. The robotic placement could therefore perform better in a real clinical scenario than the manual placement with its conventional levels of care. In this project, the registration cycle was repeated up to 7 times in some cases to achieve a detectable deviation at the target point that was close to zero. The same persistence was applied to the ensure quality of drill calibration process and the drilling execution via a slow manual advancement along the trajectory.

If the procedure is done under local anaesthetic, patient head movements during the manual drilling are expected to produce more inaccuracies for the manual placement. Even when the patient head is immobile, it should be noted that the operator in this investigation did not perform more than four zygomatic implant placement procedures per day. The level of fatigue in the real scenario may result in a wider margin of application error in manual placement. Nowadays, the patient head is often immobilised during the procedure under general anaesthetics when using the commercial robotic systems (Deng et al., 2023c, Bolding and Reebye, 2021). However, some reports stated to have used local anaesthetic but did not comment on the head fixation mechanism (Wang et al., 2024b). Most recent systems using two robotic arms claim to be tolerant of a small range of patient head movement. These systems implement a sophisticated camera in one arm that is able to achieve image acquisition and detect the position and pose of the oral structures based on one marker only (positioning device). The positional changes are then transferred in real-time to the software controlling the other operating robotic arm for trajectory adjustment (Tang et al., 2024).

The presented prototype in this project could make use of the current dynamic navigation systems if they were to be upgraded with the ability for tracking three trackers simultaneously (as suggested in section 4.6). Otherwise, the simplest solution would still be to rigidly fix the head position and operate under general anaesthetic.

6.3.3. Mechanical damage of the drilling tools

We found that the forces generated by the robotic drilling were high enough to damage the handpiece and shorten its working life. This is thought to be due to the resistance forces against the advancing drill motion along the planned trajectory, and presents as mechanical damage to the gear components of the contra-angle handpiece and the drill extension (figures 6-1 and 6-2). This is likely to be less of an issue with shorter implants.

We had to replace the handpiece used for the robotic drilling after the optimisation tests and immediately prior to conducting the comparative experiment.

This practice would be expensive and a solution to this needs to be found before the robotic prototype could be used clinically. Such damage is expected to be considerably less during the manual drilling procedure where the advancing resistance forces would cause the operator hand to adjust the advancing speed and/or the direction of the drilling force to avoid such damage.

Methods to minimise this limitation could therefore be to always use sharp drills and include smart force sensors within the robotic arm that help prevent the effects of overdue resistance forces to simulate the human manual adjustments mentioned above. Other researchers have highlighted the effect of drill wear and the drilling protocol used for robotic implant osteotomy preparation on the accuracy outcome (Deng et al., 2023c).

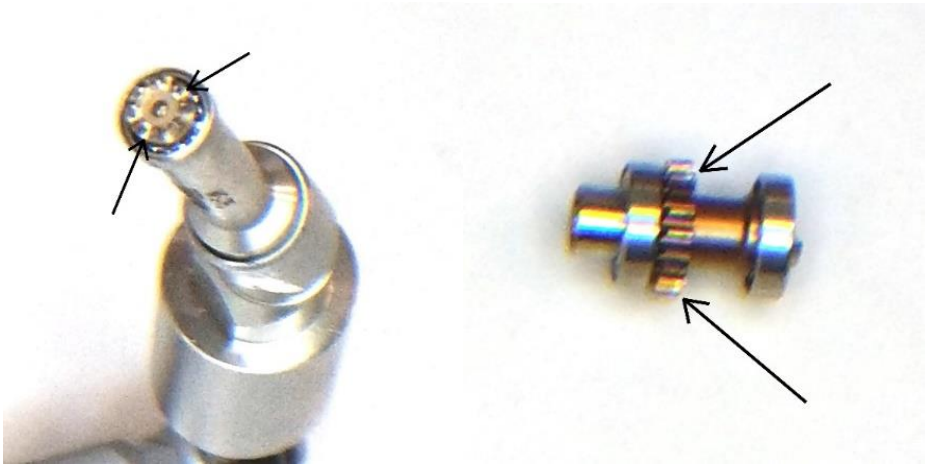

Figure 6-1. The mechanical damage to the contra-angle implant handpiece observed after completing the implant placement experiment. The shiny scratches on the gears (arrows) highlights excessive frictional forces and the potential for loosened drill grip.

Figure 6-2. The mechanical damage to the drill extension observed after completing the implant placement experiment. The metal of the ring surrounding the sleeve part had a longitudinal crack (circled area), indicating the exposure to heavy vertical and lateral forces beyond what is expected during the use of this component.

6.3.4. Modifications to overcome loose zygomatic implant junction

The junction between the zygomatic implant and its standard adapter had to be temporarily re-enforced with adhesive tape in order to prevent the excessive movement at the stage of implant placement (figure 6-3). This obviously cannot be duplicated in the clinical scenario.

Previously published literature did not report any issues using this design of ZI for manual dynamic navigation procedures (Fan et al., 2023, Aparicio et al., 2024). Studies reporting robotic ZI placement usually implement manual implant placement step and restrict the robotic tasks to drilling and tapping only (Guo et al., 2024, Olivetto et al., 2023, Li et al., 2023a), while others utilised partial initial manual placement (Deng et al., 2023c). This could be the main reason why other authors did not report this issue, as they can hold the implant and its adapter together manually during the initial stage of this step.

Therefore, implant companies need to pay a special attention to the adapter-implant locking mechanism if their implants are to be used with a robotic arm. If force feedback is to be included in future systems, it might also be useful in detecting implant adapter connection failure (i.e., a momentary drop of advancing resistance forces with a pronounced increase in lateral resistance forces).

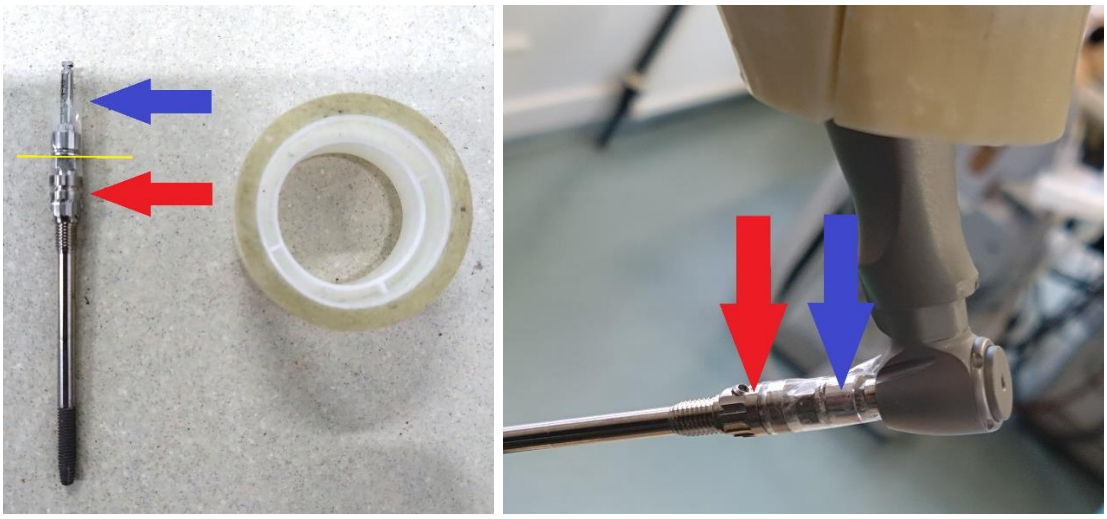

Figure 6-3. The temporary re-enforcement of the implant-adapter connection with adhesive tape during the implant insertion step. The blue arrows point to the implant adapter while the red arrows point to the zygomatic implant. The yellow line is where the two components meet in a lock-and-key fashion, but without any locking mechanism against disconnection. After the zygomatic implant threads engage the zygomatic anatomy (at around 80% of the total trajectory length), the adhesive tape was carefully removed before continuing to the final implant advancement stage (without the re-enforced fixation).

Without this temporary re-enforcement that we adapted in this project, it would have been difficult for the usually loose implant-adapter connection to resist the lateral forces arising from the anatomical features of the osteotomy site, whether initially, or during trajectory correction attempts (figure 6-4).

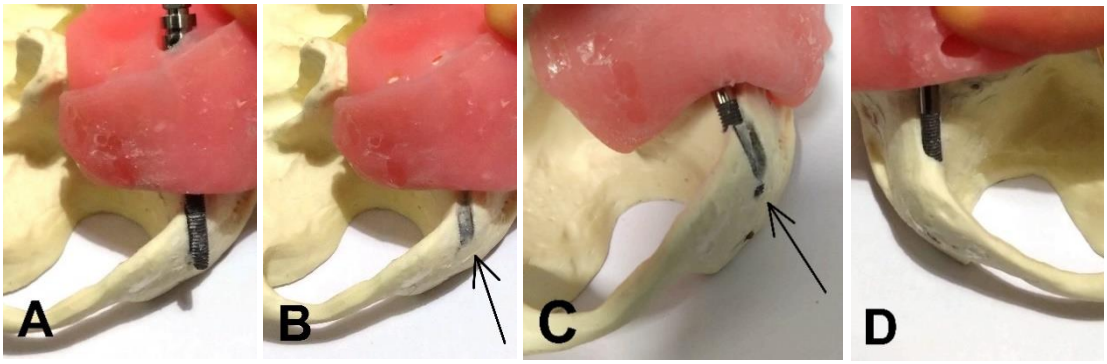

Figure 6-4. (A) a posterior zygomatic implant which was deflected outside the intended osteotomy path due to lateral forces resulting from the anatomical features of the inferior zygoma. (B) the groove that was made on the outer surface of the zygoma due to the deflected drilling path (arrow). (C) On a following session, using adhesive tape to re-enforce the implant-adapter connection, it was possible to correct the initial trajectory (arrow) and prevent the implant form going into the old deflected path. (D) the posterior zygomatic implant on the contralateral side which was placed with the help of the adhesive tape temporary re-enforcement from the first attempt.

6.3.5. The subjective nature of intra-procedure accuracy checks

Human subjective judgement is still involved in many steps of the current protocol, this includes the accuracy checks for the registration and drill calibration stages. Advancement in techniques not requiring human intervention (such as an augmented reality-based automated registration) could be the proper way to address this limitation. The threshold for registration accuracy that is recommended by the manufacturer of the dynamic navigation system is ± 0.5 mm (ClaroNavInc., 2021). This value also represents the acceptable threshold reported by other studies of robotic protocols (Guo et al., 2024), and this error type should be checked near the surgical site using the system tracer (probe) (ClaroNavInc., 2021, X-NavTechnologiesLLC, 2020, Fan et al., 2019). Since most currently available tracking cameras do not have a sophisticated way of recognising the size and location of the real objects themselves, the need for attaching trackers and subsequently establishing their spatial relationship to the real patient anatomy physically via a tracing/localisation tool is unavoidable at present.

This is also the reason why the registration accuracy checks must also depend on these localisation tools because the error in question is between the real environment and the dynamic navigation software rather than between two different system software. The robotic arm in our project depends on this registration accuracy for the identification of the proper implant trajectory, and not the other way around (i.e., coordinates obtained from the dynamic navigation system after the registration and drill calibration checks serve as input data for the robotic arm).

The prescribed drill calibration and its accuracy check procedures were difficult in the robotic group because the implant handpiece could not be rapidly detached from and re-attached to the robotic arm without risking a change in the established calibration relationship. Otherwise, if this limitation could be safely avoided, the operator would perform the drill calibration and its accuracy checks as prescribed by the manufacturer by manually approaching the accuracy checking landmarks in the real world.

Then the handpiece re-attachment to the robotic arm would not compromise the established spatial relationship, and the next step of matching to the robotic coordinates frame can progress with the hand-eye calibration method described in section 4.3.2.

Having the handpiece with an attached drill approaching the accuracy checking landmarks with the control of the robotic arm is dangerous and should not be replicated in a clinical scenario. The uncertain pressure forces and the subjective human judgment of the drill tip position in the real world will also limit objective accuracy judgement even if that robotic movement was possible in a safe manner.

6.3.6. The absence of irrigation

Irrigation to avoid overheating of the bone would be an absolute requirement in the clinical scenario, but was not addressed in this investigation. However, most *in vitro* studies do not include irrigation function (Fan et al., 2024, Guo et al., 2024), but it is a must for clinical cases (Olivetto et al., 2023).

Further work is required to develop an irrigation system alongside the robotic arm that would allow adequate cooling of the bone in the clinical setting without compromising the surgical procedure.

The cooling of the drills may have an effect on the degree of their flexibility and, therefore, the overall accuracy of implant placement.

6.4. Future Work

In relation to the current prototype robotic system, there are several aspects that are worth developing in the future that would make it more applicable for clinical work.

For the system to have more versatile applications other than zygomatic implants (Sun et al., 2023), more detailed assessment for the exact work volume inside the oral cavity may be considered for a new handpiece connection design (Wang et al., 2023c, Sin et al., 2023). This in turn would enable the design of a modified and more robust handpiece connnection to the end effector of the robotic arm.

Adding force sensing to the handpiece connection may help in making real-time micro-adjustments during the drilling process, which would reduce the contact load over the instrument and thus prolong its life (Wang et al., 2023b). The information from the force feedback could also help improve the osteotomy strategy to achive optimal primary stability (Chen et al., 2024).

The simulation environment used in this project can be applied to optimise the work volume and suitable instruments for other types of oral surgical procedures, such as harvesting autogenous bone blocks (Zhou et al., 2023). Incorporating collision detection with haptic feedback into the simulation software would make it a very beneficial training tool (Leng et al., 2024).

Improving the robotic arm software interface so that implant planning can be achieved without the need for an external planning software would also make the implementation of AI diagnostic, planning and provisionalisation features possible (Zielinski et al., 2023, Manfredini et al., 2023).

Reducing the size of the system to make it handheld (Bollars et al., 2023). This would be expected to facilitate the transport and storage of the system in addition to improving access in the clinical enviroment through the occupation of less space. However, care should be taken to avoid compromising the robustness of the mechanical components, and thus the accuracy and safety of the system.

A robotic drilling system that eliminates the effect of lateral forces could serve as a research gold standard against which the other sources of error in dynamic navigation can be improved and their acceptable error margins determined. This would be possible because the implant deviations resulting from an experimental surgical procedure will be mostly related to the other sources of errors such as registration, drill calibration, and tracking errors rather than to an application (drilling) error.

Our prototype system has used one anatomical setup and model anatomy. To enhance the validation of this system, more experiments should be carried out in a wider range of simulated scenarios before moving on to clinical studies.

Robotic placement of zygomatic implants can improve the safety of this procedure by ensuring predictable accuracy. Theoretically, operator surgical execution error would be eliminated in an ideal robotic system, and the plan put by the surgeon would be achieved with minimal final deviations.

The current difficulties in developing such an ideal system are related to the technical challenges associated with the accuracy of mapping the patient's real anatomy to their surgical plans as well as mapping the real drill tip position and orientation to the robotic system space. The mechanical drilling components should also account for the lack of tactile sensation feedback which would protect them against damage. Force sensing would ensure the detection of any abnormal resistance forces during the procedure and might compensate for the lack of detecting the position of the drill or implant itself inside the tissues. The time required to perform the preparation steps is still long from the clinical point of view and patient trust in the robotic procedure could be another challenge. Many professionals may perceive the high cost and training requirements for the use of the current commercially available robotic systems as another barrier to their application. The active involvement of all related industries and research groups would help in overcoming all the above-mentioned challenges and in creating autonomous, safe, accurate, and affordable clinical robotic systems in the future.

6.5. Clinical significance key messages

Chapter 1 highlights the clinical importance of achieving accurate implant positioning in avoiding surgical and long-term complications. The clinical protocols for guidance that are being followed in the current literature to reach the required levels of implant placement accuracy with explanation of their advantages and disadvantages. Implant placement should always be preceded with good planning practices that take prosthodontic and biological principles into consideration. Zygomatic implants provide an effective rehabilitation for atrophic maxillae, but complications due to inaccurate placement are still expected with the current guiding protocols.

Chapter 2 confirms the requirement for installation of mini-screws in a particular fashion in edentulous cases planned for zygomatic implant placement. The clinical guide resulting from this chapter is the requirement for installing six mini-screws intraorally to serve as fiducial markers in the edentulous maxillae. The accuracy for registration with this configuration was about 1 mm at the area of the frontal process of the zygoma.

Chapter 3 emphasises the importance of the drill calibration step and the degree of care that should be considered by clinicians during its application. The mean accuracy of drill calibration with the tested DN system was about 0.6 mm, and varies with the shape of the drill tip and its manufacturing material.

Chapter 4 highlights the high technical demands of the current integrated robotic systems and the associated requirement of clinical training in diagnosing and troubleshooting possible encountered issues.

Chapter 5 demonstrates that the key points for accurate zygomatic implant placement were mostly related to the registration and calibration processes rather than the drilling step itself. Robust registration and calibration protocols led to 3D deviations of the final zygomatic implants that were below 2 mm with the manual procedures. Robotic drilling produced higher deviations which could be explained by the relative simplicity of the tested integrated system.

Chapter 7

References

AALAM, A. A., KRIVITSKY-AALAM, A., KURTZMAN, G. M. & MAHESH, L. 2023. The severely atrophic maxilla: Decision making with zygomatic and pterygoid dental implants. *J Oral Biol Craniofac Res,* 13**,** 202-206.

ABDUO, J. & LAU, D. 2021. Accuracy of static computer-assisted implant placement in long span edentulous area by novice implant clinicians: A cross-sectional in vitro study comparing fully-guided, pilot-guided, and freehand implant placement protocols. *Clin Implant Dent Relat Res,* 23**,** 361-372.

AHMAD, P., ALAM, M. K., ALDAJANI, A., ALAHMARI, A., ALANAZI, A., STODDART, M. & SGHAIREEN, M. G. 2021. Dental Robotics: A Disruptive Technology. *Sensors,* 21**,** 3308.

AL-JARSHA, M. Y., ALMEZYAD, O., ALOTAIBI, N., NAUDI, K. B., ROBERTSON, D. P. & AYOUB, A. F. 2024a. The Accuracy of Intraoral Registration for Dynamic Surgical Navigation in the Edentulous Maxilla. *Int J Oral Maxillofac Implants,* 39**,** 21-46.

AL-JARSHA, M. Y., AYOUB, A. F., ALMGRAN, M. M., LIU, C. H., ROBERTSON, D. P. & NAUDI, K. B. 2024b. The precision of drill calibration for dynamic navigation. *J Dent,* 146**,** 105032.

ALTALHI, A. M., ALHARBI, F. S., ALHODAITHY, M. A., ALMARSHEDY, B. S., AL-SAAIB, M. Y., AL JFSHAR, R. M., ALJOHANI, A. S., ALSHAREEF, A. H., MUHAYYA, M. & AL-HARBI, N. H. 2023. The Impact of Artificial Intelligence on Dental Implantology: A Narrative Review. *Cureus,* 15**,** e47941.

ANADIOTI, E. & KOHLTFARBER, H. 2021. Radiographic Evaluation of Prosthodontic Patients. *Dental Clinics,* 65**,** 605-621.

APARICIO, C. 2011. A proposed classification for zygomatic implant patient based on the zygoma anatomy guided approach (ZAGA): a cross-sectional survey. *Eur J Oral Implantol,* 4**,** 269-75.

APARICIO, C., LÓPEZ-PÍRIZ, R. & PEÑARROCHA, M. 2021a. Preoperative Evaluation and Treatment Planning. Zygomatic Implant Critical Zone (ZICZ) Location. *Atlas Oral Maxillofac Surg Clin North Am,* 29**,** 185-202.

APARICIO, C., MANRESA, C., FRANCISCO, K., CLAROS, P., ALÁNDEZ, J., GONZÁLEZ-MARTÍN, O. & ALBREKTSSON, T. 2014. Zygomatic implants: indications, techniques and outcomes, and the zygomatic success code. *Periodontol 2000,* 66**,** 41-58.

APARICIO, C., POLIDO, W. D., CHEHADE, A., SHENOUDA, M., SIMON, M., SIMON, P. & AL-NAWAS, B. 2024. Round and flat zygomatic implants: effectiveness after a 3-year follow-up non-interventional study. *Int J Implant Dent,* 10**,** 30.

APARICIO, C., POLIDO, W. D., CHOW, J., DAVID, L., DAVO, R., DE MORAES, E. J., FIBISHENKO, A., ANDO, M., MCLELLAN, G., NICOLOPOULOS, C., PIKOS, M. A., ZARRINKELK, H., BALSHI, T. J. & PEÑARROCHA, M. 2021b. Identification of the Pathway and Appropriate Use of Four Zygomatic Implants in the Atrophic Maxilla: A Cross-Sectional Study. *Int J Oral Maxillofac Implants,* 36**,** 807-817.

APARICIO, C., POLIDO, W. D., CHOW, J., DAVÓ, R. & AL-NAWAS, B. 2022. Round and flat zygomatic implants: effectiveness after a 1-year follow-up non-interventional study. *Int J Implant Dent,* 8**,** 13.

APARICIO, C., POLIDO, W. D. & ZARRINKELK, H. M. 2021c. The Zygoma Anatomy-Guided Approach for Placement of Zygomatic Implants. *Atlas of the Oral and Maxillofacial Surgery Clinics of North America,* 29**,** 203-231.

ASHRY, A., ATTAR, M. S. E., ELSAMNI, O. A. & SOLIMAN, I. S. 2021. Effect of Guiding Sleeve Design on Intraosseous Heat Generation During Implant Site Preparation (In Vitro Study). *Journal of Prosthodontics,* 31**,** 147-154.

AYDEMIR, C. A. & ARıSAN, V. 2020. Accuracy of dental implant placement via dynamic navigation or the freehand method: A split-mouth randomized controlled clinical trial. *Clinical Oral Implants Research,* 31**,** 255-263.

AYOUB, A. & PULIJALA, Y. 2019. The application of virtual reality and augmented reality in Oral & Maxillofacial Surgery. *BMC Oral Health,* 19**,** 238.

BAGHERI, S. C., KHAN, H. A. & STEVENS, M. R. 2020. *Complex Dental Implant Complications*, Springer.

BATTISTA, E., GASPARRO, R., CACCIOLA, M., SAMMARTINO, G. & MARENZI, G. 2022. Dynamic Navigation System for Immediate Implant Placement in the Maxillary Aesthetic Region. *Applied Sciences,* 12**,** 5510.

BEDROSSIAN, E. 2021. Zygomatic Implants Operative Consideration to Minimize Technical Errors, Complications, and Their Management. *Atlas Oral Maxillofac Surg Clin North Am,* 29**,** 277-289.

BEDROSSIAN, E. & BEDROSSIAN, E. A. 2018. Prevention and the Management of Complications Using the Zygoma Implant: A Review and Clinical Experiences. *Int J Oral Maxillofac Implants,* 33**,** e135-e145.

BEHNIA, H., SHARIFZADEH, N. & BEHNIA, P. 2020. Aesthetic Dental Implant Complications. *In:* BAGHERI, S. C., KHAN, H. A. & STEVENS, M. R. (eds.) *Complex Dental Implant Complications*. Cham: Springer International Publishing.

BHALERAO, A., MARIMUTHU, M., WAHAB, A. & AYOUB, A. 2022. Flapless placement of zygomatic implants using dynamic navigation: An innovative technical note. *Br J Oral Maxillofac Surg,* 61**,** 136-140.

BHALERAO, A., MARIMUTHU, M., WAHAB, A. & AYOUB, A. 2023. Dynamic navigation for zygomatic implant placement: A randomized clinical study comparing the flapless versus the conventional approach. *J Dent,* 130**,** 104436.

BHALERAO, A., MARIMUTHU, M., WAHAB, A. & AYOUB, A. 2024. The Clinical Evaluation of the Dynamically Navigated Flapless Placement of Zygomatic Implants: A Randomized Controlled Trial. *Int J Oral Maxillofac Implants,* 39**,** 40-49.

BLOCK, M. S. & EMERY, R. W. 2016. Static or dynamic navigation for implant placement—choosing the method of guidance. *Journal of Oral and Maxillofacial Surgery,* 74**,** 269-277.

BLOCK, M. S., EMERY, R. W., CULLUM, D. R. & SHEIKH, A. 2017a. Implant placement is more accurate using dynamic navigation. *Journal of Oral and Maxillofacial Surgery,* 75**,** 1377-1386.

BLOCK, M. S., EMERY, R. W., LANK, K. & RYAN, J. 2017b. Implant Placement Accuracy Using Dynamic Navigation. *Int J Oral Maxillofac Implants,* 32**,** 92-99.

BOESECKE, R., BRIEF, J., RACZKOWSKY, J., SCHORR, O., DAUEBER, S., KREMPIEN, R., TREIBER, M., WETTER, T. & HASSFELD, S. Robot assistant for dental implantology. International Conference on Medical Image Computing and Computer-Assisted Intervention, 2001 Berlin, Heidelberg. Springer Berlin Heidelberg, 1302-1303.

BOLDING, S. L. & REEBYE, U. N. 2021. Accuracy of haptic robotic guidance of dental implant surgery for completely edentulous arches. *J Prosthet Dent*, 128**,** 639-647.

BOLLARS, P., JANSSEN, D., DE WEERDT, W., ALBELOOSHI, A., MESHRAM, P., NGUYEN, T. D., LACOUR, M. T. & SCHOTANUS, M. G. M. 2023. Improved accuracy of implant placement with an imageless handheld robotic system compared to conventional instrumentation in patients undergoing total knee arthroplasty: a prospective randomized controlled trial using CT-based assessment of radiological outcomes. *Knee Surg Sports Traumatol Arthrosc,* 31**,** 5446-5452.

BRÅNEMARK, P. I., GRÖNDAHL, K., OHRNELL, L. O., NILSSON, P., PETRUSON, B., SVENSSON, B., ENGSTRAND, P. & NANNMARK, U. 2004. Zygoma fixture in the management of advanced atrophy of the maxilla: technique and long-term results. *Scand J Plast Reconstr Surg Hand Surg,* 38**,** 70-85.

BRENNAND ROPER, M., VISSINK, A., DUDDING, T., POLLARD, A., GAREB, B., MALEVEZ, C., BALSHI, T., BRECHT, L., KUMAR, V., WU, Y. & JUNG, R. 2023. Long-term treatment outcomes with zygomatic implants: a systematic review and meta-analysis. *Int J Implant Dent,* 9**,** 21.

BROWN, R. A. 1979. A computerized tomography-computer graphics approach to stereotaxic localization. *J Neurosurg,* 50**,** 715-720.

CAO, Z., QIN, C., FAN, S., YU, D., WU, Y., QIN, J. & CHEN, X. 2020. Pilot study of a surgical robot system for zygomatic implant placement. *Medical Engineering & Physics,* 75**,** 72-78.

CHACKARTCHI, T., NEEMAN, T. & ZABROVSKY, A. 2020. Guided Implant Placement in Fully Edentulous Patients. The Full Retraction Protocol: Registration Technique to Improve Treatment Outcome. *Int J Periodontics Restorative Dent,* 40**,** 721-729.

CHATTERJEE, E., NASHA, A., MUSTAFA, M., CHINTHALAPUDI, S. L., PADAVALA, S., LAKSHMIPURAM, A. K. & BHATNAGAR, T. K. 2023. The Impact of Implant Angulation on the Stress Distribution and Survival Rate of Implant-Supported Fixed Dental Prostheses: A Retrospective Study. *Cureus,* 15**,** e47892.

CHEN, D., CHEN, J., WU, X., CHEN, Z. & LIU, Q. 2024. Prediction of primary stability via the force feedback of an autonomous dental implant robot. *J Prosthet Dent,* 132**,** 1299-1308.

CHEN, H. & HU, S. Research on Passive Optical Dental Implant Dynamic Navigation System Based on Binocular. 2023 IEEE 15th International Conference on Advanced Infocomm Technology (ICAIT), 2023. IEEE, 374-379.

CHEN, P. & NIKOYAN, L. 2020. Guided Implant Surgery: A Technique Whose Time Has Come. *Dental Clinics of North America,* 65**,** 67-80.

CHEN, X., WU, Y. & WANG, C. 2011. Application of a surgical navigation system in the rehabilitation of maxillary defects using zygoma implants: report of one case. *Int J Oral Maxillofac Implants,* 26**,** e29-e34.

CHHABRA, K., SELVAGANESH, S. & NESAPPAN, T. 2023. Hybrid Navigation Technique for Improved Precision in Implantology. *Cureus,* 15**,** e45440.

CHOI, Y. D., MAI, H. N., MAI, H. Y., HA, J. H., LI, L. J. & LEE, D. H. 2020. The Effects of Distribution of Image Matched Fiducial Markers on Accuracy of Computer-Guided Implant Surgery. *J Prosthodont,* 29**,** 409-414.

CHOW, J. 2016. A novel device for template-guided surgery of the zygomatic implants. *Int J Oral Maxillofac Surg,* 45**,** 1253-1255.

CHOW, J. 2020. *Zygomatic Implants: Optimization and Innovation*, Springer International Publishing.

CHRCANOVIC, B. R., OLIVEIRA, D. R. & CUSTÓDIO, A. L. 2010. Accuracy Evaluation of Computed Tomography–Derived Stereolithographic Surgical Guides in Zygomatic Implant Placement in Human Cadavers. *Journal of Oral Implantology,* 36**,** 345-355.

CLARONAVINC. 2021. Navident [User Manual For use with Navident Software Version 3.X]. Canada.

CRAIG, J. J. 2005. *Introduction to Robotics: Mechanics and Control*, Pearson/Prentice Hall.

CRISTACHE, C. M., BURLIBASA, M., TUDOR, I., TOTU, E. E., DI FRANCESCO, F. & MORARU, L. 2021. Accuracy, Labor-Time and Patient-Reported Outcomes with Partially versus Fully Digital Workflow for Flapless Guided Dental Implants Insertion—A Randomized Clinical Trial with One-Year Follow-Up. *Journal of Clinical Medicine,* 10**,** 1102.

DANIILIDIS, K. 1999. Hand-eye calibration using dual quaternions. *The International Journal of Robotics Research,* 18**,** 286-298.

DAVÓ, R. & DAVID, L. 2021. Quad Zygoma Protocol. *Atlas Oral Maxillofac Surg Clin North Am,* 29**,** 243-251.

DAVÓ, R., FAN, S., WANG, F. & WU, Y. 2023. Long-term survival and complications of Quad Zygoma Protocol with Anatomy-Guided Approach in severely atrophic maxilla: A retrospective follow-up analysis of up to 17 years. *Clin Implant Dent Relat Res,* 26**,** 343-355.

DEEB, J. G., KANDUTI, D., SKRJANC, L., CARRICO, C. K. & DEEB, G. 2022. Comparison of Accuracy and Time for Four Implant Placement Techniques Supporting Fixed-Partial Denture. *J Oral Implantol,* 48**,** 562-572.

DELONG, M. R., GANDOLFI, B. M., BARR, M. L., DATTA, N., WILLSON, T. D. & JARRAHY, R. 2019. Intraoperative image-guided navigation in craniofacial surgery: review and grading of the current literature. *Journal of Craniofacial Surgery,* 30**,** 465-472.

DEMIAN, N., PEARL, C., WOERNLEY, T. C., WILSON, J. & SEAMAN, J. 2019. Surgical navigation for oral and maxillofacial surgery. *Oral and Maxillofacial Surgery Clinics,* 31**,** 531-538.

DENG, H., BIAN, H., LI, C. & LI, Y. 2023a. Autonomous dental robotic surgery for zygomatic implants: A two-stage technique. *J Prosthet Dent,* S0022-3913**,** 00408-0.

DENG, H., BIAN, H., LIANG, Y., CAO, J., SUN, Y. & LI, Y. 2023b. Semi-autonomous two-stage dental robotic technique for zygomatic implants: An in vitro study. *J Dent,* 138**,** 104687.

DENG, H., WANG, J., LIU, L. & LI, Y. 2023c. Feasibility and accuracy of a task-autonomous robot for zygomatic implant placement. *J Prosthet Dent,* S0022-3913**,** 00710-2.

DING, Y., ZHENG, Y., CHEN, R., CAO, R., CHEN, J., WANG, L. & YANG, F. 2023. Accuracy of a novel semi-autonomous robotic-assisted surgery system for single implant placement: A case series. *Journal of Dentistry,* 139**,** 104766.

DU, C., WANG, L., YAN, J., LI, G., WU, Y., ZHAO, G., CUI, D., JIN, W. & YIN, S. 2024. The Association Between Trajectory-Skull Angle and Accuracy of Stereoelectroencephalography Electrode Implantation in Drug-Resistant Epilepsy. *World Neurosurg,* 184**,** e408-e416.

DU, Y., WANGRAO, K., LIU, L., LIU, L. & YAO, Y. 2019. Quantification of image artifacts from navigation markers in dynamic guided implant surgery and the effect on registration performance in different clinical scenarios. *Int J Oral Maxillofac Implants,* 34**,** 726–736.

DUARTE, L. R., FILHO, H. N., FRANCISCHONE, C. E., PEREDO, L. G. & BRÅNEMARK, P. I. 2007. The establishment of a protocol for the total rehabilitation of atrophic maxillae employing four zygomatic fixtures in an immediate loading system – a 30-month clinical and radiographic follow-up. *Clin Implant Dent Relat Res,* 9**,** 186-196.

EBELING, M., SCHEURER, M., SAKKAS, A., WILDE, F. & SCHRAMM, A. 2023. First-Hand Experience and Result with New Robot-Assisted Laser LeFort-I Osteotomy in Orthognathic Surgery: A Case Report. *J Pers Med,* 13**,** 287.

EDELMANN, C., WETZEL, M., KNIPPER, A., LUTHARDT, R. G. & SCHNUTENHAUS, S. 2021. Accuracy of Computer-Assisted Dynamic Navigation in Implant Placement with a Fully Digital Approach: A Prospective Clinical Trial. *Journal of Clinical Medicine,* 10**,** 1808.

EGGERT, D. W., LORUSSO, A. & FISHER, R. B. 1997. Estimating 3-D rigid body transformations: a comparison of four major algorithms. *Machine Vision and Applications,* 9**,** 272-290.

EL KHOLY, K., JANNER, S. F. M., SCHIMMEL, M. & BUSER, D. 2019. The influence of guided sleeve height, drilling distance, and drilling key length on the accuracy of static Computer-Assisted Implant Surgery. *Clin Implant Dent Relat Res,* 21**,** 101-107.

ENGKAWONG, S., MATTHEOS, N., PISARNTURAKIT, P. P., PIMKHAOKHAM, A. & SUBBALEKHA, K. 2021. Comparing patient-reported outcomes and experiences among static, dynamic computer-aided, and conventional freehand dental implant placement: A randomized clinical trial. *Clin Implant Dent Relat Res,* 23**,** 660-670.

EWERS, R., SCHICHO, K., UNDT, G., WANSCHITZ, F., TRUPPE, M., SEEMANN, R. & WAGNER, A. 2005. Basic research and 12 years of clinical experience in computer-assisted navigation technology: a review. *International journal of oral and maxillofacial surgery,* 34**,** 1-8.

FAN, S., HUNG, K., BORNSTEIN, M. M., HUANG, W., WANG, F. & WU, Y. 2019. The effect of the configurations of fiducial markers on accuracy of surgical navigation in zygomatic implant placement: An in vitro study. *Int J Oral Maxillofac Implants,* 34**,** 85–90.

FAN, S., SÁENZ-RAVELLO, G., DIAZ, L., WU, Y., DAVÓ, R., WANG, F., MAGIC, M., AL-NAWAS, B. & KÄMMERER, P. W. 2023. The Accuracy of Zygomatic Implant Placement Assisted by Dynamic Computer-Aided Surgery: A Systematic Review and Meta-Analysis. *J Clin Med,* 12**,** 5418.

FAN, X., FENG, Y., TAO, B., SHEN, Y., WU, Y. & CHEN, X. 2024. A hybrid robotic system for zygomatic implant placement based on mixed reality navigation. *Comput Methods Programs Biomed,* 249**,** 108156.

FITZPATRICK, J. M., WEST, J. B. & MAURER, C. R., JR. 1998. Predicting error in rigid-body point-based registration. *IEEE Trans Med Imaging,* 17**,** 694-702.

FORTES, J. H., DE OLIVEIRA-SANTOS, C., MATSUMOTO, W., DA MOTTA, R. J. G. & TIRAPELLI, C. 2019. Influence of 2D vs 3D imaging and professional experience on dental implant treatment planning. *Clinical oral investigations,* 23**,** 929-936.

GALLAGHER, E. J. 1990. Accuracy versus precision. *J Emerg Med,* 8**,** 641-642.

GALLO, F., ZINGARI, F., BOLZONI, A., BARONE, S. & GIUDICE, A. 2023. Accuracy of Zygomatic Implant Placement Using a Full Digital Planning and Custom-Made Bone-Supported Guide: A Retrospective Observational Cohort Study. *Dent J (Basel),* 11**,** 123.

GANTA, G. K., MOSCA, R. C., VARSANI, R., MURTHY, V. R., CHERUVU, K., LU, M. & ARANY, P. R. 2023. Automation in Dentistry with Mechanical Drills and Lasers for Implant Osteotomy: A Narrative-Scoping Review. *Dent J (Basel),* 12**,** 8.

GAO, Y., QIN, C., TAO, B., HU, J., WU, Y. & CHEN, X. 2021. An electromagnetic tracking implantation navigation system in dentistry with virtual calibration. *Int J Med Robot,* 17**,** e2215.

GARGALLO-ALBIOL, J., BAROOTCHI, S., SALOMÓ-COLL, O. & WANG, H.-L. 2019. Advantages and disadvantages of implant navigation surgery. A systematic review. *Annals of Anatomy-Anatomischer Anzeiger,* 225**,** 1-10.

GENTLE, J. E. 2024. *Matrix Algebra: Theory, Computations and Applications in Statistics,* Springer International Publishing.

GÖÇMEN, G., BAYRAKÇıOĞLU, A. & BAYRAM, F. 2023. Effect of the level of alveolar atrophy on implant placement accuracy in guided surgery for full-arch restorations supported by four implants: an in vitro study. *Head Face Med,* 19**,** 40.

GOLOB DEEB, J., BENCHARIT, S., CARRICO, C. K., LUKIC, M., HAWKINS, D., RENER-SITAR, K. & DEEB, G. R. 2019. Exploring training dental implant placement using computer-guided implant navigation system for predoctoral students: A pilot study. *European Journal of Dental Education,* 23**,** 415-423.

GONZÁLEZ-RUEDA, J. R., GALPARSORO-CATALÁN, A., DE PAZ-HERMOSO, V. M., RIAD-DEGLOW, E., ZUBIZARRETA-MACHO, Á., PATO-MOURELO, J., HERNÁNDEZ-MONTERO, S. & MONTERO-MARTÍN, J. 2023. Accuracy of zygomatic dental implant placement using computer-aided

static and dynamic navigation systems compared with a mixed reality appliance. An in vitro study. *J Clin Exp Dent,* 15**,** e1035-e1044.

GONZÁLEZ RUEDA, J. R., GALPARSORO CATALÁN, A., DE PAZ HERMOSO, V. M., RIAD DEGLOW, E., ZUBIZARRETA-MACHO, Á., PATO MOURELO, J., MONTERO MARTÍN, J. & HERNÁNDEZ MONTERO, S. 2023. Accuracy of computer-aided static and dynamic navigation systems in the placement of zygomatic dental implants. *BMC Oral Health,* 23**,** 150.

GRECCHI, F., STEFANELLI, L. V., GRIVETTO, F., GRECCHI, E., SIEV, R., MAZOR, Z., DEL FABBRO, M., PRANNO, N., FRANCHINA, A. & DI LUCIA, V. 2021. A Novel Guided Zygomatic and Pterygoid Implant Surgery System: A Human Cadaver Study on Accuracy. *International Journal of Environmental Research and Public Health,* 18**,** 6142.

GUO, H., JIANG, X. & LIN, Y. 2024. Comparison of robotic system and dynamic navigation for zygomatic implant placement: An in vitro study. *J Dent,* 150**,** 105329.

HAMILTON, A., SINGH, A., FRIEDLAND, B., JAMJOOM, F. Z., GRISETO, N. & GALLUCCI, G. O. 2022. The impact of cone beam computer tomography field of view on the precision of digital intra-oral scan registration for static computer-assisted implant surgery: A CBCT analysis. *Clin Oral Implants Res,* 33**,** 1273-1281.

HE, Y., ZHANG, Y., YU, G. Y., GUO, C. B., SHEN, G. F., PENG, X., LIU, X. J., WANG, J., ZHANG, W. B. & LIU, Y. P. 2020. Expert Consensus on Navigation-guided Unilateral Delayed Zygomatic Fracture Reconstruction Techniques. *Chin J Dent Res,* 23**,** 45-50.

HERNÁNDEZ-ALFARO, F., BERTOS-QUÍLEZ, J., VALLS-ONTAÑÓN, A., PATERNOSTRO-BETANCOURT, D., PINDAROS-GEORGIOS, F. & RAGUCCI, G. M. 2023. Three-Dimensional Evaluation of the Accuracy of Zygomatic Implant Placement Through an In-House Fully Guided Approach. *Int J Oral Maxillofac Implants,* 38**,** 747-756.

HTAY, P. E. E., LEESUNGBOK, R., LEE, S. W., JEE, Y. J., KANG, K. L. & HONG, S. O. 2023. Reliability of a chairside CAD-CAM surgical guide for dental implant surgery on the anterior maxilla: An in vitro study. *J Adv Prosthodont,* 15**,** 259-270.

HU, K. 2020. Become Competent within One Day in Generating Boxplots and Violin Plots for a Novice without Prior R Experience. *Methods Protoc,* 3**,** 64.

HUANG, L., LIU, L., YANG, S., KHADKA, P. & ZHANG, S. 2023. Evaluation of the accuracy of implant placement by using implant positional guide versus freehand: a prospective clinical study. *Int J Implant Dent,* 9**,** 45.

HUNG, K., HUANG, W., WANG, F. & WU, Y. 2016. Real-Time Surgical Navigation System for the Placement of Zygomatic Implants with Severe Bone Deficiency. *Int J Oral Maxillofac Implants,* 31**,** 1444-1449.

HUNG, K. F., WANG, F., WANG, H. W., ZHOU, W. J., HUANG, W. & WU, Y. Q. 2017. Accuracy of a real-time surgical navigation system for the placement of quad zygomatic implants in the severe atrophic maxilla: A pilot clinical study. *Clin Implant Dent Relat Res,* 19**,** 458-465.

JAYANETTI, J., SHAH, K., CHAO, D. & DRAGO, C. 2021. Double sleeve guided placement of quadruple zygomatic implants for rehabilitation of a patient with ectodermal dysplasia: A clinical report. *J Prosthet Dent,* 129**,** 824-830.

JIA, S., WANG, G., ZHAO, Y. & WANG, X. 2023. Accuracy of an autonomous dental implant robotic system versus static guide-assisted implant surgery: A retrospective clinical study. *J Prosthet Dent,* S0022-3913**,** 00284-6.

JORBA-GARCÍA, A., BARA-CASAUS, J. J., CAMPS-FONT, O., SÁNCHEZ-GARCÉS, M., FIGUEIREDO, R. & VALMASEDA-CASTELLÓN, E. 2023. Accuracy of dental implant placement with or without the use of a dynamic navigation assisted system: A randomized clinical trial. *Clin Oral Implants Res,* 34**,** 438-449.

JORBA-GARCÍA, A., FIGUEIREDO, R., GONZÁLEZ-BARNADAS, A., CAMPS-FONT, O. & VALMASEDA-CASTELLÓN, E. 2019. Accuracy and the role of experience in dynamic computer guided dental implant surgery: An in-vitro study. *Medicina oral, patologia oral y cirugia bucal,* 24**,** e76-e83.

JORBA-GARCÍA, A., GONZÁLEZ-BARNADAS, A., CAMPS-FONT, O., FIGUEIREDO, R. & VALMASEDA-CASTELLÓN, E. 2021. Accuracy assessment of dynamic computer-aided implant placement: a systematic review and meta-analysis. *Clin Oral Investig,* 25**,** 2479-2494.

KAEWSIRI, D., PANMEKIATE, S., SUBBALEKHA, K., MATTHEOS, N. & PIMKHAOKHAM, A. 2019. The accuracy of static vs. dynamic computer-assisted implant surgery in single tooth space: A randomized controlled trial. *Clinical oral implants research,* 30**,** 505-514.

KALAIVANI, G., BALAJI, V. R., MANIKANDAN, D. & ROHINI, G. 2020. Expectation and reality of guided implant surgery protocol using computer-assisted static and dynamic navigation system at present scenario: Evidence-based literature review. *Journal of Indian Society of Periodontology,* 24**,** 398-408.

KÄMMERER, P. W., FAN, S., APARICIO, C., BEDROSSIAN, E., DAVÓ, R., MORTON, D., RAGHOEBAR, G. M., ZARRINE, S. & AL-NAWAS, B. 2023. Evaluation of surgical techniques in survival rate and complications of zygomatic implants for the rehabilitation of the atrophic edentulous maxilla: a systematic review. *Int J Implant Dent,* 9**,** 11.

KHAOHOEN, A., POWCHAROEN, W., SORNSUWAN, T., CHAIJAREENONT, P., RUNGSIYAKULL, C. & RUNGSIYAKULL, P. 2024. Accuracy of implant placement with computer-aided static, dynamic, and robot-assisted surgery: a systematic review and meta-analysis of clinical trials. *BMC Oral Health,* 24**,** 359.

KIM, S. G., LEE, W. J., LEE, S. S., HEO, M. S., HUH, K. H., CHOI, S. C., KIM, T. I. & YI, W. J. 2015. An advanced navigational surgery system for dental implants completed in a single visit: an in vitro study. *J Craniomaxillofac Surg,* 43**,** 117-125.

KLASS, D., PRICE, A., DIBATTISTA, M., DIBART, S. & KERNITSKY, J. 2023. Optical accuracy assessment of robotically assisted dental implant surgery for partially edentulous patients: a single arm clinical trial. *Int J Oral Maxillofac Implants,* 39**,** 625-631.

KOO, T. K. & LI, M. Y. 2016. A Guideline of Selecting and Reporting Intraclass Correlation Coefficients for Reliability Research. *J Chiropr Med,* 15**,** 155-163.

KOVALEVSKY, J., MUELLER, I. & KOLACZEK, B. 1989. *Reference Frames. Astrophysics and Space Science Library*, Springer Netherlands.

KUNZENDORF, B., NAUJOKAT, H. & WILTFANG, J. 2021. Indications for 3-D diagnostics and navigation in dental implantology with the focus on radiation exposure: a systematic review. *Int J Implant Dent,* 7**,** 52.

LAN, K., TAO, B., WANG, F. & WU, Y. 2022. Accuracy evaluation of 3D-printed noninvasive adhesive marker for dynamic navigation implant surgery in a maxillary edentulous model: An in vitro study. *Med Eng Phys,* 103**,** 103783.

LEDDEROSE, G. J., HAGEDORN, H., SPIEGL, K., LEUNIG, A. & STELTER, K. 2012. Image guided surgery of the lateral skull base: testing a new dental splint registration device. *Comput Aided Surg,* 17**,** 13-20.

LENG, A., ZENG, B., CHEN, Y., TU, P., TAO, B. & CHEN, X. 2024. Development of a virtual reality-based zygomatic implant surgery training system with global collision detection and optimized finite element method model. *Comput Methods Programs Biomed,* 243**,** 107940.

LI, C., WANG, M., DENG, H., LI, S., FANG, X., LIANG, Y., MA, X., ZHANG, Y. & LI, Y. 2023a. Autonomous robotic surgery for zygomatic implant placement and immediately loaded implant-supported full-arch prosthesis: a preliminary research. *Int J Implant Dent,* 9**,** 12.

LI, P., CHEN, J., LI, A., LUO, K., XU, S. & YANG, S. 2023b. Accuracy of autonomous robotic surgery for dental implant placement in fully edentulous patients: A retrospective case series study. *Clin Oral Implants Res,* 34**,** 1428-1437.

LI, Y., HU, J., TAO, B., YU, D., SHEN, Y., FAN, S., WU, Y. & CHEN, X. 2020. Automatic robot-world calibration in an optical-navigated surgical robot system and its application for oral implant placement. *International Journal of Computer Assisted Radiology and Surgery,* 15**,** 1685-1692.

LIN, J., LIN, Z. & ZHENG, Z. 2021. Case report: Fabrication of a dental implant guide based on tetrahedron positioning technology. *BMC Oral Health,* 21**,** 335.

LIN, L., GAO, Y., CHAI, G., XU, H. & XIE, L. 2020. Electromagnetic Navigation in Craniofacial Surgery Based on Automatic Registration of Dental Splints. *Journal of Craniofacial Surgery,* 31**,** 393-396.

LIU, C., LIU, X., WANG, X., LIU, Y., BAI, Y., BAI, S. & ZHAO, Y. 2024. Endodontic Microsurgery With an Autonomous Robotic System: A Clinical Report. *J Endod,* 50**,** 859-864.

LIU, Q., LIU, Y., CHEN, D., WU, X., HUANG, R., LIU, R., CHEN, Z. & CHEN, Z. 2022. Placement accuracy and primary stability of implants in the esthetic zone using dynamic and static computer-assisted navigation: A retrospective case-control study. *J Prosthet Dent,* 131**,** 427-435.

LO RUSSO, L., GUIDA, L., MARIANI, P., RONSIVALLE, V., GALLO, C., CICCIÙ, M. & LAINO, L. 2023. Effect of Fabrication Technology on the Accuracy of Surgical Guides for Dental-Implant Surgery. *Bioengineering (Basel),* 10**,** 875.

LOPES, A., DE ARAÚJO NOBRE, M. & SANTOS, D. 2020. The Workflow of a New Dynamic Navigation System for the Insertion of Dental Implants in the Rehabilitation of Edentulous Jaws: Report of Two Cases. *Journal of Clinical Medicine,* 9**,** 421.

MA, F., SUN, F., WEI, T. & MA, Y. 2022. Comparison of the accuracy of two different dynamic navigation system registration methods for dental implant placement: A retrospective study. *Clin Implant Dent Relat Res,* 24**,** 352-360.

MA, Q., KOBAYASHI, E., SUENAGA, H., HARA, K., WANG, J., NAKAGAWA, K., SAKUMA, I. & MASAMUNE, K. 2020. Autonomous Surgical Robot With Camera-Based Markerless Navigation for Oral and Maxillofacial Surgery. *IEEE/ASME Transactions on Mechatronics,* 25**,** 1084-1094.

MAI, H. N., DAM, V. V. & LEE, D. H. 2023. Accuracy of Augmented Reality-Assisted Navigation in Dental Implant Surgery: Systematic Review and Meta-analysis. *J Med Internet Res,* 25**,** e42040.

MAMPILLY, M., KURUVILLA, L., TASH NIYAZI, A. A., SHYAM, A., THOMAS, P. A., ALI, A. S. & PULLISHERY, F. 2023. Accuracy and Self-Confidence Level of Freehand Drilling and Dynamic Navigation System of Dental Implants: An In Vitro Study. *Cureus,* 15**,** e49618.

MANFREDINI, M., POLI, P. P., MAIORANA, C., SALINA, F. E., TANDURELLA, M. & BERETTA, M. 2023. Computer Aided Full Arch Restoration by Means of One-Piece Implants and Stackable Guide: A Technical Note. *Dent J (Basel),* 11**,** 256.

MAO, Y., LI, X., WANG, Q. & ZHANG, J. 2023. Application of titanium 3D-printed double-sleeve guide for zygomatic implants: A technique report. *J Prosthodont,* 32**,** 752-756.

MARQUES-GUASCH, J., BOFARULL-BALLÚS, A., GIRALT-HERNANDO, M., HERNÁNDEZ-ALFARO, F. & GARGALLO-ALBIOL, J. 2023. Dynamic Implant Surgery-An Accurate Alternative to Stereolithographic Guides-Systematic Review and Meta-Analysis. *Dent J (Basel),* 11**,** 150.

MARWAN, H., SAWATARI, Y. & PELEG, M. 2020. Zygomaticomaxillary Complex Anatomy. *Management of Orbito-zygomaticomaxillary Fractures*. Cham: Springer International Publishing.

MAURER, C. R., JR., FITZPATRICK, J. M., WANG, M. Y., GALLOWAY, R. L., JR., MACIUNAS, R. J. & ALLEN, G. S. 1997. Registration of head volume images using implantable fiducial markers. *IEEE Trans Med Imaging,* 16**,** 447-462.

MILNER, M. N., ANANIA, E. C., CANDELARIA-OQUENDO, K., RICE, S., WINTER, S. R. & RAGBIR, N. K. 2020. Patient perceptions of new robotic technologies in clinical restorative dentistry. *Journal of medical systems,* 44**,** 1-10.

MIN, Z., REN, H. & MENG, M. Q.-H. Ttre: A new type of error to evaluate the accuracy of a paired-point rigid registration. 2017 IEEE/RSJ International Conference on Intelligent Robots and Systems (IROS), 2017. IEEE, 953-960.

MISCH, C. E. 2014. *Dental Implant Prosthetics*, Elsevier Mosby.

MOHAGHEGHI, S., AHMADIAN, A. & YAGHOOBEE, S. 2014. Accuracy assessment of a marker-free method for registration of CT and stereo images applied in image-guided implantology: a phantom study. *J Craniomaxillofac Surg,* 42**,** 1977-1984.

MOLINERO-MOURELLE, P., BACA-GONZALEZ, L., GAO, B., SAEZ-ALCAIDE, L.-M., HELM, A. & LOPEZ-QUILES, J. 2016. Surgical complications in zygomatic implants: A systematic review. *Medicina oral, patologia oral y cirugia bucal,* 21**,** e751-e757.

MOZER, P. S. & GUENTSCH, A. 2024. An in vitro analysis of the accuracy of static and robot-assisted implant surgery. *Clin Oral Implants Res,* 35**,** 487-497.

NASAB, M. H. A. 2019. *Handbook of Robotic and Image-Guided Surgery*, Elsevier Science.

NEUGARTEN, J. M. 2024. Accuracy and Precision of Haptic Robotic-Guided Implant Surgery in a Large Consecutive Series. *Int J Oral Maxillofac Implants,* 39**,** 99-106.

NKENKE, E., HAHN, M., LELL, M., WILTFANG, J., SCHULTZE-MOSGAU, S., STECH, B., RADESPIEL-TRÖGER, M. & NEUKAM, F. W. 2003. Anatomic site evaluation of the zygomatic bone for dental implant placement. *Clin Oral Implants Res,* 14**,** 72-79.

OLIVETTO, M., BETTONI, J., TESTELIN, S. & LEFRANC, M. 2023. Zygomatic implant placement using a robot-assisted flapless protocol: proof of concept. *Int J Oral Maxillofac Surg,* 52**,** 710-715.

PAN, Y., TSOI, J. K., LAM, W. Y. & POW, E. H. 2021. Implant framework misfit: A systematic review on assessment methods and clinical complications. *Clinical Implant Dentistry and Related Research,* 23**,** 244-258.

PAREL, S. M., BRÅNEMARK, P. I., OHRNELL, L. O. & SVENSSON, B. 2001. Remote implant anchorage for the rehabilitation of maxillary defects. *J Prosthet Dent,* 86**,** 377-381.

PARK, F. C. & MARTIN, B. J. 1994. Robot sensor calibration: solving AX=XB on the Euclidean group. *IEEE Transactions on Robotics and Automation,* 10**,** 717-721.

PARK, J. H., HWANG, C. J., CHOI, Y. J., HOUSCHYAR, K. S., YU, J. H., BAE, S. Y. & CHA, J. Y. 2020. Registration of digital dental models and cone-beam computed tomography images using 3-dimensional planning software: Comparison of the accuracy according to scanning methods and software. *Am J Orthod Dentofacial Orthop,* 157**,** 843-851.

PARRA-TRESSERRA, A., MARQUÈS-GUASCH, J., ORTEGA-MARTÍNEZ, J., BASILIO-MONNÉ, J. & HERNÁNDEZ-ALFARO, F. 2021. Current state of dynamic surgery. A literature review. *Medicina Oral, Patologia Oral y Cirugia Bucal,* 26**,** e576-e581.

PELLEGRINO, G., BASILE, F., RELICS, D., FERRI, A., GRANDE, F., TARSITANO, A. & MARCHETTI, C. 2020a. Computer-Aided Rehabilitation Supported by Zygomatic Implants: A Cohort Study Comparing Atrophic with Oncologic Patients after Five Years of Follow-Up. *Journal of Clinical Medicine,* 9**,** 3254.

PELLEGRINO, G., BELLINI, P., CAVALLINI, P. F., FERRI, A., ZACCHINO, A., TARASCHI, V., MARCHETTI, C. & CONSOLO, U. 2020b. Dynamic Navigation in Dental Implantology: The Influence of Surgical Experience on Implant Placement Accuracy and Operating Time. An in Vitro Study. *International Journal of Environmental Research and Public Health,* 17**,** 2153.

PELLEGRINO, G., GRANDE, F., FERRI, A., PISI, P., GANDOLFI, M. G. & MARCHETTI, C. 2020c. Three-Dimensional Radiographic Evaluation of the Malar Bone Engagement Available for Ideal Zygomatic Implant Placement. *Methods Protoc,* 3**,** 52.

PELLEGRINO, G., TARASCHI, V., ANDREA, Z., FERRI, A. & MARCHETTI, C. 2019. Dynamic navigation: a prospective clinical trial to evaluate the accuracy of implant placement. *Int J Comput Dent,* 22**,** 139-147.

PELLEGRINO, G., TARASCHI, V., VERCELLOTTI, T., BEN-NISSAN, B. & MARCHETTI, C. 2017. Three-Dimensional Implant Positioning with a Piezosurgery Implant Site Preparation Technique and an Intraoral Surgical Navigation System: Case Report. *Int J Oral Maxillofac Implants,* 32**,** e163-e165.

PENNESTRI`, E., CAVACECE, M. & VITA, L. On the Computation of Degrees-of-Freedom: A Didactic Perspective. ASME 2005 International Design Engineering Technical Conferences and Computers and Information in Engineering Conference, 2005. ASME, 1733-1741.

PESUN, I. J. & GARDNER, F. M. 1995. Fabrication of a guide for radiographic evaluation and surgical placement of implants. *J Prosthet Dent,* 73**,** 548-552.

POLI, P. P., MANFREDINI, M., MAIORANA, C., SALINA, F. E. & BERETTA, M. 2023. Correlation between Accuracy in Computer-Guided Implantology and Peri-Implant Tissue Stability: A Prospective Clinical and Radiological Pilot Study. *J Clin Med,* 12**,** 5098.

POMARES-PUIG, C., SÁNCHEZ-GARCÉS, M. A. & JORBA-GARCÍA, A. 2023. Dynamic and static computer-assisted implant surgery for completely edentulous patients. A proof of a concept. *J Dent,* 130**,** 104443.

PRYOR MCINTOSH, L., STRAIT, D. S., LEDOGAR, J. A., SMITH, A. L., ROSS, C. F., WANG, Q., OPPERMAN, L. A. & DECHOW, P. C. 2016. Internal Bone Architecture in the Zygoma of Human and Pan. *Anat Rec (Hoboken),* 299**,** 1704-1717.

PYO, S.-W., LIM, Y.-J., KOO, K.-T. & LEE, J. 2019. Methods used to assess the 3D accuracy of dental implant positions in computer-guided implant placement: a review. *Journal of clinical medicine,* 8**,** 54.

QIN, C., CAO, Z., FAN, S., WU, Y., SUN, Y., POLITIS, C., WANG, C. & CHEN, X. 2019a. An oral and maxillofacial navigation system for implant placement with automatic identification of fiducial points. *International Journal of Computer Assisted Radiology and Surgery,* 14**,** 281-289.

QIN, C., RAN, X., WU, Y. & CHEN, X. 2019b. The development of non-contact user interface of a surgical navigation system based on multi-LSTM and a phantom experiment for zygomatic implant placement. *International journal of computer assisted radiology and surgery,* 14**,** 2147-2154.

RIGO, L., TOLARDO, J., GIAMMARINARO, E., COVANI, U. & CASO, G. 2021. Fully Guided Zygomatic Implant Surgery. *J Craniofac Surg,* 32**,** 2867-2872.

RUßIG, L. L. & SCHULZE, R. K. 2013. Effects of minute misregistrations of prefabricated markers for image-guided dental implant surgery: an analytical evaluation. *Clin Oral Implants Res,* 24**,** 1339-46.

SALAZAR RIOS, A. L., KESTERKE, M. J., PYLANT, G. D., 3RD, BARMAK, A. B., KONTOGIORGOS, E. D. & REVILLA-LEÓN, M. 2023. Effect of print orientation, storage conditions, and storage time on intaglio surface accuracy of implant surgical guides fabricated by using a stereolithography technology. *J Prosthet Dent,* S0022-3913**,** 00552-8.

SANKAR, H., SHALINI, M., RAJAGOPALAN, A., GUPTA, S., KUMAR, A. & SHOUKET, R. 2025. Dental implant placement accuracy with robotic surgery compared to free-hand, static and dynamic computer assisted techniques: Systematic review and meta-analysis. *J Oral Biol Craniofac Res,* 15**,** 69-76.

SANZ, M., NOGUEROL, B., SANZ-SANCHEZ, I., HAMMERLE, C. H., SCHLIEPHAKE, H., RENOUARD, F., SICILIA, A., COMMITTEE, S., CORDARO, L. & JUNG, R. 2019. European Association for Osseointegration Delphi study on the trends in Implant Dentistry in Europe for the year 2030. *Clinical oral implants research,* 30**,** 476-486.

SCHERER, U., STOETZER, M., RUECKER, M., GELLRICH, N.-C. & VON SEE, C. 2015. Template-guided vs. non-guided drilling in site preparation of dental implants. *Clinical oral investigations,* 19**,** 1339-1346.

SCHEYER, E. T., MANDELARIS, G. A., MCGUIRE, M. K., ALTAKRITI, M. A. & STEFANELLI, L. V. 2020. Implant Placement Under Dynamic Navigation Using Trace Registration: Case Presentations. *Int J Periodontics Restorative Dent,* 40**,** e241-e248.

SCHIROLI, G., ANGIERO, F., SILVESTRINI-BIAVATI, A. & BENEDICENTI, S. 2011. Zygomatic implant placement with flapless computer-guided surgery: a proposed clinical protocol. *J Oral Maxillofac Surg,* 69**,** 2979-2989.

SCHIROLI, G., ANGIERO, F., ZANGERL, A., BENEDICENTI, S., FERRANTE, F. & WIDMANN, G. 2016. Accuracy of a flapless protocol for computer-guided zygomatic implant placement in human cadavers: expectations and reality. *The International Journal of Medical Robotics and Computer Assisted Surgery,* 12**,** 102-108.

SCHNEIDER, D., SAX, C., SANCHO-PUCHADES, M., HÄMMERLE, C. & JUNG, R. E. 2021. Accuracy of computer-assisted, template guided implant placement compared to conventional implant placement by hand - an in vitro study. *Clin Oral Implants Res,* 32**,** 1052-1060.

SHAH, M., EASTMAN, R. D. & HONG, T. An overview of robot-sensor calibration methods for evaluation of perception systems. Proceedings of the Workshop on Performance Metrics for Intelligent Systems, 2012 College Park, Maryland. Association for Computing Machinery, 15-20.

SHARMA, S., SUN, Y., BONYUN, J., KHADEM, M., AMADIO, J., ESKANDARI, A. H. & ALAMBEIGI, F. 2024. A Biomechanics-Aware Robot-Assisted Steerable Drilling Framework for Minimally Invasive Spinal Fixation Procedures. *IEEE Trans Biomed Eng,* 71**,** 1810-1819.

SHARMA, S., TAN, E., TRAN, B., SIOW, H. Y., TAFESSE, E., THONG, Y. H. J., TAN, R. J. M., SON, J., TODARO, L., TEO, J. & ABDUO, J. 2023. Effect of pilot-guided implant placement concept on the accuracy of osteotomy preparation and implant placement. *J Oral Sci,* 66**,** 20-25.

SHEN, Y., TAO, B., SUN, Y., HUANG, W., WANG, F. & WU, Y. 2023. The Effect of Fiducial Marker Number and Configuration on Registration Error in Dynamic Implant Surgery. *Int J Oral Maxillofac Implants,* 38**,** 727-732.

SHENGCHI, F., ZHENGGANG, C., CHUNXIA, Q., FENG, W., WEI, H., XIAOJUN, C. & YIQUN, W. 2018. The accuracy of surgical automatic robotic assisted implants placement in edentulous maxilla–an in vitro study. *Clinical Oral Implants Research,* 29**,** 283-283.

SHIMIZU, H., MINO, T., KUROSAKI, Y., ARAKAWA, H., TOKUMOTO, K., KIMURA-ONO, A., MAEKAWA, K. & KUBOKI, T. 2023. Accuracy of a novel modified single computed tomography scanning method for assisting dental implant placement: a retrospective observational study. *Int J Implant Dent,* 9**,** 42.

SHU, Q., CHEN, D., WANG, X., LIU, Q., GE, Y. & SU, Y. 2024. Accuracy of flapless surgery using an autonomous robotic system in full-arch immediate implant restoration: A case series. *J Dent,* 145**,** 105017.

SIN, M., CHO, J. H., LEE, H., KIM, K., WOO, H. S. & PARK, J. M. 2023. Development of a Real-Time 6-DOF Motion-Tracking System for Robotic Computer-Assisted Implant Surgery. *Sensors (Basel),* 23**,** 2450.

SITTIKORNPAIBOON, P., ARUNJAROENSUK, S., KABOOSAYA, B., SUBBALEKHA, K., MATTHEOS, N. & PIMKHAOKHAM, A. 2021. Comparison of the accuracy of

implant placement using different drilling systems for static computer-assisted implant surgery: A simulation-based experimental study. *Clin Implant Dent Relat Res,* 23**,** 635-643.

SMITKARN, P., SUBBALEKHA, K., MATTHEOS, N. & PIMKHAOKHAM, A. 2019. The accuracy of single-tooth implants placed using fully digital-guided surgery and freehand implant surgery. *J Clin Periodontol,* 46**,** 949-957.

SNIJDERS, T., VAN GAALEN, S. M. & DE GAST, A. 2017. Precision and accuracy of imageless navigation versus freehand implantation of total hip arthroplasty: A systematic review and meta-analysis. *Int J Med Robot,* 13**,** e1843.

STEFANELLI, L. V., MANDELARIS, G. A., DEGROOT, B. S., GAMBARINI, G., DE ANGELIS, F. & DI CARLO, S. 2020a. Accuracy of a Novel Trace-Registration Method for Dynamic Navigation Surgery. *Int J Periodontics Restorative Dent,* 40**,** 427-435.

STEFANELLI, L. V., MANDELARIS, G. A., FRANCHINA, A., PRANNO, N., PAGLIARULO, M., CERA, F., MALTESE, F., ANGELIS, F. D. & CARLO, S. D. 2020b. Accuracy of Dynamic Navigation System Workflow for Implant Supported Full Arch Prosthesis: A Case Series. *International Journal of Environmental Research and Public Health,* 17**,** 5038.

SU, X., WANG, G., ZHAO, B. & WANG, X. 2024. Maxillary sinus floor elevation for implant placement assisted by an autonomous dental implant robotic system: A clinical report. *J Prosthet Dent,* S0022-3913**,** 00241-5.

SUKSOD, N., KUNAVISARUT, C. & KITISUBKANCHANA, J. 2020. Accuracy of computer-guided implantation in the placement of one-piece ceramic dental implants in the anterior region: A prospective clinical study. *PLoS One,* 15**,** e0237229.

SUN, M., YUE, C., STUHR, S., FU, X. & WANG, H. L. 2023. Autonomous Dental Implant Robotic System Utilization for Implant Placement and Transcrestal Sinus Elevation Using Osseodensification: A Case Report. *Int J Periodontics Restorative Dent***,** In Press.

SUN, W., LIU, J., ZHAO, Y. & ZHENG, G. 2022. A Novel Point Set Registration-Based Hand-Eye Calibration Method for Robot-Assisted Surgery. *Sensors (Basel),* 22**,** 8446.

SZAUER, G. 2017. *Game Physics Cookbook: Discover over 100 easy-to-follow recipes to help you implement efficient game physics and collision detection in your games*, Packt Publishing Ltd.

TAKÁCS, A., MARADA, G., TURZÓ, K., NAGY, Á., NÉMETH, O., MIJIRITSKY, E., KIVOVICS, M. & MÜHL, A. 2023. Does implant drill design influence the accuracy of dental implant placement using static computer-assisted implant surgery? An in vitro study. *BMC Oral Health,* 23**,** 575.

TALLARICO, M., KIM, Y. J., COCCHI, F., MARTINOLLI, M. & MELONI, S. M. 2019. Accuracy of newly developed sleeve-designed templates for insertion of dental implants: A prospective multicenters clinical trial. *Clin Implant Dent Relat Res,* 21**,** 108-113.

TANG, G., LIU, S., SUN, M., WANG, Y., ZHU, W., WANG, D., LI, X., WU, H., MEN, S., ZHANG, L., FENG, C., WANG, Y. & DING, Y. 2024. High-precision all-in-one dual robotic arm strategy in oral implant surgery. *BDJ Open,* 10**,** 43.

TAO, B., FAN, X., WANG, F., CHEN, X., SHEN, Y. & WU, Y. 2024. Comparison of the accuracy of dental implant placement using dynamic and augmented reality-based dynamic navigation: An in vitro study. *J Dent Sci,* 19**,** 196-202.

TAO, B., WANG, F., SHEN, Y., FAN, S., HUANG, W., WANG, Y. & WU, Y. 2020. Accuracy and clinical outcome of a real-time surgical navigation system for the placement of quad zygomatic implants. *Zhonghua kou qiang yi xue za zhi= Zhonghua kouqiang yixue zazhi= Chinese journal of stomatology,* 55**,** 845-850.

TESTORI, T., CLAUSER, T., RAPANI, A., ARTZI, Z., AVILA-ORTIZ, G., BAROOTCHI, S., BRESSAN, E., CHIAPASCO, M., CORDARO, L., DECKER, A., DE STAVOLA, L., DI STEFANO, D. A., FELICE, P., FONTANA, F., GRUSOVIN, M. G., JENSEN, O. T., LE, B. T., LOMBARDI, T., MISCH, C., PIKOS, M., PISTILLI, R., RONDA, M., SALEH, M. H., SCHWARZ-ARAD, D., SIMION, M., TASCHIERI, S., TOFFLER, M., TOZUM, T. F., VALENTINI, P., VINCI, R., WALLACE, S. S., WANG, H. L., WEN, S. C., YIN, S., ZUCCHELLI, G., ZUFFETTI, F. & STACCHI, C. 2024. Indications for implant-supported rehabilitation of the posterior atrophic maxilla: A multidisciplinary consensus among experts in the field utilising the modified Delphi method. *Int J Oral Implantol (Berl),* 17**,** 89-100.

THOMKOVÁ, B., MARCIÁN, P., BORÁK, L., JOUKAL, M. & WOLFF, J. 2023. Biomechanical performance of dental implants inserted in different mandible locations and at different angles: A finite element study. *J Prosthet Dent,* 131**,** 128.e1-128.e10.

TIAN, Y. N., LI, B. X., ZHANG, H. & JIN, L. 2023. [Development of dental robot implantation technology]. *Zhonghua Kou Qiang Yi Xue Za Zhi,* 58**,** 1300-1306.

TRUCCO, E. & VERRI, A. 1998. *Introductory techniques for 3-D computer vision*, Prentice Hall Englewood Cliffs.

UNIVERSALROBOTSA/S 2018. Universal Robots e-Series User Manual Version 5.0.2.

UNIVERSALROBOTSA/S. 2022. Robotic Arm. Available from: https://www.universal-robots.com/in/blog/robotic-arm/.

VAN STEENBERGHE, D., MALEVEZ, C., VAN CLEYNENBREUGEL, J., BOU SERHAL, C., DHOORE, E., SCHUTYSER, F., SUETENS, P. & JACOBS, R. 2003. Accuracy of drilling guides for transfer from three-dimensional CT-based planning to placement of zygoma implants in human cadavers. *Clin Oral Implants Res,* 14**,** 131-136.

VARGHESE, K. G., GANDHI, N., KURIAN, N., DANIEL, A. Y., DHAWAN, K., JOSEPH, M. & VARGHESE, M. G. 2021. Rehabilitation of the severely resorbed maxilla by using quad zygomatic implant-supported prostheses: a systematic review and meta-analysis. *J Prosthet Dent,* 130**,** 543-552.

VERCRUYSSEN, M., COX, C., COUCKE, W., NAERT, I., JACOBS, R. & QUIRYNEN, M. 2014. A randomized clinical trial comparing guided implant surgery (bone- or mucosa-supported) with mental navigation or the use of a pilot-drill template. *Journal of Clinical Periodontology,* 41**,** 717-723.

VINCI, R., MANACORDA, M., ABUNDO, R., LUCCHINA, A., SCARANO, A., CROCETTA, C., MUZIO, L. L., GHERLONE, E. & MASTRANGELO, F. 2020. Accuracy of Edentulous Computer-Aided Implant Surgery as Compared to Virtual Planning: A Retrospective Multicenter Study. *Journal of clinical medicine,* 9**,** 774.

VOSSELMAN, N., GLAS, H. H., DE VISSCHER, S., KRAEIMA, J., MEREMA, B. J., REINTSEMA, H., RAGHOEBAR, G. M. & WITJES, M. J. H. 2021. Immediate implant-retained prosthetic obturation after maxillectomy based on zygomatic implant placement by 3D-guided surgery: a cadaver study. *Int J Implant Dent,* 7**,** 54.

VRIELINCK, L., POLITIS, C., SCHEPERS, S., PAUWELS, M. & NAERT, I. 2003. Image-based planning and clinical validation of zygoma and pterygoid implant placement in patients with severe bone atrophy using customized drill

guides. Preliminary results from a prospective clinical follow-up study. *International journal of oral and maxillofacial surgery,* 32**,** 7-14.

WACHOL, K., MORAWIEC, T., SZURKO, A., BALDI, D., NOWAK-WACHOL, A., ŚMIESZEK-WILCZEWSKA, J. & MERTAS, A. 2023. Advantages of Dynamic Navigation in Prosthetic Implant Treatment in Terms of the Clinical Evaluation and Salivary Pro-Inflammatory Biomarkers: A Clinical Study. *Applied Sciences,* 13**,** 9866.

WADDE, K., KOKITKAR, S., VENKATAKRISHNAN, L., RANGANATH, S. & KHAIRE, S. 2024. Comparative Evaluation of Sinus Complication and Survival Rates of Quad Zygoma versus Bizygoma in Combination with two Regular Implants in Atrophic Maxilla: A Systematic Review and Meta-Analysis. *J Maxillofac Oral Surg,* 23**,** 710-718.

WALKER, M. W., SHAO, L. & VOLZ, R. A. 1991. Estimating 3-D location parameters using dual number quaternions. *CVGIP: image understanding,* 54**,** 358-367.

WANG, F., TAO, B., SHEN, Y., LI, C., HUANG, W., SUN, Y. & WU, Y. 2021a. A single-arm clinical trial investigating the feasibility of the zygomatic implant quad approach for Cawood and Howell Class 4 edentulous maxilla: An option for immediate loading. *Clin Implant Dent Relat Res,* 23**,** 800-808.

WANG, F., WANG, Q. & ZHANG, J. 2021b. Role of Dynamic Navigation Systems in Enhancing the Accuracy of Implant Placement: A Systematic Review and Meta-Analysis of Clinical Studies. *J Oral Maxillofac Surg,* 79**,** 2061-2070.

WANG, M., LIU, F., YU, T., ZHAN, Y., MA, F. & RAUSCH-FAN, X. 2024a. Accuracy of an autonomous dental implant robotic system in partial edentulism: A pilot clinical study. *Clin Oral Investig,* 28**,** 385.

WANG, Q. & DECHOW, P. C. 2016. Divided Zygomatic Bone in Primates With Implications of Skull Morphology and Biomechanics. *Anat Rec (Hoboken),* 299**,** 1801-1829.

WANG, W., LI, X., YAO, C. & ZHAO, B. 2024b. Robotic dental implant placement workflow for edentulous jaws. *J Prosthet Dent,* S0022-3913**,** 00350-0.

WANG, W., XU, H., MEI, D., ZHOU, C., LI, X., HAN, Z., ZHOU, X., LI, X. & ZHAO, B. 2023a. Accuracy of the Yakebot dental implant robotic system versus fully guided static computer-assisted implant surgery template in edentulous jaw implantation: A preliminary clinical study. *Clin Implant Dent Relat Res,* 26**,** 309-316.

WANG, W., ZHUANG, M., LI, S., SHEN, Y., LAN, R., WU, Y. & WANG, F. 2022a. Exploring training dental implant placement using static or dynamic devices among dental students. *Eur J Dent Educ,* 27**,** 438-448.

WANG, W., ZHUANG, M., TAO, B., WANG, F. & WU, Y. 2024c. Learning curve of dynamic navigation-assisted zygomatic implant surgery: An in vitro study. *J Prosthet Dent,* 132**,** 178.e1-178.e12.

WANG, X. Y., LIU, L., GUAN, M. S., LIU, Q., ZHAO, T. & LI, H. B. 2022b. The accuracy and learning curves of active and passive dynamic navigation-guided dental implant surgery: An in vitro study. *J Dent***,** 104240.

WANG, Y., WANG, W., CAI, Y., ZHAO, Q. & WANG, Y. 2023b. Preliminary study of a new macro-micro robot system for dental implant surgery: Design, development and control. *Int J Med Robot***,** e2614.

WANG, Y., WANG, W., CAI, Y., ZHAO, Q. & WANG, Y. 2023c. Preoperative Planning Framework for Robot-Assisted Dental Implant Surgery: Finite-Parameter Surrogate Model and Optimization of Instrument Placement. *Bioengineering (Basel),* 10**,** 952.

WANG, Y., YU, S., WANG, Y., FENG, Y., YAN, Q. & ZHANG, Y. 2024d. Effect of implant shape and length on the accuracy of robot-assisted immediate implant surgery: An in vitro study. *Clin Oral Implants Res,* 35**,** 350-357.

WATZINGER, F., BIRKFELLNER, W., WANSCHITZ, F., ZIYA, F., WAGNER, A., KREMSER, J., KAINBERGER, F., HUBER, K., BERGMANN, H. & EWERS, R. 2001. Placement of endosteal implants in the zygoma after maxillectomy: a Cadaver study using surgical navigation. *Plast Reconstr Surg,* 107**,** 659-667.

WEI, S. M., ZHU, Y., WEI, J. X., ZHANG, C. N., SHI, J. Y. & LAI, H. C. 2021. Accuracy of dynamic navigation in implant surgery: A systematic review and meta-analysis. *Clin Oral Implants Res,* 32**,** 383-393.

WEI, T., MA, F., SUN, F. & MA, Y. 2023. Assessment of the Accuracy of Two Different Dynamic Navigation System Registration Methods for Dental Implant Placement in the Posterior Area: An In Vitro Study. *J Pers Med,* 13**,** 139.

WEST, J. B., FITZPATRICK, J. M., TOMS, S. A., MAURER, C. R., JR. & MACIUNAS, R. J. 2001. Fiducial point placement and the accuracy of point-based, rigid body registration. *Neurosurgery,* 48**,** 810-817.

WIDMANN, G., STOFFNER, R. & BALE, R. 2009. Errors and error management in image-guided craniomaxillofacial surgery. *Oral Surg Oral Med Oral Pathol Oral Radiol Endod,* 107**,** 701-715.

WIDMANN, G., STOFFNER, R., SCHULLIAN, P., WIDMANN, R., KEILER, M., ZANGERL, A., PUELACHER, W. & BALE, R. J. 2010. Comparison of the accuracy of invasive and noninvasive registration methods for image-guided oral implant surgery. *Int J Oral Maxillofac Implants,* 25**,** 491-498.

WILES, A. D., THOMPSON, D. G. & FRANTZ, D. D. Accuracy assessment and interpretation for optical tracking systems. Medical Imaging 2004: Visualization, Image-Guided Procedures, and Display, 2004. SPIE, 421-432.

WU, B. Z., MA, F. F., YAN, X. Y. & SUN, F. 2023a. Accuracy of different registration areas using active and passive dynamic navigation systems in dental implant surgery: An in vitro study. *Clin Oral Implants Res,* 35**,** 888-897.

WU, B. Z. & SUN, F. 2022. A registration-and-fixation approach with handpiece adjustment for dynamic navigation in dental implant surgery. *Heliyon,* 8**,** e10565.

WU, B. Z. & SUN, F. 2024. The impacts of registration-and-fixation device positioning on the performance of implant placement assisted by dynamic computer-aided surgery: A randomized controlled trial. *Clin Oral Implants Res,* 35**,** 386-395.

WU, B. Z., XUE, F., MA, Y. & SUN, F. 2023b. Accuracy of automatic and manual dynamic navigation registration techniques for dental implant surgery in posterior sites missing a single tooth: A retrospective clinical analysis. *Clin Oral Implants Res,* 34**,** 221-232.

WU, X. Y., SHI, J. Y., QIAO, S. C., TONETTI, M. S. & LAI, H. C. 2024. Accuracy of robotic surgery for dental implant placement: A systematic review and meta-analysis. *Clin Oral Implants Res,* 35**,** 598-608.

WU, Y., WANG, F., FAN, S. & CHOW, J. K.-F. 2019a. Robotics in dental implantology. *Oral and Maxillofacial Surgery Clinics,* 31**,** 513-518.

WU, Y., WANG, F., HUANG, W. & FAN, S. 2019b. Real-Time Navigation in Zygomatic Implant Placement: Workflow. *Oral and Maxillofacial Surgery Clinics,* 31**,** 357-367.

X-NAVTECHNOLOGIESLLC 2020. X-Guide Surgical Navigation System User Manual. Rev J. USA: X-Nav Technologies, LLC.

XI, S., HU, J., YUE, G. & WANG, S. 2024. Accuracy of an autonomous dental implant robotic system in placing tilted implants for edentulous arches. *J Prosthet Dent,* S0022-3913**,** 00521-3.

XIAOJUN, C., MING, Y., YANPING, L., YIQUN, W. & CHENGTAO, W. 2009. Image guided oral implantology and its application in the placement of zygoma implants. *Comput Methods Programs Biomed,* 93**,** 162-173.

XING GAO, B., IGLESIAS-VELÁZQUEZ, O., F, G. F. T., RODRÍGUEZ GONZÁLEZ CORTES, A., I, F. T., ORTEGA ARANEGUI, R., LÓPEZ-PINTOR, R. M., LÓPEZ-QUILES, J. & TORRES, J. 2021. Accuracy of digital planning in zygomatic implants. *Int J Implant Dent,* 7**,** 65.

XU, Z., XIAO, Y., ZHOU, L., LIN, Y., SU, E., CHEN, J. & WU, D. 2023a. Accuracy and efficiency of robotic dental implant surgery with different human-robot interactions: An in vitro study. *J Dent,* 137**,** 104642.

XU, Z., ZHOU, L., ZHENG, M., LIN, Y., HUANG, W., CHEN, J., LI, Y. & WU, D. 2023b. The effect of implant surgery experience on the learning curve of a dynamic navigation system: an in vitro study. *BMC Oral Health,* 23**,** 89.

YAN, Q., WU, X., SHI, J. & SHI, B. 2024. Does dynamic navigation assisted student training improve the accuracy of dental implant placement by postgraduate dental students: an in vitro study. *BMC Oral Health,* 24**,** 600.

YAN, Z., TANG, Q., WANG, F., GUO, R., WU, X. & LIU, Q. The Dental Implant Robot System Based on Binocular Vision. 2023 5th International Conference on Robotics and Computer Vision (ICRCV), 2023. IEEE, 283-287.

YANG, G. Z., CAMBIAS, J., CLEARY, K., DAIMLER, E., DRAKE, J., DUPONT, P. E., HATA, N., KAZANZIDES, P., MARTEL, S., PATEL, R. V., SANTOS, V. J. & TAYLOR, R. H. 2017. Medical robotics-Regulatory, ethical, and legal considerations for increasing levels of autonomy. *Sci Robot,* 2**,** eaam8638.

YANG, J. & LI, H. 2024. Accuracy assessment of robot-assisted implant surgery in dentistry: A systematic review and meta-analysis. *J Prosthet Dent,* 132**,** 747.e1-747.e15.

YOTPIBULWONG, T., ARUNJAROENSUK, S., KABOOSAYA, B., SINPITAKSAKUL, P., ARKSORNNUKIT, M., MATTHEOS, N. & PIMKHAOKHAM, A. 2023. Accuracy of implant placement with combined use of static and dynamic Computer Assisted Implant Surgery in single tooth space: a randomized controlled trial. *Clin Oral Implants Res,* 34**,** 330-341.

YU, K., UOZUMI, S., OHNISHI, K., USUDA, S., KAWANA, H. & NAKAGAWA, T. Stereo vision based robot navigation system using modulated potential field for implant surgery. 2015 IEEE International Conference on Industrial Technology (ICIT), 2015. IEEE, 493-498.

YU, X., TAO, B., WANG, F. & WU, Y. 2023. Accuracy assessment of dynamic navigation during implant placement: A systematic review and meta-analysis of clinical studies in the last 10 years. *J Dent,* 135**,** 104567.

ZHAN, Y., WANG, M., CHENG, X., LI, Y., SHI, X. & LIU, F. 2020. Evaluation of a dynamic navigation system for training students in dental implant placement. *Journal of Dental Education,* 85**,** 120-127.

ZHANG, Z., ZHANG, L. & YANG, G. Z. 2017. A computationally efficient method for hand-eye calibration. *Int J Comput Assist Radiol Surg,* 12**,** 1775-1787.

ZHOU, L., DING, J., XIAO, Y., LIU, Y., CHEN, J. & WU, D. 2023. Autogenous bone block osteotomy in the chin using a robotic system: A clinical report. *J Prosthet Dent,* S0022-3913**,** 00764-3.

ZHOU, W., FAN, S., WANG, F., HUANG, W., JAMJOOM, F. Z. & WU, Y. 2021. A novel extraoral registration method for a dynamic navigation system guiding zygomatic implant placement in patients with maxillectomy defects. *Int J Oral Maxillofac Surg,* 50**,** 116-120.

ZHOU, W., LIU, Z., SONG, L., KUO, C. L. & SHAFER, D. M. 2018. Clinical Factors Affecting the Accuracy of Guided Implant Surgery-A Systematic Review and Meta-analysis. *J Evid Based Dent Pract,* 18**,** 28-40.

ZHU, J., SUN, W., LI, L., LI, H., ZOU, Y., HUANG, B., JI, W. & SHI, B. 2023. Accuracy and patient-centered results of marker-based and marker-free registrations for dynamic computer-assisted implant surgery: A randomized controlled trial. *Clin Oral Implants Res,* 35**,** 101-113.

ZIELINSKI, R., OKULSKI, J., SIMKA, W. & KOZAKIEWICZ, M. 2023. The Zygomatic Anatomy-Guided Approach, Zygomatic Orbital Floor Classification, and ORIS Criteria-A 10-Year Follow-Up. *J Clin Med,* 12**,** 6681.